Western Mediterranean shelf foraminifera: Recent distribution, Holocene sea-level reconstructions, and paleoceanographic implications

Dissertation

Zur Erlangung des Doktorgrades der Naturwissenschaften im Department Geowissenschaften der Universität Hamburg

vorgelegt von

Yvonne Milker

aus

Leipzig

Hamburg

(2010)

Als Dissertation angenommen vom Department Geowissenschaften der Universität Hamburg

auf Grund der Gutachten von Prof. Dr. G. Schmiedl
und Prof. Dr. C. Betzler

Hamburg, den 07.07.2010

Prof. Dr. Jürgen Oßenbrügge
Leiter des Departments für Geowissenschaften

Danksagung

Zum Entstehen und Gelingen dieser Arbeit hat eine Reihe von Personen beigetragen, denen ich an dieser Stelle meinen Dank ausdrücken möchte.

Allen voran möchte ich mich bei meinem Doktorvater Prof. Dr. Gerhard Schmiedl für die Vergabe des Dissertationsthemas, für die ausgezeichnete fachliche Betreuung, die konstruktiven Diskussionen und Anregungen im Verlaufe der Arbeit sowie für die Verbesserungen der englischen Sprache herzlich bedanken. Weiterhin danke ich herzlich Prof. Dr. Christian Betzler für dessen fachliche Betreuung und die vielen anregenden Diskussionen im Verlaufe der Arbeit.

Dipl. Geol. Miriam Römer und Dipl. Geol. David Jaramillo-Vogel danke ich herzlich für die Bereitstellung der Daten aus ihren Diplomarbeiten und für die vielfältigen Diskussionen. Für seinen Einsatz bei der Aufbereitung des Probenmaterials danke ich Dipl. Geol. Robert Welti. Unserer studentischen Hilfskraft cand. Dipl. Geol. Marc Theodor gilt besonderer Dank für seine Labortätigkeiten und die vorbereitende Arbeiten mit dem Probenmaterial sowie für die vielfältigen Diskussionen und das Aushalten meiner Monologe, die der Reflektion der eigenen Arbeit dienten.

Für die vielfältigen konstruktiven Diskussionen und Anregungen bedanke ich mich bei Dr. Sebastian Lindhorst und Dipl. Geol. Jörn Fürstenau, Prof. Dr. Michal Kucera und Dr. Michael Siccha sowie Prof. Dr. Klaus Reicherter und Prof. Dr. emer. Klaus Bandel.

Dr. Nils Andersen (Leibniz Labor für Altersbestimmung und Isotopenforschung, Universität Kiel) ist für die Durchführung der Isotopenmessung und Prof. Dr. Pieter Grootes (Leibniz Labor für Altersbestimmung und Isotopenforschung, Universität Kiel) für die Durchführungen der Alterdatierungen gedankt.

Weiterhin danke ich der Promotionsförderungsstelle der Universität Hamburg, die es durch meine Anstellung möglich machte diese Arbeit durchführen zu können. Der Deutschen Forschungsgemeinschaft (DFG) ist für die finanzielle Unterstützung im Rahmen des Projektes CARBMED zu danken.

Bei meinen Eltern bedanke ich mich herzlich für die finanzielle Unterstützung während dieser Arbeit und den Rückhalt, den sie mir geben konnten. Meinem Freund Thomas danke ich vor allem für seine emotionale Unterstützung, die es möglich machte, immer wieder neu Kraft zu schöpfen und auch für seine Hilfe bei der Verbesserung des Englischen.

Summary

Modern and fossil benthic shelf foraminifera from three western Mediterranean cool-water carbonate regions (Alboran Platform, Oran Bight and the Mallorca Shelf) have been analyzed for the development of quantitative sea-level estimates and the reconstruction of changes in shelf water oceanography. The live (Rose Bengal stained) assemblages exhibit variable standing stocks and low diversity, probably reflecting seasonal population dynamics during the sampling period in late summer 2006. The dominance of “high food”-taxa in the live faunas of Oran Bight suggests the impact of an anthropogenic eutrophication on the near-coastal benthic ecosystems of this region. In contrast, the dead benthic foraminiferal assemblages are characterized by a higher diversity. In all study areas, a distinct faunal change between approximately 80 - 94 m water depth has been observed. On the shelf off Southwest Mallorca, this faunal shift coincides with the lower distribution limit of living rhodoliths, providing coarse-grained substrates that are dominated by attached epifauna. The species assemblages of the shallower sites (down to ~90 m water depth) are dominated by epifaunal species in all study areas. In contrast, the species assemblages of the deeper stations show regional differences, depending on the grain-size of the substrate and related accumulation of organic material. Fine-grained substrates, providing niches for infaunal species, are restricted to low-energy environments on the deeper Mallorca shelf. These observations demonstrate that the availability of food on the sea floor and the creation of infaunal niches in cool water carbonate shelf environments are mainly controlled by the substrate type and do not reflect differences in surface water production.

For relative sea-level reconstructions, transfer functions based on the Recent benthic foraminiferal assemblages and on Plankton/ Benthos ratios (P/B) were developed and then applied to fossil foraminiferal assemblages and P/B ratios. The transfer functions are based on regression methods such as Weighted Averaging (WA), Partial Least Squares (PLS), and WA-PLS, and further, the Modern Analoque Technique (MAT). The best predictive potential was given for the WA-PLS method, reflecting a high potential for quantitative sea-level reconstructions with an accuracy of +/- 10 m within a total sea-level rise of ~45 and ~47 m for the Alboran Platform and the southwest shelf off Mallorca, respectively. The more classical approach, based on Plankton/Benthos (P/B) transfer functions, resulted in less consistent reconstructions with higher errors. On the Alboran Platform and the Mallorca Shelf, the relative sea-level estimates correspond to the global and the Mediterranean sea-level developments during the Holocene. On the Mallorca shelf, the relative sea-level signal interferes with temporal substrate changes, resulting in minor inconsistencies during the middle Holocene period. In the Oran Bight, the estimated sea-level rise appears to be overestimated, when

compared to the global and Mediterranean sea-level histories in the middle and late Holocene. While major vertical tectonic movements in this area can be excluded, the overestimation may be attributed to a problematic age model and to redeposition processes resulting in enhanced relocation of benthic foraminifera.

The paleoclimatic evolution of the southwestern shelf off Mallorca during the Holocene has been reconstructed from stable oxygen and carbon isotope records in various benthic and planktonic foraminiferal tests and by micro- and macrofossil observations in a sediment core. The earliest Holocene is characterized by a higher seasonality as reflected by stable oxygen signals in the planktonic foraminifera *Globigerinoides ruber* (white) and *Globigerina bulloides*. The early and middle Holocene period (between 9.6 and 5.5 kyr BP) is characterized by particularly low seasonal contrasts and by the establishment of humid conditions on Mallorca Island. This resulted in a freshening of the surface mixed layer, enhanced nutrient fluxes from the island and a related eutrophication of the near-coastal marine ecosystems. This hydrological change is reflected by drops in the stable carbon isotope values of *G. ruber* (white) and the endobenthic *Bulimina aculeata* as well as in the appearances of the gastropod *Turritella communis* and the endobenthic foraminifer *Rectuvigerina phlegeri*. This humid period is nearly contemporaneous to the sapropel S1 formation in the eastern Mediterranean Sea. This demonstrates for the first time that the early Holocene warm and humid phase in the Mediterranean Sea has also affected the near-coastal ecosystems in the western part.

The detailed systematic documentation of benthic foraminiferal taxa from shallow-water carbonate environments of the western Mediterranean Sea provides a solid taxonomic base for further ecological and paleoenvironmental applications and adds significantly to already existing systematic descriptions from other areas of the Mediterranean Sea.

Kurzfassung

Im Rahmen der vorliegenden Arbeit wurden rezente und holozäne benthische Foraminiferen aus drei Karbonatschelfgebieten im westlichen Mittelmeer (Alboran-Plattform, Bucht von Oran und der Schelf von Mallorca) auf ihre Zusammensetzung, ihre Abhängigkeit von Umweltbedingungen sowie auf ihr zeitliches Auftreten hin untersucht. Wesentliches Ziel der Arbeit ist die Entwicklung von Transferfunktionen für quantitative Meeresspiegel-Rekonstruktionen und die Dokumentation von regionalen Auswirkungen der holozänen Klimadynamik auf flachmarine Ökosysteme im westlichen Mittelmeer.

Die Lebendgemeinschafftten zeichnen sich durch eine relativ geringe Diversität und schwankende Siedlungsdichten aus, was auf eine saisonal bedingte Populationsdynamik hinweist. In der Bucht von Oran werden die Lebendgemeinschaften von infaunalen Foraminiferen dominiert, was auf eine anthropogen verursachte Eutrophierung dieser Region in jüngster Vergangenheit zurückgeführt wird. Im Unterschied zu den Biozönosen sind die Thanatozönosen deutlich höher divers. Die flacheren Stationen (bis etwa 90 m Wassertiefe) im Untersuchungsgebiet werden von epifaunal lebenden Foraminiferen dominiert und weisen im Hinblick auf ihre Artenzusammensetzung Ähnlichkeiten untereinander auf. Im Gegensatz dazu zeigen die Totgemeinschaften der tieferen Stationen (~90 m - 235 m) deutlichere regionale Unterschiede, die in einem engen Zusammenhang mit dem vorhandenen Substrattyp und der damit verbundenen Akkumulation organischen Materials stehen. Dieser signifikante Faunenwechsel wurde in allen Untersuchungsgebieten beobachtet und fällt auf dem Schelf von Mallorca mit der Wassertiefe zusammen, in der noch lebende Rotalgen angetroffen werden. Die flacheren Stationen auf dem Schelf zeichnen sich durch das Vorhandensein grobkörnigen Substrats aus, auf dem epifaunal lebende Foraminiferen festgeheftet leben können, während die tieferen Stationen durch das Vorhandenensein feinkörnigen Substrats gekennzeichnet sind, welches einerseits Nischen für infaunal lebende Arten bereitstellt und anderseits auf geringe Bodenströmungen hindeutet. Diese Beobachtungen zeigen, dass die Verfügbarkeit von Nahrung und Nischen für infaunal lebende Foraminiferen eng mit dem wassertiefenabhängigen Substrat-Typ verknüpft ist, während die Oberflächenwasserproduktion die Zusammensetzung der Thanatozönosen nur wenig zu beeinflussen scheint.

Die rezenten benthischen Totgemeinschaften, die in den Untersuchungsgebieten auskartiert wurden, bilden die Grundlage für die Rekonstruktion der spätglazialen und Holozänen Meeresspiegelentwicklung. Mittels verschiedener Regressionsmethoden („Weighted Averaging“ WA, „Partial Least Squares“ PLS und WA-PLS) sowie der „Modern Analog Technique“ (MAT) wurden Transferfunktionen entwickelt, die auf die fossilen Thanatozönosen

in drei Sedimentkernen aus den Untersuchungsgebieten angewandt wurden. Darüber hinaus wurden verschiedene Transferfunktionen aus rezenten Plankton/Benthos-Verhältnissen (P/B) abgeleitet und auf fossile P/B-Verhältnisse angewandt. Die WA-PLS-Methode weist in allen Untersuchungsgebieten das größte Vorhersagepotential auf. Es wurden Genauigkeiten von +/- 10 m bei einem Gesamtmeerespiegelanstieg von ~45 m für die Alboran Platform und ~50 m für den südwestlichen Schelf von Mallorca erreicht, was das Potential benthischer Schelfforaminiferen für quantitative Meeresspiegel-Rekonstruktionen verdeutlicht. Die Rekonstruktionen, die auf den verschiedenen P/B-Transferfunktionen beruhen, zeigten hingegen größere Ungenauigkeiten. Auf der Alboran-Plattform und dem Schelf von Mallorca stimmt die rekonstruierte Meeresspiegelentwicklung im Wesentlichen mit dem globalen Trend und der mediterranen Meeresspiegelentwicklung während des Holozäns überein. Allerdings zeigen die mittels multivariaten statistischen Methoden analysierten Arten-Umwelt-Zusammenhänge auf dem Schelf von Mallorca einen signifikanten Einfluss von Substratänderungen auf die Meeresspiegel-Rekonstruktionen im mittleren Holozän, was in einer geringen Überschätzung der Paläowassertiefen in diesem Zeitabschnitt führte. In der Bucht von Oran hingegen wurde ein Meeresspiegelanstieg für das mittlere und späte Holozän rekonstruiert, der deutlich über dem globalen und denen der anderen Arbeitsgebiete liegt. Eine Beeinflussung durch tektonische Hebungsprozesse kann bei der zugrundeliegenen Genauigkeit ausgeschlossen werden. Vielmehr erscheint es wahrscheinlich, dass Umlagerungen von Foraminiferengehäusen und/ oder ein problematisches Altersmodell zu diesen Resultaten führten.

Zur Rekonstruktion der paläoökologischen and paläoozeanographischen Entwicklung des Schelfs von Mallorca wurden stabile Sauerstoff- und Kohlenstoffisotopensignale in benthischen und planktischen Foraminiferengehäusen gemessen und interpretiert. Die stabilen Sauerstoffisotopensignale in den planktischen Foraminiferen *Globigerina bulloides* und *Globigerinoides ruber* (weiß) belegen, dass das früheste Holozän durch eine höhere Saisonalität gekennzeichnet war. Im frühen und mittleren Holozän, zwischen etwa 9,5 und 5,5 ka vor heute, hingegen sanken die saisonalen Unterschiede und es stellten sich humide Bedingungen auf der Insel von Mallorca ein. Dies führte zu einer erhöhten Frischwasser- und damit Nährstoffzufuhr auf dem südwestlichen Schelf von Mallorca, was sich in den stabilen Kohlenstoffsignalen in *G. ruber* (weiß) und über erhöhte Nahrungsflüsse auch in der benthischen Foraminifere *Bulimina aculeata* widerspiegelt. Darüber hinaus weisen das gehäufte Auftreten des benthischen Gastropoden *Turritella communis* und der infaunalen benthischen Foraminifere *Rectuvigerina phlegeri* ebenfalls auf eine Eutrophierung der mallorcinischen Küstenregion in dieser Zeit hin. Das Auftreten humider Bedingungen auf der Insel von Mallorca fällt zeitlich annähernd mit der Bildungsphase des Sapropels S1 im östlichen Mittelmeer zusammen. Dies zeigt, dass die frühholozäne Feuchtphase im Mittelmeer

nicht nur das östliche Mittelmeer sondern auch die Küstenregionen im westlichen Mittelmeer beeinflusst hat.

Die systematische Untersuchung der rezenten und fossilen Benthosforaminiferen im Untersuchungsgebiet in Hinblick auf ihre taxonomische Zuordnung erfolgte mit dem Ziel, eine systematische Beschreibung dieser Foraminiferen zu erstellen. Hierdurch wurden bereits vorhandene taxonomische Arbeiten für das Mittelmeer deutlich erweitert.

Table of contents

1 Introduction

Foraminifera occur in high numerical densities in marine environments and provide an excellent tool for paleoceanographic reconstructions, relative sea-level estimates, and biodiversity studies. The Mediterranean Sea is one of the primary regions for the investigation of foraminiferal ecology and paleoecology because of its strong spatial and temporal variability of environmental conditions and high foraminiferal diversity. In this context, the comprehensive taxonomic overviews by d'Orbigny (1839), Parker (1958), Todd (1958), Hofker (1960), and more recently, by Cimerman and Langer (1991), Sgarrella and Moncharmont Zei (1993) and Rasmussen (2005) established a solid basis for further applications. Various ecological studies revealed significant spatial contrasts in the species composition. These studies showed that the diversity and microhabitat structure of Mediterranean benthic foraminiferal faunas, like in other oceans, depend on food and oxygen availability (Jorissen et al., 1995; De Rijk et al., 2000).

The distribution of shelf faunas is additionally influenced by gradients in light, temperature, salinity, the type of substrate, as well as velocity and turbulence of surface water currents (Jorissen, 1987; Cimerman & Langer, 1991; Sgarrella & Moncharmont Zei, 1993; Culver et al., 1996; Langer et al., 1998; Pawlowski et al., 2001; Saraswati, 2002; Schönfeld, 2002; Saraswati et al., 2003; Sen Gupta, 2003; Mendes et al., 2004; Lee, 2006 and Mojtahid et al., 2009). Shelf benthic foraminifera display a stenobathyal distribution, which is determined by oceanographic, trophic and sedimentological conditions. First data on the bathymetric zonation of Mediterranean benthic shallow water to deep sea foraminifera was reported by Bandy & Cherici (1966) and Cita & Zocchi (1978). More recent publications have shown that deposit feeding foraminifera decrease in number with increasing distance from the coast and increasing water depth as a response to a decreasing flux of organic matter (De Stigter et al., 1998). De Rijk et al. (1999, 2000) have illustrated that W-E shifts in the bathymetric zonation of shallow to deep benthic foraminiferal faunas in the Mediterranean Sea are basically determined by food availability.

The accurate knowledge of relative sea-level changes plays a fundamental role in the reconstruction of global circulation patterns, ice sheet dynamics, regional tectonic movements and validation of model results of future sea-level trends. The relative sea-level of the Mediterranean Sea during the late glacial and the Holocene follows that of the global sea-level development, but it is further influenced by neotectonic movements and hydro-isostatic effects (Kayan, 1988; Alessio et al., 1994; Antonioli et al., 1999; Lambeck & Bard, 2000; Antonioli et al., 2001; Morhange et al., 2001; Sivan et al., 2001; Antonioli et al., 2002; Goy et al., 2003; Lambeck et al., 2004; Pirazolli, 2005; Vouvalidis et al., 2005; Berne et al., 2007 and Stocchi &

Spada, 2007). In this context, bathymetric information is provided by both benthic and planktonic foraminifera. An older and relatively simple method for quantitative sea-level estimates is the use of transfer functions based on the ratio of planktonic to benthic foraminifera (e.g. Van der Zwaan et al. 1990; De Rijk et al., 1999 and Van Hinsbergen et al. 2005). In addition, various regression methods (e.g. Weighted Averaging, Partial Least Squares or Weighted Averaging-Partial Least Squares) have been applied on marsh foraminifera for an accurate quantification of low-amplitude sea-level changes (e.g. Horton et al. 1999; Gehrels 2000; Sabean, 2004; Horton & Edwards 2006; Boomer & Horton, 2006; Leorri et al. 2008; Nelson et al., 2008 and Hawkes et al., in press). To date, these sophisticated regression methods have never been applied to shelf sediment successions over the full range of glacio-eustatic sea-level changes.

Sediments from the Mediterranean Sea provide excellent climate archives. The ocean basin is situated between a humid and temperate climate regime in its northern part, and an arid climate regime in its southern part. Its oceanography and ecosystems respond sensitively to climatic changes. Marine sediments have been intensively studied with focus on the Neogene paleoclimatic history (e.g. Thunell et al., 1984; Rohling and de Rijk, 1999; Ariztegui et al., 2000; Cacho et al., 2000; Emeis et al., 2000; Cacho et al., 2001; Sbaffi et al., 2001; Cacho et al., 2002; Sbaffi et al., 2004; Jimenez-Espejo et al., 2007 and Kuhnt et al., 2008). The eastern Mediterranean Sea is characterized by cyclical depositions of sapropels, documenting the impact of insolation-driven hydrological changes (e.g. Rossignol-Strick et al., 1982; Rohling and Hilgen, 1991; Cramp and O'Sullivan, 1999). In the western Mediterranean Sea, sapropel-equivalent depositions have only rarely been found, implying a generally better ventilation of deep sea basins (Comas et al., 1996; Capotondi and Vigliotti, 1999). The drastic climatic and circulation changes are documented in the faunal and geochemical composition of foraminifera. The stable isotope signatures of planktonic foraminifera has been interpreted in terms of changes in temperature and freshwater discharge (e.g. Vergnaud Grazzini, 1977; Thunell et al., 1984; Vergnaud Grazzini et al., 1986; Rohling et al., 2002; Casford et al., 2003 and Rohling et al., 2004). In combination with independent proxies, this allowed the quantification of past sea surface temperatures and salinities (Thunell, 1979; Hayes et al., 1999; Emeis et al., 2000; Kucera et al., 2005 and Melki et al., 2009). In contrast, benthic foraminiferal stable isotope signals provide information on deep-water ventilation and organic matter fluxes (Vergnaud Grazzini et al., 1986; Vergnaud Grazzini & Pierre 1991, 1992; Schilman et al., 2001 and Kuhnt et al., 2008).

1.1 Aims of the study

Major target of this study is the reconstruction of the late glacial and Holocene sea-level history based on benthic and planktonic foraminifera from the western Mediterranean Sea. In a first step, the biodiversity, distribution and ecology of Recent benthic foraminifera has been studied in order to provide data on foraminiferal assemblages in neritic carbonate environments and their relation to specific environmental conditions. In a second step, this knowledge is used for the development of transfer functions for quantitative sea-level reconstructions. These major aims are complemented by the reconstruction of the paleoclimatic and paleooceanographic history of the southwestern shelf off Mallorca during the Holocene, based on planktonic and benthic stable oxygen and carbon isotope records. In order to realize the aims of this study, a comprehensive taxonomic framework is established for the benthic foraminiferal faunas. This can provide important insights into the biodiversity of shelf foraminifera in cool water carbonate environments.

1.2 Outline of thesis

This thesis is subdivided into 7 chapters. Chapter 1 contains an introduction and chapter 2 gives an overview on the present geographical and geological settings as well as on the climatic and oceanographic conditions in the Mediterranean Sea. Chapter 3 concentrates on the distribution of Recent benthic shelf foraminifera in three selected areas of the western Mediterranean Sea and their relation to the environment. The results of this chapter provide the base for chapter 4, where quantitative sea-level reconstructions for late glacial and Holocene successions are presented. These reconstructions are based on the development and application of various transfer functions using benthic foraminifera and Plankton/Benthos ratios. Chapter 5 focuses on the reconstruction of paleo-environmental changes on the southwestern shelf off Mallorca during the Holocene, recorded in the stable carbon and oxygen isotope signals of benthic and planktonic foraminifera and in faunal changes. Chapter 6 contains a systematic description of the benthic shelf foraminifera investigated in this study and chapter 7 presents the conclusions of the study and an outlook.

The basis of chapters 3 and 4 are provided by a publication in Marine Micropaleontology in 2009 and a publication submitted in Quarternary Science Reviews, respectively. Chapters 5 and 6 are based on manuscript drafts, prepared for publication in international journals.

2 Study area

2.1 Geographical and geological settings

The semi-enclosed Mediterranean Sea that represents a relict basin of the Tethys Ocean, is situated between the European and the African continent (Fig. 2.1). It covers an area of 2.5 million km^2 with an EW extent of 3700 km and an NS extent of 1600 km (Lionello et al., 2004). The average water depth is 1500 m and the maximum water depth of 5150 m is reached in the Ionian Sea (Lionello et al., 2004). The Mediterranean Sea is divided into two nearly equal sized basins - the western Mediterranean Basin and the eastern Mediterranean Basin - connected through the Strait of Sicily with approximately 330 m water depth (Wüst, 1960; Robinson et al., 2001). Via the Strait of Gibraltar (~345 m depth) it is connected with the North Atlantic Ocean and through the Marmara Sea with the Black Sea. The eastern Mediterranean Sea comprises the Levantine and Ionian Basins and the Adriatic and Aegean Seas (Fig. 2.1). The western Mediterranean Basin is subdivided into the Alboran Basin in its western part, the Provencal and Algerian Basins in its middle part and the Tyrrhenian Basin in its eastern part (Fig. 2.1).

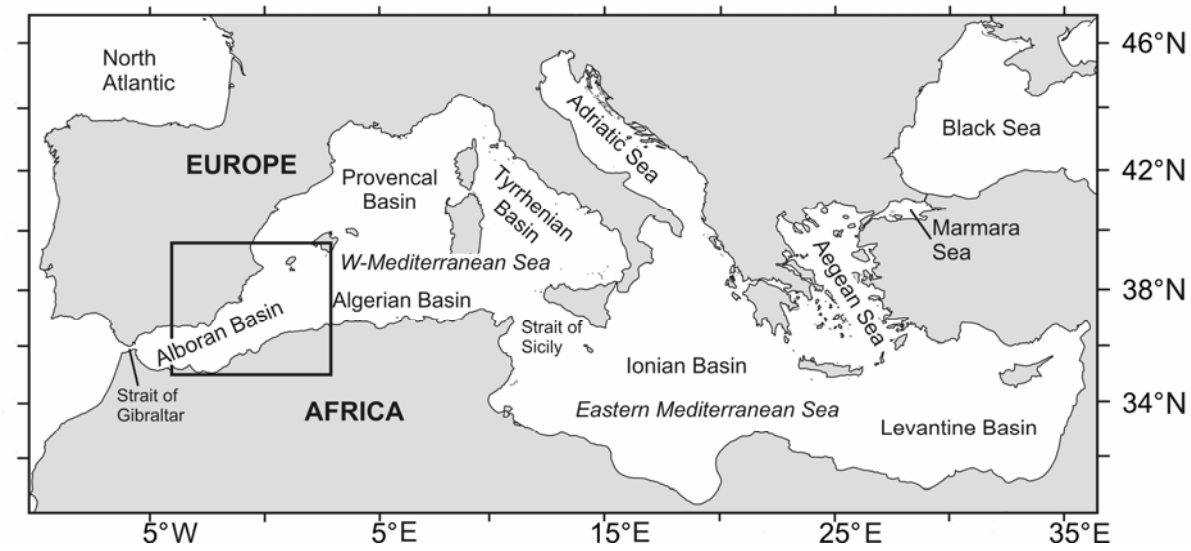

Fig. 2.1. Simplified map of the Mediterranean Sea with location of the study area in the western Mediterranean Sea.

The opening of the western Mediterranean Sea mainly took place from the late Oligocene onwards (Gueguen et al., 1998; Comas et al., 1999). The present western Mediterranean sub-basins become progressively younger eastwards. They were formed by late orogenic extension, resulting from the collision of Eurasian and African plates from the Cretaceous to the Paleogene, which is related to the spreading of the Atlantic Ocean ridge (Gueguen et al.,

1998; Comas et al., 1999). The opening of the Alboran, Provencal and Valencia basins dates back to the Oligocene and the early Miocene, whereas the Algerian and Tyrrhenian basins were formed from the Late Miocene to the Plio-Pleistocene (Dewey et al., 1989; Sanz De Galdeano, 1990; Doglioni et al., 1997; Gueguen et al., 1998) (Fig. 2.2). These basins acted as parts of a back arc-basin, related to the eastward roll back of the Apennines-Maghrebides subduction zone (Doglioni et al., 1997; Gueguen et al., 1998) (Fig. 2.2).

Recently, the Alboran region and Algerian coast are influenced by tectonic movements. Along the Alboran Ridge, uplifting processes and active subsidence occur coevally (Comas et al, 1999; Martinez-Garcia et al., submitted). Otherwise, no distinct subsidence or uplift since the Miocene is recorded for the southwestern Mallorca Island (Pomar, 1991). Recent seismicity in the western Mediterranean is almost entirely restricted to the western Alboran Sea and the North Algerian coast, where earthquakes are relatively frequent (e.g. Piromallo & Morelli, 2003; Giresse et al., 2009). The Oran region is characterized by relatively high seismicity and the occurrence of earthquakes (Bouhadad, 2001), whereas the Mallorca region shows only low seismic activity (Silva et al., 2001).

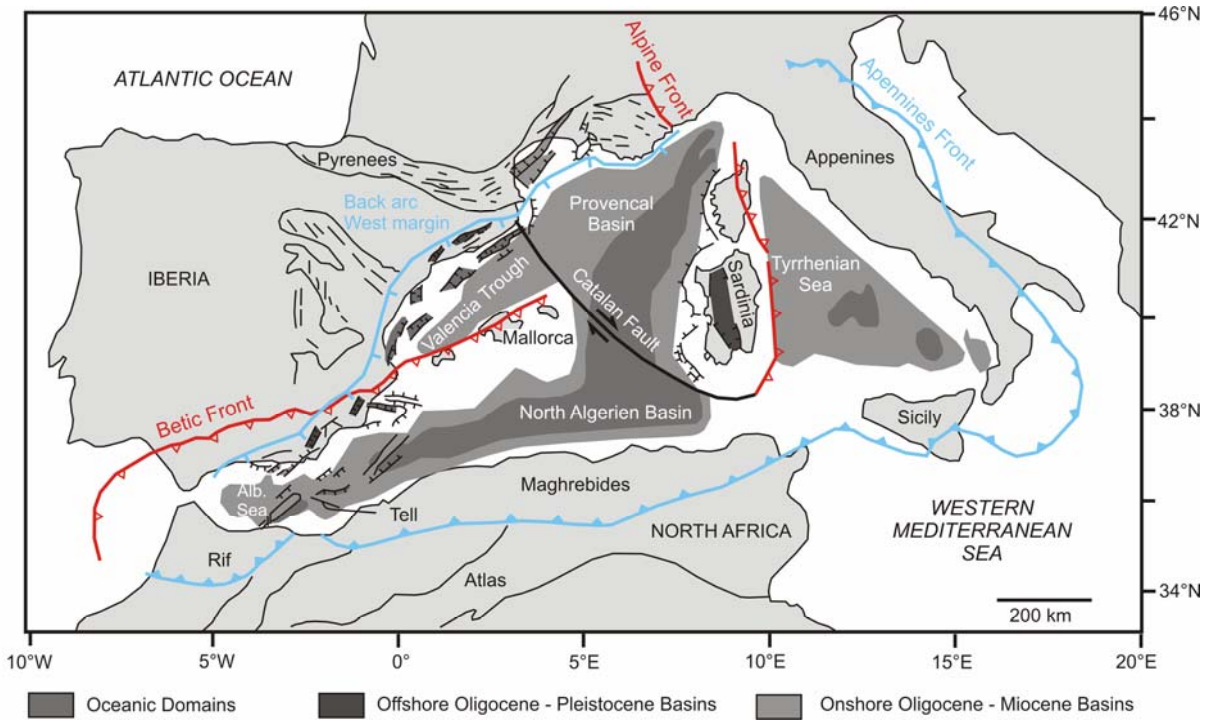

Fig. 2.2. Present tectonic situation in the western Mediterranean Sea redrawn after Gueguen et al. (1998) showing the positions of the Apennines Front and the Betic and Alpine Fronts.

2.2 Climate, hydrography and productivity

The Mediterranean Sea is situated in the transition zone between two major climate regions: a humid and temperate climate in the north and an arid climate in the south. Following an

updated Köppen & Geiger climate classification published in Peel et al. (2007), most of the northern, north-eastern and the south-western coastal regions are characterized by a temperate climate with dry and hot or warm summers with or without a dry season, while the south-eastern Mediterranean coastal regions are influenced by a warm desert climate.

The seasonal climate variability is generally linked to the North Atlantic Oscillation (NAO) during the winter season and to the position of the inner-tropical convergence zone (ITCZ) in the summer months. During the summer season, when the ITCZ and the Azores High shift towards higher latitudes, the Mediterranean region is under direct influence of the Hadley circulation - driven by deep convection in the ITCZ - and a stable high-pressure system is established across the Mediterranean resulting in hot and dry summers (Cramp & O'Sullivan, 1999; Traub et al. 2003) (Fig. 2.3). In the Mediterranean Sea, warm and dry winters are related to a positive NAO pattern, whereas cold and wet winters occur during a negative NAO pattern (Luterbacher et al., 2006). In contrast, during the winter season the eastern Mediterranean might be more affected by the North Sea Caspian Pattern (NCP) that is formed in the mid Troposphere due to geopotential height differences between the North Sea and the Caspian Sea (Gündüz & Özsoy, 2005).

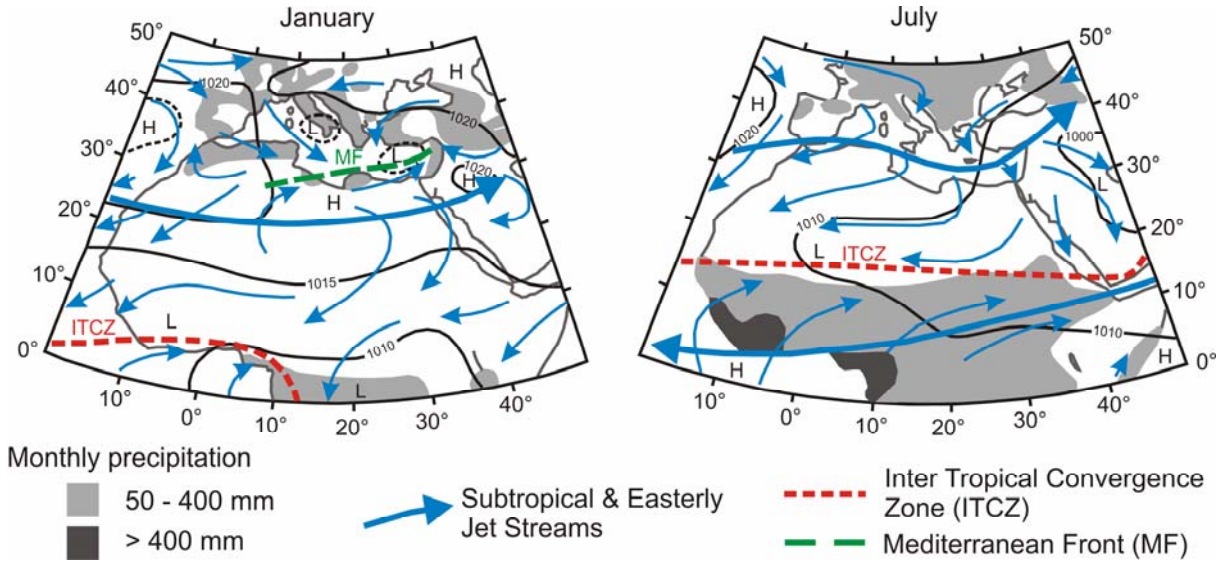

Fig. 2.3. Surface pressure (high pressure H, low pressure L), wind and precipitation in the Mediterranean region and in North Africa during January and July. The figure has been adapted from Cramp & O'Sullivan (1999).

The Mediterranean Sea is characterized by four main water masses. The surface water mass up to 75 - 150 m depth mainly consists of inflowing Atlantic Water (AW) (Wüst, 1961; Rixen et al., 2005) (Fig. 2.4). The intermediate water mass between ~150m - 600 m water depth consists of the Levantine Intermediate Water (LIW) which is formed in the eastern part of the Mediterranean (Wüst, 1961; Robinson et al., 2001). The basins below 600 m water depth are filled by deep water masses. The Western Mediterranean Deep Water (WMDW) is

formed in the Gulf of Lions, while the eastern Mediterranean Deep Water (EMDW) is formed in the southern Adriatic (Adriatic deep water, AdDW) and the Aegean Seas (Aegean deep water, AeDW) (Robinson et al, 2001; Millot & Taupier-Letage, 2005) (Fig. 2.4).

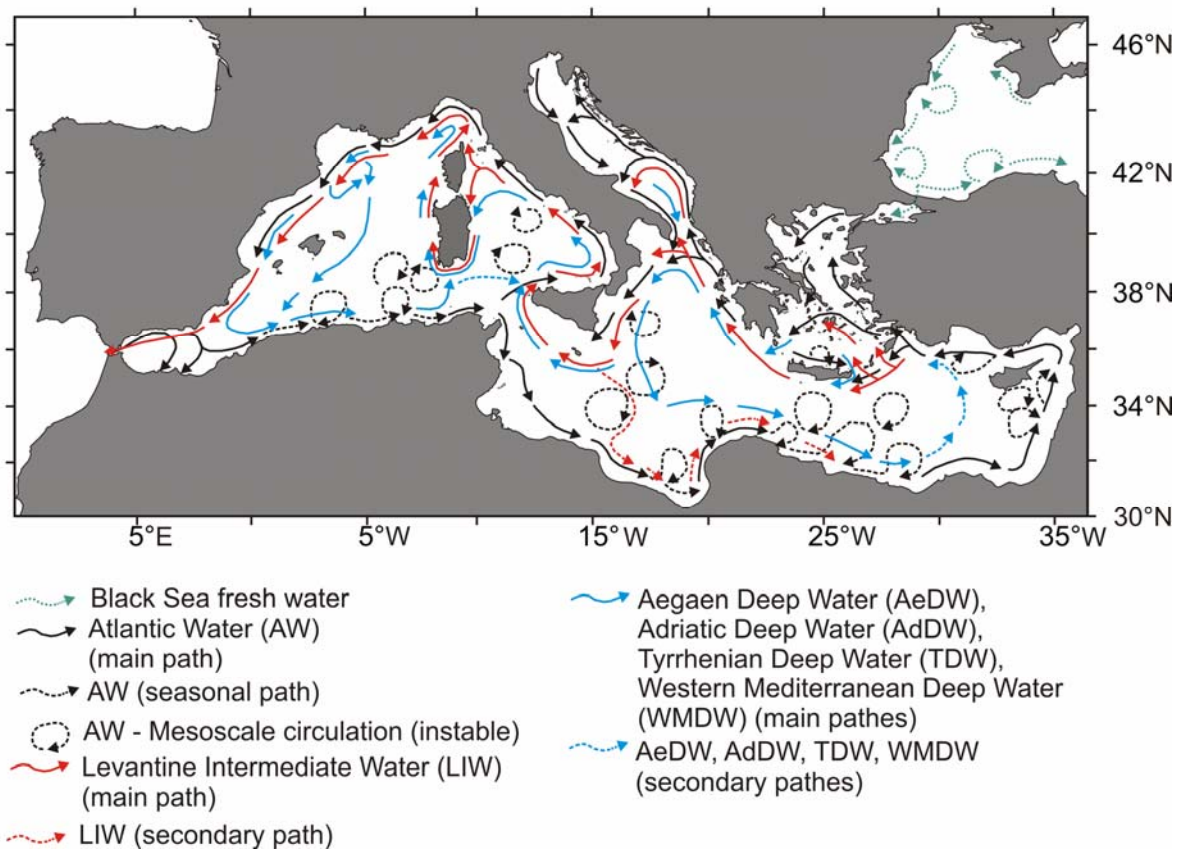

Fig. 2.4. General circulation of the Mediterranean Sea, redrawn after Millot &Taupier-Letage (2005).

In the Alboran Basin, the AW entering the Mediterranean Sea forms two anticyclonic gyres: the quasi permanent Western Alboran Gyre (WAG) and the more variable Eastern Alboran Gyre (EAG) (Tintore et al., 1988; Millot, 1999; L'Helguen et al., 2002; Vargas-Yanez et al., 2002; Masque et al., 2003; Velez-Belchi et al., 2005) (Fig. 2.5). Associated with these gyres are zones of enhanced vertical mixing and nutrient entrainment, including the Almeria-Oran-Front at the eastern edge of the EAG (Tintore et al., 1988; L'Helguen et al., 2002; Masque et al., 2003) (Fig. 2.5).

Fig. 2.5. Simplified map of the western Mediterranean Sea, showing the positions of the Western and Eastern Alboran Gyres (WAG, EAG), the Almeria-Oran Front and the Algerian Current.

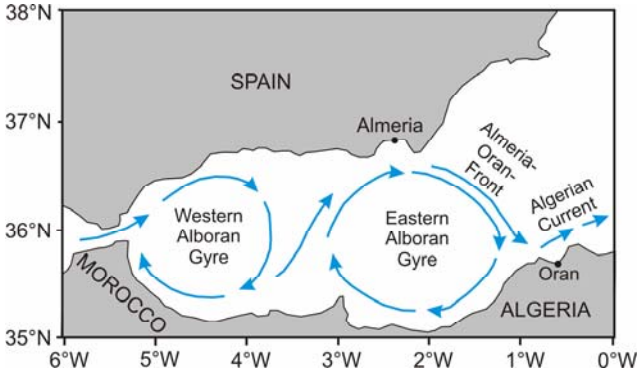

The recent anti-estuarine circulation in the Mediterranean Sea is forced by its negative water balance, e.g. increasing evaporation rates towards the eastern basins (Bethoux, 1980; Millot & Taupier-Letage, 2005). The AW (mean annual salinity of 36 - 37‰) that flows from the western Mediterranean through the Strait of Gibraltar into the eastern Mediterranean, gradually increasing in salinity to around 39‰ (Bethoux, 1980; Malanotte-Rizzoli, 1988; Millot & Taupier-Letage, 2005) (Fig. 2.4). In the winter months, vertical convection occurs in the eastern Mediterranean due to cooling of the saline AW, resulting in the formation of LIW (e.g. Millot & Taupier-Letage, 2005). The LIW flows back to the western Mediterranean, and as Mediterranean Intermediate Water (MIW) it enters the North Atlantic Ocean (Fig. 2.4). This water mass has a salinity of ~38 - 38.5‰ (Bethoux, 1980; Millot & Taupier-Letage, 2005).

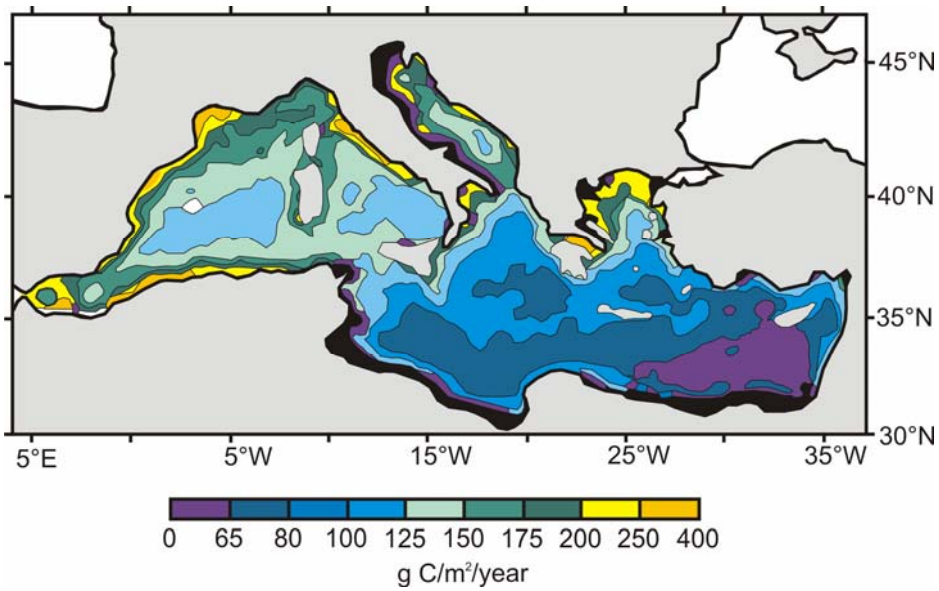

Fig. 2.6. Annual mean primary production in the Mediterranean Sea, adopted from Antoine et al. (1995).

The offshore areas of the Mediterranean Sea are oligotrophic, whereas the near-shore areas in the north-western and western parts of the Sea show higher chlorophyll a values in response to a higher riverine input of nutrients (Barale et al., 2005) (Fig. 2.6). The primary production of the Mediterranean Sea, derived from chlorophyll a data, is characterized by a distinct contrast between the eastern and western basin. In the eastern Mediterranean Sea, mean annual values of 110 g C/m^2/year are reached, whereas a higher mean annual primary production with 158 g C/m^2/year is estimated for the western basin (Antoine et al., 1995). The most productive area in the eastern Mediterranean is the Adriatic Sea with 241 g C/m^2/year mean annual primary production, and the most oligotrophic region is the southern Levantine Basin with 82 g C/m^2/year (Antoine et al., 1995) (Fig. 2.6). The Alboran Sea reaches the highest mean annual primary production in the western Mediterranean Sea with approximately 200 g C/m^2/year (Antoine et al., 1995), whereas the Balearic region is more oligotrophic with a mean annual primary production of 100 - 150 g C /m^2/year (Antione et al., 1995) (Fig. 2.6).

3 Distribution of Recent benthic foraminifera in neritic carbonate environments of the western Mediterranean Sea

Abstract

The distribution of Recent shallow-water benthic foraminifera in surface sediment samples from cool-water carbonate environments of the Oran Bight, Alboran Platform and Mallorca Shelf in the western Mediterranean Sea was studied. Multivariate statistical analyses resulted in the identification of species assemblages, representing different environmental settings. In all three regions the assemblages show a distinct bathymetric zonation that is mainly attributed to the distribution of rhodoliths and related substrates, but also to water turbulence and the availability of food at the sea floor. The live assemblages (Rose Bengal stained individuals) are characterized by rather low diversity and low standing stocks, likely reflecting seasonal population dynamics. In the Oran Bight, elevated standing stocks of “high food”-taxa suggest the impact of anthropogenic eutrophication on the near-coastal benthic ecosystems of this area. The diversity of the dead assemblages is higher than in siliclastic shelf ecosystems of the Mediterranean Sea but lower when compared to carbonate environments of the Levantine Sea. This regional difference is mainly attributed to lower sea surface temperatures and the lack of Lessepsian invaders in the western Mediterranean Sea. In all study areas, a distinct faunal change occurs between approximately 80 - 90 m water depth. This change coincides with the lower distribution limit of living rhodoliths at the shelf of Mallorca, providing coarse-grained substrates that are dominated by attached taxa. Below this depth interval, the fauna shows regional differences depending on the grain-size and related accumulation of organic material. Fine-grained substrates with infaunal niches are restricted to low-energy environments on the deeper shelf southwest off Mallorca.

This chapter is based on: Milker Y., Schmiedl, G., Betzler, C., Römer, M., David Jaramillo-Vogel, D., Siccha, M., 2009. Distribution of Recent benthic foraminifera in shelf carbonate environments of the western Mediterranean Sea. Marine Micropaleontology 73, 207-255

3.1 Introduction

Benthic foraminifera are widely used in ecological and paleoceanographic studies of various marine environments. In deep-sea benthic ecosystems, diversity, species composition and microhabitat preferences of benthic foraminifera basically reflect food and oxygen availability on the sea floor and in the upper surface sediment (e.g., Corliss, 1985; Jorissen et al., 1995; Van der Zwaan et al., 1999; De Rijk et al., 2000). Similar adaptations are observed in shelf ecosystems with fine-grained substrates (Jorissen et al., 1992; Mojtahid et al., 2009). However, shallow water (littoral and neritic) habitats can be additionally influenced by gradients in light, temperature, salinity, substrate, as well as velocity and turbulence of surface waters currents (Culver et al., 1996; Sen Gupta, 2003). These faunas commonly exhibit high foraminiferal numbers, variable diversity and a dominance of epifaunal and shallow infaunal taxa (e.g. Semeniuk, 2000; Murray, 2006). Particularly, many shallow-water taxa depend on the hydrodynamic energy at the benthic boundary layer and the corresponding substrate on the sea floor. The response of these taxa to oceanographic, trophic and sedimentological parameters is reflected by a stenobathyal distribution pattern.

In the Mediterranean Sea, the distribution of shelf foraminifera is documented in various regional studies (e.g., Jorissen, 1987; Cimerman & Langer, 1991; Sgarrella & Moncharmont Zei, 1993; Mojtahid et al., 2009). These studies revealed significant spatial contrasts in the composition of shelf faunas. In fine-grained sediments of the Adriatic Sea and the Gulf of Lions, the faunas show a distinct microhabitat zonation, depending on food availability and oxygen penetration into the sediment (Barmawidjaja et al., 1992; Jorissen et al. 1992; Schmiedl et al., 2000). In other regions, a strong correlation is observed between the diversity and abundance of symbiont-bearing shallow water foraminifera and water column illumination (Langer et al., 1998). In addition, near-coastal marine ecosystems can be affected by anthropogenic impacts. In this context, Frontalini & Coccioni (2008) and Romano et al. (2008) describe the influence of heavy metal pollution on shallow-water foraminifera on the Adriatic Sea coast and the coastal area of Bagnoli (Naples, Italy). The faunas of these areas contained a higher incidence of test deformations and a higher abundance of pollutant-tolerant species. Recently, the eastern Mediterranean shallow-water ecosystems have been invaded by various taxa from the Red Sea through the Suez Channel (Langer & Hottinger, 2000; Hyams et al., 2002; Hyams-Kaphzan et al., 2008). The number of the so-called Lessepsian invaders is still under debate, since data on the biogeography, diversity and ecology of autochthonous shallow-water faunas from various carbonate environments of the Mediterranean Sea are limited.

In this chapter, the diversity, species distribution and ecology of shelf benthic foraminifera in various cool-water carbonate environments of the western Mediterranean Sea is discussed. A

variety of multivariate analyses (Principal Component Analysis, Detrended Correspondence Analysis, and Redundancy Analysis) was applied in order to identify various assemblages and their links to different environmental parameters. In ecological studies, multivariate statistical methods are widely used to characterize community structures and to quantify the relationship between communities and environmental parameters (for summary see Ramette, 2007). Among the different methods, Principal Component Analysis and Cluster Analysis are commonly used in foraminiferal research to quantify the community structure of foraminiferal faunas (e.g. Schmiedl et al., 1997; Schönfeld, 2002; Mendes et al., 2004; Kuhnt et al., 2007). With other multivariate analyses such as Redundancy Analysis or Canonical Correspondence Analysis, faunal data can be directly related to environmental data allowing a more comprehensive analysis of foraminiferal ecology.

To date relatively little is known about the foraminiferal assemblages living in cool-water carbonate environments (Murray, 2006). Therefore, the study is designed to add new information on the diversity, distribution patterns and ecology of the Recent western Mediterranean cool-water carbonate taxa. The established relations between benthic foraminiferal faunas and environmental parameters can provide a basis for reconstructions of past environmental changes, including quantitative sea-level reconstructions (chapter 4).

3.2 Study area

The Mediterranean Sea is a semi-enclosed basin between Europe in the north and Africa in the south and can be divided into two nearly equal-sized basins (western Mediterranean and eastern Mediterranean basins) connected by the Strait of Sicily (Robinson et al., 2001) (Fig. 2.1).

The Mediterranean Sea is characterized by four main water masses. The surface waters consist of inflowing Atlantic Water (AW) (e.g. Robinson et al., 2001; Masque et al., 2003; Rixen et al., 2005). At intermediate depths, the Levantine Intermediate Water is present, which is formed in the eastern Mediterranean Sea (Robinson et al., 2001; Rixen et al., 2005). Below 600 m water depth, the basins are bathed by Western Mediterranean Deep Water formed in the Gulf of Lions, and by Eastern Mediterranean Deep Water formed in the Adriatic and Aegean seas (Robinson et al., 2001; Rixen et al., 2005) (Fig. 2.4).

In the Alboran Basin, the AW forms two anticyclonic gyres: the Western Alboran Gyre (WAG) and the Eastern Alboran Gyre (EAG) (Fig. 2.5). Surface water velocities on the Alboran Platform are relatively high, e.g. WAG velocities in October 1996 ranged between 124 and 140 cm/s (Velez-Belchi et al., 2005). In contrast, surface water velocities south-west off Mallorca are generally lower, ranging between < 15cm/s and a maximum of 50 cm/s during storm events (Werner et al., 1993). Associated with the Alboran gyres are zones of enhanced

vertical mixing and nutrient entrainment, including the Almeria-Oran-Front (Fig. 2.5). This front is marked by higher levels of primary production when compared to other open-ocean areas of the western Mediterranean Sea (L'Helguen et al., 2002; Masque et al., 2003; Velez-Belchi et al., 2005). In the Alboran basin, the annual primary production ranges between 150 and >250 g C per m^2 and year, whereas the Balearic region, with estimated annual values of 100 to 150 g C /m^2, has a more oligotrophic character than the Alboran region (Antoine et al., 1995) (Fig. 2.6).

In the western Mediterranean Sea cool-water carbonates form in areas protected from major siliciclastic input. A first comprehensive report of such carbonates was a significant part of the seminal work of Pérès and Picard (1964). Later publications corroborated and expanded these facies concepts (for example Blanc, 1972; Caulet, 1972; Fornos and Ahr, 1997; Ros et al., 1984; Carannante et al., 1988; Fornos and Ahr, 2006). The shallow subtidal facies zone (inner ramp) is dominated by *Posidonia* meadows with bioclastic sand patches down to 40 m of water depth. The middle ramp facies are dominated by coarse sediments with branching and foliose red algae, neighbouring rhodoliths may coalesce and generate a rigid coralline algal framework (corraligène de plateau) (Basso, 1997). At water depths below 90 m, muddy sands with a mixed biotic content occur.

3.3 Materials and methods

For the present study, 47 surface sediment samples were collected during Meteor cruise 69/1 in August 2006 from the Alboran Platform (14 samples), the Oran Bight (19 samples) and south-western off Mallorca (14 samples) using a grab or box corer (Fig. 3.1, Table A.1). The application of a multicorer for sampling of the sediment-water interface was not possible because of the generally coarse-grained sediments. Samples 341, 342 and 343 from the Alboran Platform were taken from the top of sediment cores drilled with a vibrocorer. The sampling depth ranges between 20 m to 235 m. After retrieval, the upper 1 to 2 cm of surface sediment was preserved in a Rose Bengal solution (1.0 - 1.5 g Rose Bengal per litre 96%-ethanol) to separate living (Rose Bengal stained) from unstained individuals except for core-top samples 341, 342 and 343. All samples were wet-sieved over a 63 µm sieve and the sample volumes were calculated. The fraction > 63 µm was dried at 40°C.

For determination of the grain-size distribution, samples were wet sieved and the weight percentages of the > 1000 µm, 1000 - 500 µm, 500 - 200 µm, 200 - 100 µm, 100 - 63 µm and < 63 µm fraction were calculated (Table A.5). Sea surface temperature and salinity data were measured during Meteor cruise 69/1 (Table A.5). As a proxy for regional primary productivity values, annual averages for chlorophyll a concentration in surface waters were extracted from the NASA SeaWiFS database (Feldmann and McClain, 2006) (Table A.5).

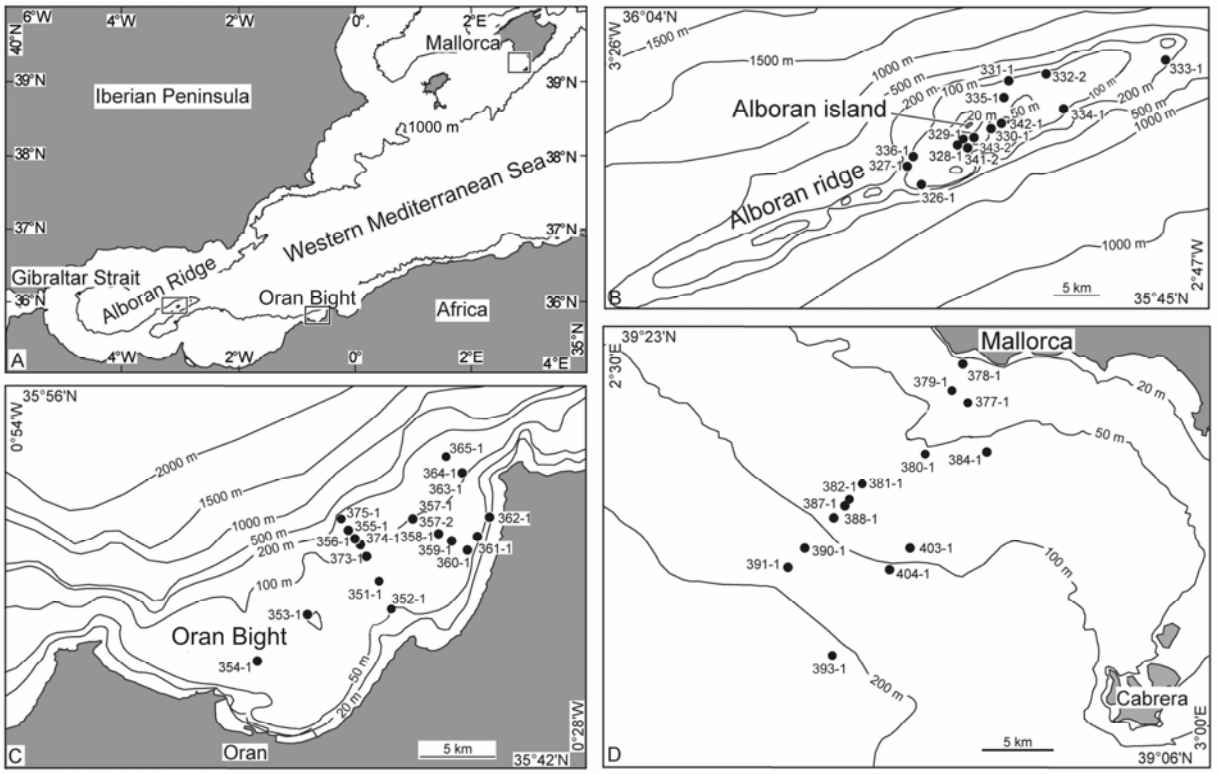

Fig. 3.1. Bathymetric survey of the western Mediterranean Sea (A) and three detailed bathymetric maps showing the studied areas Alboran Platform (B), Oran Bight (C) and Mallorca Shelf (D) (see also Table A.1) Throughout this chapter and in the following chapter figures, sample numbers are given without the suffix for better readability.

To count the foraminifera, all samples were split into two equal aliquots in order to generate sub-samples with 300 to a maximum of 1000 individuals (Fig. 3.2). The sub-samples were dry-sieved over a 125 µm - sieve. From the > 125 µm fraction, all stained and non-stained benthic foraminifera, and all planktonic foraminifera were picked and counted (electronic Tables A.17 and A.18). Only monothalamous tests with a clear pink staining and multichambered tests with more than one completely pink-stained chamber were considered as “living”. For an accurate identification of living miliolids and agglutinated specimens, tests were moistened with water. The identification of the benthic foraminiferal taxa was mainly based on the publications of Cimerman & Langer (1991), Sgarrella & Moncharmont Zei (1993), Jones (1994) and Rasmussen (2005) (see chapter 7). Test fragments and tests with yellowish-brown appearance were considered as re-deposited and counted separately. In addition to the standing stocks, the benthic foraminiferal number for empty tests (BFN) and number of taxa, the dominance D and the Shannon diversity H were calculated as defined by Hammer et al. (2008), applying the equations $D = \Sigma (n_i/n)^2$ and $H = -\Sigma n_i/n * \ln (n_i/n)$, with n_i = number of individuals of taxon i, and n = total number of individuals. Diversity values were computed with the PAST (PAlaeontological STatistics) software (Hammer et al., 2001, Hammer et al., 2008).

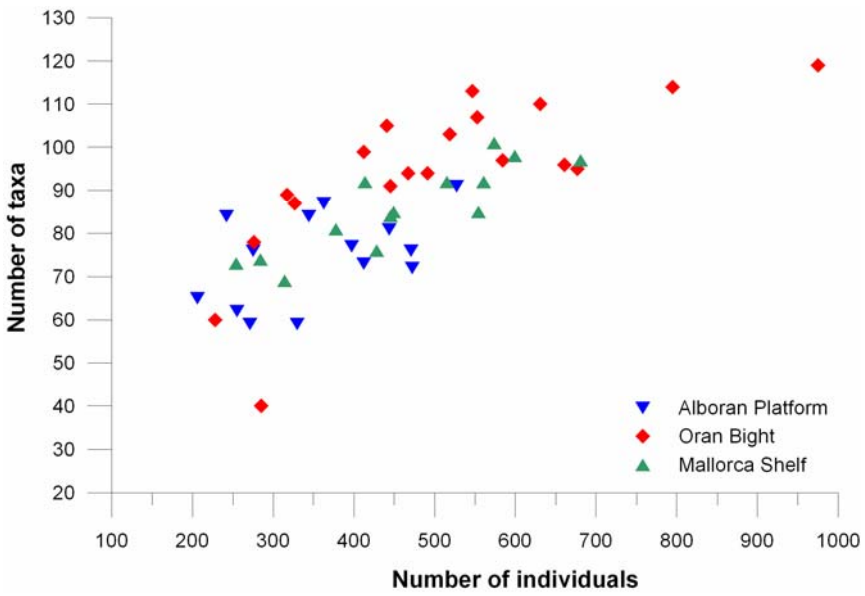

Fig. 3.2. Number of dead taxa versus number of counted dead individuals in the surface samples. It is shown that most of the taxa (74%) are captured within a total of 300 counted individuals.

Principle component analysis (PCA) was carried out to reduce the redundancy in the data set and to extract the most important foraminiferal assemblages. In PCA, the number of variables of the data matrix is reduced by extraction of uncorrelated axes, the principle components (PCs). When applied to a species matrix in Q-Mode, the correlation of a taxon to a principle component is given by its score value and the value of a principal component on a sample by its loading. For each new axis (or principle component), the explained proportion of the total variance of the data matrix can be calculated. One limitation of PCA in ecological studies is the assumption that taxa are linearly correlated with each other and the axes. For further details on methodological aspects of PCA see Leyer & Wesche (2007) and Ramette (2007). In the present study, only benthic foraminiferal taxa with a relative abundance of ≥ 1 % in at least three samples were selected and PCA was carried out with the software package Systat 12 in Q-mode for each area separately. PC loadings $\underline{\geq}$ 0.5 were defined as significant, following the suggestions of Malmgren & Haq (1982) and Backhaus et al. (2006).

A Detrended Correspondence Analysis (DCA) was performed to test whether species exhibit a unimodal or linear response to an environmental gradient (Leps & Smilauer, 2005; Leyer & Wesche, 2007). Redundancy Analyses (RDA) were carried out to quantify the relationship between the distribution of benthic foraminifera and ecological parameters such as water depth, grain-sizes, surface water chlorophyll a, surface water temperature and salinity, using the software package Canoco, version 4.5 (Ter Braak & Smilauer, 2002; Leps & Smilauer, 2005). RDA is based on a linear species-environment relationship, where the axes are linear combinations of the environmental variables (Leyer & Wesche, 2007). Both DCA and RDA were carried out on all samples except for sample 362 that contained only few foraminiferal tests. Species with values exceeding 1% in at least three samples were selected for analyses. For DCA, detrending by segments was chosen and species were centred. For RDA, species were square root transformed and environmental parameters were standardized. Partial RDAs

were used to calculate the explained variance in the foraminiferal data for each variable. Additionally, nominal variables (transformed into binary “dummy variables”) for the three areas were created for RDA analysis to explore potential local effects of environmental parameters. For both analyses, Monte Carlo permutation tests (full model, 5000 permutations) were performed with the software package Canoco (version 4.5) to test the significance of the environmental parameters.

3.4 Results

3.4.1 Surface sediment composition and grain-size

The surface sediments from the Alboran Platform consist of coarse-grained carbonates with an admixture of volcanoclastic debris. The fractions 125 µm - 2 mm and > 2 mm mainly consist of red algae, often in form of rhodoliths, gastropods, bivalves, fragments of echinoderms, foraminifera and various other biogenic components. Surface sediments of the Oran Bight resemble those from the Alboran Platform and are coarse-grained carbonates, mainly containing rhodoliths, gastropods and bivalves in the coarse fraction. The two shallowest samples (20 m and 40 m water depth) from Oran Bight are siliciclastic sands. In all other samples, siliciclastic rock fragments and mineral grains are rare. The surface sediments of the deeper stations south-western off Mallorca are fine-grained and carbonate-rich with few sea grass fragments. In contrast, samples from the shallower sites consist of coarse-grained carbonate and show a composition similar to those from the Alboran Platform and Oran Bight.

3.4.2 Distribution of living (Rose Bengal stained) benthic foraminifera

In all three areas, the total number of living benthic foraminifera, with a maximum of 535 individuals per 10 cm^3 sediment, is very low compared to the number of empty tests, with a maximum of 99,000 individuals per 10 cm^3 sediment. The highest standing stocks were observed on the Mallorca Shelf, with 33 - 535 living individuals per 10 cm^3 sediment. In the Oran Bight, 11 - 298, and on the Alboran Platform only 5 - 52 living individuals per 10 cm^3 were found (Fig. 3.3). Generally, similar species dominate the biocoenosis and the thanatocoenosis at each site, suggesting an autochthonous occurrence for most tests.

The diversity of the live fauna from the Alboran Platform shows a total of only 19 taxa, with 1 - 7 different taxa per sample (Fig. 3.3). The most abundant species are *Cassidulina crassa*, *Spirillina vivipara, Textularia pseudorugosa, Brizalina difformis* and *Brizalina striatula.* Due to their generally low densities, no significant spatial or bathymetric trends can be extracted from the census data.

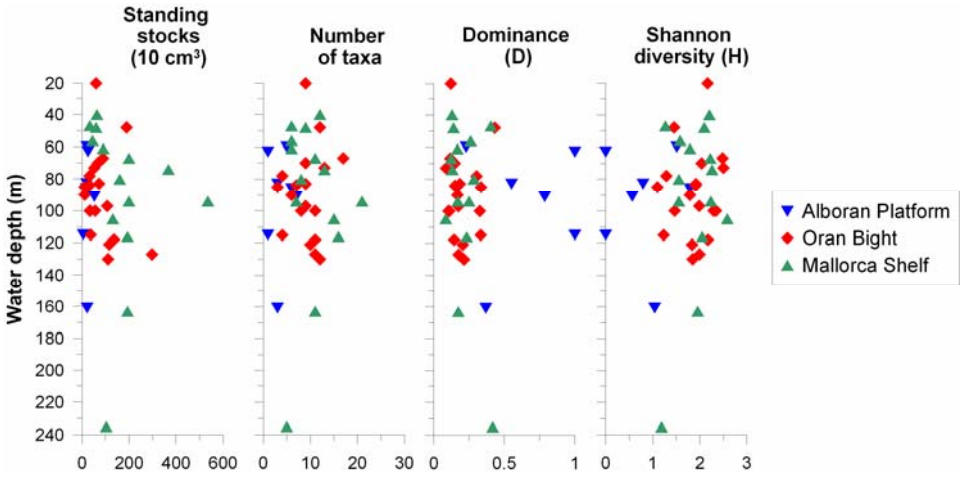

Fig. 3.3. Standing stocks (per 10cm^3 sediment) in the first centimetre of the sediment, number of individual taxa, Dominance (D) of taxa and Shannon diversity (H) for the studied areas versus water depths.

The diversity of the live fauna from the Oran Bight is higher when compared to the Alboran Platform and shows a total of 76 taxa, with 3 to 17 taxa per sample (Fig. 3.3). The biocoenosis is dominated by hyaline foraminifera with *Cancris auriculus* as the most abundant species. *Brizalina difformis, Bulimina elongata, Rectuvigerina phlegeri, Globocassidulina oblonga* and *Uvigerina peregrina* appear in different numbers in all samples from Oran Bight, except the shallowest sample 362 at 20 m. In addition, various typical shelf taxa (e.g., *Discorbinella bertheloti, Nonion fabum, Stomatorbina concentrica* and *Cibicides* spp.) occur in moderate numbers. Arenaceous and miliolid taxa are found in low numbers, except the more common *Reophax scorpiurus* and *Cibrostomoides jeffreysii*.

The live fauna from the Mallorca Shelf exhibits the highest diversities of the three study areas with a total of 83 different taxa (and 5 to 21 different taxa per sample) (Fig. 3.3). The species composition is markedly different when compared to those of the Alboran Platform and Oran Bight. The coarser-grained samples from shallower water depths (40 m - 94 m) mainly consist of various miliolids, *Neoconorbina terquemi, Textularia pala, Tritaxis challengeri* and *Asterigerinata mamilla* s.l. (with a sparse content of *Asterigerinata mariae* and *Asterigerinata adriatica*). The finer-grained samples from deeper sites (94 m - 235 m) are characterized by elevated numbers of *Cassidulina laevigata* s.l., *Hyalinea balthica, Textularia calva, Textularia gramen, Cassidulina crassa* and *Melonis affinis,* and low numbers of some other arenaceous and miliolid taxa.

The dominance D and the Shannon diversity H show a wide range, with values between 0.09 and 0.78 and 0.56 - 2.59, respectively. Exceptions are the samples 327 and 330 from Alboran Platform, where D=1 and H=0, due to the fact that only one taxon were found alive in each sample (Fig. 3.3).

3.4.3 Distribution of dead benthic foraminifera

The total benthic foraminiferal number (BFN) is highly variable, ranging between 382 and 98,987 individuals per 10 cm^3 sediment on the Alboran Platform, between 320 and 59,505 individuals per 10 cm^3 in the Oran Bight and between 1827 and 98,525 ind. per 10 cm^3 on the Mallorca Shelf (Fig. 3.4).

The Oran Bight samples contain a particularly high number of redeposited benthic foraminiferal tests with a maximum estimate of 84% in the shallowest site 362 from 20 m water depth. The number of taxa ranges between 57 and 88 on the Alboran Platform, between 16 and 112 in the Oran Bight and between 67 and 99 on the Mallorca Shelf (Fig. 3.4). The dominance D and the Shannon diversity H are quite similar in the different regions. D values range from 0.03 to 0.09 and H values from 3.1 to 3.9. Relatively high dominance and low diversity is restricted to the shallowest site 362 (20 m water depth) in the Oran Bight, with D = 0.13 and H = 2.35 (Fig. 3.4).

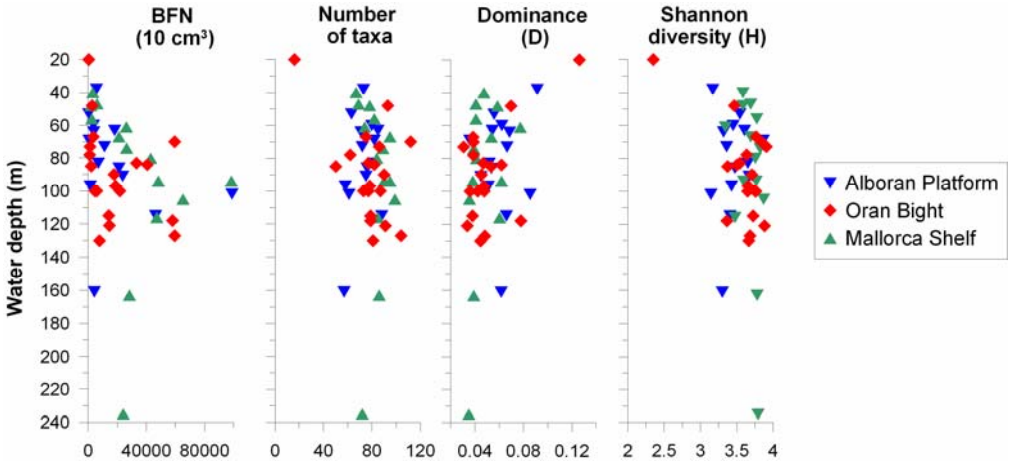

Fig. 3.4. Number of empty benthic foraminifera (BFN) per 10cm^3 sediment, number of individual taxa, Dominance (D) of taxa and Shannon diversity (H) for the studied areas versus water depth.

The PCA models reveal major faunal shifts between approximately 80 and 96 m water depth in all study areas and also show significant regional differences in the composition of faunas from similar water depths (Figs. 3.5, Tables A.2-A.4).

The 4-PC model of the Alboran Platform faunas explains 89.6% of the total variance (Table A.2). The *Asterigerinata mamilla* s.l.-assemblage (PC2) is significant in the shallower samples (38 - 62 m water depth) and includes *Elphidium complanatum* and *Cibicides lobatulus* as dominant taxa (Fig. 3.5, Table A.2). In water depth between 56 to 108 m this assemblage is replaced by an assemblage dominated by *Cibicides pseudoungerianus* (PC4) with *Cassidulina crassa* and *A. mamilla* s.l. as associated taxa. The *C. crassa*-assemblage (PC1) is significant in 80 to 138 m water depth and includes *Globocassidulina subglobosa* as dominant taxon. The

deepest sites (132 - 160 m water depth) are dominated by the *E. complanatum*-assemblage (PC3) comprising *Cibicides refulgens* as further dominant species (Fig. 3.5, Table A.2).

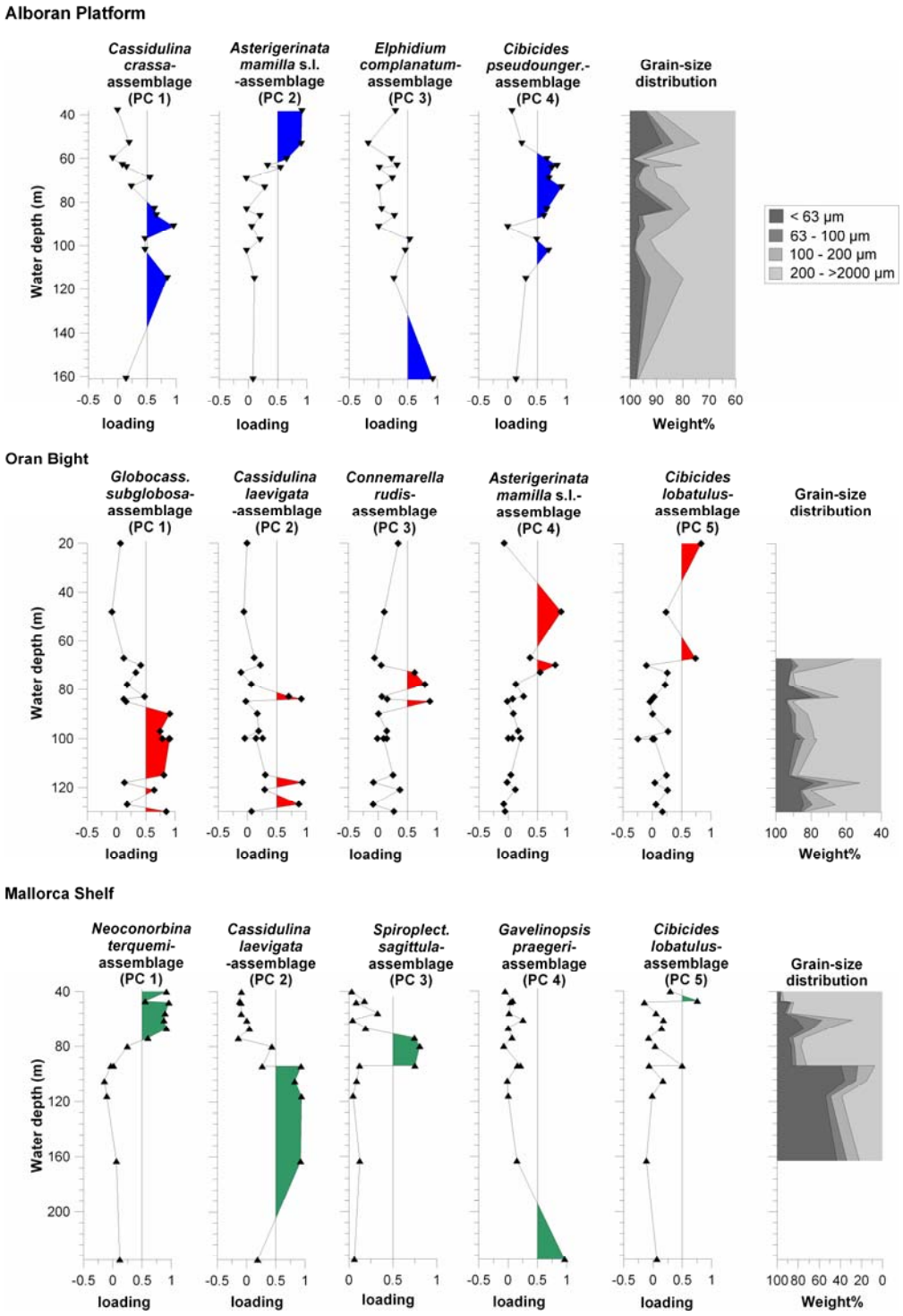

Fig. 3.5. Principal component analyses (PCAs) in Q-Mode and grain-size distribution for the Alboran Platform, Oran Bight and Mallorca Shelf surface samples versus water depths (see also Table A.2-A.4). PC loadings higher than 0.5 are defined as significant (as suggested by Malmgren & Haq (1982) and following Backhaus et al. (2006)) and are colorized.

The 5-PC model of the Oran Bight faunas explains 82.3% of the total variance (Table A.3). The shallowest sites (20 - 75 m water depth) are dominated by the *A. mamilla* s.l.-assemblage

(PC4) with *Rosalina macropora* as dominant taxon, and the *C. lobatulus*-assemblage (PC5), including *Neoconorbina terquemi* as dominant taxon (Fig. 3.5, Table A.3). In the water depth interval from 72 to 88 m a *Gaudryina rudis*-assemblage (PC3) with *C. lobatulus* as associated taxon is significant. In contrast, the deeper sites (80 - 130 m water depth) are characterized by the *G. subglobosa*-assemblage (PC1, with *C. crassa* as dominant taxon) and the *Cassidulina laevigata* s.l.-assemblage (PC2, including *Globocassidulina oblonga* as associated taxon) (Fig. 3.5, Table A.3).

The 5-PC model of the Mallorca Shelf faunas explains 90.5% of the total variance (Table A.4). The shallowest sites (40 - 75 m water depth) are characterized by significant loadings of the *Cibicides lobatulus*-assemblage (PC5, 40 - 48 m water depth) and the *N. terquemi*-assemblage (PC1, 40 - 76 m water depth) comprising *A. mamilla* s.l. as further dominant taxon (Fig. 3.5, Table A.4). A *Spiroplectinella sagittula* s.l-assemblage (PC3) dominates between 72 and 95 m water depth. Dominant taxa of this assemblage include *A. mamilla* s.l. and *C. lobatulus*. Significant loadings of the *C. laevigata* s.l.-assemblage (PC2) are restricted to the deeper sites, below approximately 96 m and down to ~210 m water depth. This assemblage contains *Bulimina elongata* as further dominant taxon. The deepest site is characterized by a *Gavelinopsis praegeri*-assemblage (PC4) with *G. subglobosa* and *C. crassa* as associated taxa (Fig. 3.5, Table A.4).

3.4.4 Relationship between foraminifera and environmental parameters

In a first step, a Detrending Correspondence Analysis (DCA) was carried out to test whether the species show a linear or unimodal relation to an environmental gradient. According to Leps & Smilauer (2005), gradient lengths with a standard deviation (SD) < 3 indicate linear, values > 4 SD unimodal species - environment relationships. The short gradient lengths of the first two axes (1.5 SD and 1.3 SD, respectively) suggest the use of a linear response model for the foraminiferal species (Table 3.1). Therefore, Redundancy Analysis (RDA) was chosen for the analyses of species-environment relationships in a second step.

Table 3.1. Statistical results of Detrended Correspondence Analysis (DCA).

	Axis 1	Axis 2	Axis 3	Axis 4
Eigenvalue	0.130	0.092	0.023	0.013
Length of gradient	1.527	1.340	0.990	0.808
Cumulative percentage variance of species data	29.8	50.9	56.1	59.0

In a first RDA setup, a total of 42.4% of the faunal variability can be explained by the included environmental variables (all canonical RDA axes). With the first two axes, 54.7% of cumulative species variance is explained (Fig. 3.6, Table A.6). With exception of the fraction

<63 µm, the environmental variables show significant F values >5, as proved by Monte Carlo tests. Temperature is negatively correlated to axis 1, and chlorophyll a as well as the fraction >1000 µm are positively correlated to this axis. The water depth shows a negative correlation to axis 2 and salinity a positive correlation. *Cassidulina crassa, Elphidium complanatum* and *Cibicides pseudoungerianus,* which have higher abundances in the Alboran Platform samples, indicate a close relation to chlorophyll a.

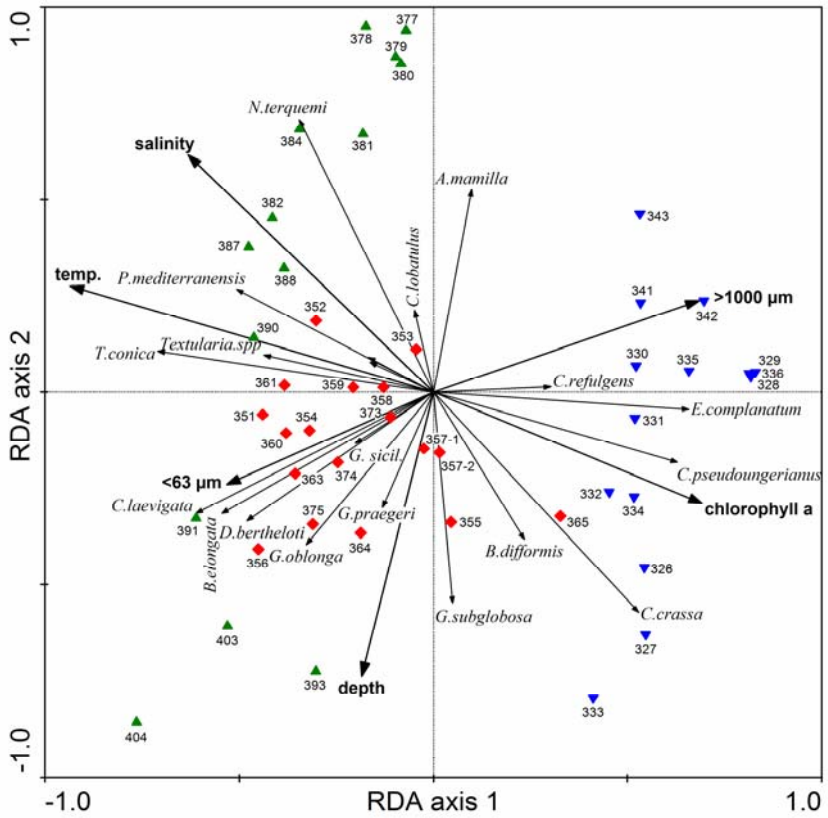

Fig. 3.6. Redundancy Analysis (RDA) for all surface samples (excluding sample 362) showing species-environment relationships (blue down triangles: Alboran Platform samples, red diamonds: Oran Bight samples and green up triangles: Mallorca Shelf samples). Only the most dominant species were selected for analysis. Names from species with very short gradients were removed from the plot for better illustration. See also Table A.6

This reflects elevated phytoplankton concentrations in surface waters of this region. *Cibicides refulgens*, which occurs in most of the Alboran samples, is probably related to coarser grained sediment. *Asterigerinata mamilla* s.l. that occurs in the shallower-water samples in all study areas is negatively correlated to water depth. A similar correlation is observed for *Cibicides lobatulus*, but with only a short gradient length. *Neoconorbina terquemi* is related to higher salinities, and *Textularia conica* and *Planorbulina mediterranensis* to higher temperatures. These two species have higher abundances in the samples from the Mallorca Shelf. These sites are marked by higher salinities and temperatures compared to those from the Alboran Platform and the Oran Bight. *Cassidulina leavigata, Bulimina elongata* and

Discorbinella bertheloti, which occur in the deeper samples from the Mallorca Shelf, exhibit a close relation to the <63 µm fraction. *Globocassidulina subglobosa* and *Gavelinopsis praegeri,* which have higher values in the Oran Bight samples, show a positive correlation with water depth. *Globocassidulina oblonga*, which occurs in all sampling areas, shows positive correlations with water depth and the content of <63 µm material (Fig. 3.6, Table A.6).

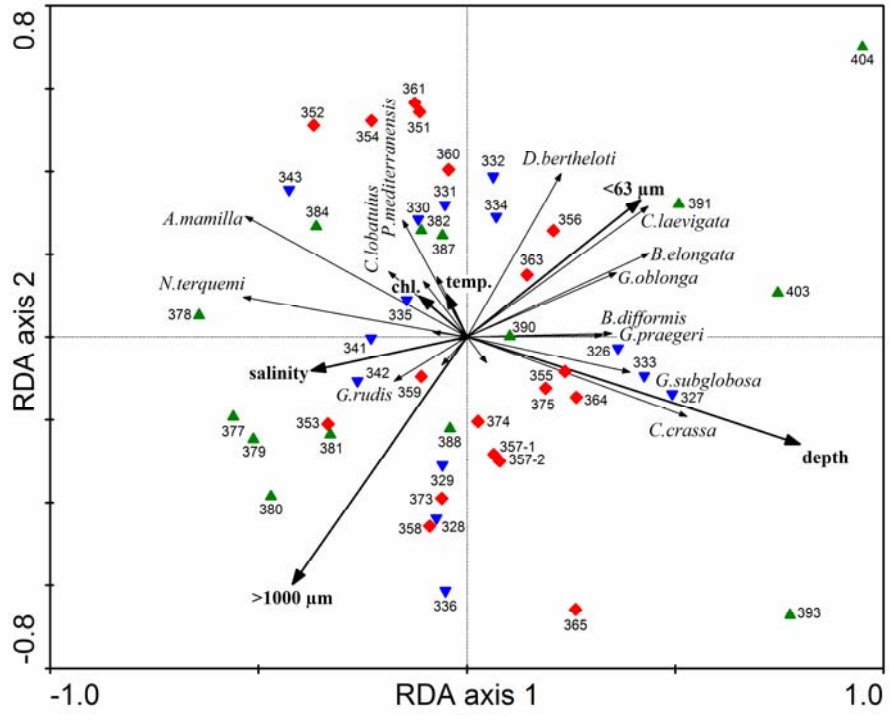

Fig. 3.7. RDA for all surface samples (excluding sample 362) with location as binary "dummy variables", used as covariables, carried out to avoid local effects and to extract environmental parameters exerting a similar influence on the faunal variability in all study areas (blue down triangles: Alboran Platform samples, red diamonds: Oran Bight samples and green up triangles: Mallorca Shelf samples). Names from species with very short gradients were removed from the plot for better illustration. See also Table A.6.

In a second RDA setup, binary "dummy variables" for the Alboran Platform, the Oran Bight and the Mallorca Shelf were introduced as covariables in order to reduce local effects and extract environmental parameters exerting a similar influence on the faunal variability in all study areas (Fig. 3.7, Table A.6). A cumulative species variance of 24.7% is explained by axis 1 and 2 (Table A.6). The water depth appeared now as the most significant parameter. It is significantly positive correlated with RDA axis 1 (Table A.6). Unlike the first RDA, *C. crassa* (besides *G. subglobosa* and probably *G. praegeri)* is now correlated to deeper water depths, whereas *N. terquemi* (besides *A. mamilla* s.l.) is now related to shallower water depths (Fig. 3.7). Similarly to the first RDA setup, *C. leavigata* s.l., *B. elongata*, *D. bertheloti* show a close relation to a higher content of fine-grained material, but *G. oblonga* could be now also related to the content of the fine-fraction.

3.5 Discussion

3.5.1 Diversity of benthic foraminifera in shelf carbonate environments

The standing stocks and diversities of the living fauna are quite variable and exhibit distinct contrasts within and between the study areas (Fig. 3.3). A patchy distribution of benthic foraminifera is common to most shelf ecosystems and attributed to highly variable environmental conditions (summary in Murray, 2006). In our study areas, standing stocks and live diversities display generally lower values when compared to faunas from siliciclastic shelf environments of the western Mediterranean Sea, e.g. from the Rhone prodelta (Mojtahid et al., 2009) and from the southern Tuscany continental shelf off the Ombrone river (Frezza & Carboni, 2009). In these siliciclastic environments, high fluxes of marine and terrestrial organic matter and fine-grained substrates generate a variety of infaunal niches that are obviously less developed in the coarser-grained carbonate environments. The relatively low diversities of the living fauna may also reflect seasonal population dynamics that are well documented from various shelf and deep sea ecosystems (Silva et al., 1995; Ohga and Kitazato, 1997; Duijnstee et al., 2004; Duchemin et al., 2007). These studies indicate an immediate or slightly lagged response of the faunas to changes in trophic conditions. In the western Mediterranean Sea, major phytoplankton blooms are restricted to February and March (Barale et al., 2005), while at the time of sampling in August 2006, phytodetritus fluxes are at a minimum. The oligotrophic summer situation likely supported only low numbers of living specimens. In addition, disturbance of the surface layer and partly loss of the living fauna during the sampling process cannot be excluded. However, such an artefact appears unlikely, since only visually intact sediment surfaces were considered for faunal analysis.

In contrast to the living faunas, the diversities of the dead faunas are similar or even higher when compared to those from siliciclastic shelf environments of the Mediterranean and other oceans (Levy et al., 1993; Scott et al., 2003; Murray; 2006, Frezza & Carboni, 2009; own unpublished data) (Fig. 3.4). Carbonate environments of the western Mediterranean Sea obviously provide a variety of (epifaunal) niches fostering the long-term development of complex benthic foraminiferal faunas. However, the mapped diversities are slightly lower than in mixed siliciclastic-carbonate ecosystems of the southeastern Levantine shelf (Hyams-Kaphzan et al., 2008). The faunas from the latter region contain various symbiont-bearing taxa, that are typical for subtropical and tropical shallow-water environments (for example the genera *Amphistegina*, *Heterostegina*, *Peneroplis*). In addition, the southeastern Levantine shelf is inhabited by a number of so-called Lessepsian invaders from the Red Sea (Hyams-Kaphzan et al., 2008). Living specimens of the Lessepsian invader *Amphistegina lobifera* are also reported from hard substrates in shallow water (0 to 3 m water depth) of the Maltese

Islands (Yokes et al., 2007). So far, none of the Lessepsian invaders have been documented in our study area except of *Cibicides* cf. C. *majori* that resembles a taxon common both on the Israeli shelf and the Gulf of Aqaba (Hottinger et al., 1993; Hyams-Kaphzan et al., 2008). In our study area, symbiont-bearing subtropical taxa are absent, except for a few living and dead specimens of *Peneroplis pertusus* and some soritids found in the Oran Bight at 20 m water depth (site 362). *P. pertusus* was described as an epiphytic species from 0 to 20 m water depth from the Adriatic and Tyrrhenian seas (Cimerman & Langer, 1991; Langer et al., 1998). The near-absence of symbiont-bearing taxa may have several reasons. In our study, all but sample 362 were recovered from water depths below 38 m, excluding the upper part of the photic zone, where the majority of Mediterranean larger foraminifera commonly lives on phytal substrates (Cimerman & Langer, 1991; Langer et al., 1998; Hyams-Kaphzan et al., 2008). In addition, most of larger benthic foraminifera exhibit a close affinity to warm-water temperatures with rather low seasonal variability (e.g., Hohenegger et al., 1999). In our study areas, winter sea-surface temperatures can be as low as 13°C and mean annual values are approximately 3 to 5°C lower than in the southeastern Levantine Sea (MEDATLAS data).

3.5.2 Impact of substrate, hydrodynamic energy at the benthic boundary layer, and food availability

3.5.2.1 Benthic foraminiferal assemblages from shallow-water sites

In all study areas, the benthic foraminiferal assemblages exhibit a marked faunal shift that is centred around 80 m on the Alboran Platform and in the Oran Bight, and around 94 m water depth on the Mallorca Shelf (Fig. 3.5). The faunas of the shallow circalittoral, between approximately 40 and 80 m, are dominated by trochospiral species, including *Asterigerinata mamilla* s.l., *Cibicides lobatulus*, *Cibicides pseudoungerianus,* and *Neoconorbina terquemi* as the most dominant taxa. These and most of the associated species are common Mediterranean shelf taxa (Jorissen, 1987; Cimerman and Langer, 1991; Sgarrella & Moncharmont Zei, 1993). They are epifaunal suspension feeders and are permanently or temporarily attached to coarse substrates, such as bioclastic sands and gravel (Sturrock and Murray, 1981; Coppa & Di Tuoro, 1995; summary in Murray, 2006). The general adaptation of these taxa to shallow water depths and coarse-grained substrate is confirmed by the results of the RDA analyses and by the grain-size distribution of the samples (Fig. 3.5 and 3.7).

On the Mallorca Shelf, the lower limit of the distribution of the shallow-water assemblages (*C. lobatulus*-, *N. terquemi- and Spiroplectinella sagittula* s.l.-assemblage) is associated with a change in grain-size composition of the substrate (Fig. 3.5). In water shallower than 94 m water depths, surface sediments are dominated by sand and gravel, while mud plays only a subordinate role. The observed shift in grain-size on the Mallorca Shelf coincides more or less with the lower limit of rhodolith growths, marking the depth of the lower photic zone (Pedley

and Carannante, 2006; own observations). No distinct bathymetric shift in substrate is present on the Alboran Platform and in the Oran Bight, whereas no rhodoliths were found deeper than 91 m on the Alboran Platform. In both areas a faunal shift has also been observed at ~80 m water depth (Fig. 3.5). The shallower sites are characterized by assemblages dominated by the *A. mamilla* s.l., *C. pseudoungerianus, Gaudryina rudis* and *C. lobatulus*, whereas in the deeper sites the assemblages are dominated by *Cassidulina crassa, Globocassidulina subglobosa* and *Cassidulina laevigata* s.l.. In the western Mediterranean Sea, the 1% light penetration depth is located at 70 - 80 m, while in the eastern Mediterranean Sea it is in 110 m water depth (Moutin & Rainbault, 2002).

It appears likely that the associated taphonomic production of coarse carbonate particles and living sciaphile algae provide suitable substrates for the observed epifaunal taxa. In shelf environments, habitat exposure to water turbulence may exert an important influence on winnowing and lateral transport of sediment and food particles. In the western Mediterranean Sea, the storm wave base is located between 30 and 60 m (Pedley and Carannante, 2006). Our own bathymetric surveys of the study areas revealed abrasion platforms at around 35 - 40 m water depths, marking the location of the average storm wave base (Betzler et al, in press). According to this finding, and the persistence of sandy substrates on the Alboran Platform and in the Oran Bight below this depth limit, wave turbulence cannot account for the observed faunal shifts at ~80 m. Instead, the impact of near-bottom currents and local sea floor topography may play a more important role for the deeper circalittoral environments. To date, no *Posidonia* meadows and associated epiphytic taxa were encountered at the studied sites. These ecosystems are restricted to the infralittoral zone (lower depth limit around 30 - 40 m) where photophile algae are associated with a variety of epiphytic benthic foraminifera (Jorissen, 1987; Langer et al., 1998).

3.5.2.2 Benthic foraminiferal assemblages from deeper sites

Below approximately 80 - 94 m water depths, the most characteristic taxa of the benthic foraminiferal assemblages belong to the family of Cassidulinidae, including *Cassidulina crassa* and *Globocassidulina subglobosa* on the Alboran Platform, *G. subglobosa, C. crassa Cassidulina laevigata* s.l., and *Globocassidulina oblonga* in the Oran Bight, and *C. laevigata* s.l. on the Mallorca Shelf. According to the results of RDA analyses, the species *C. crassa* and *G. subglobosa* are clearly related to water depth, while *C. laevigata* s.l. and probably *G. oblonga* are closely related to fine-grained substrates (Fig. 3.7).

The epifaunal to shallow infaunal species *G. oblonga* and *G. subglobosa* are commonly associated with elevated bottom water currents, vegetation cover, sandy substrates, and oligotrophic to mesotrophic conditions (Jorissen, 1987; Schmiedl et al., 1997; Martins et al.,

2007). *C. crassa* is reported from circalittoral and bathyal muds and coarser substrate and is associated with a lower flux of organic matter and strong bottom water currents in the Mediterranean Sea and the Atlantic Ocean (Sgarrella & Moncharmont Zei, 1993; Rasmussen et al., 2002; Martins et al., 2007). On the Alboran Platform, these species are associated with *Elphidium complanatum*, and the epifaunal species *Cibicides refulgens*, *Cibicides lobatulus*, *Cibicides pseudoungerianus*, and *Gavelinopsis praegeri*. These species are typically associated with high-energy shelf environments and sandy substrates in the Gulf of Cadiz, Alboran Sea and Tyrrhenian Sea (Coppa & Di Tuoro, 1995; Guimerans & Currado, 1999B; Schönfeld, 2002; Panieri et al., 2005; Martins et al., 2007). Own observations suggest that on the Alboran Platform also benthic ecosystems between 70 and 160 m water depth are influenced by winnowing and lateral transport of sediment and organic matter particles. This process can be related to the isolated position of the Alboran Platform that is influenced by surface currents of the Western Alboran Gyre (WAG) (Fig. 2.5). The WAG is approximately up to 100 km in diameter and up to 200 m deep with seasonal variants in size and strength (Gascard & Riches, 1985; Preller, 1986; Cantos-Figuerola et al., 1991). In October 1996, the WAG surface water velocities ranged between 124 and 140 cm/s (Velez-Belchi et al., 2005). Furthermore, in summer 1997 Vargas-Yanez et al. (2002) identified a third and unusual anticyclonic gyre (besides the WAG and EAG) directly centred surround the Alboran Island. Another direct influence of the WAG on the Alboran Island was also described earlier in October 1981 by Gascard & Riches (1985). A surface float that was deployed in the WAG, was circled cyclonically twice around the Island before it was returned to the WAG. As a consequence of the influence of the WAG, eutrophic conditions in the surface water of the Alboran Sea are not reflected by a well-developed infauna at the sea floor.

Similar processes can account for the faunal patterns at sites between 80 and 130 m water depth of the Oran Bight. This depth interval is dominated by sandy substrates, suggesting similar energy at the benthic-boundary layer when compared to the shallower stations of this region. The presence of *C. laevigata* s.l. that shows a higher abundance at sites with a slightly higher content of fine-grained material, indicates slightly higher food accumulation when compared to the Alboran Platform (Fig. 3.5). This cosmopolitan species is widespread from circalittoral to bathyal and mostly muddy sediment in the western Mediterranean and show higher abundances in environments with higher organic carbon contents (Jorissen, 1987; Sgarrella & Moncharmont Zei, 1993; De Stigter et al., 1998; Bartels-Jonsdottir et al., 2006).

On the Mallorca Shelf, the sites between 76 and 94 m are dominated by the *Spiroplectinella sagittula* s.l.-assemblage and the sites between 94 and ~210 m by the *C. laevigata* s.l.-assemblage (PC3, PC1; Fig. 3.5). The *S. sagittula* s.l.-assemblage marks the transition between the lower photic and aphotic zones. The dominant taxon, *S. sagittula,* is a common shelf species of the Mediterranean Sea and was described from sandy substrates of the

Adriatic Sea and in coarser-grained sediment in the Gulf of Cadiz (Jorissen, 1987; De Stigter et al., 1998; Schönfeld, 2002; Rasmussen 2005). On the Mallorca Shelf, the *S. sagittula s.l.*-fauna contains both epifaunal and shallow infaunal elements from faunas above and below. The *C. laevigata* s.l.-assemblage is closely associated with fine-grained substrates of the lower circalittoral off southwest Mallorca (Fig. 3.7). In our study area, this species is associated with *Bulimina elongata, Bulimina gibba, Hyalinea balthica, Melonis affinis* and few other taxa (Table A.4). In the Mediterranean Sea, the mentioned taxa are particularly common in fine-grained siliciclastic substrates of shelf and bathyal environments. The faunas of these ecosystems exhibit a distinct microhabitat zonation that is dependend on food availability and oxygen penetration (Barmawidjaja et al., 1992; Jorissen et al., 1992, 1995, De Stigter et al., 1998; Schmiedl et al., 2000). Besides few oxygen-limited environments in the northern Adriatic Sea, northernmost Aegean Sea and Sea of Marmara, productivity in surface waters and related fluxes of labile organic matter are the limiting environmental factors at the sea floor. Consequently, the gradient from eutrophic and mesotrophic ecosystems in the western basins and near-coastal areas to oligotrophic conditions in the eastern basins is clearly reflected in a decrease of the proportion of infaunal taxa (De Rijk et al., 2000).

In the study areas, fine-grained sediments are restricted to stations below approximately 94 m water depth on the Mallorca Shelf. The area studied on the Mallorca Shelf contains a submarine promontory, which extends perpendicular to the coastline and shelters an area situated downstream from current-induced winnowing of fines. Although surface waters around Mallorca are less productive than in the Alboran Sea or the Oran Bight (SeaWifs data; Antoine et al., 1995), the low-energy setting of the lower circalittoral off southwest Mallorca allows more particulate organic matter to accumulate on the sea floor and in fine-grained surface sediments. As predicted by the TROX model of Jorissen et al. (1995) and confirmed by own observations, the development of a mesotrophic ecosystem with infaunal niches, fostering the dominance of shallow infaunal taxa, is expected.

3.5.3 Potential anthropogenic impacts

In the Oran Bight, living and dead faunas show distinct differences. Most of the taxa observed alive prefer an infaunal microhabitat and are often associated with eutrophic and oxygen-limited conditions (Corliss, 1985; Sen Gupta & Machain-Castillo, 1993; Schmiedl et al., 2000). These taxa include *Cancris auriculus* as the most abundant taxon, *Bulimina* spp., *Brizalina* spp., *Uvigerina* spp., *Rectuvigerina phlegeri* and *Rectuvigerina bononiensis*. In samples 351, 352, 356, 360, 363 and 364 the living fauna is dominated by infaunal taxa (70 - 84%, Fig. 3.8).

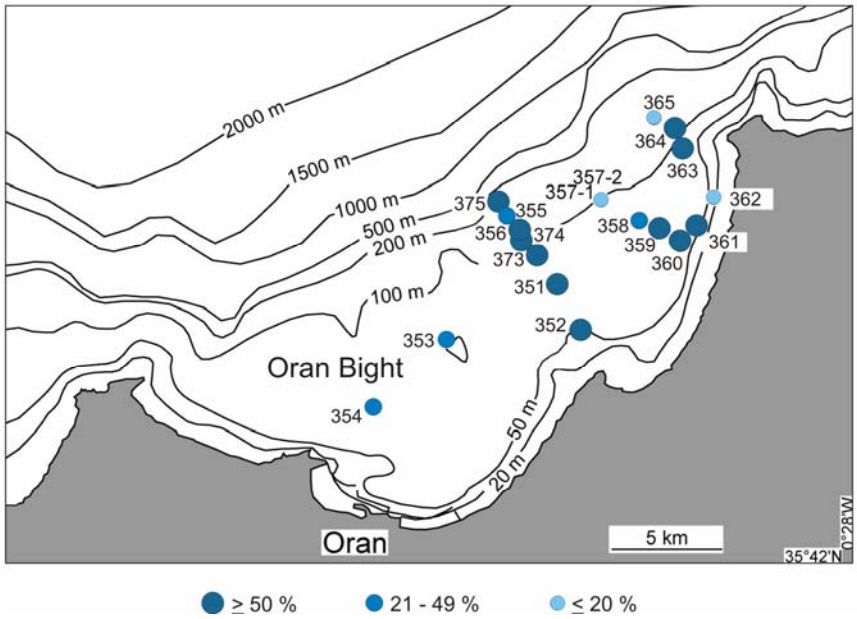

Fig. 3.8. Percentages of living infaunal taxa including *Cancris auriculus*, *Bulimina* spp., *Brizalina* spp., *Uvigerina* spp., *Rectuvigerina phlegeri* and *Rectuvigerina bononiensis* in the Oran Bight (the dark blue circles show percentages ≥ 50%, the middle blue circles 20 - 49%, and the little blue circles ≤ 20% on the total biocoenosis).

The occurrence of these high-productivity indicators in the biocoenosis, as well as noticeable contrasts to the thanatocoenses, may be attributed to the Recent anthropogenic eutrophication of this area caused by discharge of sewage from the city of Oran. Our data indicate that the potential anthropogenic impact on the benthic foraminiferal community started in recent times, and it likely was particularly strong in summer 2006. Pollution of the Oran Bight dates back at least to the 1980s and 1990s (Bakalem et al., 2009). In recent years, a total of 90 million m^3 of untreated industrial and domestic waste, polluted with nutrients, heavy metals and organic compounds, entered the Oran Bight (Taleb et al., 2007). The related eutrophication of surface waters is mirrored by regional chlorophyll a data, displaying particularly high values in the harbour region in the years 2005 and 2006 (Taleb et al., 2007). The presence of anthropogenic impacts on the benthic ecosystems of the Oran Bight is supported by data on pre-industrial benthic foraminiferal faunas from sediment cores taken in this region. These faunas contain only low portions of infaunal taxa. Some of the taxa found alive today in appreciable numbers, e.g. *Cancris auriculus*, are very rare in the sediment cores (see Fig. 4.5, Table A.7 and electronic Table A.20).

3.6 Conclusions

The shelf carbonate environments of the Oran Bight, Alboran Platform and Mallorca Shelf in the western Mediterranean Sea are inhabited by diverse benthic foraminiferal faunas with a distinct bathymetric zonation. This zonation is closely linked to the presence of coarse-grained

substrates, mainly containing rhodoliths, and is likely controlled by light penetration and the hydrodynamic energy at the benthic boundary layer.

The benthic foraminiferal biocoenoses are characterized by relatively low diversity and a wide range of standing stocks, reflecting population dynamics and variable environmental conditions in august 2006. The live assemblages of most sites in the Oran Bight are dominated by taxa typical for eutrophic conditions, such as *Cancris auriculus, Rectuvigerina* spp., bolivinids and buliminids. These species are generally rare in pre-industrial faunas from sediment cores of this region, suggesting a Recent anthropogenic impact on primary production and organic matter fluxes of coastal ecosystems in the vicinity of the city of Oran.

The diversities of the benthic foraminiferal thanatocoenoses exceed those of other Mediterranean siliciclastic shelf environments but are lower when compared to carbonate environments of the Levantine Sea. The latter difference can be mainly attributed to lower sea surface temperatures with higher seasonal contrasts in the western Mediterranean Sea.

In all three areas, a distinct faunal change occurs between approximately 80 to 94 m water depth. The upper part of the circalittoral, between approximately 40 and 80 m, is dominated by epifaunal species, such as *Asterigerinata mamilla, Neoconorbina terquemi, Cibicides* spp*., Rosalina macropora* and *Elphidium* spp*.*. These taxa are permanently or temporarily attached to carbonate fragments that are derived from rhodoliths. The lower bathymetric range of this fauna coincides with the lower distribution limit of living rhodoliths, tracing the boundary of the photic zone.

The faunas of the deeper circalittoral (below approximately 80 m water depth (Alboran Platform and Oran Bight) and 94 m water depth (Mallorca Shelf)) exhibit clear regional contrasts, depending on the energy at the benthic boundary layer and related grain-size of the substrate. High abundance of infaunal taxa, including *Cassidulina laevigata* and *Bulimina elongata,* are restricted to fine-grained sediments that have been deposited under a low-energy regime on the southwestern Mallorca Shelf. These results demonstrate that in shelf environments, the availability of food at the sea floor and the creation of infaunal niches are mainly controlled by the substrate type and do not reflect regional gradients in surface water production.

4 Holocene sea-level change in the western Mediterranean Sea: Quantitative reconstructions based on foraminiferal transfer functions

Abstract

Here, results from late glacial and Holocene relative sea-level estimates in warm-temperate shelf carbonate environments of the western Mediterranean Sea are presented. The quantitative approach is based on the evaluation of foraminiferal data with various regression methods, including Weighted Averaging (WA), Partial Least Squares (PLS), and a combination of both (WA-PLS). Further, the Modern Analog Technique (MAT) and an independent method based on Plankton/Benthos (P/B) ratios have been applied. The transfer functions were developed on the basis of Recent benthic foraminiferal assemblages in surface samples, and were then applied to sediment cores from the Alboran Platform, the Oran Bight and the Mallorca Shelf. The best predictive models were derived from the WA-PLS approach. The reconstructed relative sea-level histories in the study areas generally match the global record. Inconsistencies are attributed to the interference of the sea-level signal with redeposition processes and other environmental parameters such as substrate and food availability. Paleobathymetric estimates based on P/B ratios reflect the general sea-level development in the study areas, but exhibit a higher inaccuracy when compared to the regression methods that provides a powerful tool for sea-level reconstructions in shelf areas.

This chapter based on: Milker, Y., Schmiedl, G., Betzler, C., submitted. Holocene sea-level change in the Western Mediterranean Sea: Quantitative reconstructions based on foraminiferal transfer functions. Quarternary Science Reviews.

4.1 Introduction

Sea-level changes are mainly related to eustatic and tectonic factors and have a strong impact on sedimentation processes at continental margins and in epicontinental seas. Accurate sea-level estimates are relevant for a wide range of scientific questions, such as documentation of the ice sheet history, modeling of global circulation patterns and reconstruction of spatial and temporal variations of crustal movements. Global sea-level was approximately 120 to 130 m lower than today at the time of maximum continental glaciation during the last glacial maximum, e.g. around 22 kyr B.P. (Fairbanks, 1989). The deglaciation occurred between approximately 21 and 5 kyr B.P. and was associated with a dramatic sea-level rise, comprising two major melt-water pulses around 14 and 11 kyr B.P. and a slowing-down of sea-level rise during the Younger Dryas period and in the middle Holocene (Bard et al., 1996, 2010). In the Mediterranean Sea, sea-level changes generally follow the global development, but are also influenced by hydro-isostatic effects and neotectonic movements (Lambeck and Bard, 2000; Morhange and Pirazolli, 2005; Stocchi and Spada, 2007). In contrast to northern European shelf areas and coastlines, Holocene glacio-isostatic effects can be neglected for the Mediterranean Sea (Pirazolli, 2005). Various aspects and regional expressions of the Mediterranean sea-level change are documented by geomorphologic, geophysical and archaeological observations (Kayan, 1988; Morhange et al., 2001; Sivan et al., 2001; Goy et al., 2003; Vouvalidis et al., 2005 and Berne et al., 2007), overgrowth rates of speleothems (e.g., Alessio et al., 1994; Antonioli et al., 1999, 2001, 2002), and are simulated by numerical models (Lambeck and Bard, 2000; Lambeck et al., 2004, Pirazolli, 2005 and Stocchi and Spada, 2007).

Shelf ecosystems are particularly susceptible to relative sea-level changes, as documented by benthic foraminifera preserved in sediment successions. Shallow-water benthic foraminifera depend on various factors, such as food-availability, substrate-type, bottom current velocity, temperature, salinity, vegetation, light penetration, and the presence of endosymbionts in more tropical and oligotrophic settings (Jorissen, 1987; Langer et al., 1998; Pawlowski et al., 2001; Saraswati, 2002; Schönfeld, 2002; Saraswati et al., 2003; Mendes et al., 2004; Lee, 2006; Milker et al., 2009). In addition, the benthic foraminiferal communities in marginal marine environments, such as the Mediterranean Sea, are strongly influenced by food quality, e.g. the input, distribution and degradation of marine and terrestrial organic matter (Hyams-Kaphzan et al., 2008; Mojtahid et al. 2009). As a consequence, the specific environmental setting of the Mediterranean Sea is reflected by a distinct bathymetric zonation of the various shallow and deep-sea benthic foraminiferal taxa (Bandy and Chierici, 1966; Cita and Zocchi, 1978; Milker et al., 2009). This zonation exihibits general contrasts between the western and eastern basins of the Mediterranean Sea, reflecting a W-E decrease of surface

water productivity and related food fluxes to the sea floor (De Rijk et al., 1999, 2000). More specifically, deposit-feeding foraminifera decrease with increasing water depth and distance from the coast, responding to decreasing organic matter fluxes (De Stigter et al., 1998).

4.1.1 Quantitative sea-level reconstructions based on foraminifera

Quantitative paleobathymetric reconstructions rely on geophysical, sedimentological, geochemical and paleontological data. In this context, foraminifera proved particularly useful for accurate sea level reconstructions over a wide bathymetric range and on different time scales. Quantitative methods were developed, e.g. based on the ratio between planktonic and benthic foraminifera (P/B ratio) or the distribution patterns of certain benthic indicator taxa.

Van der Zwaan et al. (1990) developed a transfer function for paleo-water depth reconstruction using modified Plankton/Benthos (P/B) ratios from the Gulf of Mexico, Gulf of California, the west coast of the USA, and the Adriatic Sea. Van Hinsbergen et al. (2005) applied this transfer function to Lower Pliocene deposits in the Aegean Sea. De Rijk et al. (1999) compared Recent P/B ratios from the western and eastern Mediterranean and found a good correlation between the P/B ratio and water depth. They generated a transfer function that was applied by Wilson (2003) to fossil P/B ratios in the early-middle Miocene Brasso Formation of Central Trinidad. Although these studies delivered reasonable results, the confidence level of this method is limited by the interference of benthic foraminiferal abundance with oxygen and food levels at the sea floor (van Hinsbergen et al., 2005).

Alternative methods are based on the presence/ absence data of selected benthic foraminiferal taxa. Hohenegger (2005) developed transfer equations, using weighted arithmetic and geometric means of the depth ranges of benthic foraminifera and applied these equations for paleo-water depth estimates along a middle Miocene transect in the Styrian Basin in Austria. Spezzaferri and Tamburini (2007) and Fujita et al. (2010) applied these transfer equations to paleo-bathymetric reconstructions on Neogene sediments from the Eratosthenes Seamount (eastern Mediterranean Sea) and on a Pleistocene sequence off the shelf of Maraa (Tahiti), respecitively. In a similar way, Morigi et al. (2005) calculated weighted mean water depths (MWDs) based on percentages of Recent benthic foraminifera in relation to their known water depth intervals in the Adriatic Sea, and applied these MWDs to fossil foraminifera for paleo sea-level estimates of late glacial and Holocene successions.

More advanced and accurate regression methods, such as Weighted Averaging (WA), Partial Least Squares (PLS) or Weighted Averaging-Partial Least Squares (WA-PLS), were applied to marsh benthic foraminifera from the North Sea and the US-Pacific coast for sea-level reconstructions resulting in precise transfer functions (Horton et al., 1999; Horton and Murray, 2006) and Holocene sea-level estimates (Sabean, 2004; Boomer and Horton, 2006;

Horton and Edwards, 2006; Nelson et al., 2008; Hawkes et al., in press). Similar applications provided precise sea-level transfer functions for intertidal environments of the Atlantic coast of Maine and the Bay of Biscay for the latest Holocene (Gehrels, 2000; Leorri et al., 2008). Finally, the Modern Analogue Technique (MAT) approach was applied by Hayward (2004) in order to generate consistent paleobathymetric estimates for Miocene benthic foraminiferal assemblages from offshore Taranaki, New Zealand.

Here, different quantitative sea-level reconstructions for the latest glacial and Holocene based on Recent and fossil benthic foraminiferal assemblages of shelf carbonate environments from three regions with different environmental settings in the western Mediterranean Sea (Alboran Platform, Oran Bight and Mallorca Shelf) are presented. Quantitative data were generated, using regression methods (WA, WA-PLS and PLS) and MAT, as well as P/B ratios. The relative sea-level estimates have been compared with the global deglacial sea-level history, and with several regional sea-level reconstructions from the Mediterranean Sea. Major target of this study is to test the potential, applicability, and limitation of the regression methods and P/B ratios for sea-level estimates in shelf environments of the Mediterranean Sea. In contrast to previous applications of regression methods on marsh environments, the covering of a much higher water depth range is intended here.

4.2 Study area

4.2.1 Tectonic setting and sedimentation processes

The study area is located in the western Mediterranean basin (Fig. 4.1), which consists of the Alboran-, Valencia-, Provencal-, Algeria- and Tyrrhenian sub basins that were formed mainly during the Oligocene and Miocene by late orogenic extension as a result of the collision of Eurasian and African plates (Comas et al., 1999) (Fig. 2.2). Recent seismicity and tectonic movements in the western Mediterranean are concentrated in the western Alboran Sea and in the North Algerian coastal region, where earthquakes are relatively frequent (Piromallo and Morelli, 2003; Giresse et al., 2009). The Oran region is characterized by relatively high seismicity and the occurrence of earthquakes (Bouhadad, 2001), while the more offshore areas are nearly aseismic with exception of the Yusuf Fault (Domzig et al., 2006). Estimated uplift rates in the Oran Bight amount to 0.186 (+/- 0.023) mm/yr (Bouhadad, 2001). Recent uplifting and active subsidence occur coevally along the Alboran Ridge (Comas et al., 1999; Martinez-Garcia et al., submitted). Present seismic activity in the Mallorca region is low (Silva et al., 2001), and earthquakes with a magnitude higher than 4 and epicenters shallower than

30 km were not observed since 1973 (Tinti et al., 2005). No distinct vertical movements since the Miocene are documented for the southern part of the Mallorca Island (Pomar, 1991).

The specific tectonic, morphological and oceanographic settings influence the Recent sedimentation processes in the different areas. The Alboran Ridge forms a steep-flanked and rugged plateau around the small Alboran Island. The southern shelf of Mallorca, as part of the low energy and temperate Balearic carbonate platform, as well as the Algerian shelf off Oran are distally-steepened ramps (Fornos and Ahr, 2006; Betzler et al, in press). The shallow subtidal zones (uppermost 40 m water depth) of the western Mediterranean Sea are dominated by *Posidonia* meadows with bioclastic sand patches, whereas red algae and coarse-grained carbonate particles (rhodoliths, gastropods, bivalves and various other biogenic components) prevail between around 40 to 90 m water depths. Outer ramp sediments - deeper than approximately 90 m - consist of muddy sands with mixed biotic content (Betzler et al., in press). Siliciclastic components are rare in all of these cool-water carbonate environments, with exception of a quartz sand nearshore prism at the Algerian coast.

4.2.2 Oceanographic settings

The surface water mass of the western Mediterranean Sea mainly consists of inflowing Atlantic Water (AW). Subsurface water masses include the Levantine Intermediate Water, formed in the eastern part of the Mediterranean Sea, and the Western Mediterranean Deep Water (Robinson et al., 2001; Masque et al., 2003; Rixen et al., 2005) (Fig. 2.4). The AW enters the Alboran Basin as the westernmost part of the Mediterranean Sea and forms two anticyclonic gyres, the Western Alboran Gyre (WAG) and the Eastern Alboran Gyre (EAG), separated by the Alboran Ridge (Fig. 2.5). These gyres and the Almeria-Oran-Front that corresponds to the eastern edge of the EAG are zones of high primary production (Arnone, 1994; L'Helguen et al., 2002; Masque et al., 2003; Velez-Belchi et al., 2005). The Alboran Platform is directly influenced by the up to 100 km wide, and up to 200 m deep and seasonally variable WAG (Gascard and Riches, 1985; Preller, 1986; Cantos-Figuerola et al., 1991). The WAG surface water velocities measured in October 1996 ranged from 124 to 140 cm/s (Velez-Belchi et al., 2005). Geostrophic currents with velocities of ~20 cm/s at water depths of 0 to 200 m are postulated for the shelf south-west of Mallorca by model results of Werner et al. (1993). The Oran Bight is influenced by the variable Algerian Current flowing along the Algerian coast (Fig. 2.5). This current supplies the coastal regions with elevated nutrient loads and is characterized by higher chlorophyll a values when compared to the more oligotrophic Algerian Basin (Millot et al., 1990; Arnone, 1994). As a consequence of this oceanographic

setting, the Alboran Basin and the Oran Bight have higher annual primary production rates when compared to the more oligotrophic Balearic region (Antoine et al., 1995).

4.3 Materials and methods

4.3.1 Samples, sample preparation and statistical methods

Three sediment-cores were recovered with a vibro-corer during Meteor cruise 69/1 in August 2006. The cores were taken on the Alboran Platform (core 342-1) at 64 m water, in the Oran Bight (core 367-1) at 63 m water depth, and on the Mallorca Shelf (core 401-1) at 74 m water depth (Table 4.1, Fig. 4.1).

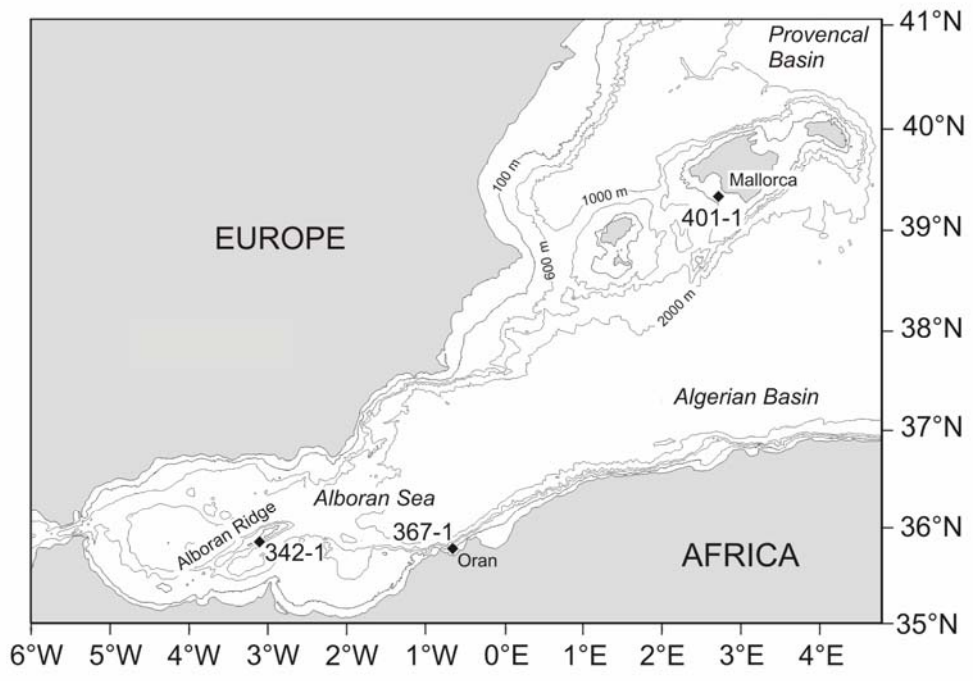

Fig. 4.1. Map of the western Mediterranean Sea showing the locations of cores 342-1 from the Alboran Platform, 367-1 from the Oran Bight, and 401-1 from the Mallorca Shelf (see also Table 4.1).

Core 342-1 consists of mostly bioturbated and cross-bedded carbonate-volcanoclastic mixed sediment in its lower part, and it contains calcarenites and calcirudites with bioclasts, bryozoa and rhodoliths in the upper part. In the lower part of core 367-1, the contact between the marlstone and sandstone basement and the overlying postglacial sediments were drilled Sediments consist of calcirudite and calcarenites with rhodoliths, lithoclasts encrusted by coralline crusts, bivalves and gastropods. The lower part of core 401-1 consists of calcirudite with warty, small and loose branching rhodoliths. The middle part contains an interval rich in the gastropod *Turritella communis* embedded in a fine- to middle-grained calcarenite, and the upper part is composed of fine-grained calcarenites with debris and shells of bivalves,

pteropods and gastropods. For detailed characterization of the core sediments see Betzler et al. (in press).

For the investigation of the foraminiferal content, the cores were sampled at 5 cm spacing, and a total of 63, 58 and 94 samples for cores 342-1, 367-1 and 401-1 were analyzed, respectively (electronic Tables A.19-A.21). The samples were wet-sieved with a 63 µm-sieve and the fraction >63 µm was dried at 40°C. The analysis of the fauna from the >125 µm faction was carried out on representative splits containing approximately 300 benthic foraminiferal individuals. Most of the samples from cores 342-1 and 367-1 contain low to moderate contents of relocated benthic foraminifera (broken tests, tests fragments, and tests with yellowish-brown coloration) that were counted separately (electronic Tables A.19-A.21). Due to the high rate of potential relocated foraminifera in the lower part of core 342-1 from the Alboran Platform, sample spacing was increased to 20 cm. The identification of the benthic foraminifera was mainly based on the studies of Cimerman and Langer (1991), Sgarrella and Moncharmont Zei (1993), Jones (1994) and Rasmussen (2005) (see chapter 6).

The Plankton/Benthos (P/B) ratios were calculated using the formula P/B(%) = PF*100/(PF+BF), where PF is the number of planktonic foraminifera and BF the number of benthic foraminifera. Q-Mode Principal Component Analysis (PCA) with Varimax rotation was carried out with the software package SYSTAT (version 12) in order to extract the dominant benthic foraminiferal assemblages (principle components; PCs) in the cores (compare with chapter 3.3). Only foraminiferal taxa with percentages $\geq$1% in at least three samples were considered. Factor loadings with eigenvalues >1 (Kaiser criterion) were selected, and loadings $\geq$0.5 for each axis were defined as significant following Backhaus et al. (2006) and the suggestions of Malmgren and Haq (1982). Detrended canonical correspondence analysis (DCCA) was carried out with CANOCO version 4.5 (Ter Braak and Smilauer, 2002; Leps and Smilauer, 2005). Gradient lengths in the surface data set were calculated in order to determine whether the species show a linear or unimodal relationship to water depth (Birks, 1998). Species-environment relationships in core 401-1 were explored with Redundancy Analysis (RDA), where the axes are linear combinations of the environmental variables (Leyer and Wesche, 2007) (Table A.14).

4.3.2 Age Model

The chronostratigraphic frameworks of the cores are based on six ^{14}C AMS dates for core 401-1, two for core 367-1 and three for core 342-1 on corallines, mollusc-shells and serpulids isolated from the cores (Fig. 4.2; Betzler et al., in press). The dating was performed at the Leibniz-Laboratory for Radiometric Dating and Stable Isotope Research, Kiel (Germany).

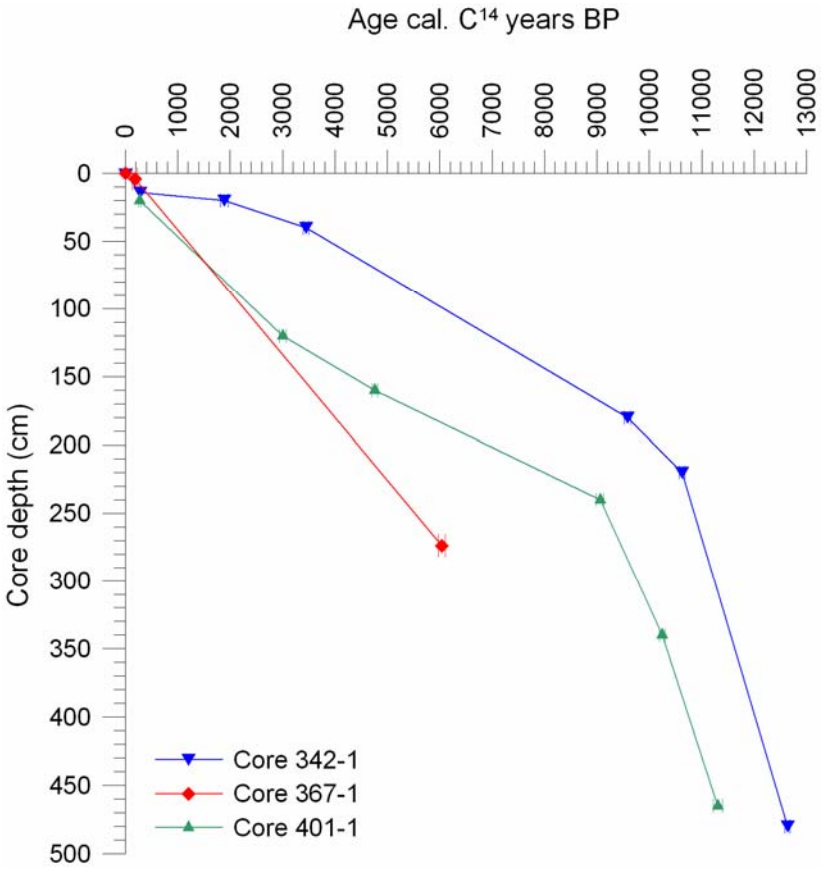

Fig. 4.2. Age-depth plots for cores 342-1 (Alboran Platform), 367-1 (Oran Bight) and 401-1 (Mallorca Shelf). The ages were calibrated with the CALIB (version 5.1.0) software package (Stuiver and Reimer, 1993). A reservoir effect of 400 years was taken into calculation (Hughen et al. 2004). Ages are given with error bars (see also Table 4.1).

Table 4.1. Location, water depths and radiocarbon dates (see also Betzler et al., in press) for cores 342-1 (Alboran Platform), 367-1 (Oran Bight) and 404-1 (Mallorca Shelf). The conventional C^{14}ages were calibrated with CALIB 5.1.0 (Stuiver and Reimer, 1993).

core	Location	Latitude/ Longitude	depth (m)	Sample	Lab code	conventional C^{14}age	calibrated C^{14}age
342-1	Alboran Platform	35°56.400´N/ 3°00.213´W	64	342-1-1, 14cm	KIA 39057	650 +/-25 BP	289 +/-24 BP
				342-1-1, 20cm	KIA 37014	2275 +/-25 BP	1887 +/-78 BP
				342-1-1, 40cm	KIA 39056	3565 +/-40 BP	3449 +/-57 BP
				342-1-2, 80cm	KIA 39057	8935 +/-50 BP	9586 +/- 63 BP
				342-1-3, 20cm	KIA 34224	9780 +/-45 BP	10624 +/-55 BP
				342-1-5, 80cm	KIA 34225	10875 +/-55 BP	12364 +/- 46 BP
367-1	Oran Bight	35°48.000´N/ 0°33.700´W	63	367-1-1, 4-6cm	KIA39043	535 +/-25 BP	185 +/-50 BP
				367-1-3, 74cm	KIA34854	5640 +/-35 BP	6041 +/-61 BP
401-1	Mallorca Shelf	39°17.101´N/ 2°48.305´E	74	401-1-1, 20cm	KIA39048	620 +/-25 BP	272 +/-22 BP
				401-1-2, 20cm	KIA 37017	3200 +/-35 BP	3004 +/-63 BP
				401-1-2, 60cm	KIA 34227	4545 +/-35 BP	4763 +/-53 BP
				401-1-3, 40cm	KIA 37018	8450 +/-55 BP	9058 +/-74 BP
				401-1-4, 40cm	KIA 34228	9410 +/-50 BP	10244+/-56 BP
				401-1-5, 65cm	KIA 34229	10335 +/-55 BP	11304 +/-87 BP

The conventional radiocarbon dates were calibrated with the CALIB (version 5.1.0) software package (Stuiver and Reimer, 1993), considering a reservoir effect of 400 years (Hughen et al., 2004) (Fig. 4.2, Table 4.1). In the upper parts of the cores, sedimentation rates range between 12 cm/kyrs (core 342-1) and 46 cm/kyrs (core 367-1). In the lower parts of cores 342-1 and 401-1, sedimentation rates are 120 cm/kyrs and 84 - 118 cm/kyrs, respectively. Accordingly, temporal resolution of this study ranges between 42 and 417 years.

4.3.3 Methods for quantitative sea-level reconstructions

4.3.3.1 Transfer functions based on Plankton/ Benthos ratios

A widely applied method for paleo-water depth reconstructions is adopted from an organic matter flux equation that was transformed into an exponential transfer function for paleo-water depth estimates: $D = \exp^{(3.58718+(0.03534*\%P_{mod}))}$, where D is the water depth and P_{mod} is the modified P/B ratio (Van der Zwaan et al., 1990). P_{mod} was calculated excluding infaunal living benthic foraminifera (stress markers), such as the genera *Bulimina, Bolivina, Uvigerina, Globobulimina* and *Fursenkoina* that do not directly depend on the accumulation of fresh organic matter following van der Zwaan et al. (1990). We have created new transfer functions based on both counted and modified P/B ratios from surface samples. Surface samples 326-1 and 334-1 from the Alboran Platform and 391-1 from the Mallorca Shelf revealed very low P/B ratios compared to the given water depth and were excluded from the model. The different transfer functions were applied on the sediment core samples.

4.3.3.2 Weighted Averaging, Partial Least Squares, Weighted Averaging - Partial Least Squares and Modern Analog Technique

The rationale behind the Weighted Averaging (WA) regression method is that a species commonly shows a unimodal distribution along an environmental gradient (Ter Braak et al., 1993). Applying this concept, mean values are calculated by weighted averaging for each species along a known environmental gradient in the training data set (surface samples). This step is followed by the estimation of the environmental parameter in the fossil data set (core samples) based on the calculated weighted averages (Birks et al., 1990; Ter Braak and Juggins, 1993). Partial Least Squares (PLS) is a method that can be used both for univariate and multivariate regression (Garthwaite, 1994). New components from independent predictors and dependent environmental variable(s) are created by maximizing the covariance between these variables (Birks, 1998; Rosipal and Krämer, 2006). In the combined approach of WA and PLS (WA-PLS), the first component is a weighted average for the environmental variable and is similar to the WA method, the further components are weighted averages for the

residuals of the environmental variable (Ter Braak and Juggins, 1993). The advantage of this method is that it can improve predictions because it considers the influence of additional environmental variables (Horton and Edwards, 2006). The Modern Analog Technique (MAT) searches in a training data-set for the nearest modern analogues for a fossil assemblage by calculating dissimilarity coefficients (Birks, 1998). The given environmental parameters in the best modern analogues are then applied to the environmental estimates in a fossil sample by (weighted) averaging of these parameters (Malmgren and Nordlund 1997).

Prior to the development of transfer functions with the above described methods, both training and fossil data sets were reduced to benthic foraminifera with abundances of $\geq$1% in more than one sample. A total of 46 surface samples with 87 species were used for the calculations. Surface sample 362-1 from the Oran Bight was excluded from the training data sets due to its low number of benthic foraminifera. Species counts were transformed into percentages for MAT, and were square-root transformed for WA, WA-PLS and PLS. All calculations were carried out with the C^2-Software (Juggins, 2003). Cross-validations for WA, WA-PLS and PLS, and bootstrapping for MAT were selected to calculate the square root error of prediction (RMSEP) in the training data-sets (Overpeck et al., 1985; Ter Braak and Juggins, 1993). Three deeper sites (393-1 from 235 m, 391-1 from 163 m and 333-1 from 161 m) were excluded step by step, because the estimated water depths recalculated in the full training data set revealed an underestimation of 12 - 36% for these samples. The number of components for WA-PLS and PLS was selected according to the lowest RMSEP values if the reduction in prediction error exceeds 5% for this component compared to the next lower component (Ter Braak and Juggins, 1993). For WA, an inverse approach was chosen because of better performance (Birks, 1998).

4.4 Results

4.4.1 Recent and Holocene Plankton/ Benthos ratios

The Recent P/B ratios in the Alboran Platform surface samples range from 63% at 163 m to 26% at 38 m water depth (Fig. 4.3). In the Oran Bight samples, P/B ratios range from 58% at 85 m to 9% at 20 m water depth (Fig. 4.3). On the Mallorca Shelf, the P/B ratios range from 44% at 235 m to 8% at 40 m water depth (Fig. 4.3). On the Mallorca Shelf, P/B ratios continuously increase with increasing water depth, whereas on the Alboran Platform and in the Oran Bight no such trend is observed (Fig. 4.3).

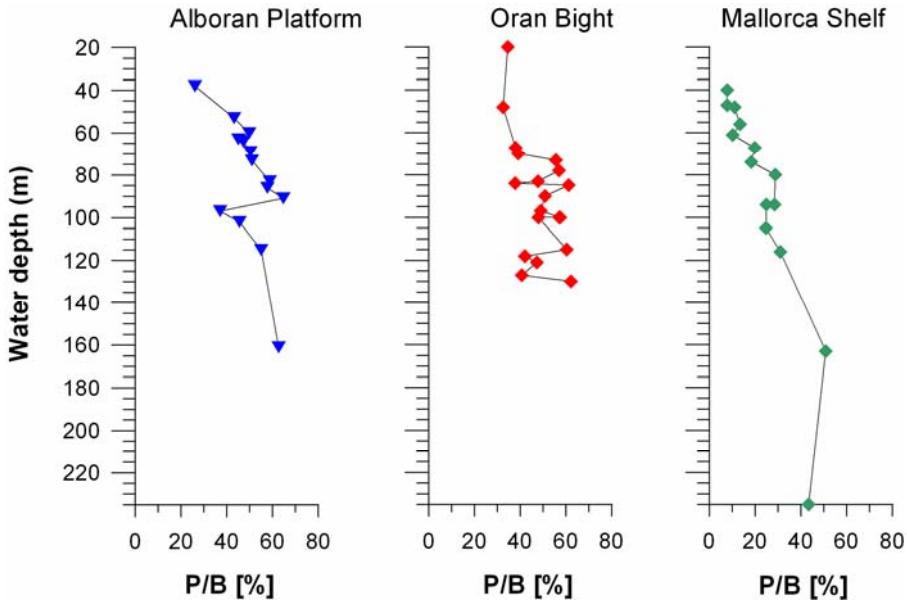

Fig. 4.3. Plankton/ Benthos ratios (P/B ratios) calculated in the surface samples from the Alboran Platform, the Oran Bight and the shelf Mallorca Shelf versus water depth.

In the late glacial interval of the Alboran Platform core, P/B ratios range from 1% to 3%. From the early Holocene to present times, P/B ratios increase continuously up to 50% (Fig. 4.4). The P/B ratios in the Oran Bight core show a generally increasing trend from 13% to a maximum of 46% during the middle and late Holocene (Fig. 4.4). P/B ratios in the Mallorca Shelf core range from approximately 5% to 8% in the earliest Holocene, followed by a strong increase to maximum values of ~27% from the early to middle Holocene, and a slight decrease to 15% in the late Holocene (Fig. 4.4).

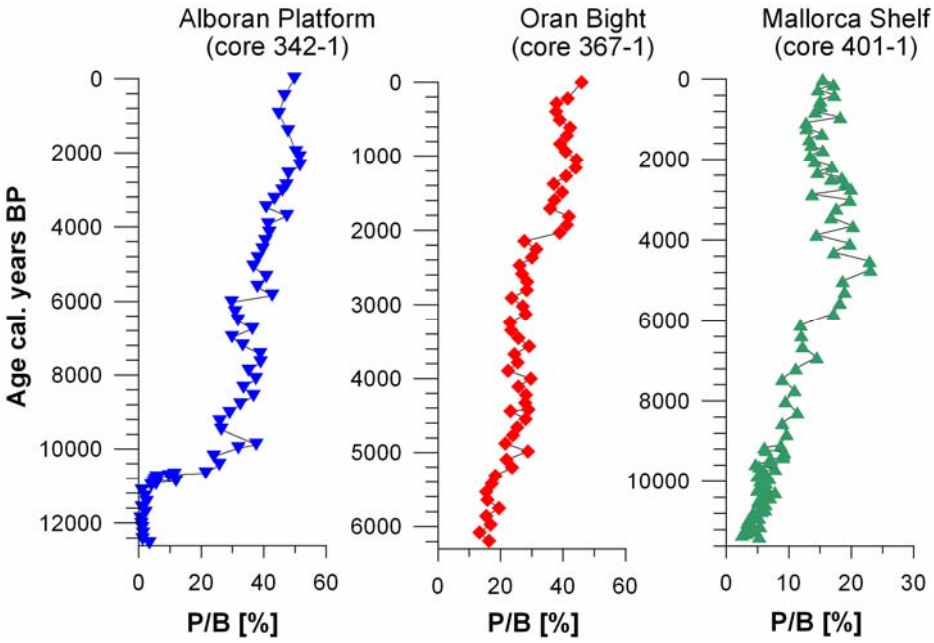

Fig. 4.4. Plankton/ Benthos ratios (P/B ratios) calculated in the cores from the Alboran Platform, the Oran Bight and the shelf Mallorca Shelf versus age.

4.4.2 Holocene benthic foraminiferal assemblages

The fossil benthic foraminiferal assemblages (principle components, PC), calculated with Principle Component Analysis (PCA), in all cores correspond to Recent assemblages in the various regions (compare Fig. 3.5).

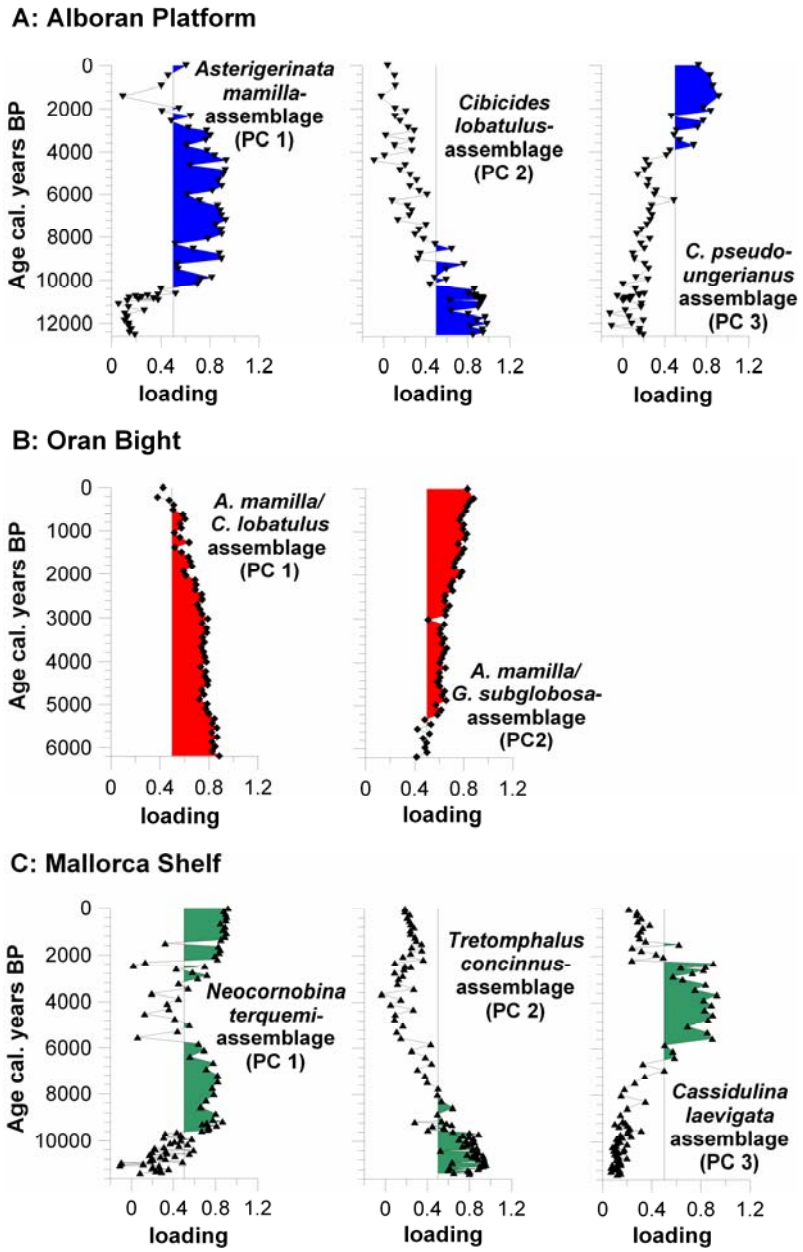

Fig. 4.5. Q-Mode Principal Component Analyses (PCAs) for the Alboran Platform core (A), the Oran Bight core (B) and the Mallorca Shelf core (C) versus age (see also Table A.7). Loadings ≥0.5 (shaded areas) are defined as significant following Backhaus et al. (2006) and the suggestions of Malmgren and Haq (1982).

The 3-PC model for the Alboran Platform core explains 85.5% of the total variance (Fig. 4.5A, Table A.7). An assemblage dominated by *Cibicides lobatulus* (PC2) with *Elphidium* sp.1, *Elphidium complanatum* forma *tyrrhenianum* as well as *Elphidium aculeatum* as dominant taxa

occurs in the late glacial and earliest Holocene period (Table A.7). This assemblage is replaced by an *Asterigerinata mamilla*-assemblage (PC1, Fig. 4.5A), including *Elphidium complanatum, Spirillina vivipara* and *Brizalina difformis* as important taxa, during the early and middle Holocene (Table A.7). A *Cibicides pseudoungerianus*-assemblage (PC3, Fig. 4.5A), with *Globocassidulina subglobosa*, *Cassidulina crassa* and *Cibicides lobatulus* as associated species, dominates the interval from late Holocene to present times (Table A.7). The percentages of observed relocated tests in this core range from approximately 84 % in the lower part to 15-30% in the upper part.

The 2-PC model for the Oran Bight core explains 95.8% of the total variance (Table A.7). The most dominant taxon throughout the core is *Asterigerinata mamilla* with percentages of 14% to 27%. This species is dominant together with *Cibicides lobatulus,* and *Rosalina macropora* and *Quinqueloculina stelligera* as important taxa in the middle Holocene (PC1, Fig. 4.5B, Table A.7). An assemblage consisting of *Asterigerinata mamilla* (PC2, Fig. 4.5B) with *Discorbinella bertheloti* and *Elphidium complanatum* as further taxa show higher loadings in the late Holocene (Table A.7). In the core, the proportion of relocated tests ranges between 27% and 52%, with lowest values in the middle core part.

The 3-PC model for core 401-1 from the Mallorca Shelf explains 85.2% of the total variance (Table A.7). A *Tretomphalus concinnus*-assemblage (PC2, Fig 4.5C), that includes *Sigmoilinita costata*, *Spirorbina* sp.1 and *Quinqueloculina stelligera* as associated taxa, dominates in the early Holocene (Table A.7). The *Neoconorbina terquemi*-assemblage (PC1), with *Tretomphalus* sp.1 as associated taxon, occurs during the Holocene, but is replaced by the *Cassidulina laevigata*-assemblage (PC3), with *Tretomphalus* sp.1, *Reussella spinulosa* and *Spirillina vivipara* as further dominant species in the interval from ~6000 to ~2400 cal. years BP (Fig. 4.5C, Table A.7).

4.4.3 Results of the quantitative sea-level reconstructions

4.4.3.1 Transfer functions based on Plankton/ Benthos ratios

Transfer functions (exponential functions) were generated both from counted and modified Plankton/Benthos ratios (P/B; P/B_{mod}) for each area separately. For the Alboran Platform surface samples, the transfer function based on counted P/B ratios (Fig. 4.6A) show a better correlation (R^2=0.60) between the estimated water depths (EWDs) and the observed water depths (OWDs) in the surface samples when compared to P/B_{mod} ratios, lacking any correlation (R^2=0.08) (Fig. 4.6B).

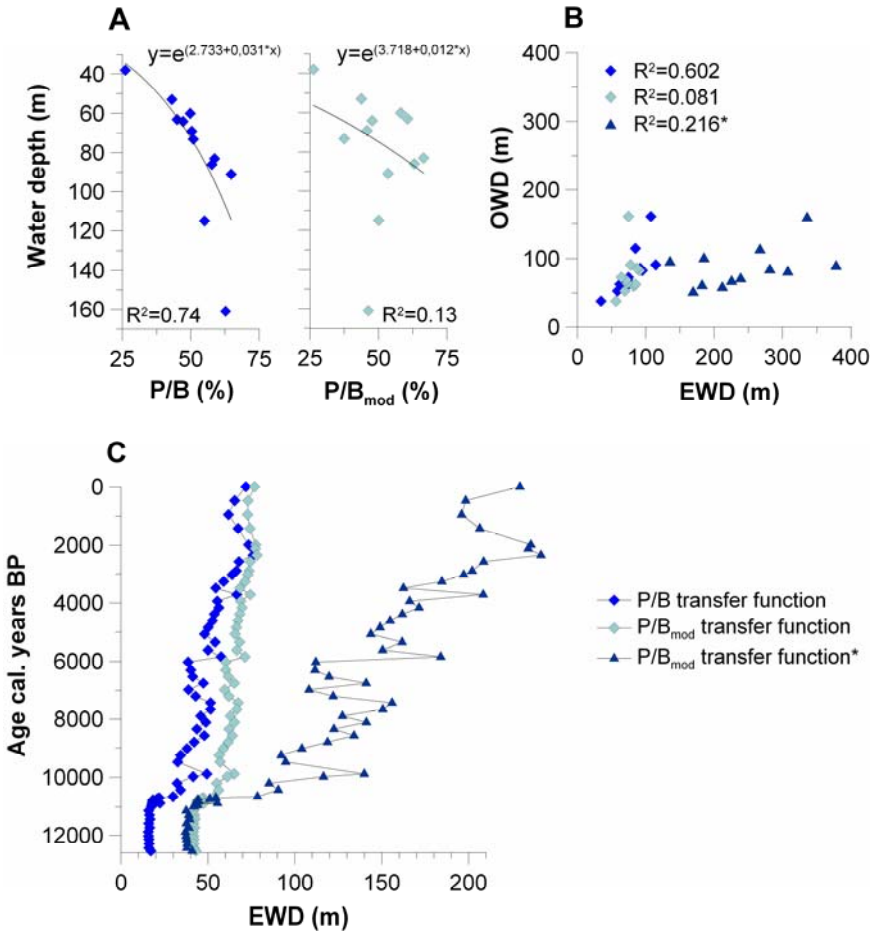

Fig. 4.6. (A) Transfer functions based on counted P/B ratios (blue squares) and modified P/B ratios (light blue squares) in surface sediments from the Alboran Platform. (B) Observed water depths (OWDs) in the surface samples from the Alboran Platform versus estimated water depths (EWDs) recalculated with the transfer functions given in (A) and the transfer function of van der Zwaan et al. (1990) (*; dark blue triangles). (C) EWDs versus age in the Alboran Platform core, calculated with the P/B and P/B_{mod} transfer functions.

The EWDs for the deeper stations are underestimated, probably due to the low sample numbers in this water depth range (Fig. 4.6B). The EWDs calculated with the transfer function of van der Zwaan et al. (1990) are generally too high when compared to the OWDs (Fig. 4.6B).

In the Alboran core, the $EWD_{P/B}$ shows a continuous increase from ~8 m in the late glacial to ~70 m at present times (Fig. 4.6C, Table A.11). The $EWD_{P/Bmod}$ has higher values throughout the core when compared to the $EWD_{P/B}$. The EWD calculated with the transfer function of van der Zwaan et al. (1990) display significantly higher values during the Holocene (Fig. 4.6C, Table A.11).

In the Oran Bight, the P/B and P/B_{mod} transfer functions based on the Oran Bight surface samples (Fig. 4.7A) and that of van der Zwaan et al. (1990) display only weak correlations between EWDs and OWDs (Fig. 4.7B). The transfer function based on counted P/B ratios provides a slightly better fit than that generated from modified P/B ratios (Fig. 4.7B).

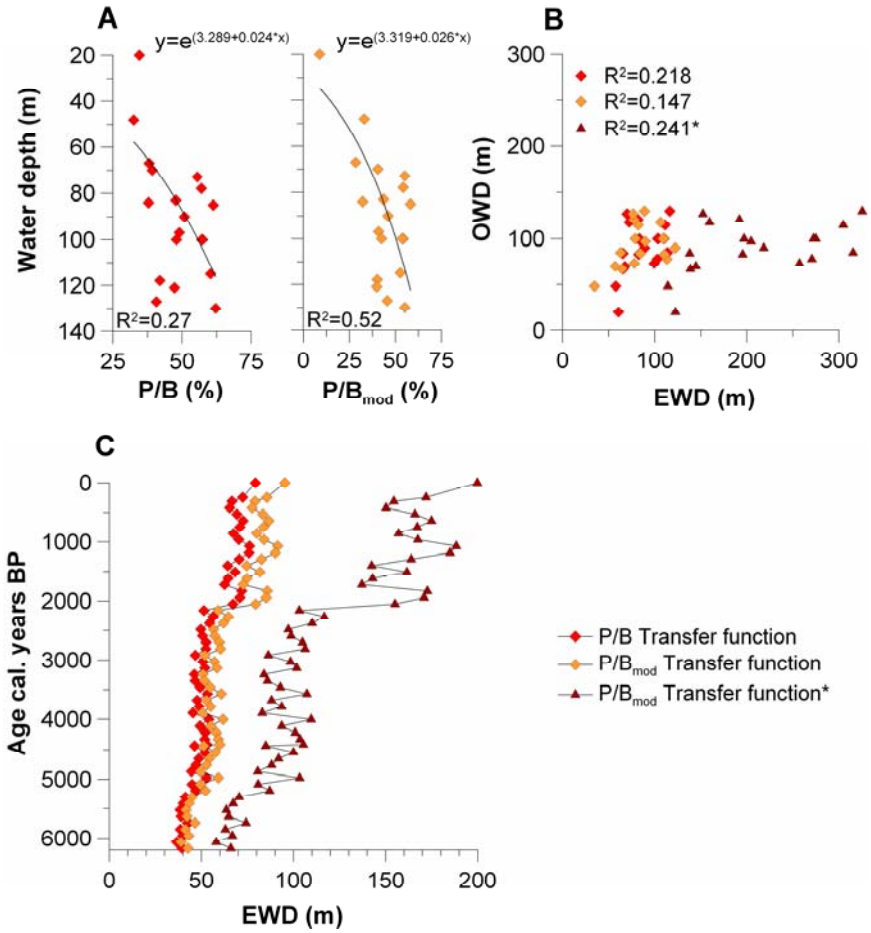

Fig. 4.7. (A) Transfer functions based on counted P/B ratios (red squares) and modified P/B ratios (light red squares) in surface sediments from the Oran Bight. (B) Observed water depths (OWDs) in the surface samples from the Alboran Platform versus estimated water depths (EWDs) recalculated with the transfer functions given in (A) and the transfer function of van der Zwaan et al. (1990) (*; dark red triangles). (C) EWDs versus age in the Oran Bight core, calculated with the P/B and P/B_{mod} transfer functions.

In the Oran Bight core, the $EWD_{P/B}$ and $EWD_{P/Bmod,}$ continuously increase from 39 - 43 m in the middle Holocene to 79 - 95 m at present times (Fig. 4.7C, Table A.12). The EWDs calculated with the transfer function of van der Zwaan et al. (1990) reveal significantly higher values (Fig. 4.7C, Table A.12).

On the Mallorca Shelf, the calculated EWDs in the surface data set show significant correlations to the OWDs for the transfer functions based on counted and modified P/B ratios (Fig. 4.8A) and that from van der Zwaan et al. (1999) (Fig 4.8B). The estimates calculated with the transfer function based on modified P/B ratios display the best fit (Fig. 4.8B).

In the Mallorca shelf core, the EWD continuously increases from approximately 40 m during the earliest Holocene to 67 m in the late Holocene (Fig. 4.8C, Table A.13). Higher than present EWDs, with maximum values around 80 to 90 m, were calculated with all P/B transfer

functions for the interval between approximately 6000 and 2000 cal. years BP (Fig. 4.8C, Table A.13).

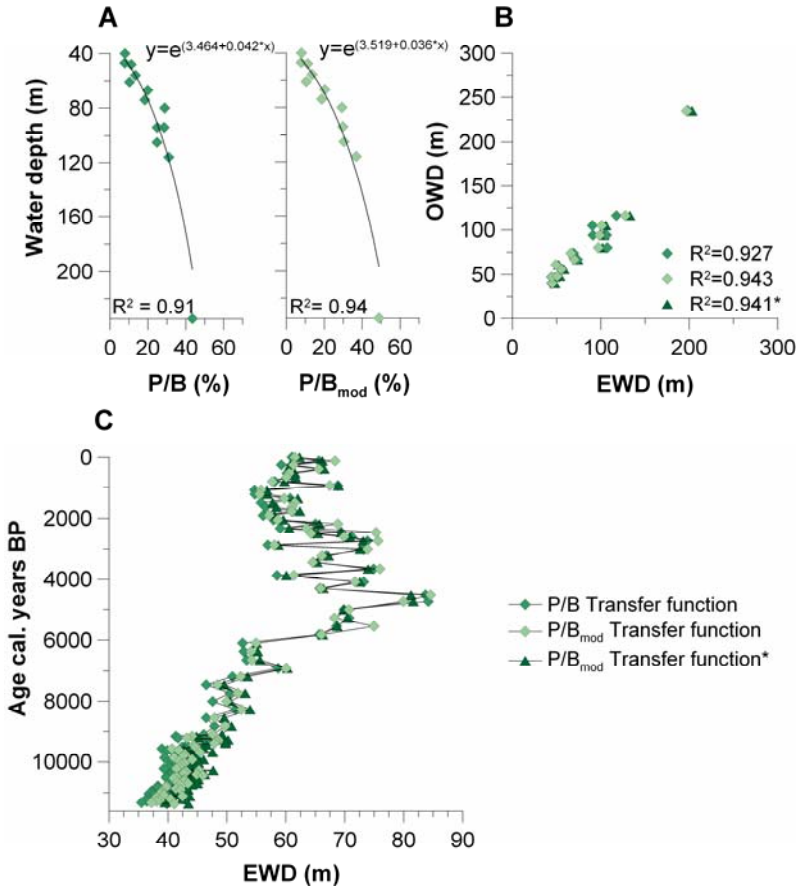

Fig. 4.8. (A) Transfer functions based on counted P/B ratios (green squares) and modified P/B ratios (light green squares) in surface sediments from the Mallorca Shelf. (B) Observed water depths (OWDs) in the surface samples from the Alboran Platform versus estimated water depths (EWDs) recalculated with the transfer functions given in (A) and the transfer function of van der Zwaan et al. (1990) (*; dark green triangles). (C) EWDs versus age in the Mallorca Shelf core, calculated with the P/B and P/B_{mod} transfer functions.

4.4.3.2 Transfer functions based on WA, PLS, WA-PLS and MAT

Detrended canonical correspondence analysis shows a gradient length of 1.71 standard deviation units (axis 1) for the surface samples in relation to water depth (Table 4.2). The unimodal-based methods WA and WA-PLS works theoretically better for a higher gradient length of the environmental parameter (>3 standard deviations (SD)), whereas for shorter gradient lengths (<2 SD) linear-based methods such as PLS could be better work (Birks, 1998). Despite the short gradient length, all regression methods have been applied.

In the Alboran Platform training (surface) data set, model fits from the estimated versus observed water depths range from R^2=0.88 for WA-PLS to R^2=0.67 for MAT (Fig. 4.9A, Table

A.8). The lowest root mean squared error of prediction (RMSEP) is given for WA-PLS, followed by WA and PLS, and the highest RMSEP is given for MAT (Table A.8).

Table 4.2. Results of Detrended Canonical Correspondence Analysis (DCCA) for the training data-set. The short gradient lengths are given in standard deviation units (SD) and indicate a linear species distribution in relation to the observed water depths.

Axis	Eigenvalue	Length of gradient
1	0.090	1.707
2	0.154	1.506
3	0.054	1.072
4	0.029	0.987

For the Alboran Platform core, the calculated paleo-water depths are lower for WA-PLS and WA and higher for PLS and MAT during the late glacial period that is characterized by high percentages of relocated tests (Fig. 4.9A). More similar paleo-water depths have been calculated with all methods for the Holocene interval (Fig. 4.9A). For the late glacial to present times, WA and WA-PLS revealed a relative sea-level rise of approximately 45-49 m, whereas MAT revealed a sea-level rise of only ~14 m (Table A.11).

In the training (surface) data set of the Oran Bight, the best model fit for the estimated versus observed water depths is shown for WA-PLS with R^2=0.91, followed by PLS and WA. MAT reveals the lowest fit with R^2=0.70 (Fig. 4.9B, Table A.9). The RMSEP ranges between 10.76 for WA-PLS and 16.45 for MAT (Table A.9).

For the Oran Bight core, the paleo-water depths calculated with WA-PLS and PLS provide similar results, while WA generates higher water depths throughout the core and for MAT no trends can be observed (Fig. 4.9B). The estimated relative sea-level rise from the middle to late Holocene ranges from ~38 m for WA to ~13 m for PLS (Table A.12).

In the training (surface) data set of the Mallorca Shelf, the best model fit for the estimated versus observed water depths resulted from WA-PLS with R^2=0.93, followed by PLS and WA (Fig. 4.9C, Table A.10). MAT reveals the lowest model fit with R^2=0.62. The lowest RMSEP of 9.9 resulted from WA-PLS (Table A.10).

For the Mallorca shelf core, earliest Holocene paleo-water depths are lowest in the WA-PLS model, slightly higher in WA and PLS models, and highest in the MAT model (Fig. 4.9C, Table A.13). All methods reveal similar water depth estimates for the late Holocene. For the middle Holocene, water depths higher than present water depths were calculated with all methods. The estimated relative sea-level rise from the earliest to the late Holocene ranges from ~43 m (WA-PLS) to ~12 m (MAT) (Table A.13).

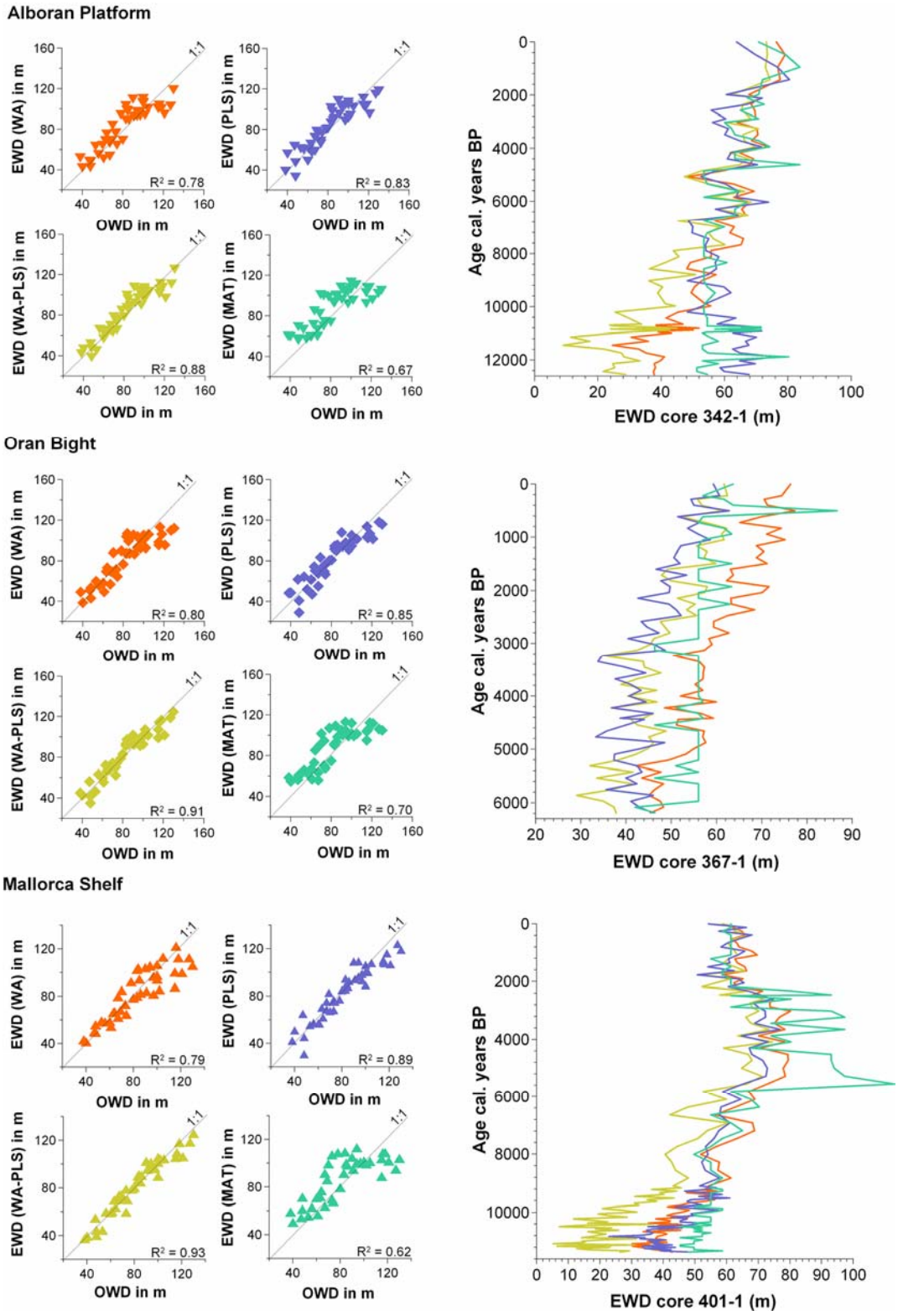

Fig. 4.9. Results of the different transfer functions, developed from Weighted Averaging (WA), Partial Least Squares (PLS), WA-PLS, and the Modern Analog Technique (MAT). On the left side, observed water depths (OWDs) versus estimated water depths (EWDs) in the training data sets (surface sediments) from the Alboran Platform (A), the Oran Bight (B) and the Mallorca Shelf (C) are plotted. On the right side, EWDs versus age in cores 342-1 from the Alboran Platform, 367-1 from the Oran Bight and 401-1 from the Mallorca Shelf, calculated with the different transfer functions, are shown (see also Tables A.8-A.10 and A.11-A.13).

4.5 Discussion

4.5.1 Comparison and significance of the different transfer functions for quantitative sea-level reconstruction

The results illustrate the advantages and disadvantages of the different methods applied. Among the developed transfer functions, WA-PLS resulted in the best prediction potential (Fig. 4.9A-C). This method revealed lowest root mean squared error of prediction (RMSEP) and the best correlations (cross-validated R^2_{jack} and R^2) for all study areas (Tables A.8-A.10). One general problem is the edge effect for models based on weighted averaging (WA, WA-PLS) resulting in underestimation of the high end and overestimation of the low end of an environmental gradient (Birks, 1998). Accordingly, the estimated water depths in the training data sets for the deeper stations are underestimated for WA and WA-PLS, but also for PLS and MAT, when compared to the observed water depths (Fig. 4.9A-C). A further problem is that WA ignores influencing environmental parameters other than the parameter of interest (Birks, 1998). This problem is solved in WA-PLS that is able to "identify" the influence of additional environmental parameters (Birks, 1998; Horton & Edwards, 2006). In this method, regression coefficients can be optimized, assuming that the influencing parameters are the same in the fossil and training data sets (Ter Braak and Juggins, 1993; Birks, 1998; Horton and Edwards, 2006). Based on this advantage, Ter Braak and Juggins (1993) and Ter Braak et al. (1993) preferred WA-PLS in their applications when compared to WA and PLS. In addition, WA-PLS performs well under no-analogue conditions, if the dominant species in a fossil data set also occur in the training data set, allowing estimation of their optima (Birks, 1998). The distribution of Recent shelf benthic foraminifera in the study areas is not only controlled by water depth, but is also influenced by other factors, such as substrate and food availability (see also 3.5). Similar effects can be expected for late glacial and Holocene faunas. These observations and methodological advantages explain the best performance of WA-PLS in our application.

The advantage of MAT is that it can handle with non-linear relationships between species and environmental parameters. However, extremes in the environmental parameters are only poorly performed, since this method is based on an interpolative technique (Kucera et al., 2005). The poor statistical performance of MAT, especially in the training data sets from the Alboran Platform and Oran Bight likely results from the no-analogue problem (Tables A.8 and A.9). This is because samples from shallower sites are under-represented in the training data set. Accordingly, the distance to the closest modern analogue increases in the down-core samples in all areas.

The applied P/B transfer functions displayed variable performance in the different regions, suggesting that the applicability of this method for accurate quantitative sea-level reconstructions is limited by local environmental conditions, such as exposure to the open ocean (shelf morphology), surface currents and trophic conditions. The P/B transfer functions that are based on the counted P/B ratios in the training data set from the Alboran Platform worked better when compared to that of van der Zwaan et al. (1990), while on the Mallorca shelf all transfer functions provide similar results. P/B transfer functions should therefore be validated by local training data sets.

4.5.2 Global versus regional sea-level evolution of the western Mediterranean Sea during the late glacial and Holocene

On the Alboran Platform and the Mallorca Shelf, the estimated relative sea-level rises calculated with WA-PLS ($ERSL_{WA\text{-}PLS}$), generally match the global sea-level development of the past 12,000 years (Bard et al., 1996; Fairbanks et al., 1989) but also resemble regional sea-level reconstructions for the Mediterranean Sea (Allesio et al., 1994; Lambeck and Bard, 2000; Antonioli et al., 2001; Sivan et al., 2001) (Fig. 4.10A). Our sea-level reconstructions exhibit a higher variability when compared to the available sea-level curves (Fig. 4.10A). This may be explained by the confidence levels of our transfer function, resulting in uncertainties of approximately +/-10 m within a total sea-level rise of ~45 and ~50 m for the Alboran Platform and the southwest shelf off Mallorca, respectively. These uncertainties prevent the detection of potential neotectonic movements on the Alboran Platform (Comas et al., 1999; Silva et al., 2001; Martinez-Garcia et al., submitted). In addition, the higher variability in the calculated $ERSL_{WA\text{-}PLS}$ values for the late glacial intervals and early Holocene on the Alboran Platform and on the Mallorca shelf are likely biased by redeposition processes resulting in relocation of foraminiferal tests. According to the reconstructions of Lambeck and Bard (2000) for the Mediterranean region, sea-level would have risen from approximately 5 to 25 m during the latest glacial and earliest Holocene period on the Alboran Platform and from approximately 14 to 30 m during the earliest Holocene period on the Mallorca Shelf, respectively. In both areas, the modern storm wave base is located at ~40 m (Betzler et al., in press), suggesting a strong influence of wave activity on sediment redeposition during this time interval. This agrees well with the high sedimentation rates in both areas during this time interval (Fig. 4.2).

In the Oran Bight, contrasting results are achieved with application of the different transfer functions. $ERSL_{WA\text{-}PLS}$ and $ERSL_{P/B}$ records revealed a sea-level rise of approximately 30 m and 36 m, respectively, during the past 6000 cal. years BP (Figs. 4.10A, 4.10B). These estimates are significantly higher when compared to the published global and regional sea-

level curves but they also exceed our estimates for the Alboran Platform and Mallorca Shelf (Figs. 4.10A, 4.10B).

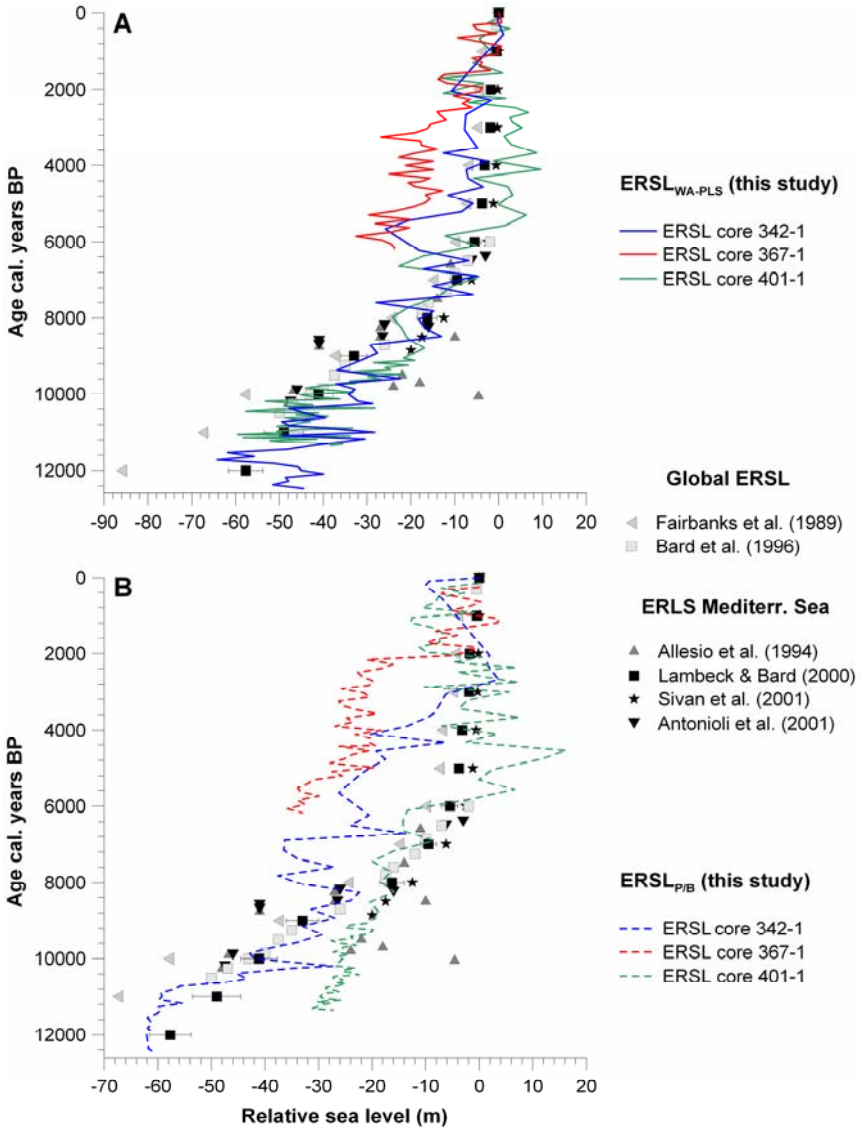

Fig. 4.10. Comparison of the estimated relative sea-level (ERSL), calculated with WA-PLS (A) and P/B ratio (B) transfer functions, for the Alboran Platform (core 342-1), the Oran Bight (core 367-1) and the Mallorca Shelf (core 401-1) with global and Mediterranean sea-level reconstructions for the latest glacial period and the Holocene.

Several reasons can account for this overestimation, including neotectonic processes along the Algerian coast, reworking of foraminiferal tests due to redeposition processes, and dating errors. Tectonic movements can likely be excluded since the documented uplift rates of approximately 0.2 mm/yr (Bouhadad, 2001) would amount to a total of only 1.2 m for the past 6 kyr. This effect is too small to be resolved by our transfer functions. The age model for the Oran Bight core is problematic because it is based on only two AMS ^{14}C dates due to a lack of datable material (e.g., pristine bivalve shells) in the recovered sediment (Fig. 4.2, Table 4.1).

The lower ^{14}C date was derived from material directly overlaying the basement identified in the lowest core part and gives an age of ~6000 years BP. However, a sedimentation gap of several thousand years above the basement is also conceivable. According to Betzler et al. (in press), the modern wave base is located at 35 m water depth in the Oran Bight, which could have resulted in permanent and local sediment erosion at site 367-1. This interpretation is supported by echosounder profiles (see Betzler et al., in press), showing a thinned sediment cover at site 367-1 in close proximity to an area with thicker sediment cover, probably containing the redeposited material permanently eroded from site 367-1. If the estimated relative sea-level reconstruction with the WA-PLS method is correct, sediment accumulation started after a sea-level in the range of 30 m had been reached and the sea-level signal could be a local one in the Oran Bight. Otherwise, significant reworking and redeposition of foraminiferal tests observed in the core would have also disturbed the sea-level signal between approximately 6 and 2 kyr BP.

4.5.3 Shelf ecosystem processes and the significance of quantitative sea-level reconstructions for the late glacial and Holocene western Mediterranean Sea

The transfer functions based on the different P/B ratios revealed consistent results only for the Mallorca Shelf (Fig. 4.8) that is presently characterized by low bottom water currents and is covered by relatively fine-grained sediments. On the Alboran Platform, the counted P/B ratios performed better than the modified P/B ratios (Fig. 4.6), while in the Oran Bight, all P/B ratio transfer functions show little applicability for bathymetric estimates (Fig. 4.7). The ratio of planktonic to benthic foraminifera depends on various environmental factors that are correlated with water depth, such as temperature, salinity, dissolved oxygen and nutrient level (Van der Zwaan et al., 1990; Sen Gupta, 2003; van Hinsbergen et al., 2005). Another important factor is the surrounding marine setting. P/B ratios appear to be higher on shelf areas with more open marine conditions when compared to shelf areas of enclosed marine basins (Sen Gupta, 2003). The Alboran Platform and the Oran Bight are exposed to open marine conditions due to narrow shelf areas associated with the particular morphologies of the Alboran Ridge and of the Algerian continental margin. In addition, surface water ecosystems of both areas contain relatively high nutrient levels (Arnone, 1994). These factors result in higher Recent P/B ratios when compared to values from surface sediments of the more oligotrophic and relatively broad southwest shelf off Mallorca at similar water depths. On the other hand, high-energy environments are stressful for benthic foraminiferal communities, particularly for infaunal species that depend on microhabitats in fine-grained sediments (Murray, 2006). Low population densities of (infaunal) benthic foraminifera are typical for high-energy ecosystems, such as the Alboran Platform and the Oran Bight (see chapter 3.5). In

conclusion, the specific environmental conditions in different shelf areas have a significant influence on the P/B ratios. Therefore, it appears necessary to generate local training sets in order to develop confident P/B ratio transfer functions.

In the modern shelf ecosystems of the study areas, benthic foraminifera exhibit distinct bathymetric zonations that, among other factors, clearly reflect the substrate type. The high-energy shelf ecosystems on the Alboran Platform and in the Oran Bight are dominated by epifaunal taxa that are often associated with elevated bottom water currents, vegetation cover and coarse-grained or sandy sediments. In both areas, fossil and modern assemblages are quite similar, suggesting that the high-energy conditions have already been established during the late glacial and prevail until today. Therefore it appears likely, that on the Alboran Platform and the Oran Bight, the obtained ERSL reconstructions are not biased by energy-related substrate effects. However, at times of significantly lower sea-level during the late glacial and early Holocene, the accuracy of ERSL reconstructions on the Alboran Platform may suffer from the elevated proportion of relocated tests (compare 4.5.2).

In contrast, a major change in substrate and hydrodynamic energy at the sea floor is observed at site 401-1 on the southwest shelf off Mallorca, disturbing the developed sea-level transfer functions. The earliest Holocene benthic foraminiferal assemblages are dominated by epifaunal species, such as *Tretomphalus concinnus* that has been associated with sandy substrates and/ or the presence of seagrass meadows (Casieri et. al., 2008; Frezza and Carboni, 2009) (PC2, Fig. 4.5C). This result implies high-energy conditions during this time interval on the Mallorca Shelf similar to those which prevailed in the other areas. The epifaunal suspension feeder *Neoconorbina terquemi* dominates the early and late Holocene intervals (PC1, Fig. 4.5C). This species is typical for the present Mallorca Shelf, where it is associated with sandy substrates (see also chapter 3.5). In other areas, this epifaunal suspension feeder is permanently or temporarily attached to coarse substrates, such as bioclastic sands and is also related to vegetation cover (Sturrock and Murray, 1981; Jorissen, 1987; Coppa and Di Tuoro, 1995; summary in Murray, 2006).

Our ERSL records for core 401-1 (Fig. 4.10A) suggest an overestimation of water depth for the time interval between approximately 6000 and 2400 cal. years B.P. that is dominated by the *Cassidulina laevigata* assemblage (PC3; Fig. 4.5C). Redundancy Analyses underlined the relevance of this assemblage for the ERSL calculation but also revealed a close relation of *C. leavigata* to the fine fraction of the sediment (Fig. 3.7, Fig. 4.11, Table A.15). Recently, *C. leavigata* occurs in areas with elevated content of fine-grained sediment and shows a higher abundance at water depths from 80 m and deeper southwest off Mallorca and in the Oran Bight (Fig. 3.5). Similar observations have been reported from other circalittoral to bathyal environments of the Mediterranean Sea, where this shallow infaunal species prefers muddy sediments with elevated organic carbon content (Jorissen, 1987; Sgarrella and Moncharmont

Zei, 1993; De Stigter et al., 1998; Bartels-Jonsdottir et al., 2006). These results demonstrate that changes in substrate and associated microhabitat niches influence the accuracy of sea-level transfer functions based on benthic foraminifera.

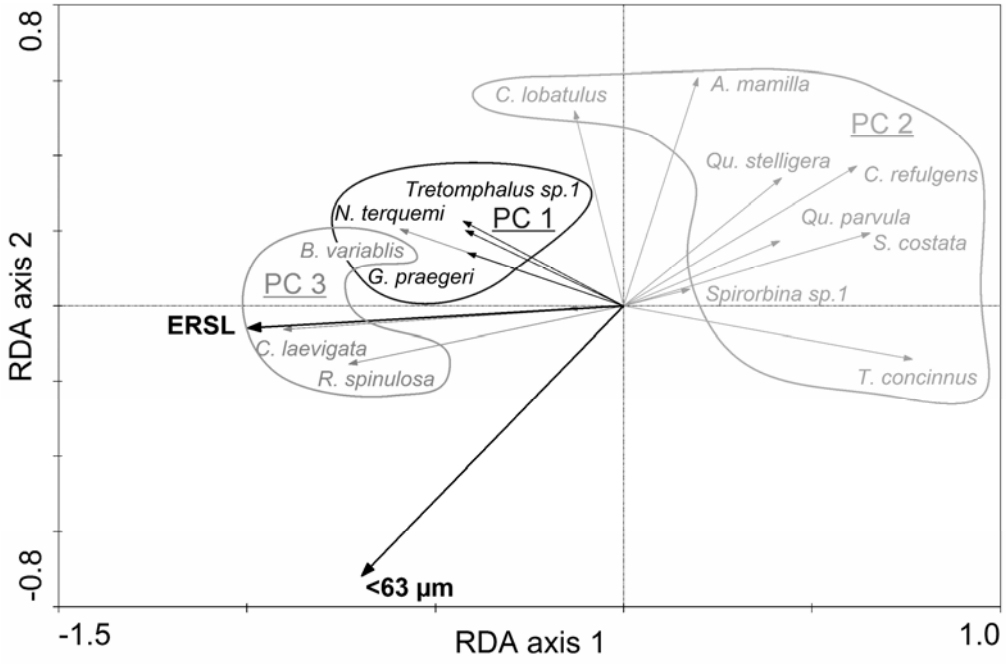

Fig. 4.11. Redundancy Analysis (RDA) for the most important species in core 401-1 from the Mallorca Shelf. PC1 species are shown in black, PC2 species in light grey and PC3 species in middle grey. The *Cassidulina laevigata*-assemblage (PC3) is strongly related to the estimated relative sea-level ($ERSL_{WA-PLS}$) and to some extent to the content of fine-grained substrate of this core (see also Fig. 4.5C and Table A.15).

4.5. Conclusions

Benthic foraminifera from cool-water carbonate environments of the western Mediterranean shelf exhibit a high potential for quantitative sea-level reconstructions with an accuracy of +/- 10 m within a total sea-level rise of ~45 and ~50 m for the Alboran Platform and the southwest shelf off Mallorca, respectively. Among various transfer functions, the best predicted model is provided by the Weighted Averaging-Partial Least Squares (WA-PLS) regression method. In contrast, Modern Analog Technique (MAT) and the more “classical” approach based on counted or modified Plankton/Benthos (P/B) ratios resulted in less consistent reconstructions with higher errors. The latter method is influenced by exposure to the open ocean, nutrient conditions, and energy at the sea floor. Therefore, regional training data sets should be used for paleobathymetric applications of this method.

The paleobathymetric trends for the Alboran Platform and the Mallorca Shelf regions reflect the global and Mediterranean sea-level histories during the Holocene. In contrast, the calculated middle to late Holocene sea-level rise in the Oran Bight appears to be overestimated when compared to the global signal. Major tectonic vertical movements can be excluded for this region, and thus cannot account for the observed inconsistencies. Instead, the results may be attributed to redeposition processes with enhanced relocation of benthic foraminifera and/ or a problematic age model. On the Mallorca shelf, the sea-level signal interferes with temporal changes in substrate and microhabitat niches, resulting in minor inconsistencies during the middle Holocene period.

5 Impact of an early Holocene humid phase on shelf environments off Southwest Mallorca, western Mediterranean Sea

Abstract

Stable oxygen and carbon isotope records of different planktonic and benthic foraminifera from a shelf sediment core off southwest Mallorca document major climatic, hydrological and trophic changes during the Holocene. A change in sediment facies between approximately 9.6 and 5.5 kyr BP is attributed to humid conditions on Mallorca Island. This humid interval is nearly contemporaneous to the formation of sapropel S1 in the eastern Mediterranean Sea and resulted in a freshening of the surface mixed layer, enhanced nutrient input from land and related eutrophication of near-coastal marine ecosystems off SW Mallorca. These results demonstrate that the early Holocene warm and humid phase also affected surface water hydrography, organic carbon cycling and marine ecosystems in the western Mediterranean Sea. Comparison with records from more open-ocean settings of different areas in the western Mediterranean Sea suggests that the climate impacts were likely restricted to near-coastal systems.

This chapter is based on: Milker, Y., Schmiedl, G., Betzler, C., Andersen, N., Theodor, M., in prep. Impact of an early Holocene humid phase on shelf environments off Southwest Mallorca, western Mediterranean Sea.

5.1 Introduction

Mediterranean marine and terrestrial climate archives recorded major hydrological changes during the late Quaternary. These changes occurred on orbital and suborbital timescales and bear climate signals of the high northern latitudes and the African monsoon system. They are associated with high-amplitude shifts in circulation, biogeochemical cycles and marine ecosystems of the Mediterranean Sea. The eastern Mediterranean deep basins are characterized by periodic deposition of sapropels, associated with maxima in northern hemisphere insolation and related hydrological changes of the African tropical rain belt (e.g., Rossignol-Strick et al., 1982; Rohling and Hilgen, 1991; Cramp and O'Sullivan, 1999). Times of sapropel formation coincide with humid phases in northern Africa (Rohling et al., 2002; Kuper and Kröpelin, 2006), enhanced Nile River runoff (Fontugne et al., 1994; Emeis et al., 2000; Almogi-Labin et al., 2009) and with precipitation increase over the northern borderlands (Kotthoff et al., 2008). These climate changes resulted in stagnation of eastern Mediterranean deep-water masses but the knowledge on the exact sequence of ecological and biogeochemical impacts and regional expression over the whole Mediterranean is still fragmentary. The most recent sapropel layer S1 was deposited in the early Holocene, between approximately 9.6 and 6 kyr BP (Mercone et al., 2000).

Sediment records from the western Mediterranean Sea only occasionally contain sapropel-equivalent organic rich layers (Comas et al., 1996; Capotondi and Vigliotti, 1999; Cramp and O'Sullivan, 1999) and lack an organic rich layer equivalent to Holocene sapropel S1 (Martinez-Ruiz et al., 2003). Geochemical and faunal records from the Alboran Sea suggest a reduction of intermediate and deep-water ventilation and a fertility increase of surface waters during the earliest Holocene, e.g. between approximately 10 and 8 kyr BP (Vergnaud Grazzini and Pierre, 1991, 1992; Jimenez-Espejo et al., 2008). This time interval coincides with sea surface temperature (SST) maxima in various western Mediterranean records, as part of a series of abrupt warm and cool events associated with the North Atlantic climate variability (Cacho et al., 2001; Sbaffi et al., 2001, 2004).

Planktonic and benthic stable isotope data delivered a wealth of information on the Mediterranean paleoenvironmental evolution. Planktonic foraminiferal $\delta^{18}O$ and alkenone records imply major drops in sea surface salinities in Levantine surface waters during times of sapropel formation (Emeis et al., 2000, 2003). Multi-species planktonic foraminiferal $\delta^{13}C$ records documented major changes in surface water stratification and identified the early Holocene interval as a phase of enhanced input of dissolved inorganic carbon from terrestrial sources (Casford et al., 2002). The $\delta^{13}C$ signal of epibenthic deep-sea foraminifera provided information on past changes in deep-water sources and residence times, while the $\delta^{13}C$ signal

of shallow infaunal taxa revealed short-term changes of organic matter fluxes to the sea floor (Vergnaud Grazzini and Pierre, 1991; Schilman et al., 2001; Kuhnt et al., 2008).

The general paleoceanographic contrasts between the western and eastern basins of the Mediterranean Sea can be attributed to different hydrological balances and the influence of North Atlantic and African climate systems. For a detailed reconstruction of regional climate impacts and evaluation of land-to-sea couplings, records from shelf and coastal marine settings are required. To date, very little information is available on the Holocene variability of western Mediterranean shelf environments, mainly because the retrieval of sediment cores with gravity or piston corers is hampered by high sand contents in these depositional systems.

For this study, a unique sediment record from the southwest Mallorca shelf of the western Mediterranean Sea that was drilled with a vibrocorer has been analyzed. The stable isotope records of various planktonic and benthic foraminiferal species have been compared with faunal records from the same site and with records from other areas of the western Mediterranean Sea. This approach allowed for the reconstruction of regional trends in Holocene surface water characteristics and productivity, and the detection of local climatic and hydrological signals.

5.2 Regional settings

The island of Mallorca, the largest of the Balearic Islands, extends over an area of 3667 km^2 and is situated in the Balearic Basin, approximately 200 km east of the Iberian Peninsula (Werner et al., 1993). The island represents an emergent area of the Balearic promontory that is located between the Valencia Trough and the Algerian Basin (Fig. 5.1). This 350 km long and 104 km wide promontory presents the prolongation of the Betic system and consists of three blocks separated by the Ibiza, Mallorca and Menorca channels (Acosta et al, 2004) (Fig. 5.1). The Mallorca channel is situated west off the island and consists of two depressions in the north-west and south-east, connected by a narrow north-trending channel with a sill depth of 740 m (Acosta et al., 2004). The island of Mallorca is surrounded by a narrow shelf with sills and a smooth upper slope south-west of the island (Garcia et al., 1994; Acosta et al., 2004).

The hydrography of the Balearic Basin is characterized by a strong seasonal thermocline in summer (from May to October) and by the formation of Mediterranean Deep Water in the winter months (Garcia et al., 1994; Fernandez de Puelles et al., 2004A). In the surface waters, two permanent density fronts are established: the Continental Front on the continental shelf slope with a south-westward flow in the upper 300 m, and the Balearic Front along the Balearic Islands shelf slope, with a north-eastward flow (Fig. 5.2). The latter front separates the open ocean Mediterranean Water from the Modified Mediterranean Water that enters the

Balearic Basin through the Ibiza channel (Garcia et al., 1994). The southwest shelf of Mallorca is characterized by geostrophic currents that follow the topographic features and reach velocities of approximately 20 cm/s (Werner et al., 1993).

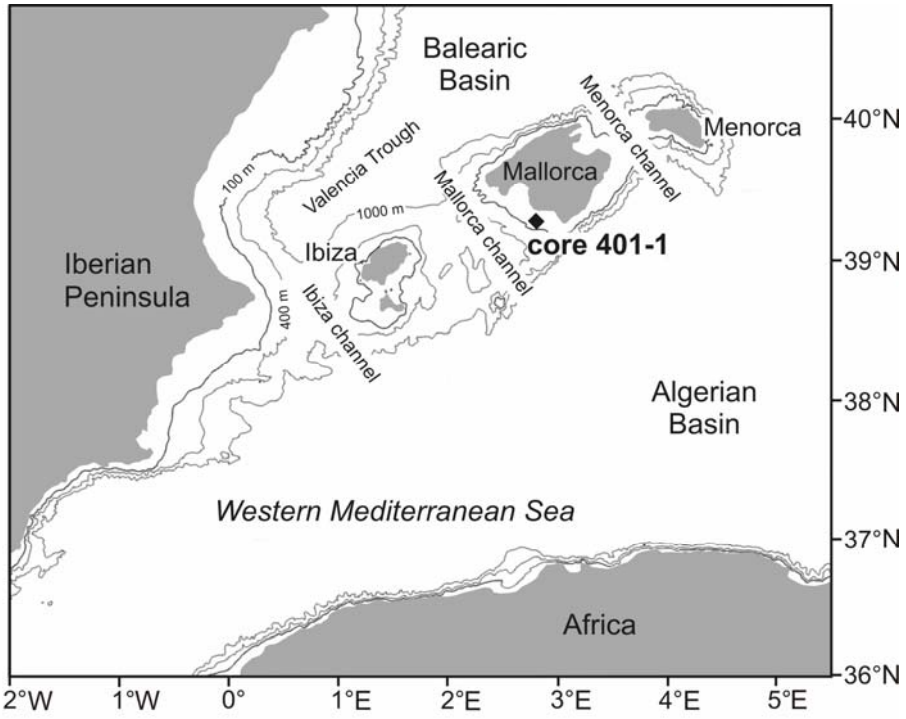

Fig. 5.1. Bathymetric map of the western Mediterranean Sea showing the location of core 401-1 on the south-western shelf off Mallorca.

The salinities of the shelf off Mallorca show no annual seasonality but an interannual monthly variability (Fernandez de Puelles et al., 2004A). They range from 37.3 to 37.5‰ at 10 m water depth (Brasseur et al., 1996). Sea surface salinities measured in the working area during Meteor-Cruise 69/1 in august 2006 were in the same range (37.3-37.4‰; Table A.5). Mean sea surface temperatures on the shelf show an annual seasonality and range from 21.5 - 27.4°C in summer and 13.4 - 14.3°C in winter (Fernandez de Puelles et al., 2004A). Sea surface temperatures measured during Meteor-cruise in august 2008 were in the range of 25.4 to 26.3°C (Table A.5).

Recently, the Balearic region has an oligotrophic character with estimated an annual primary production of 100 to 150 g C/m^2/year (Antoine et al., 1995). The Mallorca Channel is characterized by very low chlorophyll a values in the surface waters, with a deep chlorophyll a maximum between 50 m and 75 m (Fernandez de Puelles et al., 2004B). Elevated chlorophyll a concentrations are restricted to the coastal areas and the frontal systems (Fernandez de Puelles et al., 2004B).

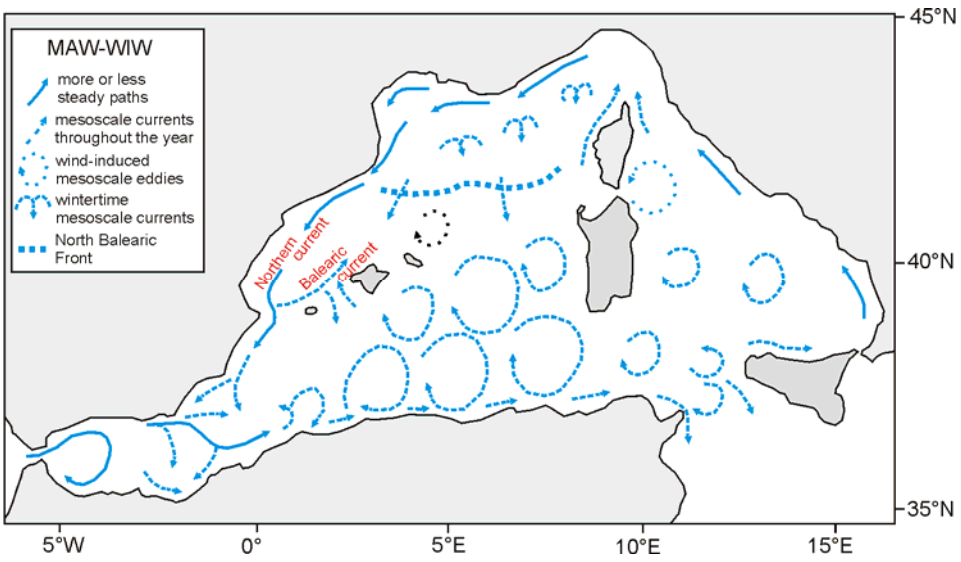

Fig. 5.2. Circulation of the Modified Atlantic Water (MAW) and the Winter Intermediate Water (WIW) in the western Mediterranean Sea adapted from Millot (1999) and Pinot et al. (2002). For the Balearic region, the Northern and the Balearic Currents are indicated.

5.3 Materials and Methods

The 470 cm long sediment core 401-1 was recovered by means of a vibrocorer on the south-western shelf of Mallorca at 74 m water depth, at 39°17.10' N and 2°48.31' E, during Meteor cruise 69/1 (Fig. 5.1). The lower part of the core consists of calcirudites containing rhodoliths, shells and debris of molluscs. The middle part is characterized by fine to middle calcarenites with a high content of shells of the benthic gastropod *Turritella communis*. The upper part is composed of fine to middle calcarenites with debris and shells of molluscs (Betzler et al., in press).

For the stable oxygen and carbon isotope measurements, benthic and planktonic foraminifera were picked from the fraction >125 µm of 94 core samples (Table A.16). Approximately 30 tests of the planktonic species *Globigerina bulloides* and *Globigerinoides ruber* (white) and approximately 10 tests of the benthic species *Bulimina aculeata*, *Cibicides lobatulus* and *Rectuvigerina phlegeri* were picked. The latter species was only picked in the core interval from 176.5 cm and 301.5 cm because of its low abundance or absence in the other core sections. For the isotopic analyses, only the compact type of *G. ruber* (*G. ruber gomitulus*) was selected because this phenotype shows different $\delta^{13}C$ and $\delta^{18}O$ values when compared to the larger specimens of *G. ruber* (*G. ruber ruber*) (Emiliani, 1971; Weiner, 1975). All specimens were cleaned with ethanol in an ultrasonic bath. The isotopic composition was measured with a Finnigan MAT 251 mass spectrometer at the Leibniz-Laboratory for Radiometric Dating and Isotope Research, Kiel (Germany). The data are given in δ-notation, standardized to the Vienna Pee Dee Belemnite (VPBD). The external precision ranges from

+/-0.01 and +/-0.04‰. From the fraction >125 µm, benthic gastropods were picked throughout the core at 5 cm spacing. For chronostratigraphy of core 401-1, six AMS ^{14}C measurements were performed at the Leibniz-Laboratory for Radiometric Dating and Isotope Research, Kiel (Germany) and were transferred to calendar years according to the procedures described in chapter 4.3.2 and in Betzler et al. (in press) (compare Fig. 4.2 and Table 4.1).

5.4. Results

The $\delta^{18}O$ values of *Globigerina bulloides* range from -0.15 to 1.11‰ VPDB (Fig. 5.3). *Globigerinoides ruber* (white) exhibits generally lower values, ranging from -0.87 to 0.54‰. The benthic foraminiferal $\delta^{18}O$ records reveal lowest values for *Cibicides lobatulus* with 0.17 to 1.49‰. The $\delta^{18}O$ values of *Rectuvigerina phlegeri* range from 1.07 to 1.41‰. The highest values were measured in *Bulimina aculeata* tests with 1.16 to 2.25‰ (Fig. 5.3). For all species (except for *R. phlegeri*), a change from heavier values to lighter $\delta^{18}O$ values is observed during the earliest Holocene. The $\delta^{18}O$ values of *G. ruber* (white) return to heavier values from ~9 to 7.2 kyr BP and then remain more or less constant from 7.2 kyr BP to present. In contrast, the $\delta^{18}O$ values of *G. bulloides* show a continuous increase from 9 kyr BP to present. The $\delta^{18}O$ values of *C. lobatulus* and *B. aculeata* are relatively low in the interval from ~9 to ~6 kyr BP and exhibit slight subsequent increases (Fig. 5.3).

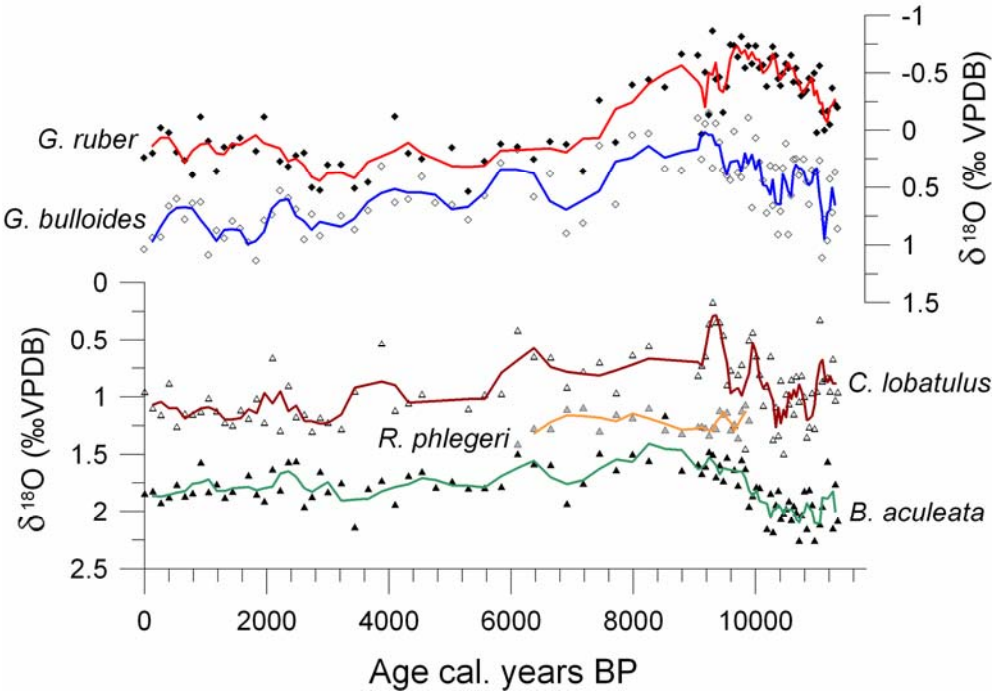

Fig. 5.3. Stable oxygen isotope records of the planktonic foraminfera *Globigerinoides ruber* (white), *Globigerina bulloides* and the benthic foraminifera *Cibicides lobatulus, Bulimina aculeata* and *Rectuvigerina phlegeri* in core 401-1 versus age (the curves are smoothed with a running average of 3).

The $\delta^{13}C$ values of *G. ruber* (white) range from 0.49 to 1.66‰ while *G. bulloides* shows significantly lower values, ranging from -1.66 to -0.10‰ (Fig. 5.4). Among the benthic foraminifera, *R. phlegeri* has the lowest $\delta^{13}C$ values, ranging between -1.29 and -0.62‰. The highest $\delta^{13}C$ values were measured in *C. lobatulus* tests with 0.46 and 1.83‰, the $\delta^{13}C$ values of *B. aculeata* range from -0.71 to 0.41‰ (Fig. 5.4). During the early Holocene, the $\delta^{13}C$ values of *G. ruber* (white) exhibit a general decrease while the $\delta^{13}C$ values of *G. bulloides* exhibit no clear trend with relatively high variability. From ~9 kyr BP on, $\delta^{13}C$ values of *G. ruber* (white) return to earliest Holocene values and remain more or less constant from ~5 kyr BP to present. In contrast, the $\delta^{13}C$ values of *G. bulloides* exhibit a general decrease from ~9 kyr BP to present. The $\delta^{13}C$ record of *C. lobatulus* shows a continuous decrease over the whole time interval investigated (Fig. 5.4). In contrast, the $\delta^{13}C$ record of *B. aculeata* exhibits relatively lower $\delta^{13}C$ values during the early to middle Holocene interval (~9 to ~6 kyr BP) followed by a general increase until present.

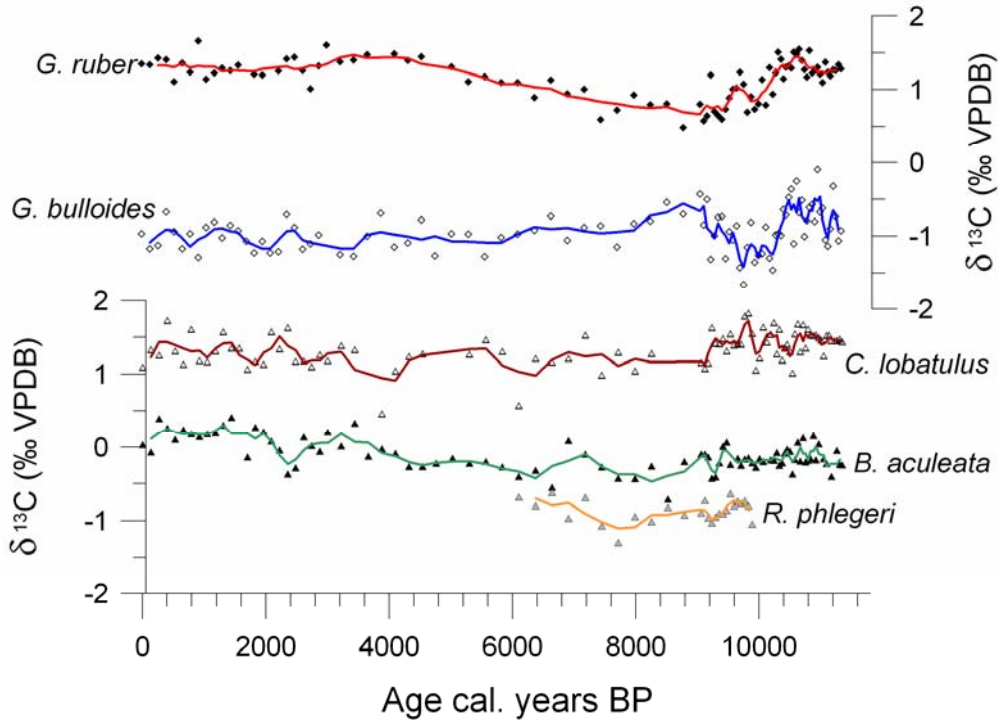

Fig. 5.4. Stable carbon isotope records of the planktonic foraminfera *Globigerinoides ruber* (white), *Globigerina bulloides* and the benthic foraminifera *Cibicides lobatulus, Bulimina aculeata* and *Rectuvigerina phlegeri* in core 401-1 versus age (the curves are smoothed with a running average of 3).

5.5 Discussion

5.5.1 Regional climate trends and seasonality

The general $\delta^{18}O$ shift from heavier to lighter values in the different species during the earliest Holocene includes a glacio-eustatic signal of ~0.3‰ (Lambeck and Chappell, 2001) but also a general warming and/or freshening of western Mediterranean surface water masses (Fig. 5.3). This result is consistent with alkenone temperature reconstructions for the southern Tyrrhenian Sea that revealed an early Holocene mean annual temperature increase from ~16°C to ~20°C (Sbaffi et al., 2001, 2004). A similar temperature increase was also documented for the Alboran Sea based on palynological data (Dormoy et al., 2009). On a basin-wide comparison, the early and middle Holocene mean $\delta^{18}O$ values of *G. bulloides* from the Mallorca Shelf are between 0.5 and 1.0 ‰ lighter relative to records from the open Alboran Sea and Tyrrhenian Sea (Cacho et al., 1999, 2001; Fig. 5.5). This regional contrast is particularly expressed in the time interval between 11.5 and ~9 kyr BP and disappears during the late Holocene. Earliest Holocene relative sea-level at core site 401-1 was ~50 m lower than today resulting in a more near-shore setting of the study area (Fig. 5.6). The observed $\delta^{18}O$ depletion could thus be attributed to the influence of mesoscale climate effects, e.g. warmer temperatures, in the near-coastal setting off Mallorca when compared to open-oceanic settings. The local $\delta^{18}O$ depletion during this time interval could also reflect lower salinities of near-coastal waters resulting from moist conditions and enhanced freshwater run-off from the Mallorca Island. The presence of a fresh surface layer in coastal waters off Mallorca would also explain the inter-specific $\delta^{18}O$ contrasts, with higher depletions in the planktonic taxa and lower depletions in benthic taxa (Fig. 5.3). This interpretation is supported by various palynological studies documenting increased (winter) precipitation during the early Holocene in the northern borderlands of the western and eastern Mediterranean Sea (Magny et al., 2002; Kotthoff et al., 2008; Dormoy et al., 2009). The timing of surface water freshening off Mallorca would be largely consistent with the African Humid Period between 14.8 to 5.5 kyr BP (de Menocal et al., 2000) and the time window of sapropel formation in the eastern Mediterranean Sea between approximately 9.6 to 6 kyr BP (Mercone et al., 2000).

Depending on their preferred (seasonal) habitats, different planktonic foraminiferal species respond to hydrographic and climatic change with isotopic variations of variable amplitude (Rohling and De Rijk, 1999; Casford et al., 2002). The surface dwelling species *G. ruber* has a minimum temperature requirement of ~14°C (Hemleben et al., 1999; Bijma et al., 1990; Reiss et al., 2000). In the Mediterranean Sea, *G. ruber* (white) mainly occurs at times of high surface sea surface temperatures (SST) in the thin mixed layer above the seasonal thermocline during summer and fall (Tolderlund and Be, 1971; Pujol and Vergnaud-Grazzini, 1995; Rohling and

De Rijk, 1999; Rohling et al., 2004; Capotondi et al., 2006). In contrast, *G. bulloides* inhabits a greater depth range and appears in the mixed layer during the colder transitional periods, mainly from late winter to spring (Tolderlund and Be, 1971; Pujol and Vergnaud-Grazzini, 1995). During this transitional period, *G. bulloides* depends on the wind-induced entrainment of nutrients from subsurface waters (Schiebel et al., 2001; Rohling et al., 2004). The $\Delta\delta^{18}O$ signal between *G. bulloides* and *G. ruber* can thus be interpreted as a proxy for the seasonal contrasts in sea surface temperature and salinity (SST, SSS) (Fig. 5.6). Accordingly, seasonality of shelf waters off SW Mallorca was highest during the earliest Holocene and dropped significantly around 9.5 kyr BP, coinciding with the onset of sapropel deposition in the eastern Mediterranean Sea. In the Tyrrhenian Sea, strong seasonal contrasts with efficient vertical mixing in winter and stratified water column in summer has been reported by Carboni et al. (2005) for the interval between 10.9 to 8.3 kyr BP. This result is in accordance with paleolimnological records around the Mediterranean Sea and shows that the earliest Holocene climate was characterized by colder winters and warmer summers than today (Watts et al., 1996; Magny et al., 2002).

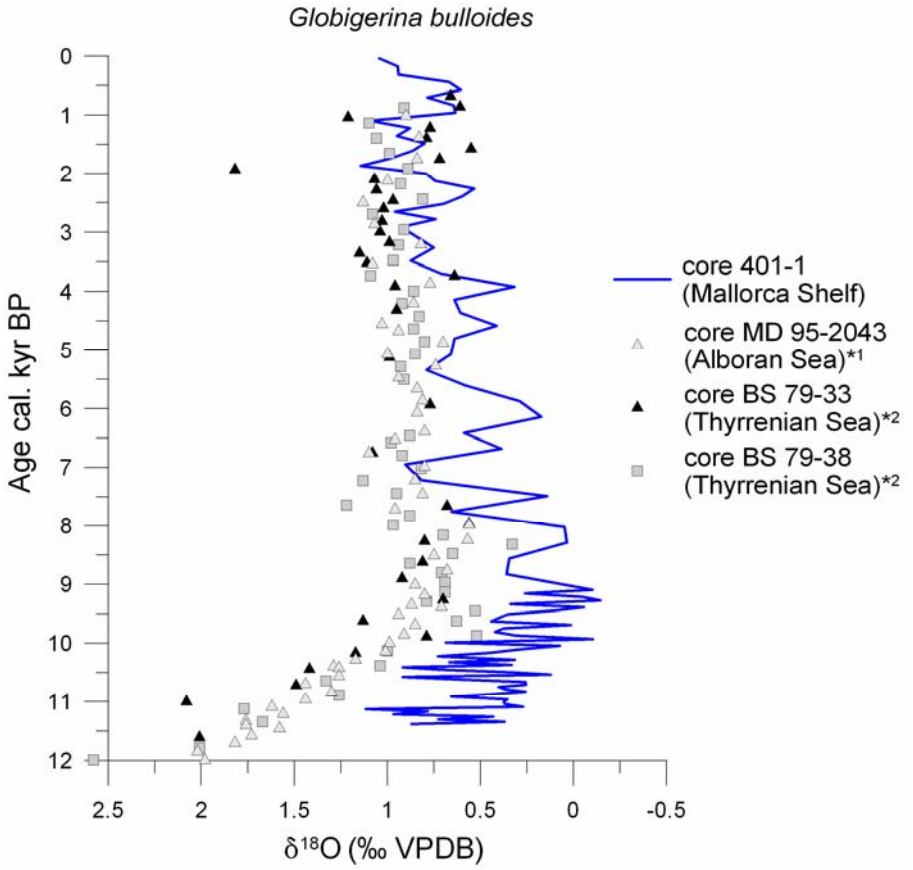

Fig. 5.5. Comparison of the stable $\delta^{18}O$ record of *Globigerina bulloides* in core 401-1 from the shelf off Mallorca (blue line) with deep water isotope records of this species (symbols) from the Alboran and Tyrrhenian Seas (*[1] Cacho et al., 1999; *[2] Cacho et al., 2001).

The time interval between 9.5 and 6 kyr BP is characterized by generally low but strongly fluctuating $\delta^{18}O$ values with an overall trend to cooler and/or saltier Mallorcan surface waters and a shift from moderate to low seasonality (Figs. 5.3 and 5.6). This result is in accordance with decreasing temperatures from ~20°C to ~15°C in the time interval of 9 to 5.4 kyr BP in the Tyrrhenian Sea (Sbaffi et al., 2001, 2004). A comparable seasonality trend was reported from the northeastern borderlands of the eastern Mediterranean Sea (Pross et al., 2009). There, abrupt cold events (e.g., the 8.2 kyr event) resulted in short-lived increase of seasonal temperature contrasts. Similarly, short-term climate changes may account for the strong fluctuations in the $\Delta\delta^{18}O$ values during this time in our record although the $\delta^{13}C$ record of *G. ruber* implies significant input of isotopically light terrestrial dissolved organic carbon (DOC) and thus enhanced summer rainfall during the same time period (Fig. 5.6, see also discussion below). The late Holocene $\Delta\delta^{18}O$ values imply an overall trend from low to moderate seasonality, marking the establishment of modern hydrographic conditions and seasonal contrasts (Fig. 5.6). A slight trend to heavier $\delta^{18}O$ values is documented in *G. bulloides* and *C. lobatulus*, likely documenting calcification of these species in well-mixed surface waters and under the influence of increasingly cooler winter/early spring temperatures (Fig. 5.3). A similar trend is reported for the Alboran Sea (Cacho et al., 2001) indicating a super-regional climate signal.

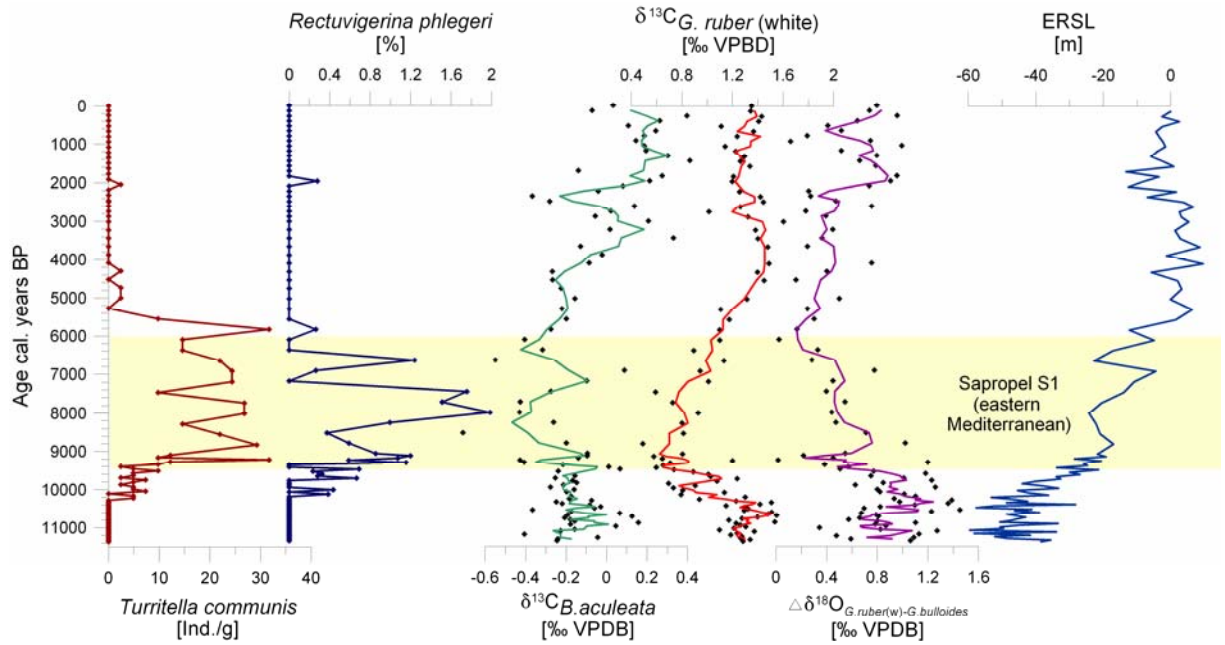

Fig. 5.6. Abundance of the gastropod *Turritella communis* (Individuals per 10 g sediment), percentages of *Rectuvigerina phlegeri*, stable carbon isotope ($\delta^{13}C$) records of *Bulimina aculeata* and *Globigerinoides ruber* and $\Delta\ \delta^{18}O$ of *Globigerinoides ruber* (white)-*Globigerina bulloides* in core 401-1 in comparison with the estimated relative sea-level (ERSL) on the Mallorca shelf. The highlighted time interval shows the sapropel S1 deposition in the eastern Mediterranean (Mercone et al., 2000).

5.5.2 Regional hydrology, organic matter fluxes and benthic shelf ecosystem dynamics

The interval between approximately 10.5 and 5 kyr BP is marked by low $\delta^{13}C$ values of *G. ruber* (white) that are depleted by up to 1 ‰ around 9 kyr BP relative to the earliest Holocene and late Holocene values (Figs. 5.4 and 5.6). The $\delta^{13}C$ record of *G. bulloides* exhibits only a short-lived depletion between ~10.5 and 9.5 kyr BP while the $\delta^{13}C$ record of the epibenthic *C. lobatulus* lacks a comparable signal (Fig. 5.4). These $\delta^{13}C$ signatures suggest that the environmental signal is mainly restricted to the summer season and localized in the thin mixed surface layer. In the eastern Mediterranean Sea, similar $\delta^{13}C$ drops of *G. ruber* have been reported for the time interval of sapropel S1 formation and have been related to input of isotopically light carbon of terrestrial sources (Casford et al., 2002). Similarly, the $\delta^{13}C$ signal of *G. ruber* from the Mallorca shelf likely indicates the increased input of terrestrial DOC with enhanced freshwater runoff. This documents the establishment of humid conditions and related summer rainfall on Mallorca Island. The local expression of this early to middle Holocene runoff signal is validated by lighter $\delta^{13}C$ values of *G. ruber* when compared to open-ocean records from the Alboran Sea (Pujol and Vergnaud Grazzini, 1989). Although this interpretation appears reasonable, the planktonic foraminiferal signals may also interfere with the ^{12}C removal in surface waters through the process of phytoplankton production (Pujol and Vergnaud Grazzini, 1989; Ortiz et al., 1996).

The early to middle Holocene climatic and hydrological changes had a strong impact on shelf sedimentation processes and benthic ecosystem dynamics. The time interval between approximately 9.6 and 5.5 kyr BP is characterized by a unique sediment facies consisting of fine to middle calcarenites with a high content of shells of the benthic gastropod *Turritella communis* and the appearance of the infaunal benthic foraminifer *Rectuvigerina phlegeri* (Fig. 5.6). This facies is documented in several sediment cores from the south-western shelf of Mallorca (Betzler et al., in press). The infaunal suspension feeder *Turritella communis* is characteristic for muddy substrates and soft bottoms in various Atlanto-Mediterranean shallow- to mid-shelf environments and favors ecosystems with a high content of suspended organic matter (Fretter and Graham, 1981; Allmon, 1988, 1992; Koulouri et al., 2006). In the western Mediterranean Sea, it also occurs in sandy substrates with carbonate detritus together with green algae and calcareous red algae (Simboura and Zenetos, 2002; Massuti and Renoues, 2005; Poirier et al., 2009). In the Bay of Banyuls (south-western France) it is very abundant and co-occurs with *Rectuvigerina phlegeri* in pelitic substrates around 30-40 m water depth, representing a mesotrophic setting (unpublished data of G. Schmiedl). To date, this facies has not been documented on the modern shelf off SW Mallorca (Betzler et al., in press; own observations).

The presence of this facies correlates with the drop in $\delta^{13}C$ of *G. ruber* during the early and middle Holocene, documenting a rise in freshwater runoff and associated nutrient input from land (Fig. 5.6). This nutrient supply finally resulted in higher organic matter fluxes and food availability at the sea floor, where it is reflected by the presence of *T. communis* and the increase in abundance of the benthic foraminifer *Rectuvigerina phlegeri* (Fig. 5.6). *R. phlegeri* occupies a shallow to intermediate infaunal microhabitat and occurs in muddy shelf environments with relatively high organic matter content (Guimerans and Currado, 1999A; Bartels-Jonsdottir et al., 2006). In the western Mediterranean Sea, *R. phlegeri* is particularly abundant in ecosystems influenced by river plumes where it feeds from fresh organic matter (Frezza and Carboni, 2009; Mojtahid et al., 2009). A relatively deep infaunal habitat of *R. phlegeri* at site 401-1 is confirmed by its low $\delta^{13}C$ values relative to *B. aculeata* and *C. lobatulus*, reflecting a strong pore water influence (Fig. 5.4).

The early Holocene eutrophication is corroborated by a decrease in the $\delta^{13}C$ values of *B. aculeata* (Figs. 5.4 and 5.6). *Bulimina aculeata* is abundant in shelf and bathyal environments where it responds to seasonal phytodetritus pulses and occupies a predominantly shallow infaunal microhabitat in organic-rich muddy sediments with a shallow oxygen penetration (Rathburn and Corliss, 1994; Mendes et al., 2004; Murgese and de Deckker, 2007). Its $\delta^{13}C$ signal depends on the organic carbon fluxes and site-specific $\delta^{13}C$ of pore water dissolved inorganic carbon (Mackensen et al., 2000). Accordingly, the $\delta^{13}C$ signal of *B. aculeata* reflects the remineralisation rate of organic matter in the uppermost surface sediment that is correlated to organic matter flux rates (McCorkle et al., 1985, 1990; Holsten et al., 2004; Schmiedl et al., 2004). The high fluctuations of the various trophic signals imply high-amplitude short-term changes in freshwater runoff and nutrient fluxes during the early to middle Holocene period. The inferred environmental shifts are likely linked to abrupt climate change although the limited temporal resolution of our record for this interval does not allow for a more comprehensive evaluation.

The humid phase on Mallorca Island between 9.6 and 5.5 kyr BP is nearly synchronous to sapropel S1 formation in the eastern Mediterranean Sea that is dated to approximately 9.6 to 6 kyr B.P. (Mercone et al., 2000; Fig. 5.6). The eastern Mediterranean climate during S1 formation was characterized by generally warmer and wetter conditions in both southern and northern Mediterranean borderlands when compared to present conditions (Rossignol-Strick, 1999; Bar-Matthews et al., 2000; Kotthoff et al., 2008; Dormoy et al., 2009). More specifically, the high abundance of deciduous tree pollen in sediment archives has been related to high annual precipitation rates and absence of summer drought (Rossignol-Strick, 1995, 1999). Increased Mediterranean rainfalls co-occur with an intensification of the African monsoon system and northward shift of the African tropical rain belt (Rossignol-Strick, 1983; de Menocal

et al. 2000) and likely resulted from the formation and eastward movement of more summer depressions in the western Mediterranean (Rohling and Hilgen, 1991; Rossignol-Strick, 1999). This early Holocene humid period is associated with low $\delta^{18}O$ and $\delta^{13}C$ values of *G. ruber* (white) in eastern Mediterranean sediment cores documenting enhanced freshwater input (Rossignol-Strick et al., 1982; Emeis et al., 2000; Rohling et al, 2002; Capotondi et al, 2006).

Pollen records from the western Mediterranean region also document a more humid and warmer climate during the time interval of S1 formation (Ariztegui et al., 2000; Drescher-Schneider et al., 2007; Ninyerola et al., 2007). Specifically, moist conditions during the early Holocene (8 - 5 kyr BP) have also been documented for the Balearic islands, based on higher abundances of *Quercus, Buxus* and other mesophilous taxa in lagoonal and marshland sediments (Yll et al. 1997). However, the impact of early Holocene warm and humid conditions on marine environments is less well constrained in temperature and salinity proxies (Emeis et al., 2000; Cacho et al., 2001; Melki et al., 2009). Evidence for enhanced freshwater runoff and enhanced stratification during this time period (e.g., 8.3 to 5.2 kyr BP) is restricted to the Tyrrhenian Sea (Ariztegui et al., 2000; Carboni et al., 2005). In addition, deep-sea records from the Algerian and Balearic basins did not show any comparable productivity increase for this time interval (Weldeab et al., 2003; Jimenez-Espejo et al., 2007). In the Alboran Basin, however, Vergnaud Grazzini and Pierre (1992) found higher percentages of *U. peregrina* with depleted $\delta^{13}C$ values in the interval between 9 and 6 kyr BP implying a regional productivity increase. This increase is linked to the history of the gyre and frontal system of the Alboran Sea and therefore is likely influenced by early Holocene sea-level rise and the hydrography of Atlantic surface waters.

The rather abrupt drops in the abundance of *T. communis* and *R. phlegeri* imply a rapid termination of meso- to oligotrophic conditions on the southwest shelf off Mallorca around 5.5 kyr BP (Fig. 5.6) coinciding with the abrupt termination of the African Humid Period (de Menocal et al., 2000). In both regions, these signals may reflect rapid ecosystem shifts rather than rapid climate changes. This interpretation is corroborated by a gradual increase of $\delta^{13}C$ values of *B. acuelata* and planktonic foraminiferal $\delta^{18}O$ and $\delta^{13}C$ values suggesting a gradual hydrological change (Figs. 5.3, 5.4 and 5.6). This result is confirmed by a gradual decrease in total biomass, *Buxus* and *Corylus*, and a dominance of *Olea* heralding the modern xeric conditions and an increasing anthropogenic influence (Yll et al., 1997; Ninyerola et al., 2007; Perez-Obiol, 2007). Generally, the late Holocene Mediterranean climate is characterized by drier summers and more humid winters, similar to present conditions (Watts et al., 1996; Dormoy et al., 2009). During the past 5 kyr, annual sea surface temperatures in the southern Tyrrhenian Sea decreased from ~17°C to ~15°C (Sbaffi et al., 2001).

5.6 Conclusions

The stable isotope records of two surface-dwelling planktonic and three benthic foraminiferal species, together with micro- and macrofaunal data from a shelf sediment core off southwest Mallorca (western Mediterranean Sea) provide insights into the hydrographic evolution and ecosystem dynamics of this region during the Holocene.

The establishment of humid conditions with enhanced summer rainfalls on Mallorca Island during the early and middle Holocene (e.g. between 9.6 and 5.5 kyr BP) resulted in increased freshwater runoff, input of terrestrial dissolved organic matter and nutrients into the coastal marine system. In the upper surface layer, these hydrological changes are documented by decreased $\delta^{18}O$ and $\delta^{13}C$ values of *Globigerinoides ruber* (white). On the sea floor, elevated organic matter fluxes resulted in a lowering of $\delta^{13}C$ values of *Bulimina aculeata,* and the appearance of the suspension feeding gastropod *Turritella communis* and the infaunal benthic foraminifer *Rectuvigerina phlegeri*.

Differences in the $\delta^{18}O$ signals of *Globigerina bulloides* (representing the late winter/spring situation) and *Globigerinoides ruber* (representing the late summer situation) reveal higher seasonality during the earliest Holocene and an abrupt drop of seasonal contrasts with onset of the humid phase around 9.6 kyr.

The timing of the Mallorca humid interval is nearly synchronous to the formation of sapropel S1 (9.6-6.0 kyr BP) in the eastern Mediterranean Sea, corroborating previous evidence from pollen records. For the first time, a major impact of this humid period on western Mediterranean marine ecosystems is documented here. Comparisons with open-ocean records from the Alboran, Balearic and Tyrrhenian basins illustrate that the marine response to enhanced precipitation in the western Mediterranean during the early Holocene is probably confined to near-coastal settings.

6 Taxonomy of modern benthic shelf foraminifera in the western Mediterranean Sea

Abstract

A total of 280 modern benthic foraminifera from carbonate shelf environments of three areas in the western Mediterranean Sea (Alboran Platform, Oran Bight and the south-western shelf off Mallorca) have been studied and are systematically listed here. The systematic description provides a list of synonyms, short remarks about morphological features of various taxa and some annotations about taxa with problematic generic status. 111 taxa are illustrated by SEM photographs.

This chapter is based on: Milker, Y. and Schmiedl, G., in prep. Taxonomy of modern benthic shelf foraminifera in the western Mediterranean Sea.

6.1 Introduction

Foraminifera are a widely distributed and diverse order of protists in marine environments. They play an important role in ecological and paleo-ecological studies due to their high numerical density in marine sediments and the excellent preservation potential of their shells. Benthic foraminifera show a great diversity with more than 10,000 modern taxa while planktonic foraminifera are less diverse with 40-50 modern species. The oldest benthic foraminifera were found in Cambrian deposits, and the oldest planktonic species occur in the Jurassic (Sen Gupta, 2003).

An accurate knowledge of the taxonomy of foraminifera provides the basis for any applications in paleoenvironmental or biostratigraphic studies of these protozoa. In the early 18th century, Scheuchzer was the first who identified foraminifera as animals, and he assigned them to the gastropoda (Nuglisch, 1985). Lamarck established independent foraminiferal orders such as *Discorbis, Rotalia*, *Lenticulina* and *Nummulites* in 1801 and 1804 (Nuglisch, 1985). D'Orbigny, who played an important role in foraminiferal research, categorized foraminifera as their own order inside the cephalopoda in 1826, and Dujardin assigned them to the protozoa in 1841 (Nuglisch, 1985). Since the first investigations, more systematic studies were carried out by Reuss, Ehrenberg and later by Thalman. An important monograph about modern foraminifera based on the material collected during the Challenger expedition (1872 - 1876) was published by Brady in 1884 and later republished in revised forms by Barker (1960) and Jones (1994). In the early 20th century, Cushman was one of the leading researchers of foraminiferal taxonomy (e.g., Cushman, 1910, 1911, 1914, 1915, 1917, 1918, 1920, 1929, 1930, 1931). The last *magnum opus* on foraminifera dates back to 1988, when Loeblich and Tappan published a comprehensive work about the taxonomy of foraminifera with a description of 878 genera.

The Mediterranean Sea represents a classical region for investigations in foraminiferal taxonomy. D'Orbigny described numerous current taxa from the Mediterranean region in 1826 (Cimerman and Langer, 1991). Further, scientists such as Parker (1958) and Todd (1958) investigated deep sea benthic and planktonic foraminifera from the eastern and western Mediterranean Sea, collected during the Swedish Deep Sea Expedition (1946 - 1948) and the Atlantic cruise 151 (1948). Hofker (1960) investigated in the taxonomy of shallow water benthic foraminifera from the Gulf of Naples.

More recent comprehensive and systematic descriptions were provided by Cimerman and Langer (1991) for the Adriatic and Tyrrhenian Seas, by Sgarrella and Moncharmont Zei (1993) for the Gulf of Naples, and by Rasmussen (2005) for the southern Aegean Sea. Beside these works, there are many additional publications about foraminiferal taxonomy from the

Mediterranean Sea (e.g. Jorissen, 1987; Alberola et al 1987, 1991; Mendes et al., 2004; Frezza & Carboni, 2009), and the Sea of Marmara (e.g. Kaminski et al., 2002; Chendes et al, 2004; Avsar et al., 2006, 2009).

6.2 Materials and methods

This chapter provides a taxonomic summary for a total of 280 Recent, Holocene and late glacial benthic shelf foraminifera from the western Mediterranean Sea, ranging from 20 m to 235 m water depth. A total of 98 living (Rose Bengal stained) species have been identified in the surface samples (electronic Table A.17). In addition, a total of 163, 175 and 173 Recent species, represented by empty tests, have been identified on the Alboran Platform, the Oran Bight and the Mallorca Shelf, respectively (compare Fig. 3.1 and electronic Table A.18). In the sediment-cores 342-1 (Alboran Platform), 367-1 (Oran Bight) and 401-1 (Mallorca Shelf) a total of 172, 178 and 194 late glacial and Holocene species have been identified (compare Fig. 4.1; electronic Tables A.19-A.21). Rare species or species with problematic systematic position have been summarized in higher taxonomic units (genera, families).

The classification of Loeblich and Tappan (1988) provides the basis for the generic classification of this study. Identification on the species level is primarily based on the publications of Cimerman & Langer (1991), Sgarrella & Moncharmont Zei (1993) and Rasmussen (2005). Furthermore, other publications about the Mediterranean Sea were studied (e.g., Hofker, 1950; Parker, 1958; Jorissen, 1987; Alberola et al., 1987, 1991, Mendes et al., 2004; Frezza and Carboni, 2009). Valuable information was also provided by comprehensive taxonomic studies from other areas, such as the Atlantic Ocean (Jones, 2004) or the Red Sea (Hottinger et al., 1993).

In the systematic description, species within the same genus are listed in alphabetical order. The given references include publications that have an extensive list of synonyms, useful illustrations and taxa descriptions. The given remarks contain short morphological descriptions of those species, for which the classification was restricted to family or genus level, and for which no illustrations in the literature were available. Furthermore, annotations on controversial species classifications are given. SEM photographs of 111 taxa, performed with a Zeiss LEO 1455VP, are appended to this chapter.

6.3 Systematic benthic foraminiferal descriptions

Order Foramiferida Eichwald, 1830

Suborder Textulariina Delage & Herouard, 1896

Superfamily: Astrorhizacea Brady, 1881

Family: Bathysiphonidae Arnimelech, 1952

Genus: *Rhabdamminella* de Folin, 1887

***Rhabdamminella cylindrica* (Brady)**

1884 *Marsipella cylindrica* Brady
1910 *Marsipella cylindrica* Brady - Cushman, p. 30, text-figs. 15 & 16
1918 *Marsipella cylindrica* Brady - Cushman, p. 24, Pl. 9, figs. 8 & 9
1988 *Rhabdamminella cylindrica* (Brady) - Loeblich & Tappan, p. 4, Pl. 14, figs. 2 & 3
1994 *Marsipella cylindrica* Brady - Jones, p. 34, Pl. 24, figs. 20-22

Family: Saccamminidae Brady, 1884

Subfamily: Saccammininae Brady, 1884

Genus: *Lagenammina* Rhumbler, 1911

***Lagenammina difflugiformis* (Brady)**

1879 *Reophax difflugiformis* Brady
1910 *Proteonina difflugiformis* (Brady) - Cushman, p. 41, text-figs. 40 & 41
1918 *Proteonina difflugiformis* (Brady) - Cushman, p. 47, Pl. 21, figs. 1 & 2
1945 *Proteonina difflugiformis* (Brady) - Cushman, p. 545, Pl. 71, fig. 1
1960 *Proteonina difflugiformis* (Brady) - Hofker, p. 235, Pl. A, fig. 7
1988 *Lagenammina difflugiformis* (Brady) - Loeblich & Tappan, p. 6, Pl. 21, figs. 7 & 8
1992 *Reophax difflugiformis* Brady - Schiebel, p. 21, Pl. 8, fig. 9
1992 *Lagenammina difflugiformis* (Brady) - Wollenburg, p. 15, Pl. 2, fig. 4
1994 *Lagenammina arenulata* (Skinner) - Jones, p. 37, Pl. 30, fig. 5

Remarks: The test is unilocular and pyriform. The wall is composed of coarse-grained quartz particles that are strongly cemented together. The aperture is terminal on the end of a short neck. This species has been assigned to *Lagenammina difflugiformis* and not to *Lagenammina atlantica* due the visible short neck (Jones, 1994).

Superfamily: Ammodiscacea Reuss, 1862

Family: Ammodiscidae Reuss, 1862

Subfamily: Ammodiscinae Reuss, 1862

Genus: *Ammodiscus* Reuss, 1862

***Ammodiscus minimus* Hoeglund**

1947 *Ammodiscus minimus* Hoeglund
1960 *Ammodiscus minimus* Hoeglund - Hofker, p. 236, Pl. A, fig. 13

Remarks: The specimens have a small and circular test with rounded periphery. The coils are in a single plane and increase in size when added. The wall is finely agglutinated and smooth. The aperture is arch-shaped at the open end of the undivided tube.

Superfamily: Hormosinacea Haeckel, 1894

Family: Hormosinidae Haeckel, 1894

Subfamily: Reophacinae Cushman, 1910

Genus: *Reophax* De Montfort, 1808

***Reophax scorpiurus* De Montfort**

(Pl. 1, fig. 1)

1808 *Reophax scorpiurus* De Montfort
1910 *Reophax scorpiurus* De Montfort - Cushman, p. 83, text-figs. 114-116
1920 *Reophax scorpiurus* De Montfort - Cushman, p. 6, Pl. 1, figs. 5-7
1988 *Reophax scorpiurus* De Montfort - Loeblich & Tappan, p. 13, Pl. 44, figs. 1-3
1991 *Reophax scorpiurus* De Montfort - Cimerman & Langer, p. 17, Pl. 4, figs. 1 & 2
1993 *Reophax scorpiurus* De Montfort - Sgarrella & Moncharmont Zei, p. 156, Pl. 2, figs. 3 & 4
2004 *Reophax scorpiurus* De Montfort - Chendes et al., p. 76, Pl. 1, fig. 2

2009 *Reophax scorpiurus* De Montfort - Avsar et al., p. 134, Pl. 1, figs. 3 & 4

Superfamily: Lituolacea de Blainville, 1827

Family: Haplophragmoididae Maync, 1952

Genus: *Cibrostomoides* Cushman, 1910

***Cibrostomoides jeffreysii* (Williamson)**

(Pl. 1, fig. 3)

1858 *Nonionina jeffreysii* Williamson
1991 *Cibrostomoides jeffreysii* (Williamson) - Alberola et al., p. 80, Pl. 1, figs. 1 & 5
1991 *Labrospira kosterensis* Hoeglund - Cimerman & Langer, p. 18, Pl. 4, figs. 11-13
1992 *Labrospira jeffreysii* (Williamson) - Schiebel, p. 17, Pl. 7, fig. 4
1992 *Cibrostomoides jeffreysii* (Williamson) - Wollenburg, p. 27, Pl. 5, figs. 1 & 4
1993 *Cibrostomoides jeffreysii* (Williamson) - Sgarrella & Moncharmont Zei, p. 157, Pl. 2, figs. 8 & 9
1993 *Labrospira jeffreysii* (Williamson) - Hottinger et al., p. 29, Pl. 2, figs. 5-9
1994 *Veleroninoides jeffreysii* (Williamson) - Jones, p. 41, Pl. 35, figs. 1-3 & 5
2003 *Cibrostomoides jeffreysii* (Williamson) - Murray, p. 11, fig. 2, no. 5

***Cribrostomoides subglobosum* (Sars)**

(Pl. 1, fig. 2)

1869 *Lituola subglobosa* Sars
1910 *Haplophragmoides subglobosa* (Sars) - Cushman, p. 105, text-figs. 162-164
1920 *Haplophragmoides subglobosa* (Sars) - Cushman, p. 45, Pl. 8, fig. 5
1960 *Labrospira nitida* (Goes) - Hofker, p. 236, Pl. A, fig. 14
1991 *Labrospira subglobosa* (Sars) - Cimerman & Langer, p.18, Pl. 5, figs. 1-3
1993 *Cibrosomoides subglobosum* (Sars) - Sgarrella & Moncharmont Zei, p. 157, Pl. 2, figs. 15-16
1994 *Cibrostomoides subglobosus* (Cushman) - Jones, p. 40, Pl. 34, figs. 8-10

Genus: *Haplophragmoides* Cushman, 1910

?*Haplophragmoides* sp. 1

Remarks: The test is involute, planispirally enrolled and subcircular in lateral view. The wall is coarsely agglutinated. The aperture is an equatorial slit at the base of the apertual face. Five to six chambers are visible that gradually increase in size when added.

Family: Discamminidae Mikhalevich, 1980

Genus: *Glaphyrammina* Loeblich & Tappan, 1984

***Glaphyrammina americana* (Cushman)**

1910 *Ammobaculitus americanus* Cushman, p. 118, text-figs. 184 & 185
1920 *Ammobaculitus americanus* Cushman - Cushman, p. 64, Pl. 12, figs. 6 & 7
1888 *Glaphyrammina americana* (Cushman) - Loeblich & Tappan, p. 15, Pl. 51, figs. 7-10
1994 *Glaphyrammina americana* (Cushman) - Jones, p. 40, Pl. 34, figs. 1-4

Superfamily: Verneuilinacea Cushman, 1911

Family: Verneuilinidae Cushman, 1911

Subfamily: Verneuilininae Cushman, 1911

Genus: *Gaudryina* d'Orbigny, 1839

***Gaudryina rudis* Wright**

(Pl. 1, fig. 4)

1900 *Gaudryina rudis* Wright
1987 *Gaudryina rudis* Wright - Alberola et al., p. 305, Pl. 2, figs. 8 & 9
1991 *Connemarella rudis* (Wright) - Cimerman & Langer, p. 23, Pl. 8, figs. 1-4
2003 *Gaudryina rudis* Wright - Murray, p.13, fig. 2, no. 12 & 13

***Gaudryina siciliana* Cushman**

(Pl. 1, figs. 5 & 6)

1936 *Gaudryina siciliana* Cushman
1993 *Sahulia* cf. *S. barkeri* Hofker - Hottinger et al., p. 33, Pl. 8, figs. 7-11
1993 *Connemarella rudis* (Wright) - Sgarrella & Moncharmont Zei, p. 167, Pl. 4, figs. 6-7
2005 *Gaudryina siciliana* Cushman - Rasmussen, p. 55, Pl. 1, figs. 7 & 8

Superfamily: Trochamminacea Schwager, 1877

Family: Trochamminidae Schwager, 1877

Subfamily: Polystomammininae Broennimann & Beurlen, 1977

Genus: *Deuterammina* Broennimann, 1976

***Deuterammina dublinensis* Broennimann and Whittaker**

1983 *Deuterammina dublinensis* Broennimann & Whittaker
1988 *Deuterammina dublinensis* Broennimann & Whittaker - Loeblich & Tappan, p. 131, Pl. 135, figs. 1-5

Subfamily: Trochammininae Schwager, 1877

Genus: *Polystomammina* Seigli, 1965

***Polystomammina nitida* (Brady)**

1881 *Trochammina nitida* Brady
1920 *Trochammina nitida* Brady - Cushman, p. 75, Pl. 15, fig. 2
1988 *Polystomammina nitida* (Brady) - Loeblich & Tappan, p. 35, Pl. 135, figs. 6-9

Genus: *Ammoglobigerina* Eimer & Fickert, 1899

***Ammoglobigerina globigeriniformis* (Parker & Jones)**

(Pl. 1, fig. 7)

1865 *Lituola nautiloidea* Lamarck var. *globigeriformes* Parker & Jones
1910 *Trochammina globigeriformis* (Parker & Jones) - Cushman, p. 124, text-figs. 193-195
1920 *Trochammina globigeriformis* (Parker & Jones) - Cushman, p. 78, Pl. 16, figs. 5 & 6
1987 *Trochammina globigeriformis* (Parker & Jones) - Alberola et al., p. 305, Pl. 2, figs. 4 & 5
1988 *Ammoglobigerina globigeriformis* (Parker & Jones) - Loeblich & Tappan, p. 33, Pl. 128, figs. 9 & 10
1991 *Ammoglobigerina globigeriformis* (Parker & Jones) - Cimerman & Langer, p. 20, Pl. 7, figs. 4-6
1992 *Trochammina globigeriformis* (Parker & Jones) - Schiebel, p. 63, Pl. 7, fig. 9
1993 *Trochammina globigeriformis* (Parker & Jones) - Sgarrella & Moncharmont Zei, p. 161, Pl. 3, figs. 9 & 10

Genus: *Tritaxis* Schubert, 1921

***Tritaxis challengeri* (Hedley, Hurdle & Burdet)**

1964 *Trochammina challengeri* Hedley, Hurdle & Burdet
1994 *Tritaxis challengeri* (Hedley, Hurdle & Burdet) - Jones, p. 46, Pl. 41, fig. 3

Remarks: The test is planoconvex and trochospirally enrolled with a few whorls. Three chambers per whorl are visible. Sutures are radial and oblique on the spiral side. The final chamber occupies about one-half of the face of the umbilical side. The wall is agglutinated and imperforate. The aperture is interiomarginal.

Superfamily: Textulariacea Ehrenberg, 1838

Family: Eggerellidae Cushman, 1937

Subfamily: Eggerellinae Cushman, 1937

Genus: *Eggerelloides* Haynes, 1973

***Eggerelloides scabrus* (Williamson)**

(Pl. 1, fig. 8)

1958 *Bulimina scabra* Williamson
1960 *Eggerella scabra* (Williamson) - Hofker, p. 236, Pl. A, figs. 11 & 12
1988 *Eggereloides scabrus* (Williamson) - Loeblich & Tappan, p. 48, Pl. 189, figs. 5-7
1991 *Eggerella scabra* (Williamson) - Alberola et al., p. 80, Pl. 1, fig. 2
1995 *Eggereloides scabrus* (Williamson) - Coppa & Di Tuoro, p. 166, Pl. 1, fig. 5
1992 *Eggerelloides scabra* (Williamson) - Schiebel, p. 16, Pl. 8, fig. 4
1993 *Eggerella scabra* (Williamson) - Sgarrella & Moncharmont Zei, p. 162, Pl. 4, fig. 13
2003 *Eggerelloides scaber* (Williamson) - Murray, p. 13, fig. 2, no. 11
2004 *Eggerelloides scaber* (Williamson) - Chendes, p. 76, Pl. 1, fig. 4
2004 *Eggerelloides scaber* (Williamson) - Mendes et al., p. 178, Pl. 1, fig. 3
2009 *Eggerelloides scabrus* (Williamson) - Avsar et al., p. 134, Pl. 1, fig. 7
2009 *Eggerelloides scabrus* (Williamson) - Frezza & Carboni, p. 55 & 47, Pl. 1, fig. 8; Pl. 2, fig. 10

Family: Textulariidae Ehrenberg, 1838

Subfamily: Textulariinae Ehrenberg, 1838

Genus: *Bigenerina* d'Orbigny, 1826

***Bigenerina nodosaria* d'Orbigny**

(Pl. 1, fig. 9)

1826 *Bigenerina nodosaria* d'Orbigny
1911 *Bigenerina nodosaria* d'Orbigny - Cushman, p. 27, text-figs. 46-48

1960 *Bigenerina nodosaria* d'Orbigny - Hofker, p. 238, Pl. A, figs. 19 & 20
1987 *Bigenerina nodosaria* d'Orbigny - Alberola et al., p. 304, Pl. 1, fig. 1
1987 *Bigenerina nodosaria* d'Orbigny - Jorissen, p. 34, Pl. 1, fig. 10
1988 *Bigenerina nodosaria* d'Orbigny - Loeblich & Tappan, p. 48, Pl. 191, figs. 1 & 2
1991 *Bigenerina nodosaria* d'Orbigny - Cimerman & Langer, p. 21, Pl. 9, figs. 1-6
1993 *Bigenerina nodosaria* d'Orbigny - Sgarrella & Moncharmont Zei, p. 164, Pl. 4, fig. 12
1994 *Bigenerina nodosaria* d'Orbigny - Jones, p. 49, Pl. 44, figs. 14-18
2002 *Bigenerina nodosaria* d'Orbigny - Kaminski et al., p. 170, Pl. 1, fig. 9
2003 *Bigenerina nodosaria* d'Orbigny - Murray, p. 11, fig. 2, no. 4
2004 *Bigenerina nodosaria* d'Orbigny - Chendes et al., p. 76, Pl. 1, fig. 5
2005 *Bigenerina nodosaria* d'Orbigny - Rasmussen, p. 56, Pl. 1, figs. 12 & 13
2009 *Bigenerina nodosaria* d'Orbigny - Avsar et al., p. 134, Pl. 1, fig. 8

Genus: *Sahulia* Loeblich & Tappan, 1985

Sahulia cf. *S. kerimbaensis* (Said)

1949 *Textularia kerimbaensis* Said
1993 *Sahulia kerimbaensis* (Said) - Hottinger et al., p. 34, Pl. 9, figs. 8-12

Genus: *Textularia* Defrance, 1824

Textularia agglutinans d'Orbigny

(Pl. 1, fig. 10)

1839 *Textularia agglutinans* d'Orbigny
1911 *Textularia agglutinans* d'Orbigny - Cushman, p. 9, text-fig. 10
1932 *Textularia agglutinans* d'Orbigny - Cushman, p. 10, Pl. 2, figs. 5-7
1960 *Textularia agglutinans* d'Orbigny - Hofker, p. 237, Pl. A, fig. 18
1987 *Textularia agglutinans* d'Orbigny - Alberola et al., p. 304, Pl. 1, fig. 13; Pl. 2, fig. 1
1991 *Textularia agglutinans* d'Orbigny - Alberola et al., p. 80, Pl. 1, fig. 3
1991 *Textularia agglutinans* d'Orbigny - Cimerman & Langer, p. 21, Pl. 10, figs. 1 & 2
1993 *Textularia agglutinans* d'Orbigny - Hottinger et al., p. 36, Pl. 13, figs. 1-9
1994 *Textularia agglutinans* d'Orbigny - Jones, p. 48, Pl. 43, figs. 1-3

Remarks: *Textularia agglutinans* shown in Hottinger et al. (1993) and Jones (1994) differs from that shown by the other authors and the specimens in this work.

Textularia calva Lalicker

1935 *Textularia calva* Lalicker
1958 *Textularia calva* Lalicker - Parker, p. 254, Pl. 1, fig. 4
1991 *Textularia bocki* (Hoeglund) - Cimerman & Langer, p. 21, Pl. 10, fig. 6
2002 *Textularia bocki* (Hoeglund) - Kaminski et al., p. 170, Pl. 1, figs. 1 & 2
1993 *Textularia calva* Lalicker - Sgarrella & Moncharmont Zei, p. 164, Pl. 3, fig. 11
2005 *Textularia gramen* d'Orbigny - Rasmussen, p. 56, Pl. 1, fig. 17

Textularia conica d'Orbigny

1839 *Textularia conica* d'Orbigny
1932 *Textularia conica* d'Orbigny - Cushman, p. 11, Pl. 2, figs. 8-10; Pl. 3, figs. 1-3
1958 *Textularia conica* d'Orbigny - Parker, p. 254, Pl. 1, figs. 5 & 6
1991 *Textularia conica* d'Orbigny - Cimerman & Langer, p. 22, Pl. 10, figs. 7-9
1993 *Textularia conica* d'Orbigny - Sgarrella & Moncharmont Zei, p. 166, Pl. 3, figs. 4 & 5
2005 *Textularia conica* d'Orbigny - Rasmussen, p. 56, Pl. 1, figs. 14 & 15

Textularia gramen d'Orbigny

1846 *Textularia gramen* d'Orbigny, p. 248, Tab. 15, figs. 4-6
1911 *Textularia gramen* d'Orbigny - Cushman, p. 8, text-figs. 6-9
1991 *Textularia bocki* Hoeglund - Cimerman & Langer, p. 21, Pl. 10, fig. 5
2002 *Textularia* sp. - Kaminski et al., p. 170, Pl. 1, figs. 8 a & b
2009 *Textularia bocki* Hoeglund - Avsar et al., p. 134, Pl. 1, figs. 9 & 10

Textularia pala Czjzek

(Pl. 1, fig. 11)

1848 *Textularia pala* Czjzek
1991 *Textularia truncata* Hoeglund - Cimerman & Langer, p. 22, Pl. 12, figs. 1-3
1993 *Textularia pala* Czjzek - Sgarrella & Moncharmont Zei, p. 166, Pl. 3, fig. 8

Textularia pseudorugosa Lacroix

(Pl. 1, fig. 12)

1932 *Textularia pseudorugosa* Lacroix

1991 *Textularia pseudorugosa* Lacroix - Cimerman & Langer, p. 22, Pl. 11, figs. 5-8
1993 *Textularia pseudorugosa* Lacroix - Sgarrella & Moncharmont Zei, p. 166, Pl. 3, figs. 6 & 7
1995 *Textularia pseudorugosa* Lacroix - Coppa & Di Tuoro, p. 166, Pl. 1, fig. 8

Subfamily: Siphotextularinnae Loeblich & Tappan, 1985

Genus: *Siphotextularia* Finlay, 1939

***Siphotextularia concava* (Karrer)**

(Pl. 1, fig. 13)

1868 *Plecanium concavum* Karrer
1911 *Textularia concava* (Karrer) - Cushman, p. 22, text-fig. 38
1932 *Textularia concava* (Karrer) - Cushman, p. 13, Pl. 3, fig. 6
1991 *Siphotextularia concava* (Karrer) - Cimerman & Langer, p. 23, Pl. 12, figs. 4-6
1993 *Siphotextularia concava* (Karrer) - Sgarrella & Moncharmont Zei, p. 166, Pl. 3, fig. 12
1994 *Siphotextularia concava* (Karrer) - Jones, p. 47, Pl. 42, figs. 13 & 14
2005 *Siphotextularia concava* (Karrer) - Rasmussen, p. 58, Pl. 2, fig. 6

***Siphotextularia flintii* Cushman**

(Pl. 1, fig. 14)

1911 *Textularia flintii* Cushman, p. 21, text-fig. 36
1987 *Siphotextularia flintii* (Cushman) - Aberola et al., p. 304, Pl. 1, figs. 9 & 10
1992 *Siphotextularia bermudezi* Mikhalevich - Schiebel, p. 25, Pl. 6, fig. 16
2003 *Siphotextularia flintii* (Cushman) - Murray, p. 15, fig. 3, no. 11
2009 *Siphotextularia concava* (Karrer) - Avsar et al., p. 134, Pl. 1, fig. 11

Family: Pseudogaudryinidae Loeblich & Tappan, 1985

Subfamily: Pseudogaudryininae Loeblich & Tappan, 1985

Genus: *Pseudoclavulina* Cushman, 1936

***Pseudoclavulina crustata* Cushman**

(Pl. 1, fig. 15)

1936 *Pseudoclavulina crustata* Cushman
1958 *Pseudoclavulina crustata* Cushman - Parker, p. 254, Pl. 1, fig. 7
1960 *Pseudoclavulina crustata* Cushman - Hofker, p. 239, Pl. A, figs. 27 & 28
1987 *Pseudoclavulina crustata* Cushman - Jorissen, p. 34, Pl. 1, fig. 1
1991 *Pseudoclavulina crustata* Cushman - Cimerman & Langer, p. 23, Pl. 11, figs. 9 & 10
1993 *Clavulina crustata* (Cushman) - Sgarrella & Moncharmont Zei, p. 167, Pl. 4, fig. 10

Family Valvulinidae Berthelin, 1880

Subfamily: Valvulininae Berthelin, 1880

Genus: *Clavulina* d'Orbigny, 1826

***Clavulina cylindrica* (Cushman)**

1922 *Bigenerina cylindrica* Cushman
1960 *Goesella obscura* (Chaster) - Hofker, p. 236, Pl. A, fig. 15
1993 *Bigenerina cylindrica* Cushman - Sgarrella & Moncharmont Zei, p. 164, Pl. 4, fig. 11

Remarks: This species has been assigned to the genus *Clavulina* due to its morphological characteristics following Loeblich & Tappan (1988).

Superfamily: Spiroplectamminacea Cushman, 1927

Family: Spiroplectamminidae Cushman, 1927

Subfamily: Spiroplectammininae Cushman, 1927

Genus: *Spiroplectinella* Kisel'man, 1972

***Spiroplectinella sagittula* s.l. (Defrance)**

(Pl. 1, figs. 16 & 17)

1824 *Textularia sagittula* Defrance
1960 *Spiroplectammina sagittula* (Defrance) - Hofker, p. 237, Pl. A, fig. 17
1987 *Spiroplectammina wrightii* (Silvestri) - Alberola et al., p. 304, Pl. 1, figs. 11 & 12
1987 *Textularia sagittula* Defrance - Jorissen, p. 41, Pl. 3, fig. 12
1988 *Spiroplectinella wrightii* (Silvestri) - Loeblich & Tappan, p. 30, Pl. 120, figs. 1-10
1991 *Spiroplectinella sagittula* (d'Orbigny) - Cimerman & Langer, p. 19, Pl. 6, figs. 5 & 6
1992 *Spiroplectinella sagittula* (Defrance) - Schiebel, p. 26, Pl. 6, fig. 14
2002 *Spirorutilus* sp. - Kaminski et al., p. 171, Pl. 1, figs. 3 & 4
2005 *Textularia sagittula* Defrance - Rasmussen, p. 57, Pl. 2, fig. 3

2009 *Spiroplectinella sagittula* (d'Orbigny) - Avsar et al., p. 134, Pl. 1, fig. 5

Remarks: There is some confusion about *Textularia sagittula* Defrance and *Spiroplectinella sagittula* (d'Orbigny) in the literature. *Spiroplectinella sagittula* s.l. in this work contains also species shown as *Spiroplectinella wrightii* in Cimerman & Langer (1991, p. 20, Pl. 6, figs. 1-4).

***Spiroplectinella* sp. 1**

Remarks: This species has a planispiral initial stage and a more compact test than *Spiroplectinella sagittula* with a low slit at the base of the final chamber. Further, it differs from *S. sagittula* due to the lower number of chambers. A juvenile stage of *S. sagittula* cannot be excluded.

***Spiroplectinella* sp. 2**

2002 *Textularia* sp. - Kaminski, p. 171, Pl. 1, fig. 7
2004 *Textularia* sp. - Chendes et al., p. 76, Pl. 1, fig. 7
2006 *Spiroplectinella sagittula* (d'Orbigny) - Asvar et al., p. 132, Pl. 1, fig. 1

Remarks: This species has a smaller early planispiral stage when compared to *Spiroplectinella sagittula*. The chambers show a stronger increase when added. The test is more angular in outline than that of *S. sagittula.*

Suborder Involutinina Hohenegger & Piller, 1977

Family Planispirillinidae Piller, 1978
Genus *Trocholinopsis* Piller, 1983

***Trocholinopsis porosuturalis* Piller**

1983 *Trocholinopsis porosuturalis* Piller
1988 *Trocholinopsis porosuturalis* Piller - Loeblich & Tappan, p. 83, Pl. 316, figs. 12-17

Suborder Spirillinina Hohenegger & Piller, 1975

Family: Spirillinidae Reuss & Fritsch, 1861

***Spirillinid* sp. 1**

1993 *Spirillinid* genus? sp. A - Hottinger et al., p. 75, Pl. 87, figs. 1-6

Genus: *Sejunctella* Loeblich & Tappan, 1957

Sejunctella* cf. *S. lateseptata

1875 *Spirillina lateseptata* Terquem
1931 *Spirillina lateseptata* Terquem - Cushman, p. 6, Pl. 1, fig. 12 & 13; Pl. 2, fig. 1
1988 *Sejunctella lateseptata* (Terquem) - Loeblich & Tappan, p. 83, Pl. 318, fig. 8
1993 *Sejunctella*? sp. A - Hottinger et al., p. 74, Pl. 85, figs. 6-8

Remarks: The species in this work differ from that shown in Cushman (1931) and Loeblich & Tappan (1988) by the presence of numerous larger pores on the convex side.

***Sejunctella* sp. 1**

Remarks: This species has a discoidal test with a hyaline wall. On the keel, it has relatively short spines. One side is perforate, and the other side is imperforate. The aperture is a simple rounded opening at the end of the tubular chamber.

Genus: *Spirillina* Ehrenberg, 1843

***Spirillina limbata* Brady**

(Pl. 1, fig. 19)

1884 *Spirillina limbata* Brady
1991 *Spirillina limbata* Brady - Cimerman & Langer, p. 24, Pl. 14, figs. 1-3
1994 *Spirillina limbata* Brady - Jones, p. 92, Pl. 85, figs. 18-21

Remarks: The specimens shown in Jones (1994) differ from that shown in Cimerman & Langer (1991) by more numerous coils. The specimens in this work resemble that shown in Cimerman & Langer (1991).

***Spirillina vivipara* Ehrenberg**

(Pl. 1, fig. 18)

1841 *Spirillina vivipara* Ehrenberg
1931 *Spirillina vivipara* Ehrenberg - Cushman, p. 3, Pl. 1, figs. 1-4
1958 *Spirillina vivipara* Ehrenberg - Parker, p. 264, Pl. 3, fig. 4
1960 *Spirillina vivipara* Ehrenberg - Hofker, p. 252, Pl. D, fig. 109
1988 *Spirillina vivipara* Ehrenberg - Loeblich & Tappan, p. 83, Pl. 318, figs. 4-7
1991 *Spirillina vivipara* Ehrenberg - Cimerman & Langer, p. 24, Pl. 14, fig. 6
1992 *Spirillina vivipara* Ehrenberg - Schiebel, p. 69, Pl. 5, fig. 16
1994 *Spirillina vivipara* Ehrenberg - Jones, p. 92, Pl. 85, figs. 1-4

***Spirillina wrightii* Heron-Allen & Earland**

(Pl. 1, fig. 20)

1930 *Spirillina wrightii* Heron-Allen & Earland
1958 *Spirillina wrightii* Heron-Allen & Earland - Parker, p. 264, Pl. 3, figs. 1-3

Remarks: This species is very similar to *Spirillina limbata*, but in difference it shows tubercles on one side.

Family: Patellinidae Rhumbler, 1906

Subfamily: Patellininae Rhumbler, 1906

Genus: *Patellina* Williamson, 1858

***Patellina corrugata* Williamson**

1858 *Patellina corrugata* Williamson
1931 *Patellina corrugata* Williamson - Cushman, p. 11, Pl. 2, figs. 6 & 7
1988 *Patellina corrugata* Williamson - Loeblich & Tappan, p. 84, Pl. 320, figs. 7-14
1991 *Patellina corrugata* Williamson - Cimerman & Langer, p. 24, Pl. 14, figs. 7-12
1993 *Patellina corrugata* Williamson - Hottinger et al., p. 76, Pl. 87, figs. 7-11
1994 *Patellina corrugata* Williamson - Jones, p. 93, Pl. 86, figs. 1-7
2003 *Patellina corrugata* Williamson - Murray, p. 24, fig. 9, no. 6 & 7

Suborder Miliolina Delage & Herouard, 1896

Superfamily: Cornuspiracea Schultze, 1854

Family: Cornuspiridae Schultze, 1854

Subfamily: Cornuspirinae Schultze, 1854

Genus: *Cornuspira* Schultze, 1854

***Cornuspira foliacea* (Philippi)**

1844 *Orbis foliaceus* Philippi
1865 *Cornuspira foliacea* (Philippi) - Reuss, p. 5, Pl. 1, figs. 8 & 9
1917 *Cornuspira foliacea* (Philippi) - Cushman, p. 24, Pl. 1, fig. 1; Pl. 2, fig. 2
1929 *Cornuspira foliacea* (Philippi) - Cushman, p. 79, Pl. 20, figs. 3-5
1960 *Cornuspiroides foliaceum* (Phillipi) - Hofker, p. 240, Pl. B, fig. 34
1991 *Cornuspira foliacea* (Philippi) - Cimerman & Langer, p. 24, Pl. 15, figs. 1-3
1994 *Cornuspira foliacea* (Philippi) - Jones, p. 27, Pl. 11, figs. 5-6
2005 *Cornuspira foliacea* (Philippi) - Rasmussen, p. 59, Pl. 3, fig. 3

***Cornuspira involvens* (Reuss)**

1850 *Operculina involvens* Reuss
1917 *Cornuspira involvens* (Reuss) - Cushman, p. 25, Pl. 1, fig. 2; Pl. 2, fig. 2
1929 *Cornuspira involvens* (Reuss) - Cushman, p. 80, Pl. 20, figs. 6 & 8
1932 *Cornuspira involvens* (Reuss) - Cushman, p. 67, Pl. 16, fig. 2
1991 *Cornuspira involvens* (Reuss) - Cimerman & Langer, p. 25, Pl. 15, figs. 4-7
1994 *Cornuspira involvens* (Reuss) - Jones, p. 26, Pl. 11, figs. 1-3
1995 *Cyclogira involvens* (Reuss) - Coppa & Di Tuoro, p. 166, Pl. 1, fig. 9
2003 *Cornuspira involvens* (Reuss) - Murray, p. 15, fig. 4. no. 5

Family: Fischerinidae Millett, 1898

Subfamily: Fischerininae Millett, 1898

Genus: *Trisegmentina* Wiesner, 1920

***Trisegmentina compressa* Wiesner**

1923 *Trisegmentina compressa* Wiesner
1988 *Trisegmentina compressa* Wiesner - Loeblich & Tappan, p. 87, Pl. 329, figs. 7-9

1991 *Trisegmentina compressa* Wiesner - Cimerman & Langer, p. 25, Pl. 15, figs. 9-11
1993 *Fischerina compressa* (Wiesner) - Sgarrella & Moncharmont Zei, p. 168, Pl. 6, fig. 15

Subfamily: Nodobacullariellinae Bogdanovich, 1981

Genus: *Vertebralina* d'Orbigny, 1826

***Vertebralina striata* d'Orbigny**

1826 *Vertebralina striata* d'Orbigny
1917 *Vertebralina striata* d'Orbigny - Cushman, p. 38, Pl. 22, figs. 3 & 4
1932 *Vertebralina striata* d'Orbigny - Cushman, p. 73, Pl. 10, figs. 8-10
1988 *Vertebralina striata* d'Orbigny - Loeblich & Tappan, p. 87, Pl. 330, figs. 17-19
1991 *Vertebralina striata* d'Orbigny - Cimerman & Langer, p. 25, Pl. 16, figs. 1-5
1993 *Vertebralina striata* d'Orbigny - Sgarrella & Moncharmont Zei, p. 169, Pl. 6, fig. 7
1993 *Vertebralina striata* d'Orbigny - Hottinger et al., p. 43, Pl. 23, figs. 8-15
1994 *Vertebralina striata* d'Orbigny - Jones, p. 28, Pl. 12, figs. 12-14

Genus: *Wiesnerella* Cushman, 1933

***Wiesnerella auriculata* (Egger)**

1893 *Planispira auriculata* Egger
1929 *Planispirina auriculata* (Egger) - Cushman, p. 93, Pl. 22, fig. 3
1932 *Planispirina auriculata* (Egger) - Cushman, p. 72, Pl. 16, fig. 6
1988 *Wiesnerella auriculata* (Egger) - Loeblich & Tappan, p. 87, Pl. 330, figs. 11-13
1993 *Wiesnerella auriculata* (Egger) - Hottinger et al., p. 43, Pl. 24, figs. 1-4

Family: Nubeculariidae Jones, 1875

Subfamily: Nubecularrinae Jones, 1875

Genus: *Nubecularia* Defrance, 1825

***Nubecularia lucifuga* Defrance**

1825 *Nubecularia lucifuga* Defrance
1917 *Nubecularia lucifuga* Defrance - Cushman, p. 41, Pl. 8, fig. 6
1960 *Nubecularia lucifuga* Defrance - Hofker, p. 244, Pl. C, fig. 62
1988 *Nubecularia lucifuga* Defrance - Loeblich & Tappan, p. 88, Pl. 332, figs. 1-3
1991 *Nubecularia lucifuga* Defrance - Cimerman & Langer, p. 26, Pl. 17, figs. 5-7

Genus *Nubeculina* Cushman, 1924

***Nubeculina divaricata* (Brady)**

1879 *Sagrina divaricata* Brady
1932 *Nubeculina divaricata* (Brady) - Cushman, p. 48, Pl. 11, figs. 5 & 6
1988 *Nubeculina divaricata* (Brady) - Loeblich & Tappan, p. 88, Pl. 331, figs. 13 & 14
1991 *Nubeculina divaricata* (Brady) - Cimerman & Langer, p. 25, Pl. 16, figs. 6-10

Family: Ophthalmidiidae Wiesner, 1920

Genus: *Ophthalmidium* Kübler & Zwingli, 1870

***Ophthalmidium acutimargo* (Brady)**

1884 *Spiroloculina acutimargo* Brady
1988 *Spirophthalmidium acutimargo* (Brady) - Loeblich & Tappan, p. 336, Pl. 334, figs. 10 & 11
1991 *Spirophthalmidium acutimargo* (Brady) - Cimerman & Langer, p. 26, Pl. 17, figs. 11-13
1993 *Ophthalmidium acutimargo* (Brady) - Sgarrella & Moncharmont Zei, p. 168, Pl. 5, figs. 1 & 2
1994 *Spirophthalmidium acutimargo* (Brady) - Jones, p. 26, Pl. 10, fig. 13

***Ophthalmidium* sp. 1**

Remarks: The test is oval and flattened in lateral view, with a carinate periphery. The globular proloculus is followed by a narrow tubular flexostyle. Later chambers are broader at the base and tapering towards the aperture. The wall is porcelaneous and imperforate. The rounded aperture is on the end of a neck and has a lip, but no tooth was visible.

Superfamily: Miliolacea Ehrenberg, 1839

Family: Spiroloculinidae Wiesner, 1920

Genus: *Adelosina* d'Orbigny, 1826

***Adelosina dubia* (d'Orbigny)**

1826 *Triloculina dubia* d'Orbigny
1991 *Adelosina dubia* (d'Orbigny) - Cimerman & Langer, p. 26, Pl. 18, figs. 5-7

***Adelosina intricata* (Terquem)**

1878 *Quinqueloculina intricata* Terquem
1991 *Adelosina intricata* (Terquem) - Cimerman & Langer, p. 27, Pl. 18, figs. 9-10
1993 *Adelosina intricata* (Terquem) - Sgarrella & Moncharmont Zei, p. 178, Pl. 8, figs. 4 & 5
1994 *Adelosina intricata* (Terquem) - Jones, p. 22, Pl. 6, figs. 11 & 12

***Adelosina italica* (Terquem)**

1878 *Quinqueloculina italica* Terquem
1993 *Adelosina italica* (Terquem) - Sgarrella & Moncharmont Zei, p. 179, Pl. 7, figs. 13 & 14

***Adelosina laevigata* d'Orbigny**

1825 *Adelosina laevigata* d'Orbigny
1846 *Adelosina laevigata* d'Orbigny - D'Orbigny, p. 302, Tab. 20, figs. 22-24
1988 *Adelosina laevigata* d'Orbigny - Loeblich & Tappan, p. 90, Pl. 337, figs. 5-12

***Adelosina longirostra* (d'Orbigny)**

1826 *Quinqueloculina longirostra* d'Orbigny
1846 *Quinqueloculina longirostra* d'Orbigny - D'Orbigny, p. 291, Tab. 18, figs. 25-27
2005 *Adelosina longirostra* (d'Orbigny) - Rasmussen, p. 60, Pl. 3, figs. 7 & 8

***Adelosina mediterranensis* (Le Calvez & Le Calvez)**

(Pl. 2, fig. 2)

1958 *Quinqueloculina mediterranensis* Le Calvez & Le Calvez
1987 *Quinqueloculina mediterranensis* Le Calvez & Le Calvez - Alberola et al., p. 306, Pl. 3, fig. 8
1991 *Adelosina mediterranensis* (Le Calvez & Le Calvez) - Cimerman & Langer, p. 28, Pl. 19, figs. 1-16
1993 *Adelosina mediterranensis* (Le Calvez & Le Calvez) - Sgarrella & Moncharmont Zei, p. 179, Pl. 7, figs. 9-11
2005 *Adelosina mediterranensis* (Le Calvez & Le Calvez) - Rasmussen, p. 60, Pl. 3, fig. 6
2009 *Adelosina mediterranensis* (Le Calvez & Le Calvez) - Avsar et al., p. 134, Pl. 1, fig. 14

***Adelosina* sp.1**

(Pl. 2, fig. 1)

1991 *Adelosina* sp. 1 - Cimerman & Langer, p. 28, Pl. 21, fig. 1 (juvenile specimen)
1994 *Miliolid juvenaria* - Jones, p. 19, Pl. 3, fig. 11

Remarks: This species is a juvenile *Adelosina* form with a megalospheric proloculus followed by a embracing and planispirally enrolled second chamber provided with a neck. No further determination is possible.

Genus: *Spiroloculina* d'Orbigny, 1826

***Spiroloculina dilatata* d'Orbigny**

1846 *Spiroloculina dilatata* d'Orbigny, p. 271, Pl. 16, figs. 16-18
1991 *Spiroloculina dilatata* d'Orbigny - Cimerman & Langer, p. 30, Pl. 22, figs. 5-8

***Spiroloculina excavata* d'Orbigny**

(Pl. 2, fig. 3)

1846 *Spiroloculina excavata* d'Orbigny, p. 271, Tab. 16, figs. 19-21
1960 *Spiroloculina excavata* d'Orbigny - Hofker, p. 239, Pl. A, fig. 30
1987 *Spiroloculina excavata* d'Orbigny - Alberola et al., p. 306, Pl. 2, fig. 11
1991 *Spiroloculina excavata* d'Orbigny - Cimerman & Langer, p. 30, Pl. 23, figs.1-3
1993 *Spiroloculina excavata* d'Orbigny - Sgarrella & Moncharmont Zei, p. 169, Pl. 5, fig. 6
2002 *Spiroloculina excavata* d'Orbigny - Kaminski et al., p. 170, Pl. 1, fig. 11
2003 *Spiroloculina excavata* d'Orbigny - Murray, p. 17, fig. 4, no. 13 & 14
2004 *Spiroloculina excavata* d'Orbigny - Chendes et al., p. 76, Pl. 1, fig. 9
2005 *Spiroloculina excavata* d'Orbigny - Rasmussen, p. 61, Pl. 3, fig. 11
2006 *Spiroloculina excavata* d'Orbigny - Avsar et al., p. 132, Pl. 1, fig. 3
2009 *Spiroloculina excavata* d'Orbigny - Avsar et al., p. 134, Pl. 1, fig. 16

***Spiroloculina* cf. *S. rostrata* Reuss**

1850 *Spiroloculina rostrata* Reuss
1993 cf. *Spiroloculina rostrata* Reuss - Sgarrella & Moncharmont Zei, p. 169, Pl. 5, fig. 5

Remarks: The specimens in this work differ from that shown in Sgarrella & Moncharmont Zei (1993) due to their shorter necks. The aperture is nearly rounded with a rim and provided with a short tooth.

***Spiroloculina tenuiseptata* Brady**

(Pl. 2, fig. 4)

1884 *Spiroloculina tenuiseptata* Brady
1958 *Spiroloculina canaliculata* d'Orbigny - Parker, p. 257, Pl. 1, figs. 26-28
1960 *Spiroloculina canaliculata* d'Orbigny - Hofker, p. 240, Pl. A, fig. 32
1987 *Spiroloculina canaliculata* d'Orbigny - Alberola et al., p. 306, Pl. 2, fig. 16
1991 *Spiroloculina tenuiseptata* Brady - Cimerman & Langer, p. 31, Pl. 24, figs. 6-9
1993 *Spiroloculina tenuiseptata* Brady - Sgarrella & Moncharmont Zei, p. 169, Pl. 5, fig. 7
1994 *Spiroloculina tenuiseptata* Brady - Jones, p. 26, Pl. 10, figs. 5 & 6
2002 *Spiroloculina tenuiseptata* Brady - Kaminski et al., p. 170, Pl. 1, fig. 10
2005 *Spiroloculina tenuiseptata* Brady - Rasmussen, p. 61, Pl. 3, fig. 12

***Spiroloculina* sp. 1**

Remarks: The test is ovate in lateral view. The proloculus is followed by a second chamber of one whorl in length. The periphery margin is broad. The wall is porcelaneous and imperforate. The aperture, at the open end, is relatively broad and oval. This species is likely a juvenile stage of *Spiroloculina excavata*.

***Spiroloculina* sp. 2**

Remarks: The test is fusiform in side view, biconcave in end view, and evolute. The wall is porcelaneous and imperforate with a slightly rough test surface. The aperture is rounded with a rim and provided with a short bifite tooth.

***Spiroloculina* sp. 3**

Remarks: The test is fusiform in outline, biconcave in end view, and evolute. The wall is porcelaneous and imperforate with a slightly rough test surface. The aperture is rounded with a small rim and, provided with a relatively short bifite tooth.

Family: Hauerinidae Schwager, 1876

***Miliolid* sp. 1**

(Pl. 2, fig. 5)

Remarks: The test of these small specimens is nearly rounded and partly ornamented with longitudinal striae. The periphery margin is carinate in lateral view. Three chambers are visible from one side, and two from the other side. The wall is porcelaneous and imperforate. The terminal aperture is oval and bordered by a rim, provided with a short simple tooth. These specimens have been assigned to the Hauerinidae and not to the Miliolidae, due to the absence of pseudopores defined by Loeblich and Tappan (1988) for the latter family.

***Miliolid* sp. 2**

(Pl. 2, fig. 6)

Remarks: The test of these small specimens is oval, with a rounded periphery margin in lateral view. Three chambers are visible on both sides. The wall is porcelaneous and imperforate. The terminal aperture is oval. The tooth is long, but mostly broken. These specimens have been assigned to the Hauerinidae and not to the Miliolidae, due to the absence of pseudopores defined by Loeblich and Tappan (1988) for the latter family.

Subfamily: Siphonapertinae Saidova, 1975
Genus: *Siphonaperta* Vella, 1957

***Siphonaperta agglutinans* (d'Orbigny)**

(Pl. 2, fig. 7)

1839 *Quinqueloculina agglutinans* d'Orbigny
1929 *Quinqueloculina agglutinans* d'Orbigny - Cushman, p. 22, Pl. 1, fig. 1

1991 *Siphonaperta agglutinans* (d'Orbigny) - Cimerman & Langer, p. 31, Pl. 25, figs. 1-3
1993 *Siphonaperta agglutinans* (d'Orbigny) - Hottinger et al., p. 62, Pl. 61, figs. 10 & 11; Pl. 62, figs. 1-3

***Siphonaperta aspera* (d'Orbigny)**

1826 *Quinqueloculina aspera* d'Orbigny
1987 *Quinqueloculina aspera* d'Orbigny - Jorissen, p. 40, Pl. 3, fig. 2
1991 *Siphonaperta aspera* (d'Orbigny) - Cimerman & Langer, p. 31, Pl. 25, figs. 4-6
1993 *Siphonaperta aspera* (d'Orbigny) - Sgarrella & Moncharmont Zei, p. 185, Pl. 6, fig. 12
1995 *Siphonaperta aspera dilatata* Le Calvez & Le Calvez - Coppa & Di Tuoro, p. 166, Pl. 1, fig. 7
2005 *Siphonaperta aspera* (d'Orbigny) - Rasmussen, p. 61, Pl. 4, fig. 1
2009 *Siphonaperta aspera* (d'Orbigny) - Frezza & Carboni, p. 55, Pl. 1, fig. 21

***Siphonaperta dilatata* (Le Calvez & Le Calvez)**

1958 *Quinqueloculina aspera* d'Orbigny var. *dilatata* Le Calvez & Le Calvez
1991 *Siphonaperta dilatata* (Le Calvez & Le Calvez) - Cimerman & Langer, p. 31, Pl. 26, figs. 1-3

***Siphonaperta horrida* (Cushman)**

1947 *Quinqueloculina horrida* Cushman
1993 *Siphonaperta horrida* (Cushman) - Hottinger et al., p. 63, Pl. 63, figs. 7-12

***Siphonaperta irregularis* (d'Orbigny)**

1826 *Quinqueloculina irregularis* d'Orbigny
1991 *Siphonaperta irregularis* (d'Orbigny) - Cimerman & Langer, p. 32, Pl. 26, figs. 4-6

***Siphonaperta* sp. 1**

1991 *Siphonaperta* sp. 2 - Cimerman & Langer, p. 32, Pl. 26, figs. 7-9

***Siphonaperta* sp. 2**

Remarks: The test is subelliptical in lateral and peripheral view. The chamber arrangement is quinqueloculine. The wall is imperforate and has an agglutinated outer coating. The aperture is terminal and rounded at the end of a short neck. The tooth is simple and narrow. This species looks close to *Siphonaperta* sp.1, but it is generally smaller.

Subfamily: Hauerininae Schwager, 1876

Genus: *Cycloforina* Luczkowksa, 1972

***Cycloforina contorta* (d'Orbigny)**

(Pl. 2, fig. 8)

1846 *Quinqueloculina contorta* d'Orbigny, p. 298, Tab. 20, figs. 4-6
1929 *Quinqueloculina contorta* d'Orbigny - Cushman, p. 29, Pl. 3, fig. 6
1988 *Cycloforina contorta* (d'Orbigny) - Loeblich & Tappan, p. 91, Pl. 342, figs. 4-9
1991 *Cycloforina contorta* (d'Orbigny) - Cimerman & Langer, p. 32, Pl. 27, figs. 7-11
1993 *Quinqueloculina contorta* d'Orbigny - Sgarrella & Moncharmont Zei, p. 170, Pl. 6, figs. 5 & 6

***Cycloforina tenuicollis* (Wiesner)**

1923 *Miliolina tenuicollis* Wiesner
1991 *Cycloforina tenuicollis* (Wiesner) - Cimerman & Langer, p. 33, Pl. 28, figs. 5-6
1993 *Quinqueloculina tenuicollis* (Wiesner) - Sgarrella & Moncharmont Zei, p. 175, Pl. 6, figs. 10 & 11
2009 *Cycloforina tenuicollis* (Wiesner) - Avsar et al., p. 134, Pl. 1, fig. 18

***Cycloforina villafranca* Le Calvez & Le Calvez**

1958 *Quinqueloculina villafranca* Le Calvez & Le Calvez
1991 *Cycloforina villafranca* (Le Calvez & Le Calvez) - Cimerman & Langer, p. 33, Pl. 28, figs. 7-9
1993 *Quinqueloculina villafranca* Le Calvez & Le Calvez - Sgarrella & Moncharmont Zei, p. 176, Pl. 7, figs. 3 & 4
2005 *Cycloforina villafranca* (Le Calvez & Le Calvez) - Rasmussen, p. 62, Pl. 4, fig. 3
2009 *Cycloforina villafranca* (Le Calvez & Le Calvez) - Avsar et al., p. 134, Pl. 1, fig. 19

***?Cycloforina* sp. 1**

Remarks: The test is elongate. The chambers are arranged in a quinqueloculine manner and

are one-half coil in length. Four chambers are visible from one side and three chambers from the other side. The wall is porcelaneous and imperforate with weak and minute longitudinal anastoming microstriae. The aperture is ovate at the end of the final chamber and provided with a peristomal rim and a relatively long slender tooth with a short bifite termination.

Genus: *Lachlanella* Vella, 1957

***Lachlanella bicornis* (Walker and Jacob) emend. Haynes**

1973 *Quinqueloculina bicornis* (Walker and Jacob) emend. Haynes
1987 *Quinqueloculina bicornis* Walker & Jacob - Alberola et al., p. 305, Pl. 2, figs. 10 & 14
1991 *Lachlanella bicornis* ((Walker and Jacob) emend. Haynes) - Cimerman & Langer, p. 34, Pl. 29, figs. 1-3
1994 *Adelosina bicornis* ((Walker & Jacob) emend. Haynes) - Jones, p. 22, Pl. 6, fig. 9
2006 *Quinqueloculina bicornis* Walker & Jacob - Avsar et al., p. 132, Pl. 1, fig. 5

***Lachlanella bradyana* Cushman**

1917 *Quinqueloculina bradyana* Cushman
1929 *Quinqueloculina bradyana* Cushman - Cushman, p. 23, Pl. 1, fig. 3
1994 *Quinqueloculina bradyana* Cushman - Jones, p. 22, Pl. 6, figs. 6 & 7
1995 *Quinqueloculina bradyana* Cushman - Coppa & Di Tuoro, p. 166, Pl. 1, fig. 12

***Lachlanella undulata* (d'Orbigny)**

(Pl. 2, fig. 9)

1826 *Quinqueloculina undulata* d'Orbigny
1991 *Lachlanella undulata* (d'Orbigny) - Cimerman & Langer, p. 34, Pl. 30, figs. 3-6
1993 *Quinqueloculina undulata* d'Orbigny - Sgarrella & Moncharmont Zei, p. 175, Pl. 7, fig. 6
2005 *Lachlanella undulata* (d'Orbigny) - Rasmussen, p. 62, Pl. 4, fig. 4

***Lachlanella variolata* (d'Orbigny)**

1826 *Quinqueloculina variolata* d'Orbigny
1929 *Triloculina carinata* d'Orbigny - Cushman, p. 65, Pl. 17, fig. 5
1991 *Lachlanella variolata* (d'Orbigny) - Cimerman & Langer, p. 35, Pl. 31, figs. 1-12
1993 *Quinqueloculina variolata* d'Orbigny - Sgarrella & Moncharmont Zei, p. 175, Pl. 8, fig.1

***Lachlanella* sp. 1**

Remarks: The test is elongate-ovate, with a quinqueloculine chamber arrangement. The wall is porcelaneous and imperforate. The test surface is ornamented by numerous striae. The large aperture consists of two nearly parallel sides and an everted rim provided with a long, slender tooth with short bifite termination.

Genus: *Quinqueloculina* d'Orbigny, 1826

***Quinqueloculina* cf. *Q. annectens* (Schlumberger)**

1893 *Massilina annectens* Schlumberger
1960 *Quinqueloculina annectens* (Schlumberger) - Hofker, p. 241, Pl. B, fig. 38
1991 *Quinqueloculina annectens* (Schlumberger) - Cimerman & Langer, p. 35, Pl. 32, figs. 1 & 2

Remarks: These large specimens are oval in outline. The periphery is broadly rounded. Four chambers are visible from the exterior. On the wall few dark sand grains are visible. The aperture is oval with a bifite tooth. In contrast to the specimen shown in Hofker (1960) and Cimerman & Langer (1991), the specimens in this work have a lower width to length ratio.

***Quinqueloculina auberiana* d'Orbigny**

1826 *Quinqueloculina auberiana* d'Orbigny
1917 *Quinqueloculina auberiana* d'Orbigny - Cushman, p. 46, Pl. 12, fig. 1
1991 *Quinqueloculina auberiana* d'Orbigny - Cimerman & Langer, p. 36, Pl. 32, figs. 8 & 9

Quinqueloculina berthelotiana d'Orbigny

1839 *Quinqueloculina berthelotiana* d'Orbigny
1987 *Quinqueloculina berthelotiana* d'Orbigny - Alberola et al., p. 305, Pl. 3, fig. 2
1991 *Quinqueloculina berthelotiana* d'Orbigny - Cimerman & Langer, p. 36, Pl. 32, figs. 5-7
1993 *Quinqueloculina berthelotiana* d'Orbigny - Sgarrella & Moncharmont Zei, p. 170, Pl. 6, figs. 1 & 2
2005 *Quinqueloculina berthelotiana* d'Orbigny - Rasmussen, p. 62, Pl. 4, fig. 5
2006 *Quinqueloculina berthelotiana* d'Orbigny - Avsar et al., p. 132, Pl. 1, fig. 6

Quinqueloculina disparilis d'Orbigny

1826 *Quinqueloculina disparilis* d'Orbigny
1929 *Quinqueloculina disparilis* d'Orbigny - Cushman, p. 32, Pl. 5, fig. 4
1991 *Quinqueloculina disparilis* d'Orbigny - Cimerman & Langer, p. 36, Pl. 33, figs. 1 & 2
1993 *Quinqueloculina disparilis* d'Orbigny - Sgarrella & Moncharmont Zei, p. 170, Pl. 8, fig. 2
1995 *Quinqueloculina disparilis* d'Orbigny - Coppa & Di Tuoro, p. 168, Pl. 2, fig. 2

Quinqueloculina lata Terquem

1876 *Quinqueloculina lata* Terquem
1993 *Quinqueloculina lata* Terquem - Sgarrella & Moncharmont Zei, p. 172, Pl. 5, fig. 15
2003 *Quinqueloculina lata* Terquem - Murray, p. 17, fig. 4, no. 9 & 10

Quinqueloculina laevigata d'Orbigny

1839 *Quinqueloculina laevigata* d'Orbigny
1929 *Quinqueloculina laevigata* d'Orbigny - Cushman, p. 30, Pl. 4, fig. 3
1965 *Quinqueloculina laevigata* d'Orbigny - Phleger, p. 53, Pl. 1, fig. 23
1991 *Quinqueloculina laevigata* d'Orbigny - Cimerman & Langer, p. 37, Pl. 33, figs. 8-11

Quinqueloculina limbata d'Orbigny

1826 *Quinqueloculina limbata* d'Orbigny
1991 *Quinqueloculina limbata* d'Orbigny - Cimerman & Langer, p. 37, Pl. 34, figs. 1-5

Quinqueloculina neapolitana Sgarrella & Moncharmont Zei

1993 *Quinqueloculina neapolitana* n.sp. - Sgarrella & Moncharmont Zei, p. 173, Pl. 5, figs. 10-12

Quinqueloculina padana Perconi

(Pl. 2, fig. 10)

1954 *Quinqueloculina padana* Perconig
1987 *Quinqueloculina badenensis* d'Orbigny - Jorissen, p. 43, Pl. 4, fig. 10
1993 *Quinqueloculina padana* Perconig - Sgarrella & Moncharmont Zei, p. 172, Pl. 7, fig. 1
2005 *Quinqueloculina padana* Perconig - Rasmussen, p. 63, Pl. 4, figs. 8 & 9
2009 *Quinqueloculina padana* Perconig - Frezza & Carboni, p. 55, Pl. 1, fig. 9

Quinqueloculina parvula Schlumberger

(Pl. 2, fig. 11)

1894 *Quinqueloculina parvula* Schlumberger
1991 *Quinqueloculina parvula* Schlumberger - Cimerman & Langer, p. 37, Pl. 34, figs. 6-8
1993 *Quinqueloculina parvula* Schlumberger - Sgarrella & Moncharmont Zei, p. 174, Pl. 5, fig. 16

Quinqueloculina pseudobuchiana Luczkowksa

1974 *Quinqueloculina pseudobuchiana* Luczkowska
1991 *Quinqueloculina pseudobuchiana* Luczkowska - Cimerman & Langer, p. 38, Pl. 35, figs. 1-4

Quinqueloculina seminula (Linné)

(Pl. 2, fig. 12)

1758 *Serpula seminula* Linné
1917 *Quinqueloculina seminulum* (Linné) - Cushman, p. 44, pl. 11, fig. 2
1929 *Quinqueloculina seminulum* (Linné) - Cushman, p. 24, Pl. 2, figs. 1 & 2
1960 *Quinqueloculina seminulum* (Linné) - Hofker, p. 241, Pl. B, fig. 41
1988 *Quinqueloculina seminula* (Linné) - Loeblich & Tappan, p. 92, Pl. 344, figs. 8-13
1991 *Quinqueloculina seminula* (Linné) - Cimerman & Langer, p. 38, Pl. 34, fig. 9-12
1992 *Quinqueloculina seminula* (Linné) - Schiebel, p. 64, Pl. 5, fig. 3
1992 *Quinqueloculina seminula* (Linné) - Wollenburg, p. 40, Pl. 10, fig. 8
1994 *Quinqueloculina seminulum* (Linné) - Jones, p. 21, Pl. 5, fig. 6
2006 *Quinqueloculina seminula* (Linné) - Avsar et al., p. 132, Pl. 1, fig. 7
2009 *Quinqueloculina seminula* (Linné) - Frezza & Carboni, p. 55, Pl. 1, figs. 10 & 11

***Quinqueloculina stalkeri* Loeblich & Tappan**

1953 *Quinqueloculina stalkeri* Loeblich & Tappan
1991 *Quinqueloculina stalkeri* Loeblich & Tappan - Sgarrella & Moncharmont Zei, p. 174, Pl. 5, figs. 13 & 14
2005 *Quinqueloculina stalkeri* Loeblich & Tappan - Rasmussen, p. 63, Pl. 4, figs. 10 & 11

***Quinqueloculina stelligera* Schlumberger**

(Pl. 2, fig. 13)

1893 *Quinqueloculina stelligera* Schlumberger
1929 *Quinqueloculina stelligera* Schlumberger - Cushman, p. 28, Pl. 3, figs. 3 & 4
1991 *Quinqueloculina stelligera* Schlumberger - Cimerman & Langer, p. 38, Pl. 34, fig. 13-15
1993 *Quinqueloculina stelligera* Schlumberger - Sgarrella & Moncharmont Zei, p. 175, Pl. 6, figs. 13 & 14

***Quinqueloculina viennensis* Le Calvez & Le Calvez**

(Pl. 2, fig. 14)

1958 *Quinqueloculina viennensis* Le Calvez & Le Calvez
1993 *Quinqueloculina viennensis* Le Calvez & Le Calvez - Sgarrella & Moncharmont Zei, p. 176, Pl. 7, fig. 8
2005 *Quinqueloculina viennensis* Le Calvez & Le Calvez - Rasmussen, p. 64, Pl. 4, fig. 13

***Quinqueloculina* sp. 1**

Remarks: The test of these small specimens is lenticular in outline, with a quinqueloculine chamber arrangement. The length-width ratio is nearly one. Five chambers are visible from the exterior. The wall is porcelaneous and imperforate with a smooth surface. The oval aperture is terminal, provided with a short bifite tooth.

Subfamily: Miliolinellinae Vella, 1957

Genus: *Affinetrina* Luczkowska, 1972

***Affinetrina* sp. 1**

Remarks: The test is ovate in outline and in section. The chamber arrangement is triloculine and three chambers are visible. The wall is porcelaneous and imperforate. The aperture is a long slit with a long, slender tooth. The test surface is smooth with elongated microstriae.

***Affinetrina* sp.2**

Remarks: The test is ovate in outline and in section. The chamber arrangement is triloculine and three chambers are visible. The wall is porcelanous and imperforate. The test surface is smooth. The aperture is a long slit with a long, slender tooth.

Genus: *Biloculinella* Wiesner, 1931

***Biloculinella globula* (Bornemann)**

(Pl. 2, fig. 15)

1855 *Biloculina globulus* Bornemann
1917 *Biloculina globulus* Bornemann - Cushman, p. 78, Pl. 31, fig. 2
1932 *Pyrgo globula* (Bornemann) - Cushman, p. 65, Pl. 15, figs. 6-8
1991 *Biloculinella globula* (Bornemann) - Cimerman & Langer, p. 40, Pl. 36, figs. 1 & 2
2003 *Biloculinella globula* (Bornemann) - Kaminski et al., p. 172, Pl. 2, fig. 1
2005 *Biloculinella globula* (Bornemann) - Rasmussen, p. 64, Pl. 4, fig. 14

***Biloculinella inflata* (Wright)**

1902 *Biloculina inflata* - Wright
1988 *Biloculinella inflata* Wright - Sgarrella & Moncharmont Zei, p. 188, Pl. 10, fig. 12

***Biloculinella labiata* (Schlumberger)**

1891 *Biloculina labiata* Schlumberger
1958 *Biloculinella labiata* (Schlumberger) - Parker, p. 255, Pl. 1, figs. 10 &11
1988 *Biloculinella labiata* (Schlumberger) - Loeblich & Tappan, p. 93, Pl. 348, figs. 1-4
1991 *Biloculinella labiata* (Schlumberger) - Cimerman & Langer, p. 40, Pl. 36, fig. 12

2009 *Biloculinella labiata* (Schlumberger) - Avsar et al., p. 134, Pl. 1, fig. 20

?*Biloculinella* sp. 1

Remarks: The test is ovate in outline and narrow. In section, the test is ovate and the periphery is rounded. The wall is porcelaneous and imperforate. The apertural flap is terminal, but smaller when compared to other *Biloculinella* species.

Genus: *Miliolinella* Wiesner, 1931

***Miliolinella dilatata* (d'Orbigny)**

1839 *Quinqueloculina dilatata* d'Orbigny
1991 *Miliolinella dilatata* (d'Orbigny) - Cimerman & Langer, p. 41, Pl. 37, figs. 9-11

***Miliolinella elongata* Kruit**

1955 *Miliolinella circularis* (Bornemann) var. *elongata* Kruit
1991 *Miliolinella elongata* Kruit - Cimerman & Langer, p. 41, Pl. 37, fig. 8
1993 *Miliolinella circularis elongata* Kruit - Sgarrella & Moncharmont Zei, p. 187, Pl. 10, fig. 5
2009 *Miliolinella elongata* Kruit - Avsar et al., p. 134, Pl. 1, fig. 21

***Miliolinella* cf. *M. hybrida* (Terquem)**

1878 *Quinqueloculina hybrida* Terquem
1993 *Miliolinella* cf. *M. hybrida* (Terquem) - Hottinger et al., p. 52, Pl. 39, figs. 1-6

Remarks: The test is porcelaneous, oval to subcircular in section. The test surface is smooth. The chambers are strongly inflated and often distorted. Sutures are distinct and depressed. The aperture is terminal, arch-shaped or triangular, mostly rounded, but also irregular. The specimens in this work have no thick rim that bordered the aperture and no basal flap (probably broken?) as described in Hottinger et al. (1993).

***Miliolinella labiosa* (d'Orbigny)**

1839 *Triloculina labiosa* d'Orbigny
1839 *Triloculina labiosa* d'Orbigny - Cushman, p. 53, Pl. 11, fig. 12
1960 *Miliolinella labiosa* (d'Orbigny) - Hofker, p. 243, Pl. B, fig. 54
1991 *Miliolinella labiosa* (d'Orbigny) - Cimerman & Langer, p. 41, Pl. 38, figs. 1-3

***Miliolinella semicostata* (Wiesner)**

(Pl. 2, fig. 16)

1923 *Miliolina semicostata* Wiesner
1991 *Miliolinella semicostata* (Wiesner) - Cimerman & Langer, p. 42, Pl. 38, figs. 10-15
1993 *Miliolinella semicostata* (Wiesner) - Sgarrella & Moncharmont Zei, p. 187, Pl. 10, fig. 7

***Miliolinella subrotunda* (Montagu)**

(Pl. 2, fig. 17)

1803 *Vermiculum subrotundum* Montagu
1929 ?*Quinqueloculina subrotunda* (Montagu) - Cushman, p. 25, Pl. 2, fig. 4
1988 *Miliolinella subrotunda* (Montagu) - Loeblich & Tappan, p. 93, Pl. 350, figs. 1-12
1991 *Miliolinella subrotunda* (Montagu) - Cimerman & Langer, p. 42, Pl. 38, figs. 4-9
1992 *Miliolinella subrotunda* (Montagu) - Schiebel, p. 28, Pl. 5, fig. 1
1994 *Miliolinella subrotunda* (Montagu) - Jones, p. 20, Pl. 4, fig. 3
2003 *Miliolinella subrotunda* (Monatgu) - Murray, p. 15, fig. 4, no. 6
2005 *Miliolinella subrotunda* (Montagu) - Rasmussen, p. 64, Pl. 4, fig. 15
2009 *Miliolinella subrotunda* (Montagu) - Avsar et al., p. 134, Pl. 1, figs. 22 & 23

***Miliolinella webbiana* (d'Orbigny)**

(Pl. 2, fig. 18)

1839 *Triloculina webbiana* d'Orbigny
1987 *Miliolinella webbiana* (d'Orbigny) - Alberola et al., p. 306, Pl. 2, fig. 12
1991 *Miliolinella webbiana* (d'Orbigny) - Cimerman & Langer, p. 42, Pl. 39, figs. 1-3
1993 *Miliolinella webbiana* (d'Orbigny) - Sgarrella & Moncharmont Zei, p. 187, Pl. 10, fig. 6

***Miliolinella* sp. 1**

1991 c.f. *Miliolinella* sp. 2 - Cimerman & Langer, p. 42, Pl. 39, figs. 6 & 7

Remarks: The test is porcelaneous, with a smooth surface, and ovate in lateral view. The periphery margin is broadly rounded. The chambers are initially arranged in a quinqueloculine pattern but later nearly planispirally. They are inflated and increasing when added. Three chambers are visible from the exterior. The terminal aperture is provided with an apertual flap.

Genus: *Pseudotriloculina* Cherif, 1970

***Pseudotriloculina laevigata* (d'Orbigny)**

1826 *Triloculina leavigata* d'Orbigny
1991 *Pseudotriloculina laevigata* (d'Orbigny) - Cimerman & Langer, p. 43, Pl. 39, figs. 8-12

***Pseudotriloculina planciana* (d'Orbigny)**

1839 *Triloculina planciana* d'Orbigny
1929 *Triloculina planciana* d'Orbigny - Cushman, p. 62, Pl. 15, fig. 6

***Pseudotriloculina* sp. 1**

Remarks: The test of these small specimens is ovate in outline with a broadly rounded periphery. Three chambers are visible from the exterior. The wall is porcelaneous and imperforate with a smooth surface. The large aperture, at the end of the final chamber, is subrounded and provided by a long bifite? tooth.

Genus: *Ptychomiliola* Eimer & Fickert, 1899

***?Ptychomiliola separans* (Brady)**

1881 *Miliolina separans* Brady
1988 c.f. *Ptychomiliola separans* (Brady) - Loeblich & Tappan, p. 94, Pl. 353, figs. 10 & 11
1994 c.f. *Ptychomiliola separans* (Brady) - Jones, p. 23, Pl. 7, figs. 1-4

Remarks: The specimens were mostly broken, and the apertural tooth was not visible. Therefore, the correct identification is questionable.

Genus: *Pyrgoella* Cushman & White, 1936

***Pyrgoella sphaera* (d'Orbigny)**

1839 *Biloculina sphaera* d'Orbigny, p. 66, Pl. 8, figs. 13-16
1960 *Planispirina sphaera* (d'Orbigny) - Hofker, p. 244, Pl. B, fig. 59
1958 *Pyrgoella sphaera* (d'Orbigny) - Parker, p. 256, Pl. 1, fig. 14
1958 *Pyrgoella sphaera* (d'Orbigny) - Todd, p. 188, Pl. 1, fig. 4
1988 *Pyrgoella sphaera* (d'Orbigny) - Loeblich & Tappan, p. 94, Pl. 351, figs. 1-4
1992 *Pyrgoella sphaera* (d'Orbigny) - Wollenburg, p. 41, Pl. 11, fig. 2
1991 *Pyrgoella sphaera* (d'Orbigny) - Cimerman & Langer, p. 45, Pl. 41, figs. 1 & 2
1994 *Pyrgoella sphaera* (d'Orbigny) - Jones, p. 18, Pl. 2, fig. 4

Genus: *Pyrgo* Defrance, 1824

***Pyrgo anomala* (Schlumberger)**

(Pl. 3, fig. 1)

1891 *Biloculina anomala* Schlumberger
1917 *Biloculina anomala* Schlumberger - Cushman, p. 79, Pl. 32, fig. 1
1958 *Pyrgo anomala* (Schlumberger) - Parker, p. 255, Pl. 1, figs. 22 & 23
1960 *Pyrgo fischeri* (Schlumberger) - Hofker, p. 243, Pl. B, fig. 56
1991 *Pyrgo anomala* (Schlumberger) - Cimerman & Langer, p. 44, Pl. 41, figs. 3-5
1993 *Pyrgo anomala* (Schlumberger) - Sgarrella & Moncharmont Zei, p. 180, Pl. 9, fig. 3

***Pyrgo depressa* (d'Orbigny)**

1826 *Biloculina depressa* d'Orbigny
1929 *Pyrgo depressa* (d'Orbigny) - Cushman, p. 71, Pl. 19, figs. 4 & 5
1960 *Pyrgo depressa* (d'Orbigny) - Hofker, p. 243, Pl. B, fig. 53
1990 *Pyrgo depressa* (d'Orbigny) - Hasegawa et al., p. 475, Pl. 2, fig. 1

1994 *Pyrgo depressa* (d'Orbigny) - Jones, p. 19, Pl. 3, figs. 1 & 2
2003 *Biloculinella depressa* (d'Orbigny) - Murray, p. 15, fig. 4, no. 2 & 3
2005 *Pyrgo depressa* (d'Orbigny) - Rasmussen, p. 65, Pl. 4, fig. 17

***Pyrgo elongata* (d'Orbigny)**

1826 *Biloculina elongata* d'Orbigny
1917 *Biloculina elongata* d'Orbigny - Cushman, p. 78, Pl. 31, fig. 1
1929 *Pyrgo elongata* (d'Orbigny) - Cushman, p. 70, Pl. 19, figs. 2 & 3
1960 *Pyrgo elongata* (d'Orbigny) - Hofker, p. 244, Pl. B, fig. 58
1991 *Pyrgo elongata* (d'Orbigny) - Cimerman & Langer, p. 44, Pl. 41, figs. 6-8
1993 *Pyrgo elongata* (d'Orbigny) - Sgarrella & Moncharmont Zei, p. 182, Pl. 9, fig. 1
1994 *Pyrgo elongata* (d'Orbigny) - Jones, p. 18, Pl. 2, fig. 9

Remarks: The specimen shown in Sgarrella & Moncharmont Zei (1993) differs from that shown by the other authors, and from that in this work, by its not so elongate test.

***Pyrgo oblonga* (d'Orbigny)**

1839 *Biloculina oblonga* d'Orbigny
1988 *Pyrgo oblonga* (d'Orbigny) - Loeblich & Tappan, p. 94, Pl. 351, figs. 11-13
2003 *Pyrgo oblonga* (d'Orbigny) - Hottinger et al., p. 57, Pl. 50, figs. 1-6

***Pyrgo* sp. 1**

2006 *Pyrgo elongata* (d'Orbigny) - Avsar et al., p. 132, Pl. 1, fig. 13

Remarks: The specimen shown in Avsar et al. (2006) differs from *Pyrgo elongata* shown in Cimerman & Langer (1991) and Sgarrella & Moncharmont Zei (1993). The specimens in this work and that in Avsar et al. (2006) are broader than *P. elongata* in outline, and contain a rectangle-like attachment at the base of the test.

Genus: *Triloculina* d'Orbigny, 1826

?*Triloculina eburnea* d'Orbigny

1839 *Triloculina eburnea* d'Orbigny
1993 *"Quinqueloculina" eburnea* (d'Orbigny) - Hottinger et al., p. 59, Pl. 53, figs. 9-11; Pl. 54, figs. 1-5

Remarks: The generic position of this species is questionable due to the chamber arrangement, the absence of an everted lip and a bifite tooth termination (see also Hottinger et al., 2003).

***Triloculina oblonga* (Montagu)**

1803 *Vermiculum oblongum* Montagu
1917 *Triloculina oblonga* (Montagu) - Cushman, p. 69, Pl. 26, fig. 3
1929 *Triloculina oblonga* (Montagu) - Cushman, p. 57, Pl. 13, fig. 4
1991 *Pseudotriloculina oblonga* (Montagu) - Cimerman & Langer, p. 43, Pl. 40, figs. 1-4
2005 *Triloculina oblonga* (Montagu) - Rasmussen, p. 67, Pl. 5, fig. 4
2009 *Pseudotriloculina oblonga* (Montagu) - Avsar et al., p. 134, Pl. 1, fig. 24

***Triloculina plicata* Terquem**

(Pl. 2, fig. 19)

1878 *Triloculina plicata* Terquem
1991 *Triloculina plicata* Terquem - Cimerman & Langer, p. 46, Pl. 43, figs. 8-10
2005 *Triloculina plicata* Terquem - Rasmussen, p. 67, Pl. 5, fig. 5

***Triloculina tricarinata* d'Orbigny**

(Pl. 2, fig. 20)

1826 *Triloculina tricarinata* d'Orbigny
1917 *Triloculina tricarinata* d'Orbigny - Cushman, p. 66, Pl. 25, fig. 2
1929 *Triloculina tricarinata* d'Orbigny - Cushman, p. 56, Pl. 13, fig. 3
1932 *Triloculina tricarinata* d'Orbigny - Cushman, p. 59, Pl. 13, fig. 3
1960 *Triloculina tricarinata* d'Orbigny - Hofker, p. 242, Pl. B, fig. 47
1990 *Triloculina tricarinata* d'Orbigny - Hasegawa et al., p. 475, Pl. 2, figs. 10 & 11
1991 *Triloculina tricarinata* d'Orbigny - Cimerman & Langer, p. 46, Pl. 44, figs. 3 & 4
1993 *Triloculina tricarinata* d'Orbigny - Hottinger et al., p. 64-65, Pl. 68, figs. 7-12
1993 *Triloculina tricarinata* d'Orbigny - Sgarrella & Moncharmont Zei, p. 187, Pl. 9, figs. 14 & 15

1994 *Triloculina tricarinata* d'Orbigny - Jones, p. 20, Pl. 3, fig. 17
2004 *Triloculina tricarinata* d'Orbigny - Chendes et al., p. 76, Pl. 1, fig. 11
2005 *Triloculina tricarinata* d'Orbigny - Rasmussen, p. 67, Pl. 5, fig. 6

***Triloculina* sp. 1**

Remarks: The test is ovate in outline and subtriangular in section. The chambers are one-half coil in length. The chamber arrangement is triloculine in the adult stage. Three chambers are visible from the exterior. The wall is porcelaneous and imperforate. The subrounded aperture, at the end of the last chamber, is surrounded by a thick peristomal rim and provided with a short bifite tooth.

Subfamily: Sigmoilinitinae Luczkowska, 1974

Genus: *Pseudoschlumbergerina* Cherif, 1970

***Pseudoschlumbergerina ovata* (Side-bottom)**

1904 *Sigmoilina ovata* Sidebottom
1988 *Pseudoschlumbergerina ovata* (Side-bottom) - Loeblich & Tappan, p. 95, Pl. 355, figs. 7-10
1993 *Pseudoschlumbergerina ovata* (Side-bottom) - Hottinger et al., p. 55, Pl. 46, figs. 1-6

Genus: *Sigmoilina* Schlumberger, 1887

***Sigmoilina distorta* Phleger & Parker**

1951 *Sigmoilina distorta* Phleger & Parker
1958 *Sigmoilina distorta* Phleger & Parker - Parker, p. 256, Pl. 1, fig. 25
1993 *Sigmoilina distorta* Phleger & Parker - Sgarrella & Moncharmont Zei, p. 185, Pl. 9, fig. 5

***Sigmoilina sigmoidea* (Brady)**

1884 *Planispirina sigmoidea* Brady
1917 *Sigmoilina sigmoidea* (Brady) - Cushman, p. 61, Pl. 24, figs. 2 & 3
1929 *Sigmoilina sigmoidea* (Brady) - Cushman, p. 50, Pl. 11, figs. 5 & 6
1988 *Sigmoilina sigmoidea* (Brady) - Loeblich & Tappan, p. 95, Pl. 356, figs. 21-23
1992 *Sigmoilina sigmoidea* (Brady) - Wollenburg, p. 43, Pl. 11, fig. 9
1993 *Sigmoilina sigmoidea* (Brady) - Sgarrella & Moncharmont Zei, p. 184, Pl. 9, fig. 13
1994 *Sigmoilina sigmoidea* (Brady) - Jones, p. 18, Pl. 2, figs. 1-3

Remarks: The specimen shown in Loeblich & Tappan (1988) has a short simple tooth and not a flap-like tooth as shown by the other authors and also observed in this work.

Genus: *Sigmoilinita* Seiglie, 1965

***Sigmoilinita costata* (Schlumberger)**

(Pl. 3, fig. 2)

1893 *Sigmoilina costata* Schlumberger
1987 *Sigmoilina costata* Schlumberger - Alberola et al., p. 306, Pl. 2, fig. 15
1991 *Sigmoilinita costata* (Schlumberger) - Cimerman & Langer, p. 47, Pl. 45, figs. 1-6
1993 *Sigmoilina costata* Schlumberger - Sgarrella & Moncharmont Zei, p. 184, Pl. 9, figs. 6-8
2009 *Sigmoilinita costata* (Schlumberger) - Avsar et al., p. 134, Pl. 1, fig. 27

***Sigmoilinita* cf. *S. tricosta* (Cushman & Todd)**

1944 *Spiroloculina tricosta* Cushman & Todd
1993 c.f. *Sigmoilina tricosta* (Cushman & Todd) - Sgarrella & Moncharmont Zei, p. 185, Pl. 5, figs. 8 & 9

Remarks: The test is fusiform in lateral view and flattened in peripheral view. The chambers are one-half coil in length. Early chambers are arranged in sigmoid pattern and later nearly planispirally. The wall is porcelaneous and imperforate. The surface is ornamented by longitudinal costae. The aperture at the end of the final chamber is small and ovate to rounded. A tooth was not visible.

Genus: *Subedentostomina* McCulloch, 1981

***Subedentostomina* sp. 1**

Remarks: The test is elongate-oval with flattened sites. The chambers are one-half coil in length, added in various planes and are various in numbers. The chambers are mostly broader at the base and narrowing towards the aperture and overlapping more strongly on one side than on the other side. The wall is imperforate and calcareous. The toothless aperture is terminal at the end of the last chamber and provided by a narrow slit bordered by a lip.

Subfamily: Sigmoilopsinae Vella, 1957

Genus: *Sigmoilopsis* Finlay, 1947

***Sigmoilopsis minuta* (Collins)**

1958 *Massilina minuta* Collins
1993 *Sigmoilopsis minuta* (Collins) - Hottinger et al., p. 62, Pl. 61, figs. 4-9

***Sigmoilopsis schlumbergeri* (Silvestri)**

(Pl. 3, fig. 3)

1904 *Sigmoilina schlumbergeri* Silvestri
1929 *Sigmoilina schlumbergeri* Silvestri - Cushman, p. 49, Pl. 11, figs. 1-3
1960 *Sigmoilina schlumbergeri* Silvestri - Hofker, p. 244, Pl. C, fig. 61
1987 *Sigmoilopsis schlumbergeri* (Silvestri) - Jorissen, p. 43, Pl. 4, fig. 9
1988 *Sigmoilopsis schlumbergeri* (Silvestri) - Loeblich & Tappan, p. 95, Pl. 356, figs. 8-13
1993 *Sigmoilopsis schlumbergeri* (Silvestri) - Sgarrella & Moncharmont Zei, p. 185, Pl. 9, fig. 4
1994 *Sigmoilopsis schlumbergeri* (Silvestri) - Jones, p. 23, Pl. 8, figs. 1-4
2004 *Sigmoilopsis schlumbergeri* (Silvestri) - Chendes et al., p. 76, Pl. 1, fig. 12
2005 *Sigmoilopsis schlumbergeri* (Silvestri) - Rasmussen, p. 68, Pl. 5, fig. 8
2009 *Sigmoilopsis schlumbergeri* (Silvestri) - Avsar et al., p. 134, Pl. 1, fig. 28
2009 *Sigmoilopsis schlumbergeri* (Silvestri) - Frezza & Carboni, p. 57, Pl. 2, fig. 21

Subfamily: Tubinellinae Rhumbler, 1906

Genus: *Articulina* d'Orbigny, 1826

***Articulina mucronata* (d'Orbigny)**

1839 *Vertebralina mucronata* d'Orbigny
1993 *Articulina mucronata* (d'Orbigny) - Sgarrella & Moncharmont Zei, p. 190, Pl. 10, fig. 11

Superfamily: Soritacea Ehrenberg, 1839

Family: Peneroplidae Schultze, 1854

Genus: *Peneroplis* De Montfort, 1808

***Peneroplis pertusus* (Forskal)**

(Pl. 3, fig. 4)

1775 *Nautilus pertusus* Forskal
1917 *Peneroplis pertusus* (Forskal) - Cushman, p. 86, Pl. 37, figs. 1, 2 & 6
1930 *Peneroplis pertusus* (Forskal) - Cushman, p. 35, Pl. 12, figs. 3-6
1991 *Peneroplis pertusus* (Forskal) - Cimerman & Langer, p. 49, Pl. 49, figs. 1-7
1993 *Peneroplis pertusus* (Forskal) - Sgarrella & Moncharmont Zei, p. 190, Pl. 10, fig. 13
1994 *Peneroplis pertusus* (Forskal) - Jones, p. 29, Pl. 13, figs. 16 & 17, 23

Family: Soritidae Ehrenberg, 1839

Subfamily: Archaiasinae Cushman, 1927

Genus: *Parasorites* Seiglie & Rivera, 1977

***Parasorites marginales* (Lamarck)**

1816 *Orbulites marginales* Lamarck
1994 *Parasorites marginales* (Lamarck) - Jones, p. 30, Pl. 15, figs. 1-3 & 5

Suborder Lagenina Delage & Herouard, 1896

Superfamily: Nodosariacea Ehrenberg, 1838

Family: Nodosariidae Ehrenberg, 1838

Genus: *Dentalina* Risso, 1826

***Dentalina guttifera* d'Orbigny**

1846 *Dentalina guttifera* d'Orbigny, p. 49, Tab. 2, figs. 11 & 13
1993 *Dentalina guttifera* d'Orbigny - Sgarrella & Moncharmont Zei, p. 192, Pl. 11, fig. 7
2005 *Dentalina pyrula* (d'Orbigny) - Rasmussen, p. 69, Pl. 5, fig. 13

Subfamily: Nodosariinae Ehrenberg, 1838

Genus: *Laevidentalina* Loeblich & Tappan, 1986

***Laevidentalina* sp. 1**

Remarks: The test is elongate and arcuate. The chambers are uniserially arranged. Sutures are oblique. The wall is calcareous and hyaline with a smooth and unornamented surface. The aperture is terminal and consists of a serial of radial slits

Genus: *Pyramidulina* Fornasini, 1894

***Pyramidulina catesbyi* (d'Orbigny)**

1839 *Nodosaria catesbyi* d'Orbigny
1993 *Pyramidulina catesbyi* (d'Orbigny) - Hottinger et al., p. 76, Pl. 88, figs. 1-19

Remarks: The specimens in this work have two uniserial chambers, where the first is globular and larger than the second chamber that is more pyriform. In difference to the specimens shown in Hottinger et al. (1993), the specimens have more distinct striae.

Family: Vaginulinidae Reuss, 1860

Subfamily: Lenticulininae Chapman, Parr & Collins, 1934

Genus: *Lenticulina* Lamarck, 1804

***Lenticulina calcar* (Linné)**

(Pl. 3, fig. 5)

1758 *Nautilus calcar* Linné
1846 *Robulina calcar* d'Orbigny - D'Orbigny, p. 99, Tab. 4, figs. 18-20
1933 *Robulina calcar* (Linné) - Cushman, p. 7, Pl. 2, fig. 3
1991 *Lenticulina calcar* (Linné) - Cimerman & Langer, p. 51, Pl. 53, figs. 1-4
1993 *Lenticulina calcar* (Linné) - Sgarrella & Moncharmont Zei, p. 194, Pl. 12, fig. 11
1994 *Lenticulina calcar* (Linné) - Jones, 1994, p. 81, Pl. 70, figs. 9-12
2005 *Lenticulina calcar* (Linné) - Rasmussen, p. 69, Pl. 6, fig. 5

***Lenticulina orbicularis* (d'Orbigny)**

(Pl. 3, fig. 6)

1826 *Robulina orbicularis* d'Orbigny
1991 *Lenticulina orbicularis* (d'Orbigny) - Cimerman & Langer, p. 51, Pl. 53, fig. 12
1993 *Lenticulina orbicularis* (d'Orbigny) - Sgarrella & Moncharmont Zei, p. 194, Pl. 12, fig. 8
1994 *Lenticulina orbicularis* (d'Orbigny) - Jones, p. 81, Pl. 69, fig. 17
2005 *Lenticulina orbicularis* (d'Orbigny) - Rasmussen, p. 70, Pl. 6, fig. 8

Genus: *Neolenticulina* McCulloch, 1977

***Neolenticulina peregrina* (Schwager)**

1866 *Cristellaria peregrina* Schwager
1960 *Lenticulina peregrina* (Schwager) - Hofker, p. 245, Pl. C, fig. 71
1988 *Neolenticulina peregrina* (Schwager) - Loeblich & Tappan, p. 115, Pl. 447, figs. 9-12 & 16
1993 *Neolenticulina peregrina* (Schwager) - Sgarrella & Moncharmont Zei, p. 195, Pl. 12, fig. 4
1994 *Neolenticulina variablis* (Reuss) - Jones, p. 80, Pl. 68, figs. 11-16
2005 *Lenticulina peregrina* (Schwager) - Rasmussen, p. 70, Pl. 6, fig. 9

Subfamily: Marginulininae Wedekind, 1937

Genus: *Amphicoryna* Schlumberger, 1881

***Amphicoryna scalaris* (Batsch)**

(Pl. 3, figs. 7 & 8)

1791 *Nautilus (Ortoceras) scalaris* Batsch
1958 *Lagenonodosaria scalaris* (Batsch) - Parker, p. 258, Pl. 1, figs. 32 & 33
1960 *Nodogenerina scalaris* (Batsch) - Hofker, p. 244, Pl. C, figs. 63-65
1988 *Amphicoryna scalaris* (Batsch) - Loeblich & Tappan, p. 116, Pl. 450, figs. 11-14
1991 *Amphicoryna scalaris* (Batsch) - Cimerman & Langer, p. 52, Pl. 54, figs. 1-9
1993 *Amphicoryna scalaris* (Batsch) - Sgarrella & Moncharmont Zei, p. 191, Pl. 11, figs. 2-3
1994 *Amphicoryna scalaris* (Batsch) - Jones, p. 75, Pl. 63, figs. 28-31; Pl. 65, figs. 7-9
2003 *Amphicoryna scalaris* (Batsch) - Murray, p. 17, fig. 5, no. 1
2004 *Amphicoryna scalaris* (Batsch) - Chendes et al., p. 76, Pl. 1, fig. 14
2009 *Amphicoryna scalaris* (Batsch) - Frezza & Carboni, p. 57, Pl. 2, figs. 19 & 20

Genus: *Marginulina* d'Orbigny, 1826

***Marginulina costata* (Batsch)**

1791 *Nautilus costatus* Batsch
1993 *Marginulina costata* (Batsch) - Sgarrella & Moncharmont Zei, p. 195, Pl. 12, fig. 5
1994 *Marginulina costata* (Batsch) - Jones, p. 77, Pl. 65, fig. 13
2005 *Marginulina costata* (Batsch) - Rasmussen, p. 71, Pl. 6, fig. 17

Genus: *Hemirobulina* Stache, 1864

***Hemirobulina* sp. 1**

Remarks: The test is elongate and circular in section. The chambers are added in a slightly curve at the base and later become rectilinear. Sutures are oblique and depressed. The wall is calcareous and hyaline, with a smooth surface. The aperture is terminal at the dorsal angle.

Subfamily: Vaginulininae Reuss, 1860

Genus: *Vaginulina* d'Orbigny, 1826

***Vaginulina* cf. V. *americana* Cushman**

1923 *Vaginulina americana* Cushman
1994 c.f. *Vaginulina americana* Cushman - Jones, p. 79, Pl. 67, figs. 10-12

Remarks: The species in this work shows, in difference to that shown in Jones (1994), only a few striae on the test.

Family: Lagenidae Reuss, 1862

Genus: *Hyalinonetrion* Patterson & Richardson, 1987

***Hyalinonetrion gracillimum* (Sequenza)**

1862 *Amphorina gracillima* Sequenza
1988 *Hyalinonetrion sahulense* (Patterson & Richardson) - Loeblich & Tappan, p. 117, Pl. 455, figs. 6 & 7
1991 *Hyalinonetrion gracillimum* (Sequenza) - Cimerman & Langer, p. 52, Pl. 55, figs. 1 & 2
1994 *Procerolagena gracillima* (Sequenza) - Jones, p. 62, Pl. 56, figs. 19-22 & 24-29
1993 *Hyalinonetrion gracillis* (Costa) - Hottinger et al., p. 78, Pl. 90, figs. 7 & 8
2005 *Lagena gracillima* (Sequenza) - Rasmussen, p. 72, Pl. 7, figs. 4 & 5
2009 *Hyalinonetrion gracillimum* (Sequenza) - Avsar et al., p. 134, Pl. 2, fig. 1

Genus: *Lagena* Walker & Jacob, 1798

***Lagena doveyensis* Haynes**

1973 *Lagena doveyensis* Haynes
1991 *Lagena doveyensis* Haynes - Cimerman & Langer, p. 53, Pl. 55, figs. 3-5
2009 *Lagena doveyensis* Haynes - Avsar et al., p. 134, Pl. 2, fig. 2

***Lagena striata* (d'Orbigny)**

1839 *Oolina striata* d'Orbigny
1933 *Lagena striata* (d'Orbigny) - Cushman, p. 32, Pl. 8, figs. 11 & 13
1991 *Lagena striata* (d'Orbigny) - Cimerman & Langer, p. 53, Pl. 55, figs. 6-7
1992 *Lagena striata* (d'Orbigny) - Wollenburg, p. 46, Pl. 12, fig. 3
1993 *Lagena striata* (d'Orbigny) - Sgarrella & Moncharmont Zei, p. 198, Pl. 12, figs. 2-3
1994 *Lagena striata* (d'Orbigny) - Jones, p. 64, Pl. 57, figs. 22 & 24
2005 *Lagena striata* (d'Orbigny) - Rasmussen, p. 73, Pl. 7, fig. 8
2005 *Lagena striata* (d'Orbigny) - Avsar et al., p. 134, Pl. 2, figs. 3 & 4

***Lagena strumosa* Reuss**

1858 *Lagena striata* (d'Orbigny) var. *strumosa* Reuss
1833 *Lagena striata* (d'Orbigny) var. *strumosa* Reuss - Cushman, p. 32, Pl. 8, figs. 11 & 13
1993 *Lagena strumosa* Reuss - Hottinger et al., p. 79, Pl. 90, figs. 18-25
2002 *Amphycorina proxima* (Silvestri) - Kaminski et al., p. 173, Pl. 2, fig. 5

Family: Polymorphinidae d'Orbigny, 1839

Subfamily: Polymorphininae d'Orbigny, 1839

Genus: *Globulina* d'Orbigny, 1839

***Globulina gibba* (d'Orbigny)**

1826 *Polymorphina (Globuline) gibba* d'Orbigny
1960 *Globulina gibba* (d'Orbigny) - Hofker, p. 247, Pl. C, figs. 79 & 81

1993 *Globulina gibba* (d'Orbigny) - Hottinger et al., p. 79, Pl. 91, figs. 6-12
2005 *Globulina gibba* (d'Orbigny) - Rasmussen, p. 74, Pl. 7, figs. 11 & 12

Remarks: Under the name *Globulina gibba* only the fistulose form of this species has been counted.

***Globulina myristiformis* (Williamson)**

1858 *Polymorphina myristiformis* Williamson
1991 *Globulina myristiformes* (Williamson) - Cimerman & Langer, p. 53, Pl. 56, figs. 13 & 14
1994 *Globulina myristiformes* (Williamson) - Jones, p. 85, Pl. 73, figs. 9 & 10

Family: Ellipsolagenidae Silvestri, 1923

Subfamily: Oolinininae Loeblich & Tappan, 1961

Genus: *Lagnea* Popescu, 1983

***Lagnea* sp. 1**

Remarks: The test is unilocular, flask-shaped and compressed. The periphery is broadly carinate, with plate-like struts forming polygonal and tubular structures extending completely around the periphery. The wall is calcareous and hyaline, with a smooth test surface. The aperture is rounded and terminal at the end of the neck, and bordered by a thickened rim.

Genus: *Oolina* d'Orbigny, 1839

***Oolina acuticosta* (Reuss)**

1862 *Lagena acuticosta* Reuss
1933 *Lagena acuticosta* Reuss - Cushman, p. 34, Pl. 8, figs. 9, 10 & 12
1983 *Oolina acuticosta* (Reuss) - Boltovskoy, p. 301, Pl. 1, figs. 8 & 9
1993 *Oolina acuticosta* (Reuss) - Sgarrella & Moncharmont Zei, p. 199, Pl. 12, fig. 12
1994 *Oolina* sp. nov. - Jones, p. 65, Pl. 57, fig. 31
2006 *Oolina acuticosta* (Reuss) - Avsar et al., p. 133, Pl. 1, fig. 17

***Oolina foveolata* (Sequenza)**

1862 *Orbulina foveolata* Sequenza
1993 *Oolina foveolata* (Sequenza) - Sgarrella & Moncharmont Zei, p. 199, Pl. 12, fig. 14

***Oolina hexagona* (Williamson)**

(Pl. 3, fig. 9)

1848 *Entesolenia squamosa* (Montagu) var. *hexagona* Williamson
1988 *Favulina hexagona* (Williamson) - Loeblich & Tappan, p. 120, Pl. 463, figs. 1 & 2
1991 *Favulina hexagona* (Williamson) - Cimerman & Langer, p. 55, Pl. 58, figs. 8 & 9
1992 *Favulina hexagona* (Williamson) - Wollenburg, p. 46, Pl. 12, fig. 9
1993 *Oolina hexagona* (Williamson) - Sgarrella & Moncharmont Zei, p. 199, Pl. 12, fig. 15
1994 *Oolina hexagona* (Williamson) - Jones, p. 66, Pl. 58, fig. 33
2004 *Favulina hexagona* (Williamson) - Chendes et al., p. 76, Pl. 1, fig. 16
2005 *Oolina hexagona* (Williamson) - Rasmussen, p. 76, Pl. 8, fig. 10

Subfamily: Ellipsolageninae Silvestri, 1923

Genus: *Fissurina* Reuss, 1850

***Fissurina castanea* (Flint)**

1899 *Lagena castanea* Flint
1993 *Fissurina castanea* (Flint) - Sgarrella & Moncharmont Zei, p. 201, Pl. 13, fig. 10

***Fissurina crebra* (Matthes)**

1939 *Lagena crebra* Matthes
1983 *Fissurina crebra* (Matthes) - Boltovskoy, p. 301, Pl. 1, figs. 1 & 2

***Fissurina fasciata* (Egger)**

1857 *Oolina fasciata* Egger
1983 *Fissurina fasciata* (Egger) - Boltovskoy, p. 301, Pl. 2, figs. 6 & 7
1993 *Fissurina orbignyana* Sequenza - Sgarrella & Moncharmont Zei, p. 204, Pl. 13, figs. 2 & 3

***Fissurina lacunata* (Burrows & Holland)**

1895 *Lagena orbignyana* Sequenza var. *lacunata* Burrows & Holland

1933 *Lagena orbignyana* Sequenza var. *lacunata* Burrows & Holland - Cushman, p. 27, Pl. 7, figs. 1-5 & 8
1994 *Fissurina castanea* (Burrows & Holland) - Jones, p. 69, Pl. 60, figs. 1 & 2
2005 *Fissurina orbignyana* Sequenza var. *lacunata* (Burrows & Holland) - Rasmussen, p. 77, Pl. 9, fig. 4

***Fissurina orbignyana* Sequenza**

1862 *Fissurina orbignyana* Sequenza
1933 *Lagena orbignyana* (Sequenza) - Cushman, p. 26, Pl. 6, figs, 7, 8 & 11
1991 *Palliolatella orbignyana* (Sequenza) - Cimerman & Langer, p. 56, Pl. 59, figs. 5-7
1994 *Fissurina cucculata* (Silvestri) - Jones, p. 68, Pl. 59, fig. 18
2003 *Fissurina orbignyana* Sequenza - Murray, p. 17, fig. 5, no. 5 & 6
2005 *Fissurina orbignyana* Sequenza - Rasmussen, p. 77, Pl. 9, figs. 2 & 3

***Fissurina submarginata* Boomgaart**

1949 *Fissurina submarginata* Boomgaart
1994 *Fissurina submarginata* Boomgaart - Jones, p. 68, Pl. 59, figs. 21 & 22

Subfamily: Parafissurininae Jones, 1984

Genus: *Parafissurina* Parr, 1947

***Parafissurina lateralis carinata* (Buchner)**

1940 *Lagena lateralis* Cushman var. *carinata* Buchner
1983 *Parafissurina lateralis carinata* (Buchner) - Boltovskoy, p. 303, Pl. 1, fig. 28
1993 *Parafissurina lateralis* (Cushman) - Sgarrella & Moncharmont Zei, p. 205, Pl. 13, fig. 11

Superfamily: Ceratobuliminacea Cushman, 1927

Family: Ceratobuliminidae Cushman, 1927

Subfamily: Ceratobulimininae Cushman, 1927

Genus: *Lamarckina* Berthelin, 1881

***Lamarckina scabra* (Brady)**

1884 *Pulvinulina oblonga* (Williamson) var. *scabra* Brady
1931 *Lamarckina scabra* (Brady) - Cushman, p. 35, Pl. 7, fig. 6
1993 *Lamarckina scabra* (Brady) - Sgarrella & Moncharmont Zei, p. 242, Pl. 26, figs. 3 & 4

Family: Epistominidea Wedekind, 1937

Subfamily: Epistomininae Wedekind, 1937

Genus: *Hoeglundina* Brotzen, 1948

***Hoeglundina elegans* (d'Orbigny)**

1826 *Rotalia elegans* d'Orbigny
1931 *Epistomina elegans* (d'Orbigny) - Cushman, p. 65, Pl. 13, fig. 6
1979 *Hoeglundina elegans* (d'Orbigny) - Corliss, p. 12, Pl. 5, figs. 11-13
1991 *Hoeglundina elegans* (d'Orbigny) - Cimerman & Langer, p. 56, Pl. 59, figs. 10-12
1992 *Hoeglundina elegans* (d'Orbigny) - Schiebel, p. 49, Pl. 5, fig. 8
1993 *Hoeglundina elegans* (d'Orbigny) - Sgarrella & Moncharmont Zei, p. 242, Pl. 26, figs. 7 & 8
1994 *Hoeglundina elegans* (d'Orbigny) - Jones, p. 104, Pl. 105, figs. 3-6
2005 *Hoeglundina elegans* (d'Orbigny) - Rasmussen, p. 78, Pl. 9, fig. 11

Superfamily: Robertinacea Reuss, 1850

Family: Robertinidae Reuss, 1850

Subfamily: Alliatininae Mc Gowran, 1966

Genus: *Robertina* d'Orbigny, 1846

***Robertina translucens* Cushman & Parker**

1936 *Robertina translucens* Cushman & Parker
1958 *Robertina translucens* Cushman & Parker - Parker, p. 263, Pl. 2, fig. 34
1993 *Robertina translucens* Cushman & Parker - Sgarrella & Moncharmont Zei, p. 244, Pl. 26, fig. 13
2004 *Robertina translucens* Cushman & Parker - Chendes et al., p. 76, Pl. 1, fig. 17
2005 *Robertina translucens* Cushman & Parker - Rasmussen, p. 79, Pl. 9, fig. 12

Suborder Rotaliina Delage & Hertouard, 1896

Superfamily: Bolivinacea Glaessner, 1937

Family: Bolivinidae Glassner, 1937

Genus: *Bolivina* d'Orbigny, 1839

***Bolivina cistina* Cushman**

1936 *Bolivina cistina* Cushman

1990 *Bolivina cistina* (Cushman) - Hasegawa et al., p. 476, Pl. 3, figs. 1 & 2
1991 *Abditodentrix rhomboidales* (Millett) - Cimerman & Langer, p. 60, Pl. 61, figs. 4-6

***Bolivina plicatella* Cushman**

1930 *Bolivina plicatella* Cushman
1990 *Bolivina plicatella* Cushman - Hasegawa et al., p. 476, Pl. 3, figs. 3 & 4
1993 *Bolivina plicatella plicatella* Cushman - Mehrnusch, p. 11, figs. 22-27

***Bolivina pseudoplicata* Heron-Allen & Earland**

(Pl. 3, fig. 10)

1858 *Bolivina pseudoplicata* Heron-Allen & Earland
1958 *Bolivina pseudoplicata* Heron-Allen & Earland - Parker, p. 261, Pl. 2, fig. 8
1960 *Bolivina pseudoplicata* Heron-Allen & Earland - Hofker, p. 251, Pl. D, fig. 108
1990 *Bolivina pseudoplicata* Heron-Allen & Earland - Hasegawa, p. 476, Pl. 3, figs. 5 & 6
1991 *Bolivina pseudoplicata* Heron-Allen & Earland - Cimerman & Langer, p. 58, Pl. 61, figs. 1 & 2
1993 *Bolivina pseudoplicata* Heron-Allen & Earland - Sgarrella & Moncharmont Zei, p. 208, Pl. 14, figs. 9 & 10
2003 *Bolivina pseudoplicata* Heron-Allen & Earland - Murray, p. 19, fig. 5, no. 17
2005 *Bolivina pseudoplicata* Heron-Allen & Earland - Rasmussen, p. 80, Pl. 9, figs. 16 & 17

***Bolivina subspinescens* Cushman**

1922 *Bolivina subspinescens* Cushman
1990 *Bolivina subspinescens* Cushman - Hasegawa et al., p. 476, Pl. 3, fig. 10
1992 *Bolivina subspinescens* Cushman - Schiebel, p. 34, Pl. 1, fig. 5
1993 *Bolivina subspinescens* Cushman - Sgarrella & Moncharmont Zei, p. 210, Pl. 14, figs. 12 & 13
2005 *Sagrina subspinescens* (Cushman) - Rasmussen, p. 85, Pl. 11, fig. 2
2008 *Bolivina subspinescens* Cushman - Leiter, p. 24, Pl. 3, fig. 4

***Bolivina variablis* (Williamson)**

(Pl. 3, fig. 11)

1858 *Textularia variablis* Williamson
1965 *Bolivina variablis* (Williamson) - Phleger, p. 51, Pl. 1, fig. 8
1991 *Bolivina variablis* (Williamson) - Cimerman & Langer, p. 59, Pl. 61, figs. 7 & 8
1992 *Bolivina variablis* (Williamson) - Schiebel, p. 32, Pl. 1, fig. 6a
1993 *Bolivina variablis* (Williamson) - Hottinger et al., p. 91, Pl. 110, figs. 1-4; Pl. 111, figs. 1 & 2

***Bolivina* sp. 1**

Remarks: The test is elongate and triangular in outline. The periphery is rounded. The chambers are broad, low and biserially arranged. The test surface is ornamented with flat rips and ridges. It is less densely perforate on the older chambers, and more densely perforate on the last chamber. The wall is calcareous and hyaline. The aperture is a narrow loop at the base of the apertural face.

Genus: *Brizalina* Costa, 1856

***Brizalina difformis* (Williamson)**

(Pl. 3, fig. 12)

1858 *Textularia variablis* var. *difformis* Williamson
1958 *Bolivina difformis* (Williamson) - Parker, p. 260, Pl. 2, fig. 9
1991 *Brizalina difformis* (Williamson) - Cimerman & Langer, p. 59, Pl. 61, figs. 9-11
2003 *Brizalina difformis* (Williamson) - Murray, p. 19, fig. 6, no. 2

***Brizalina dilatata* (Reuss)**

1850 *Bolivina dilatata* Reuss
1911 *Bolivina dilatata* Reuss - Cushman, p. 33, text-fig. 54
1991 *Brizalina dilatata* (Reuss) - Cimerman & Langer, p. 59, Pl. 62, fig. 2
1992 *Bolivina dilatata* Reuss - Schiebel, p. 31, Pl. 1, fig. 4a
2002 *Brizalina dilatata* (Reuss) - Kaminski, p. 173, Pl. 2, fig. 13
2004 *Bolivina dilatata* Reuss - Mendes et al., p. 180, Pl. 2, fig. 1
2008 *Bolivina dilatata* Reuss - Leiter, p. 22, Pl. 3, fig. 6

***Brizalina spathulata* (Williamson)**

(Pl. 3, fig. 14)

1858 *Textularia variablis* var. *spathulata* Williamson
1987 *Bolivina spathulata* (Williamson) - Jorissen, p. 34, Pl. 1, fig. 5
1991 *Brizalina spathulata* (Williamson) - Cimerman & Langer, p. 60, Pl. 62, figs. 3-5

1993 *Bolivina spathulata* (Williamson) - Sgarrella & Moncharmont Zei, p. 210, Pl. 14, fig. 3
1994 *Brizalina spathulata* (Williamson) - Jones, p. 57, Pl. 52, figs. 20 & 21
2003 *Brizalina spathulata* (Williamson) - Murray, p. 19, fig. 6, no. 3
2004 *Brizalina spathulata* (Williamson) - Chendes et al., p. 76, Pl. 2, fig. 3
2004 *Brizalina spathulata* (Williamson) - Mendes et al., p. 180, Pl. 2, fig. 7
2005 *Brizalina spathulata* (Williamson) - Rasmussen, p. 81, Pl. 9, fig. 23
2006 *Brizalina spathulata* (Williamson) - Avsar et al., p. 133, Pl. 1, fig. 19

***Brizalina striatula* (Cushman)**

(Pl. 3, fig. 13)

1922 *Bolivina striatula* Cushman
1960 *Bolivina striatula* Cushman - Hofker, p. 251, Pl. D, fig. 106
1965 *Bolivina striatula* Cushman - Phleger, p. 51, Pl. 1, fig. 4
1991 *Brizalina striatula* (Cushman) - Cimerman & Langer, p. 60, Pl. 62, figs. 6-9
1992 *Bolivina striatula* Cushman - Schiebel, p. 32, Pl. 1, fig. 9
1993 *Brizalina striatula* (Cushman) - Hottinger et al., p. 92, Pl. 112, figs. 3-8
1993 *Bolivina striatula* Cushman - Sgarrella & Moncharmont Zei, p. 210, Pl. 14, fig. 16
2003 *Brizalina striatula* (Cushman) - Kaminski et al., p. 172, Pl. 2, fig. 10
2005 *Brizalina striatula* (Cushman) - Rasmussen, p. 82, Pl. 9, fig. 24

***Brizalina* sp. 1**

Remarks: This species has an elongate, compressed and lancelote test. The wall is hyaline and calcareous. The chambers are biserially arranged and broad. The last chambers contain pores. The final chamber has an irregular form. The aperture is an elongate, interiomarginal loop with an internal toothplate.

Superfamily: Cassidulinacea d'Orbigny, 1839
Family: Cassidulinidae d'Orbigny, 1839
Subfamily: Cassidulininae d'Orbigny, 1839

***Cassidulinid* sp. 1**

Remarks: The test is circular and flattened. The early chambers are biserially enrolled and later chambers are uniserially enrolled. Chambers increase in size when added. The wall is calcareous and finely perforate. The test surface is smooth. The aperture, at the base of the last chamber, is rounded.

Genus: *Cassidulina* d'Orbigny, 1826

***Cassidulina crassa* d'Orbigny**

(Pl. 3, fig. 15)

1839 *Cassidulina crassa* d'Orbigny, p. 56, Pl. 7, figs. 18-20
1911 *Cassidulina crassa* d'Orbigny - Cushman, p. 97, text-fig. 151
1945 *Cassidulina crassa* d'Orbigny - Cushman, p. 288, figs.18 & 19
1958 *Cassidulina crassa* d'Orbigny - Parker, p. 271, Pl. 4, fig. 12
1987 *Cassidulina crassa* d'Orbigny - Jorissen, p. 41, Pl. 1, fig. 3
1992 *Cassidulina crassa* d'Orbigny - Schiebel, p. 39, Pl. 2, fig. 13
1993 *Cassidulina crassa* d'Orbigny - Sgarrella & Moncharmont Zei, p. 236, Pl. 23, figs. 10 & 11
1994 *Cassidulina crassa* d'Orbigny - Jones, p. 60, Pl. 54, fig. 4
2003 *Cassidulina obtusa* Williamson - Murray, p. 21, fig. 6, no. 11 & 12
2005 *Cassidulina obtusa* Williamson - Rasmussen, p. 82, Pl. 10, figs. 2-4

***Cassidulina laevigata* s.l. d'Orbigny**

(Pl. 3, fig. 16)

1826 *Cassidulina leavigata* d'Orbigny
1896 *Cassidulina laevigata* d'Orbigny var. *carinata* Silvestri
1911 *Cassidulina leavigata* d'Orbigny - Cushman, p. 96, text-fig. 150
1960 *Cassidulina laevigata* d'Orbigny - Hofker, p. 250, Pl. D, fig. 103
1988 *Cassidulina leavigata* d'Orbigny - Loeblich & Tappan, p. 144, Pl. 555, figs. 1-5
1990 *Cassidulina carinata* Silvestri - Hasegawa, p. 477, Pl. 4, figs. 1 & 2
1991 *Cassidulina leavigata* d'Orbigny - Cimerman & Langer, p. 61, Pl. 63, figs. 1-3
1992 *Cassidulina leavigata* d'Orbigny - Schiebel, p. 39, Pl. 2, fig. 11
1993 *Cassidulina carinata* Silvestri - Sgarrella & Moncharmont Zei, p. 236, Pl. 23, figs. 8 & 9
2004 *Cassidulina carinata* Silvestri - Chendes et al., p. 76, Pl. 2, fig. 4
2004 *Cassidulina leavigata* d'Orbigny - Mendes et al., p. 180. Pl. 2, fig. 11

2005 *Cassidulina carinata* Silvestri - Rasmussen, p. 82, Pl. 10, fig. 1
2006 *Cassidulina carinata* Silvestri - Avsar et al., p. 133, Pl. 1, fig. 20
2009 *Cassidulina carinata* Silvestri - Frezza & Carboni, p. 57, Pl. 2, fig. 12

Remarks: In this work, the species *Cassidulina laevigata* d'Orbigny and *Cassidulina carinata* Silvestri has been summarized to *Cassidulina leavigata* s.l.. *Cassidulina carinata* is a subspecies of *C. laevigata* with an acute margin and a thin keel.

Genus: *Cassidulinoides* Cushman, 1927

***Cassidulinoides bradyi* (Norman)**

1880 *Cassidulina bradyi* Norman
1911 *Cassidulina bradyi* Norman - Cushman, p. 99, text-fig. 153
1993 *Cassidulinoides bradyi* (Norman) - Sgarrella & Moncharmont Zei, p. 211, Pl. 14, fig. 15
1994 *Cassidulinoides bradyi* (Norman) - Jones, p. 60, Pl. 54, figs. 6-9
2005 *Cassidulinoides bradyi* (Norman) - Rasmussen, p. 83, Pl. 10, fig. 8

Genus: *Globocassidulina* Voloshinova, 1960

***Globocassidulina oblonga* (Reuss)**

(Pl. 3, fig. 18)

1850 *Cassidulina oblonga* Reuss
1987 *Globocassidulina oblonga* (Reuss) - Alberola et al., p. 308, Pl. 4, fig. 12
1987 *Cassidulina oblonga* Reuss - Jorissen, p. 41, Pl. 3, fig. 11
1988 *Globocassidulina oblonga* (Reuss) - Loeblich & Tappan, p. 145, Pl. 557, figs. 1-4
1990 *Globocassidulina subglobosa* (Brady) - Hasegawa, p. 477, Pl. 4, figs. 5 & 6
2004 *Globocassidulina oblonga* (Reuss) - Rasmussen, p. 83, Pl. 10, figs. 9 & 10
2006 *Globocassidulina subglobosa* (Brady) - Avsar et al., p. 133, Pl. 2, figs. 1 & 2
2009 *Globocassidulina subglobosa* (Brady) - Frezza & Carboni, p. 57, Pl. 2, fig. 13

***Globocassidulina subglobosa* (Brady)**

(Pl. 3, fig. 17)

1881 *Cassidulina subglobosa* Brady
1911 *Cassidulina subglobosa* Brady - Cushman, p. 98, text-fig. 152
1958 *Globocassidulina subglobosa* (Brady) - Parker, p. 272, Pl. 4, fig. 13
1979 *Globocassidulina subglobosa* (Brady) - Corliss, p. 8, Pl. 3, figs. 12 & 13
1988 *Globocassidulina subglobosa* (Brady) - Loeblich & Tappan, p. 145, Pl. 557, figs. 18-23
1990 *Globocassidulina oblonga* (Reuss) - Hasegawa et al., p. 477, Pl. 4, figs. 3 & 4
1991 *Globocassidulina subglobosa* (Brady) - Cimerman & Langer, p. 61, Pl. 63, figs. 4-6
1992 *Globocassidulina subglobosa* (Brady) - Schiebel, p. 47, Pl. 2, fig. 14
1993 *Globocassidulina subglobosa* (Brady) - Sgarrella & Moncharmont Zei, p. 236, Pl. 24, figs. 1 & 2
1994 *Globocassidulina subglobosa* (Brady) - Jones, p. 60, Pl. 54, fig. 17
2003 *Globocassidulina subglobosa* (Brady) - Murray, p. 24, fig. 8, no. 7
2005 *Globocassidulina subglobosa* (Brady) - Rasmussen, p. 84, Pl. 10, fig. 11

Superfamily: Turrilinacea Cushman, 1927

Family: Turrilinidae Cushman, 1927

Genus: *Floresina* Revets, 1990

***Floresina* sp. 1**

1991 *Floresina* sp. 1 - Cimerman & Langer, p. 61, Pl. 65, figs. 4-6
1993 *Floresina* sp. A - Hottinger et al., p. 95, Pl. 117, figs. 8-11

Family: Stainforthiidae Reiss, 1963

Genus: *Stainforthia* Hofker, 1956

***Stainforthia complanata* (Egger)**

1893 *Virgulina schreibersiana* Czjzek var. *complanata* Egger
1958 *Virgulina complanata* Egger - Parker, p. 272, Pl. 4, fig. 20
1988 *Stainforthia concava* (Hoeglund) - Loeblich & Tappan, p. 148, Pl. 565, figs. 9-12
1992 *Stainforthia concava* (Hoeglund) - Wollenburg, p. 57, Pl. 16, fig. 1
1993 *Stainforthia complanata* (Egger) - Sgarrella & Moncharmont Zei, p. 214, Pl. 15, fig. 4
2005 *Stainforthia complanata* (Egger) - Rasmussen, p. 84, Pl. 10, figs. 16 & 17

Superfamily: Buliminacea Jones, 1875

Family: Siphogenerinoididae Saidova, 1981

Subfamily: Tubulogenerininae Saidova, 1987

Genus: *Rectuvigerina* Mathews, 1945

***Rectuvigerina bononiensis* (Fornasini)**

(Pl. 3, fig. 19)

1888 *Uvigerina bononiensis* Fornasini
1992 *Rectuvigerina bononiensis* (Fornasini) - Schiebel, p. 54, Pl. 3, fig. 8
2008 *Uvigerina bononiensis* Fornasini - Leiter, p. 55, Pl. 4, fig. 10

***Rectuvigerina phlegeri* Le Calvez**

(Pl. 3, fig. 20)

1959 *Rectuvigerina phlegeri* Le Calvez
1992 *Rectuvigerina phlegeri* Le Calvez - Schiebel, p. 55, Pl. 3, fig. 10
1993 *Rectuvigerina phlegeri* Le Calvez - Sgarrella & Moncharmont Zei, p. 215, Pl. 16, figs. 3 & 4
2004 *Rectuvigerina phlegeri* Le Calvez - Chendes et al., p. 76, Pl. 2, fig. 5
2006 *Rectuvigerina phlegeri* Le Calvez - Avsar et al., p. 133, Pl. 2, fig. 3
2009 *Rectuvigerina phlegeri* Le Calvez - Frezza & Carboni, p. 55, Pl. 1, fig. 6

Family: Buliminidae Jones, 1875

Genus: *Bulimina* d'Orbigny, 1826

***Bulimina aculeata* d'Orbigny**

(Pl. 3, fig. 21)

1826 *Bulimina aculeata* d'Orbigny
1911 *Bulimina aculeata* d'Orbigny - Cushman, p. 86, text-fig. 139
1958 *Bulimina aculeata* d'Orbigny - Parker, p. 261. Pl. 2, figs. 17 & 18
1987 *Bulimina marginata* forma *aculeata* d'Orbigny - Jorissen, p. 43, Pl. 4, fig. 5
1990 *Bulimina aculeata* d'Orbigny - Hasegawa, p. 476, Pl. 3, figs. 14 & 15
1991 *Bulimina aculeata* d'Orbigny - Cimerman & Langer, p. 61, Pl. 63, figs. 10 & 11
1992 *Bulimina aculeata* d'Orbigny - Schiebel, p. 35, Pl. 2, fig. 1
1993 *Bulimina aculeata* d'Orbigny - Sgarrella & Moncharmont Zei, p. 211, Pl. 15, fig. 1
1994 *Bulimina aculeata* d'Orbigny - Jones, p. 56, Pl. 51, figs. 7-9
2003 *Bulimina aculeata* d'Orbigny - Kaminski et al., p. 174, Pl. 3, fig. 3
2004 *Bulimina aculeata* d'Orbigny - Chendes et al., p. 76, Pl. 2, fig. 8
2004 *Bulimina aculeata* d'Orbigny - Mendes et al., p. 180. Pl. 2, fig. 3
2008 *Bulimina aculeata* d'Orbigny - Leiter, p. 24, Pl. 3, fig. 11

***Bulimina costata* d'Orbigny**

1852 *Bulimina costata* d'Orbigny
1958 *Bulimina costata* d'Orbigny - Parker, p. 261, Pl. 2, figs. 19 & 20
1987 *Bulimina costata* d'Orbigny - Jorissen, p. 34, Pl. 1, fig. 9
1991 *Bulimina* cf. *B. alazaensis* Cushman - Cimerman & Langer, p. 62, Pl. 64, figs. 1 & 2
1993 *Bulimina costata* d'Orbigny - Sgarrella & Moncharmont Zei, p. 211, Pl. 15, fig. 3
2003 *Bulimina costata* d'Orbigny - Kaminski et al., p. 174, Pl. 3, figs. 5 & 6
2004 *Bulimina costata* d'Orbigny - Chendes et al., p. 76, Pl. 2, fig. 6
2005 *Bulimina costata* d'Orbigny - Rasmussen, p. 85, Pl. 11, fig. 3

***Bulimina elongata* d'Orbigny**

(Pl. 3, fig. 22)

1846 *Bulimina elongata* d'Orbigny, p. 187, Tab. 11, figs. 19 & 20
1911 *Bulimina elongata* d'Orbigny - Cushman, p. 79, text-fig. 131
1991 *Bulimina elongata* d'Orbigny - Cimerman & Langer, p. 62, Pl. 64, figs. 3-8
1993 *Bulimina elongata* d'Orbigny - Hottinger et al., p. 99, Pl. 124, figs. 3-6
1993 *Bulimina elongata* d'Orbigny - Sgarrella & Moncharmont Zei, p. 211, Pl. 15, figs. 10 & 11
1994 *Bulimina elongata* d'Orbigny - Jones, p. 55, Pl. 50, figs. 3 & 4; Pl. 51, figs. 1 & 2
2002 *Bulimina elongata* d'Orbigny - Kaminski et al., p. 175, Pl. 3, fig. 4
2004 *Bulimina elongata* d'Orbigny - Chendes et al., p. 76, Pl. 2, fig. 7

Remarks: The specimens have often basal spines, but differ from *B. aculeata* by its elongate test.

***Bulimina gibba* Fornasini**

(Pl. 3, fig. 23)

1901 *Bulimina gibba* Fornasini
1958 *Bulimina gibba* Fornasini - Parker, p. 261, Pl. 2, figs. 21 & 22
1960 *Bulimina gibba* Fornasini - Hofker, p. 248, Pl. D, figs. 91-95
1994 *Bulimina gibba* Fornasini - Jones, p. 54, Pl. 50, figs. 1 & 2
2005 *Bulimina gibba* Fornasini - Rasmussen, p. 86, Pl. 11, fig. 5

***Bulimina marginata* d'Orbigny**

1826 *Bulimina marginata* d'Orbigny
1911 *Bulimina marginata* d'Orbigny - Cushman, p. 83, text-fig. 136

1958 *Bulimina marginata* d'Orbigny - Parker, p. 262, Pl. 2, fig. 23
1987 *Bulimina marginata* forma *marginata* d'Orbigny - Jorissen, p. 43, Pl. 4, figs. 6 a & b
1988 *Bulimina marginata* d'Orbigny - Loeblich & Tappan, p. 150, Pl. 571, figs. 1-3
1991 *Bulimina marginata* d'Orbigny - Cimerman & Langer, p. 62, Pl. 64, figs. 9-11
1992 *Bulimina marginata* d'Orbigny - Schiebel, p. 36, Pl. 2, fig. 2
1993 *Bulimina marginata* d'Orbigny - Sgarrella & Moncharmont Zei, p. 212, Pl. 15, figs. 5-7
1994 *Bulimina marginata* d'Orbigny - Jones, p. 55, Pl. 51, figs. 3-5
2004 *Bulimina marginata* d'Orbigny - Mendes et al., p. 180, Pl. 2, fig. 3
2005 *Bulimina marginata* d'Orbigny - Rasmussen, p. 86, Pl. 11, fig. 6
2008 *Bulimina marginata* d'Orbigny - Leiter, p. 26, Pl. 3, fig. 12

Genus: *Globobulimina* Cushman, 1927

***Globobulimina affinis* d'Orbigny**

1839 *Globobulimina affinis* d'Orbigny
1993 *Globobulimina affinis* d'Orbigny - Sgarrella & Moncharmont Zei, p. 212, Pl. 15, figs. 8 & 9
2005 *Globobulimina affinis* d'Orbigny - Rasmussen, p. 87, Pl. 11, fig. 7
2006 *Globobulimina affinis* d'Orbigny - Avsar et al., p. 133, Pl. 2, fig. 6
2008 *Globobulimina affinis* d'Orbigny - Leiter, p. 40, Pl. 4, fig. 4

Family: Uvigerinidae Haeckel, 1894

Subfamily: Uvigerininae Haeckel, 1894

Genus: *Siphouvigerina* Parr, 1950

?*Siphouvigerina* sp. 1

1991 cf. *Siphouvigerina* sp. 1 - Cimerman & Langer, p. 62, Pl. 66, figs. 1 & 2

Remarks: The test is elongate with a triserial and appressed arrangement of the earlier chambers. Later chambers are loosely triserial and then biserial and umbrella-like. The wall is calcareous and perforate. The test surface is irregularly ornamented by longitudinally ridges. The rounded aperture is terminal at the end of a short neck and bordered by a rim.

Genus: *Uvigerina* d'Orbigny, 1826

***Uvigerina peregrina* Cushman**

(Pl. 4, fig. 1)

1932 *Uvigerina peregrina* Cushman
1958 *Uvigerina peregrina* Cushman - Parker, p. 263, Pl. 2, figs. 37 & 38
1988 *Uvigerina peregrina* Cushman - Loeblich & Tappan, p. 151, Pl. 573, figs. 24-28
1993 *Uvigerina peregrina* Cushman - Sgarrella & Moncharmont Zei, p. 215, Pl. 16, fig. 5
2004 *Uvigerina peregrina* Cushman - Mendes et al., p. 180, Pl. 2, fig. 12
2005 *Uvigerina peregrina* Cushman - Rasmussen, p. 88, Pl. 11, figs. 14 & 15
2009 *Uvigerina peregrina* Cushman - Frezza & Carboni, p. 57, Pl. 2, fig. 15

***Uvigerina* sp. 1**

Remarks: The test is elongate and rounded in section. Early chambers are appressed and triserially arranged. Later chambers are more loosely triserial and larger. Sutures are distinct and depressed. The wall is calcareous and perforate. The test surface is ornamented by longitudinally ridges. The aperture is terminal and bordered by a lip provided with a hemicylindrical toothplate.

Subfamily: Angulogerininae Galloway, 1933

Genus: *Angulogerina* Cushman, 1927

***Angulogerina angulosa* (Williamson)**

(Pl. 4, fig. 2)

1858 *Uvigerina angulosa* Williamson
1958 *Angulogerina angulosa* (Williamson) - Parker, p. 259, Pl. 2, figs. 1 & 2
1988 *Angulogerina angulosa* (Williamson) - Loeblich & Tappan, p. 151, Pl. 574, figs. 5-9
1991 *Angulogerina angulosa* (Williamson) - Cimerman & Langer, p. 63, Pl. 66, figs. 3 & 4
1992 *Trifarina angulosa* (Williamson) - Schiebel, p. 56, Pl. 3, fig. 1
1993 *Angulogerina angulosa* (Williamson) - Sgarrella & Moncharmont Zei, p. 215, Pl. 16, fig. 8
2003 *Trifarina angulosa* (Williamson) - Murray, p. 26, fig. 10, no. 5

2005 *Trifarina angulosa* (Williamson) - Rasmussen, p. 89, Pl. 12, fig. 1

Genus: *Trifarina* Cushman 1923

***Trifarina fornasinii* (Selli)**

1948 *Angulogerina fornasinii* Selli
1992 *Trifarina fornasinii* (Selli) - Schiebel, p. 56, Pl. 3, fig. 2
2005 *Trifarina fornasinii* (Selli) - Rasmussen, p. 89, Pl. 12, fig. 3

Family: Reussellidae Cushman, 1933

Genus: *Reussella* Galloway, 1933

***Reussella spinulosa* (Reuss)**

(Pl. 4, fig. 3)

1850 *Verneuilina spinulosa* Reuss
1911 *Verneuilina spinulosa* Reuss - Cushman, p. 55, text-fig. 88
1987 *Reussella spinulosa* (Reuss) - Alberola et al., p. 322, Pl. 4, fig. 14
1987 *Reussella spinulosa* (Reuss) - Jorissen, p. 41, Pl. 3, fig. 7
1988 *Reussella spinulosa* (Reuss) - Loeblich & Tappan, p. 152, Pl. 575, figs. 9-12
1991 *Reussella spinulosa* (Reuss) - Cimerman & Langer, p. 63, Pl. 66, figs. 5-8
1993 *Reussella spinulosa* (Reuss) - Sgarrella & Moncharmont Zei, p. 214, Pl. 15, fig. 14
2005 *Reussella spinulosa* (Reuss) - Rasmussen, p. 90, Pl. 12, fig. 4
2006 *Reussella spinulosa* (Reuss) - Avsar et al., p. 133, Pl. 2, fig. 7
2009 *Reussella spinulosa* (Reuss) - Avsar et al., p. 134, Pl. 2, fig. 9

Superfamily: Fursenkoinacea Loeblich & Tappan, 1961

Family: Fursenkoinidae Loeblich & Tappan, 1961

Genus: *Fursenkoina* Loeblich & Tappan, 1961

***Fursenkoina acuta* (d'Orbigny)**

1846 *Polymorphina acuta* d'Orbigny
1991 *Fursenkoina acuta* (d'Orbigny) - Cimerman & Langer, p. 64, Pl. 67, figs. 1 & 2
1993 *Fursenkoina acuta* (d'Orbigny) - Sgarrella & Moncharmont Zei, p. 235, Pl. 23, fig. 7
2002 *Fursenkoina acuta* (d'Orbigny) - Kaminski et al., p. 174, Pl. 3, figs. 11 & 12
2005 *Fursenkoina acuta* (d'Orbigny) - Rasmussen, p. 90, Pl. 12, fig. 8
2006 *Fursenkoina acuta* (d'Orbigny) - Avsar et al., p. 133, Pl. 2, fig. 8
2009 *Fursenkoina acuta* (d'Orbigny) - Avsar et al., p. 135, Pl. 2, fig. 10

Genus: *Sigmavirgulina* Loeblich & Tappan, 1957

***Sigmavirgulina tortuosa* (Brady)**

1881 *Bolivina tortuosa* Brady
1988 *Sigmavirgulina tortuosa* (Brady) - Loeblich & Tappan, p. 153, Pl. 579, figs. 1-5
1994 *Sigmavirgulina tortuosa* (Brady) - Jones, p. 58, Pl. 52, figs. 31-34

***Sigmavirgulina* sp. 1**

1990 *Sigmavirgulina* sp. 1 - Cimerman & Langer, p. 64, Pl. 67, figs. 3-7

Remarks: The test is flatter than the typical flaring test of *Sigmavirgulina* species, and biserial. The early chambers show a sigmoidal alignment and the later chambers increase in breadth and are arranged in a single plane. The periphery is carinate. The wall is calcareous and later chambers are coarsely perforate. The aperture is elongate and oval at the inner margin of the final chamber, and surrounded by a small lip.

Superfamily: Discorbacea Ehrenberg, 1838

Family: Bagginidae Cushman, 1927

Subfamily: Baggininae Cushman, 1927

Genus: *Cancris* De Montfort, 1808

***Cancris auriculus* (Fichtel & Moll)**

(Pl. 4, figs. 4 & 5)

1798 *Nautilus auricula* Fichtel & Moll
1931 *Cancris auricula* (Fichtel & Moll) - Cushman, p. 72, Pl. 15, fig. 1
1988 *Cancris auriculus* (Fichtel & Moll) - Loeblich & Tappan, p. 157, Pl. 591, figs. 1-3
1993 *Cancris auriculus* (Fichtel & Moll) - Hottinger et al., p. 106, Pl. 136, figs. 6-14
1994 *Cancris auriculus* (Fichtel & Moll) - Jones, p. 105, Pl. 106, fig. 4

2005 *Cancris auricula* (Fichtel & Moll) - Rasmussen, p. 91, Pl. 12, figs. 14 & 15

Genus: *Valvulineria* Cushman, 1926

***Valvulineria bradyana* (Fornasini)**

(Pl. 4, figs. 6 & 7)

1900 *Discorbina bradyana* Fornasini
1958 *Valvulineria complanata* (d'Orbigny) - Parker, p. 268, Pl. 3, figs. 42-44
1987 *Valvulineria bradyana* (Fornasini) - Jorissen, p. 43, Pl. 4, figs. 2 a & b
1991 *Valvulineria bradyana* (Fornasini) - Cimerman & Langer, p. 64, Pl. 67, figs. 8-10
1993 *Valvulineria bradyana* (Fornasini) - Sgarrella & Moncharmont Zei, p. 220, Pl. 18, figs. 1 & 2
1995 *Valvulineria bradyana* (Fornasini) - Coppa & Di Tuoro, p. 170, Pl. 3, figs. 3 & 6
2004 *Valvulineria bradyana* (Fornasini) - Chendes et al., p. 76, Pl. 2, fig. 12
2005 *Valvulineria complanata* (d'Orbigny) - Rasmussen, p. 91, Pl. 12, figs. 16 & 17
2006 *Valvulineria complanata* (d'Orbigny) - Avsar et al., p. 133, Pl. 2, figs. 9 & 10
2009 *Valvulineria bradyana* (Fornasini) - Avsar et al., p. 135, Pl. 2, figs. 11 & 12
2009 *Valvulineria bradyana* (Fornasini) - Frezza & Carboni, p. 55, Pl. 1, figs. 1 & 2

***Valvulineria minuta* Parker**

1954 *Valvulineria minuta* Parker
1993 *Valvulineria minuta* Parker - Sgarella & Moncharmont Zei, p. 220, Pl. 18, figs. 3 & 4

***Valvulineria* sp. 1**

Remarks: The test is rounded in outline and trochospirally enrolled. Two and a half whorls are visible. The chambers are inflated and gradually increase when added. Six chambers are visible in the final whorl. The periphery is rounded. The spiral side is flattened. On the umbilical side, the umbilicus is depressed. Sutures are curved, radial and depressed. The wall is calcareous, more finely perforate than *Valvulineria bradyana,* and hyaline with a smooth surface. The aperture is an interiomarginal arch on the base of the last chamber with a flap that partly covers the umbilicus.

Family: Eponididae Hofker, 1951

Subfamily: Eponidinae Hofker, 1951

Genus: *Eponides* De Montfort, 1808

***Eponides concameratus* (Williamson)**

(Pl. 4, figs. 8 & 9)

1858 *Rotalina concamerata* Williamson
1931 *Eponides repanda* var. *concamerata* (Williamson) - Cushman, p. 51, Pl. 11, fig. 4
1988 *Eponides repandus* (Fichtel & Moll) - Loeblich & Tappan, p. 158, Pl. 594, figs. 1-3
1991 *Eponides concameratus* (Williamson) - Cimerman & Langer, p. 64, Pl. 67, figs. 11-14
1993 *Eponides repandus* (Fichtel & Moll) - Hottinger et al., p. 106, Pl. 137, figs. 1-10
1993 *Eponides repandus* var. *concamerata* (Williamson) - Sgarrella & Moncharmont Zei, 232, Pl. 22, figs. 4 & 5
1995 *Eponides repandus* (Fichtel & Moll) - Coppa & Di Tuoro, p. 172, Pl. 4, figs. 8 & 10
2005 *Eponides repandus* (Fichtel & Moll) - Rasmussen, p. 92, Pl. 13, figs. 1 & 2

***Eponides* sp. 1**

1991 cf. *Eponides* sp. 1 - Cimerman & Langer, p. 64, Pl. 68, figs. 1 & 2

Remarks: The test is trochospiral and planoconvex. The spiral side is evolute. The umbilical side is convex and involute. Sutures are backwards curved, depressed on umbilical side, and thickened on the spiral side. The aperture is an interiomarginal, extraumbilical large arched slit. This species differs from *Eponides repandus* by the larger and curved apertural opening. The specimens in this study are generally larger and more oval in outside than *E. repandus*.

Family: Mississippinidae Saidova, 1981

Subfamily: Stomatorbininae Saidova, 1981

Genus: *Stomatorbina* Doreen, 1948

***Stomatorbina concentrica* (Parker & Jones)**

(Pl. 4, figs. 10 & 11)

1846 *Pulvinulina concentrica* Parker & Jones
1931 *Eponides concentrica* (Parker & Jones) - Cushman, p. 43, Pl. 9, figs. 4 & 5
1991 *Stomatorbina concentrica* (Parker & Jones) - Cimerman & Langer, p. 65, Pl. 68, figs. 7-9
1993 *Stomatorbina concentrica* (Parker & Jones) - Sgarrella & Moncharmont Zei, p. 232, Pl. 26, figs. 9 & 10
2005 *Stomatorbina concentrica* (Parker & Jones) - Rasmussen, p. 92, Pl. 13, figs. 3 & 4

***Stomatorbina* sp. 1**

Remarks: The test is flat, subelliptical in outline, very low trochospiral, evolute on the spiral side, and involute on the umbilical side. Six chambers are visible in the last whorl that increase in size. Sutures are narrower and not very elevated when compared to *Stomatorbina* described by Loeblich & Tappan (1988), but curved, oblique, depressed and nearly radiate on the umbilical side. The periphery is rounded. The wall is calcareous and finely perforate with a smooth surface. The aperture is an interio-marginal slit, partly covered by a triangular umbilical flap.

Family Discorbidae Ehrenberg, 1838

Genus: *Discorbis* Lamarck, 1804

***Discorbis williamsoni* Chapman & Parr**

(Pl. 4, figs. 12 & 13)

1932 *Discorbis williamsoni* Chapman & Parr
2003 *Discorbinoides milletti* (Wright) - Murray, p. 21, fig. 7, no. 3 & 4
2005 *Discorbis williamsoni* Chapman & Parr - Rasmussen, p. 93, Pl. 13, figs. 7 & 8

Family: Rosalinidae Reiss, 1963

Genus: *Gavelinopsis* Hofker, 1951

***Gavelinopsis praegeri* (Heron Allen & Earland)**

(Pl. 4, figs. 14 & 15)

1913 *Discorbina praegeri* Heron Allen & Earland
1931 ?*Discorbis praegeri* (Heron-Allen & Earland) - Cushman, p. 30, Pl. 6, fig. 4
1958 *Gavelinopsis praegeri* (Heron Allen & Earland) - Parker, p. 264, Pl. 3, figs. 24 & 25
1960 *Gavelinopsis praegeri* (Heron Allen & Earland) - Hofker, p. 252, Pl. D, fig. 114
1987 *Gavelinopsis praegeri* (Heron Allen & Earland) - Jorissen, p. 41, Pl. 3, fig. 13
1988 *Gavelinopsis praegeri* (Heron Allen & Earland) - Loeblich & Tappan, p. 161, Pl. 608, figs. 6-12
1991 *Gavelinopsis praegeri* (Heron Allen & Earland) - Cimerman & Langer, p. 66, Pl. 70, figs. 3 & 4
1992 *Gavelinopsis praegeri* (Heron Allen & Earland) - Schiebel, p. 46, Pl. 4, fig. 6
1993 *Gavelinopsis praegeri* (Heron Allen & Earland) - Sgarrella & Moncharmont Zei, p. 218, Pl. 17, figs. 1 & 2
2003 *Gavelinopsis praegeri* (Heron Allen & Earland) - Murray, p. 24, fig. 8, no. 5 & 6

Genus: *Neoconorbina* Hofker, 1951

***Neoconorbina terquemi* (Rzehak)**

(Pl. 4, figs. 16 & 17)

1888 *Discorbina terquemi* Rzehak
1958 *Neoconorbina terquemi* (Rzehak) - Parker, p. 267, Pl. 3, figs. 26 & 27
1960 *Neoconorbina neapolitana* Hofker - Hofker, p. 252, Pl. D, fig. 115
1987 *Neoconorbina terquemi* (Rzehak) - Alberola, p. 308, Pl. 4, fig. 9
1987 *Neoconorbina terquemi* (Rzehak) - Jorissen, p. 40, Pl. 3, figs. 3 & 4
1988 *Neoconorbina terquemi* (Rzehak) - Loeblich & Tappan, p. 161, Pl. 609, figs. 8-10
1991 *Neoconorbina terquemi* (Rzehak) - Cimerman & Langer, p. 66, Pl. 70, figs. 5-7
1993 *Neoconorbina terquemi* (Rzehak) - Sgarrella & Moncharmont Zei, p. 218, Pl. 17, fig. 3
1994 *Neoconorbina terquemi* (Rzehak) - Jones, p. 94, Pl. 88, figs. 5-8
2005 *Neoconorbina terquemi* (Rzehak) - Rasmussen, p. 93, Pl. 13, figs. 11 & 12
2006 *Neoconorbina terquemi* (Rzehak) - Avsar et al., p. 133, Pl. 2, fig. 16

Genus: *Planodiscorbis* Bermudez, 1952

***Planodiscorbis rarescens* (Brady)**

1884 *Discorbis rarescens* Brady
1915 *Discorbis rarescens* Brady - Cushman, p. 20, Pl. 7, fig. 4

1958 *Planodiscorbis* rarescens (Brady) - Todd, p. 196, Pl. 1, fig. 17

Genus: *Rosalina* d'Orbigny, 1826

***Rosalina anomala* Terquem**

(Pl. 4, figs. 18 & 19)

1875 *Rosalina anomala* Terquem
2003 *Rosalina anomala* Terquem - Murray, p. 26, fig. 9, no. 9 & 10
2006 *Rosalina anomala* Terquem - Wisshak & Rueggenberg, p. 4, fig. 3, figs. J & K

***Rosalina bradyi* Cushman**

(Pl. 4, figs. 20 & 21)

1915 *Rosalina bradyi* Cushman
1987 *Rosalina bradyi* Cushman - Jorissen, p. 41, Pl. 3, figs. 6 a & b
1991 *Rosalina bradyi* Cushman - Cimerman & Langer, p. 66, Pl. 71, figs. 1-5
1993 *Rosalina bradyi* Cushman - Hottinger et al., p. 110, Pl. 142, fig. 12; Pl. 143, figs. 1-6
1994 *Rosalina bradyi* Cushman - Jones, p. 93, Pl. 86, fig. 8
1995 *Rosalina globularis* d'Orbigny - Coppa & Di Tuoro, p. 170, Pl. 3, figs. 8 & 9

***Rosalina globularis* d'Orbigny**

1926 *Rosalina globularis* d'Orbigny
1988 *Rosalina globularis* d'Orbigny - Loeblich & Tappan, p. 161, Pl. 610, figs. 1-5; Pl. 611, figs. 1-3
1993 *Rosalina globularis* d'Orbigny - Sgarrella & Moncharmont Zei, p. 219, Pl. 17, figs. 7 & 8
2005 *Rosalina globularis* d'Orbigny - Rasmussen, p. 94, Pl. 14, fig. 1

***Rosalina macropora* (Hofker)**

(Pl. 5, figs. 1 & 2)

1951 *Discopulvinulina macropora* Hofker
1960 *Discopulvinulina macropora* Hofker - Hofker, p. 253, Pl. D, fig. 122
1991 *Rosalina macropora* (Hofker) - Cimerman & Langer, p. 67, Pl. 71, figs. 6 & 7
1993 *Rosalina bradyi* (Cushman) - Sgarrella & Moncharmont Zei, p. 218, Pl. 17, figs. 4 & 5
1995 *Rosalina bradyi* (Cushman) - Coppa & Di Tuoro, p. 168, Pl. 2, figs. 12 & 13
2004 *Mississipina concentrica* (Parker & Jones) - Mendes et al., p. 178, Pl. 1, fig. 4
2005 *Rosalina macropora* (Hofker) - Rasmussen, p. 95, Pl. 14, figs. 3 & 4

***Rosalina obtusa* d'Orbigny**

1846 *Rosalina obtusa* d'Orbigny, p. 179, Tab. 11, figs. 4-6
1958 *Rosalina obtusa* d'Orbigny - Parker, p. 268, Pl. 3, figs. 33, 34 & 39
1993 *Rosalina obtusa* d'Orbigny - Sgarrella & Moncharmont Zei, p. 219, Pl. 17, figs. 9 & 10
1995 *Rosalina obtusa* d'Orbigny - Coppa & Di Tuoro, p. 170, Pl. 3, figs. 1 & 2
2006 *Rosalina bradyi* Cushman - Avsar et al., p. 133, Pl. 2, figs. 13 & 14

***Rosalina* sp. 1**

1993 cf. *Rosalina* sp. A - Hottinger et al., p. 112, Pl. 145, figs. 1-4

Remarks: The test is large, trochospiral and flat. The spiral side is slightly convex and evolute, the umbilical side is involute. The test shape is often irregular. Six to seven chambers are visible in the adult coil, rapidly increasing in size when added. Sutures are thickened, curved on the spiral side, depressed and curved on the umbilical side. The test is coarsely perforated on the spiral side, but shows no perforation on the umbilical side.

Genus: *Spirorbina* Sellier de Civrieux, 1977

?*Spirorbina* sp. 1

Remarks: The test is low trochospiral and planoconvex. The spiral side is weakly convex and evolute with one and a half whorls of broad and low semilunate chambers. Six to seven chambers are visible in the final whorl. Sutures are backcurved, oblique, flush and obscure on both sides, but the first, second or three first sutures can be depressed on the spiral side. The umbilical side is flat and partially involute with large pustules in the umbilical region. The periphery is subacut. The wall is calcareous and finely perforate on

the spiral side. The umbilical side is not perforate or has a few large pores parallel to the sutures. The aperture is a low slit extending from near the periphery along the umbilical chamber margin to the preceding suture for much of the final whorl.

Genus: *Tretomphalus* Moebius, 1880

***Tretomphalus concinnus* (Brady)**

(Pl. 5, fig. 3)

1884 *Discorbina concinna* Brady
1915 *Discorbis concinna* (Brady) - Cushman, p. 16, Pl. 5, fig. 3
1988 *Tretomphalus concinnus* (Brady) - Loeblich & Tappan, p. 162, Pl. 613, figs. 1-6
1991 *Tretomphalus bulloides* (d'Orbigny) - Cimerman & Langer, p. 67, Pl. 72, figs. 3-5
1993 *Tretomphalus concinnus* (Brady) - Sgarrella & Moncharmont Zei, p. 219, Pl. 17, figs. 11 & 12
1994 *Tretomphalus concinnus* (Brady) - Jones, p. 96, Pl. 90, fig. 7

***Tretomphalus* sp. 1**

(Pl. 5, fig. 4)

Remarks: The test is trochospiral and planoconvex. Chambers rapidly increase when added and are slightly inflated. Five chambers are visible in the adult coil. On the spiral side, sutures are strongly backcurved, depressed and oblique. On the umbilical side, chambers are triangular and overlapping. The final chamber occupies about one third of the circumference. The chamber interior is simple and undivided. The periphery is subacut. The wall is calcareous and smooth. The spiral side is non-perforate or with a perforation of only one chamber. The umbilical side is densely and coarsely perforate. The aperture is a low interiomarginal arch with a bordering lip near the periphery on the umbilical side.

Family: Sphaeroidinidae Cushman, 1927

Genus: *Sphaeroidina* d'Orbigny, 1826

***Sphaeroidina bulloides* d'Orbigny**

1832 *Sphaeroidina bulloides* d'Orbigny
1914 *Sphaeroidina bulloides* d'Orbigny - Cushman, p. 18, Pl. 12, figs. 1 a & b
1960 *Sphaeroidina bulloides* d'Orbigny - Hofker, p. 251, Pl. D, fig. 107
1988 *Sphaeroidina bulloides* d'Orbigny - Loeblich & Tappan, p. 162, Pl. 617, figs. 1-6
1990 *Sphaeroidina bulloides* d'Orbigny - Hasegawa et al., p. 477, Pl. 4, figs. 10 & 11
1994 *Sphaeroidina bulloides* d'Orbigny - Jones, p. 91, Pl. 84, figs. 1 & 2
2005 *Sphaeroidina bulloides* d'Orbigny - Rasmussen, p. 95, Pl. 14, fig. 11

Superfamily: Glabratellacea Loeblich & Tappan, 1964

Family: Glabratellidae Loeblich & Tappan, 1964

Genus: *Conorbella* Hofker, 1951

***Conorbella imperiatoria* (d'Orbigny)**

1846 *Rosalina imperiatoria* d'Orbigny, p. 176, Tab. 10, figs. 16-18
1991 *Conorbella imperiatoria* (d'Orbigny) - Cimerman & Langer, p. 68, Pl. 72, figs. 9-11
1993 *Schackoinella imperiatoria* (d'Orbigny) - Sgarrella & Moncharmont Zei, p. 222, Pl. 18, figs. 5 & 6

***Conorbella pulvinata* (Brady)**

(Pl. 5, figs. 5 & 6)

1884 *Discorbina pulvinata* Brady
1915 *Discorbina pulvinata* Brady - Cushman, p. 19, Pl. 7, fig. 2
1988 *Conorbella pulvinata* (Brady) - Loeblich & Tappan, p. 163, Pl. 618, figs. 4-6
1991 *Conorbella pulvinata* (Brady) - Cimerman & Langer, p. 68, Pl. 73, figs. 4-7
1994 *Glabratella pulvinata* (Brady) - Jones, p. 94, Pl. 88, fig. 10
2005 *Glabratella pulvinata* (Brady) - Rasmussen, p. 96, Pl. 14, figs. 12 & 13

Genus: *Glabratella* Doreen, 1948

***Glabratella erecta* (Sidebottom)**

1908 *Discorbina erecta* Sidebottom

1991 *Conorbella erecta* (Sidebottom) - Cimerman & Langer, p. 68, Pl. 72, figs. 6-8
1993 *Glabratella erecta* (Sidebottom) - Sgarrella & Moncharmont Zei, p. 220, Pl. 18, figs. 7 & 8

***Glabratella hexacamerata* Seigle & Bermudez**

(Pl. 5, figs. 7 & 8)

1965 *Glabratella hexacamerata* Seigle & Bermudez
1993 *Glabratella hexacamerata* Seigle & Bermudez - Sgarrella & Moncharmont Zei, p. 222, Pl. 18, figs. 9 & 10

***Glabratella patelliformis* (Brady)**

1884 *Discorbis patelliformis* Brady
1915 *Discorbis patelliformis* Brady - Cushman, p. 17, Pl. 5, fig. 5
1994 *Glabratella patelliformes* (Brady) - Jones, p. 94, Pl. 88, figs. 3 a-c
1991 *Glabratella patelliformis* (Brady) - Cimerman, p. 68, Pl. 73, figs. 1-3

Genus: *Planoglabratella* Seiglie & Bermudez, 1965

***Planoglabratella opercularis* (d'Orbigny)**

(Pl. 5, figs. 9 & 10)

1939 *Rosalina opercularis* d'Orbigny
1915 *Discorbis opercularis* (d'Orbigny) - Cushman, p. 18, Pl. 11, fig. 3
1988 *Planoglabratella opercularis* (d'Orbigny) - Loeblich & Tappan, p. 164, Pl. 621, figs. 21-23
1994 *Planoglabratella opercularis* (d'Orbigny) - Sgarrella & Moncharmont Zei, p. 222, Pl. 19, figs. 4 & 5
2009 *Planoglabratella opercularis* (d'Orbigny) - Avsar et al. p. 135, Pl. 2, figs. 15 & 16

***Planoglabratella* sp. 1**

Remarks: The test is planoconvex and trochospiral, with a subconical spiral side and a flat umbilical side. On the spiral side, rapidly enlarging whorls are visible. The up to ten chambers are low, broad and strongly curved on both sides. The periphery is subangular with short spines. The wall is calcareous and perforate. On the umbilical side, there are fine radial striae with pustules in the center. The aperture is an interiomarginal slit near the periphery margin of the last chamber.

***Planoglabratella* sp. 2**

Remarks: The test is planoconvex and trochospiral, with a subconical spiral side and a flat umbilical side. More than eight backcurved chambers are visible. Sutures are relatively broad, backcurved on the spiral and umbilical side. The wall is calcareous and densely perforate with a smooth surface on the spiral side. The umbilical side provides radial microstriae and a pustulose region in its center. The aperture is a low interiomarginal slit near the peripheral margin of the final chamber.

Family: Heronalleniidae Loeblich & Tappan, 1986
Genus: *Heronallenia* Chapman & Parr, 1931

***Heronallenia lingulata* (Burrows & Holland)**

1895 *Discorbina lingulata* Burrows & Holland
1994 *Heronallenia lingulata* (Burrows & Holland) - Jones, p. 96, Pl. 91, fig. 3
1991 *Heronallenia* sp.1 - Cimerman & Langer, p. 69, Pl. 73, figs. 9-10
2005 *Heronallenia lingulata* (Burrows & Holland) - Rasmussen, p. 96, Pl. 14, figs. 16 & 17

Superfamily: Siphoninacea Cushman, 1927
Family: Siphoninidae Cushman, 1927
Subfamily: Siphonininae Cushman, 1927
Genus: *Siphonina* Reuss, 1850

***Siphonina reticulata* (Czjzek)**

1848 *Rotalina reticulata* Czjzek
1931 *Siphonina reticulata* (Czjzek) - Cushman, p. 68, Pl. 14, fig. 1
1958 *Siphonina reticulata* (Czjzek) - Parker, p. 273, Pl. 4, fig. 25
1988 *Siphonina reticulata* (Czjzek) - Loeblich & Tappan, p. 164, Pl. 624, figs. 4-6
1990 *Siphonina reticulata* (Czjzek) - Hasegawa et al., p. 477, Pl. 4, figs. 12-14

1991 *Siphonina reticulata* (Czjzek) - Cimerman & Langer, p. 69, Pl. 73, figs. 11-13
1993 *Siphonina reticulata* (Czjzek) - Sgarrella & Moncharmont Zei, p. 222, Pl. 19, figs. 7 & 8
2004 *Siphonina reticulata* (Czjzek) - Chendes et al., p. 76, Pl. 2, fig. 13
2005 *Siphonina reticulata* (Czjzek) - Rasmussen, p. 97, Pl. 14, fig. 18
2009 *Siphonina reticulata* (Czjzek) - Avsar et al., p. 135, Pl. 2, figs. 17 & 18

Genus: *Siphoninella* Cushman, 1927

***Siphoninella soluta* (Brady)**

1884 *Truncatulina soluta* Brady
1988 *Siphoninella soluta* (Brady) - Loeblich & Tappan, p. 164, Pl. 624, figs. 7-9
1994 *Siphoninella soluta* (Brady) - Jones, p. 100, Pl. 96, fig. 4

Superfamily: Discorbinellacea Sigal, 1952

Family: Discorbinellidae Sigal, 1952

Subfamily: Discorbinellinae Sigal, 1952

Genus: *Discorbinella* Cushman & Martin, 1935

***Discorbinella bertheloti* (d'Orbigny)**

(Pl. 5, figs. 11 & 12)

1839 *Rosalina bertheloti* d'Orbigny
1931 *Discorbis bertheloti* (d'Orbigny) - Cushman, p. 16, Pl. 2, fig. 2
1988 *Discorbinella bertheloti* (d'Orbigny) - Loeblich & Tappan, p. 166, Pl. 630, figs. 4-6
1993 *Discorbinella bertheloti* (d'Orbigny) - Hottinger et al., p. 114, Pl. 150, figs. 1-4
1993 *Discorbinella bertheloti* (d'Orbigny) - Sgarrella & Moncharmont Zei, p. 216, Pl. 16, figs. 11 & 12
2004 *Discorbinella bertheloti* (d'Orbigny) - Chendes et al., p. 76, Pl. 3, fig. 3
2005 *Discorbinella bertheloti* (d'Orbigny) - Rasmussen, p. 98, Pl. 14, figs. 25 & 26
2006 *Discorbinella bertheloti* (d'Orbigny) - Avsar et al., p. 133, Pl. 2, fig. 15
2009 *Discorbinella bertheloti* (d'Orbigny) - Avsar et al., p. 135, Pl. 2, figs. 19 & 20

Superfamily: Planorbulinacea Schwager, 1877

Family: Planulinidae Bermudez, 1952

Genus: *Hyalinea* Hofker, 1951

***Hyalinea balthica* (Schroeter)**

(Pl. 5, fig. 13)

1783 *Nautilus balthicus* Schroeter
1931 *Anomalina balthica* (Schroeter) - Cushman, p. 108, Pl. 19, fig. 3
1958 *Hyalinea balthica* (Schroeter) - Parker, p. 275, Pl. 4, fig. 39
1960 *Hofkerinella baltica* (Schroeter) - Hofker, p. 255, Pl. E, fig. 137
1988 *Hyalinea balthica* (Schroeter) - Loeblich & Tappan, p. 167, Pl. 632, figs. 5-8
1993 *Hyalinea balthica* (Schroeter) - Sgarrella & Moncharmont Zei, p. 234, Pl. 22, fig. 12
1994 *Hyalinea balthica* (Schroeter) - Jones, p. 110, Pl. 112, figs. 1-2
2002 *Hyalinea balthica* (Schroeter) - Kaminski et al., p. 174, Pl. 3, fig. 13
2003 *Hyalinea balthica* (Schroeter) - Murray, p. 24, fig. 8, no. 8-10
2005 *Hyalinea balthica* (Schroeter) - Rasmussen, p. 98, Pl. 14, figs. 27 & 28
2006 *Hyalinea balthica* (Schroeter) - Avsar et al., p. 133, Pl. 2, fig. 17
2009 *Hyalinea balthica* (Schroeter) - Frezza & Carboni, p. 57, Pl. 2, fig. 18

Genus: *Planulina* d'Orbigny, 1826

***Planulina ariminensis* d'Orbigny**

1826 *Planulina ariminensis* d'Orbigny
1988 *Planulina ariminensis* d'Orbigny - Loeblich & Tappan, p. 167, Pl. 633, figs. 1-4
1990 *Planulina ariminensis* d'Orbigny - Hasegawa et al., p. 477, Pl. 4, figs. 15 & 16
1993 *Planulina ariminensis* d'Orbigny - Sgarrella & Moncharmont Zei, p. 234, Pl. 22, fig. 9

Family: Cibicididae Cushman, 1927

Subfamily: Cibicidinae Cushman, 1927

Genus: *Cibicides* De Montfort, 1808

***Cibicides lobatulus* s.l. (Walker & Jacob)**

(Pl. 5, figs. 14 & 15)

1798 *Nautilus lobatulus* Walker & Jacob
1846 *Truncatulina lobatula* d'Orbigny - D'Orbigny, p. 168, Tab. 9, figs. 18-23
1931 *Cibicides lobatula* (Walker & Jacob) - Cushman, p. 118, Pl. 21, fig. 3
1945 *Cibicides lobatulus* (Walker & Jacob) - Cushman, p. 288, fig. 21
1979 *Cibicidoides lobatulus* (Walker & Jacob) - Corliss, p. 10, Pl. 3, figs. 7-9
1987 *Cibicides lobatulus* (Walker & Jacob) - Alberola et al., p. 308, Pl. 4, fig. 11
1988 *Lobatula lobatula* (Walker & Jacob) - Loeblich & Tappan, p. 168, Pl. 637, figs. 10-13
1991 *Lobatula lobatula* (Walker & Jacob) - Cimerman & Langer, p. 71, Pl. 75, figs. 1-4

1992 *Lobatula lobatulus* (Walker & Jacob) - Wollenburg, p. 63, Pl. 19, fig. 3
1993 *Lobatula lobatulus* (Walker & Jacob) - Hottinger et al., p. 118, Pl. 154, figs. 5-11
1993 *Cibicides pseudolobatulus* (Perelis & Reiss) - Hottinger et al., p. 116, Pl. 152, figs. 7-11
1993 *Cibicides lobatulus* (Walker & Jacob) - Sgarrella & Moncharmont Zei, p. 234, Pl. 22, figs. 10 & 11
1994 *Cibicides lobatulus* (Walker & Jacob) - Jones, p. 97, Pl. 92, fig. 10; Pl. 93, figs. 1 & 4-5
1995 *Cibicides lobatulus* (Walker & Jacob) - Coppa & Di Tuoro, p. 170, Pl. 3, figs. 7 & 10
2003 *Cibicides lobatulus* (Walker & Jacob) - Murray, p. 21, fig. 6, no. 13-15
2005 *Cibicides lobatulus* (Walker & Jacob) - Rasmussen, p. 99, Pl. 15, figs. 4-6
2006 *Lobatula lobatula* (Walker & Jacob) - Avsar et al., p. 133, Pl. 3, figs. 1 & 2
2009 *Lobatula lobatula* (Walker & Jacob) - Frezza & Carboni, p. 55, Pl. 1, figs. 18-20

Remarks: In this work, *Cibicides lobatulus* s.l. contains the species *Cibicides pseudo-lobatulus* that is characterized by a lower pore density on the umbilical side, and *Cibicides lobatulus* s.s. that is coarsely and uniformly perforate on both sides.

***Cibicides* cf. *C. mayori* (Cushman)**

1924 *Truncatulina mayori* Cushman
1993 ?*Cibicides mayori* (Cushman) - Hottinger et al., p. 116, Pl. 152, figs. 1-6

Remarks: The test is lamellar, trochospiral and mostly plano-convex. The peripheral margin is acute with thin fringe-like carina. Six to seven chambers are visible in the adult stage. Chambers are partly irregularly formed. Sutures are backcurved on both sides, limbate on the spiral side and depressed on the umbilical side. The calcareous test is densely perforated on the spiral side. The perforation on the umbilical side is restricted to the last chambers. On the umbilical side, a small imperforate, umbilical knob is sometimes present. The aperture is interiomarginal.

***Cibicides pseudoungerianus* (Cushman)**

(Pl. 5, figs. 16 & 17)

1922 *Truncatulina pseudoungerianus* Cushman
1931 *Cibicides pseudoungeriana* (Cushman) - Cushman, p. 123, Pl. 22, figs. 3-7
1991 *Cibicidoides pseudoungerianus* (Cushman) - Cimerman & Langer, p. 69, Pl. 74, figs. 2 & 3
2005 *Cibicides ungerianus* (Cushman) - Rasmussen, p. 100, Pl. 15, figs. 12 & 13
2008 *Cibicidoides pseudoungerianus* (Cushman) - Leiter, p. 33, Pl. 1, fig. 9

***Cibicides refulgens* De Montfort**

(Pl. 5, figs. 18 & 19)

1808 *Cibicides refulgens* De Montfort
1931 *Cibicides refulgens* De Montfort - Cushman, p. 116, Pl. 21, fig. 2
1988 *Cibicides refulgens* De Montfort - Loeblich & Tappan, p. 167, Pl. 634, figs. 1-3
1991 *Cibicides refulgens* De Montfort - Cimerman & Langer, p. 70, Pl. 75, figs. 5-9
2003 *Cibicides refulgens* De Montfort - Murray, p. 21, fig 7, no. 1 & 2
2004 *Cibicides refulgens* De Montfort - Chendes et al., p. 76, Pl. 3, fig. 2
2005 *Cibicides refulgens* De Montfort - Rasmussen, p. 100, Pl. 15, figs. 7 & 8

***Cibicides* sp. 1**

Remarks: The test is trochospiral, planoconvex and ovate to subcircular in outline. The spiral side is evolute and flat for the first chambers, but slightly convex for the last chambers. The spiral side is coarsely and densely perforated. Sutures are backcurved and thickened on the spiral side. The umbilical side is convex, involute and finely perforate with a knob-like feature in the umbilical region. Sutures are depressed on the umbilical side. The apertural face is angular, and the periphery is subcarinate. Eight chambers that increase in size when added, are visible in the final whorl. The wall is calcareous. The aperture is a low interiomarginal opening.

Family: Planorbulinidae Schwager, 1877
Subfamily: Planorbulininae Schwager, 1877
Genus: *Planorbulina* d'Orbigny, 1826

***Planorbulina mediterranensis* d'Orbigny**

(Pl. 5, fig. 20)

1825 *Planorbulina mediterranensis* d'Orbigny
1846 *Planorbulina mediterranensis* d'Orbigny - D'Orbigny, p. 166, Tab. 9, figs. 15-17
1931 *Planorbulina mediterranensis* d'Orbigny - Cushman, p. 129, Pl. 24, figs. 5-8
1958 *Planorbulina mediterranensis* d'Orbigny - Parker, p. 276, Pl. 4, fig. 44
1960 *Planorbulina mediterranensis* d'Orbigny - Hofker, p. 254, Pl. E, figs. 128 & 129
1988 *Planorbulina mediterranensis* d'Orbigny - Loeblich & Tappan, p. 170, Pl. 645, figs. 1-4
1991 *Planorbulina mediterranensis* d'Orbigny - Cimerman & Langer, p. 71, Pl. 78, figs. 1-8
1993 *Planorbulina mediterranensis* d'Orbigny - Sgarrella & Moncharmont Zei, p. 235, Pl. 23, fig. 4
1995 *Planorbulina mediterranensis* d'Orbigny - Coppa & Di Tuoro, p. 168, Pl. 2, figs. 8 & 11
2004 *Planorbulina mediterranensis* d'Orbigny - Chendes et al., p. 76, Pl. 3, fig. 5
2004 *Planorbulina mediterranensis* d'Orbigny - Mendes et al., p. 178, Pl. 1, fig. 5
2005 *Planorbulina mediterranensis* d'Orbigny - Rasmussen, p. 100, Pl. 15, fig. 14
2006 *Planorbulina mediterranensis* d'Orbigny - Avsar et al., p. 133, Pl. 3, fig. 3
2009 *Planorbulina mediterranensis* d'Orbigny - Avsar et al., p. 135, Pl. 3, figs. 2 & 3

***Planorbulina variablis* (d'Orbigny)**

1839 *Truncatulina variablis* d'Orbigny
1988 *Planorbulina variablis* (d'Orbigny) - Loeblich & Tappan, p. 170, Pl. 645, figs. 5 & 6
1991 *Cibicidella variablis* (d'Orbigny) - Cimerman & Langer, p. 72, Pl. 77, figs. 1-10
1993 *Cibicidella variablis* (d'Orbigny) - Sgarrella & Moncharmont Zei, p. 234, Pl. 23, figs. 2 & 3

Family: Cymbaloporidae Cushman, 1927

Subfamily: Cymbaloporinae Cushman, 1927

Genus: *Cymbaloporetta* Cushman, 1928

***Cymbaloporetta bulloides* (d'Orbigny)**

1839 *Rosalina bulloides* d'Orbigny
1988 *Cymbaloporetta bulloides* (d'Orbigny) - Loeblich & Tappan, p. 170, Pl. 649, figs. 11-15
1991 *Cymbaloporetta* sp.1 - Cimerman & Langer, p. 72, Pl. 80, figs. 1-5

Superfamily: Acervulinacea Schultze, 1854

Family: Acervulinidae Schultze, 1854

Genus: *Acervulina* Schultze, 1854

***Acervulina inhaerens* Schultze**

1854 *Acervulina inhaerens* Schultze
1988 *Acervulina inhaerens* Schultze - Loeblich & Tappan, p. 597, Pl. 659, figs. 1-6

Genus: *Sphaerogypsina* Galloway, 1933

***Sphaerogypsina globula* (Reuss)**

1848 *Ceriopora globula* Reuss
1988 *Sphaerogypsina globula* (Reuss) - Loeblich & Tappan, p. 173, Pl. 662, figs. 4-6
1991 *Sphaerogypsina globula* (Reuss) - Cimerman & Langer, p. 72, Pl. 80, figs. 6-9
1993 *Sphaerogypsina globula* (Reuss) - Sgarrella & Moncharmont Zei, p. 235, Pl. 23, fig. 6
1993 *Sphaerogypsina globula* (Reuss) - Hottinger et al., p. 128, Pl. 173, figs. 1-10

Family: Homotrematidae Cushman, 1927

Genus: *Miniacina* Galloway, 1933

***Miniacina miniacea* (Pallas)**

1766 *Millepora miniacea* Pallas
1988 *Miniacina miniacea* (Pallas) - Loeblich & Tappan, p. 173, Pl. 663, figs. 4-6; Pl. 664, figs. 1-5
1991 *Miniacina miniacea* (Pallas) - Cimerman & Langer, p. 73, Pl. 81, figs. 1-6
1993 *Miniacina miniacea* (Pallas) - Hottinger et al., p. 122, Pl. 175, figs. 9 & 10; Pl. 176, figs. 1-6; Pl. 177, figs. 1-7
1993 *Miniacina miniacea* (Pallas) - Sgarrella & Moncharmont Zei, p. 235, Pl. 23, fig. 5
1994 *Miniacina miniacea* (Pallas) - Jones, p. 101, Pl. 100, figs. 5-9; Pl. 101, fig. 1

Superfamily: Asterigerinacea d'Orbigny, 1839

Family: Asterigerinatidae Reiss, 1963

Genus: *Asterigerinata* Bermudez, 1949

***Asterigerinata adriatica* Haake**

(Pl. 6, fig. 1 & 2)

1977 *Asterigerinata adriatica* Haake
1991 *Asterigerinata* sp.1 - Cimerman & Langer, p. 73, Pl. 82, figs. 5 & 6
1993 *Asterigerinata adriatica* Haake - Sgarrella & Moncharmont Zei, p. 224, Pl. 19, figs. 11 & 12

2004 *Asterigerinata adriatica* Haake - Chendes et al., p. 76, Pl. 3, fig. 6
2006 *Asterigerinata adriatica* Haake - Avsar et al., p. 133, Pl. 3, fig. 4

Asterigerinata mamilla (Williamson)

(Pl. 6, figs. 3 & 4)

1858 *Rotalina mamilla* Williamson
1931 *Discorbis mamilla* (Williamson) - Cushman, p. 23, Pl. 5, fig. 1
1958 *Asterigerinata mamilla* (Williamson) - Parker, p. 264, Pl. 3, figs. 5 & 6
1960 *Asterigerinata mamilla* (Williamson) - Hofker, p. 252, Pl. D, fig. 111
1987 *Asterigerinata mamilla* (Williamson) - Alberola et al., p. 322, Pl. 4, fig. 10
1987 *Asterigerinata mamilla* (Williamson) - Jorissen, p. 41, Pl. 3, fig. 1
1991 *Asterigerinata mamilla* (Williamson) - Cimerman & Langer, p. 73, Pl. 83, figs. 1-4
1993 *Asterigerinata mamilla* (Williamson) - Sgarrella & Moncharmont Zei, p. 224, Pl. 19, figs. 9 & 10
1995 *Asterigerinata mamilla* (Williamson) - Coppa & Di Tuoro, p. 170, Pl. 3, figs. 11 & 12
2004 *Asterigerinata mamilla* (Williamson) - Mendes et al., p. 178, Pl. 1, fig. 2
2005 *Asterigerinata mamilla* (Williamson) - Rasmussen, p. 101, Pl. 15, figs. 17 & 18
2006 *Asterigerinata mamilla* (Williamson) - Avsar et al., p. 133, Pl. 3, figs. 5-7
2009 *Asterigerinata mamilla* (Williamson) - Avsar et al., p. 135, Pl. 3, figs. 5 & 6

Asterigerinata mariae Sgarrella

(Pl. 6, figs. 5 & 6)

1990 *Asterigerinata mariae* Sgarrella
1993 *Asterigerinata mariae* Sgarrella - Sgarrella & Moncharmont Zei, p. 224, Pl. 20, fig. 1

Superfamily: Nonionacea Schultze, 1854

Family: Nonionidae Schultze, 1854

Subfamily: Nonioninae Schultze, 1854

Genus: *Haynesina* Banner & Calver, 1978

Haynesina depressula (Walker & Jacob)

(Pl. 6, fig. 7)

1798 *Nautilus depressula* Walker & Jacob
1914 *Nonionina depressula* (Walker & Jacob) - Cushman, p. 23, Pl. 17, figs. 3 a & b
1987 *Nonion depressulum* (Walker & Jacob) - Jorissen, p. 39, Pl. 2, figs. 7 a & b
1991 *Haynesina depressula* (Walker & Jacob) - Cimerman & Langer, p. 81, Pl. 83, figs. 1-4
1993 *Nonion depressulum* (Walker & Jacob) - Sgarrella & Moncharmont Zei, p. 238, Pl. 24, figs. 3 & 4
2004 *Haynesina depressula* (Walker & Jacob) - Chendes et al., p. 76, Pl. 3, fig. 7
2005 *Haynesina depressula* (Walker & Jacob) - Rasmussen, p. 102, Pl. 16, fig. 3
2009 *Nonion depressulum* (Walker & Jacob) - Avsar et al., p. 135, Pl. 3, figs. 7 & 8

Haynesina sp. 1

Remarks: The test is planispirally enrolled, biumbilicate and circular with involute coiling. The umbilical region is depressed and completely filled with tubercles. Sutures are backcurved. The periphery is rounded. Seven to eight slightly inflated chambers are visible on the final whorl, extending near the periphery. The chambers slightly increase when added. The wall is calcareous, finely and densely perforate, with a smooth surface. The interlocular spaces are ornamented with minute pseudospines. The aperture is a low interiomarginal arch at the base of the apertural face, extending nearly to the umbilicus and is covered by granules.

Haynesina sp. 2

(Pl. 6, fig. 8)

1958 *Nonion* sp. B - Parker, p. 259, Pl. 1, figs. 40 & 41

Remarks: The test is planispiral, circular in outline and compressed. Up to twelve chambers are visible in the final whorl. The umbilicus is partly filled with pustules. The incised sutures are backcurved, and also filled with pustules. The periphery is subrounded. The wall is calcareous and smooth, except the umbilical region and the sutures, and finely perforate. The aperture is an interiomarginal slit covered by pustules.

The species in this work has similarities to *Haynesina* sp. shown and described in

Rasmussen (2005; p. 102, Pl. 16, fig. 4), but has more chambers.

Genus: *Nonion* De Montfort, 1808

***Nonion fabum* (Fichtel & Moll)**

(Pl. 6, fig. 19)

1798 *Nautilus faba* Fichtel & Moll
1988 *Nonion fabum* (Fichtel & Moll) - Loeblich & Tappan, p. 179, Pl. 690, figs. 1-7
1994 *Nonion fabum* (Fichtel & Moll) - Jones, p. 108, Pl. 109, figs. 12 & 13
2004 *Nonion fabum* (Fichtel & Moll) - Mendes et al., p. 178. Pl. 1, fig. 10
2005 *Nonion fabum* (Fichtel & Moll) - Rasmussen, p. 102, Pl. 16, fig. 5
2008 *Nonion asterizans* (Fichtel & Moll) - Leiter, p. 46, Pl. 2, fig. 5

Genus: *Nonionella* Cushman, 1926

***Nonionella turgida* (Williamson)**

(Pl. 6, figs. 10 & 11)

1858 *Rotalina turgida* Williamson
1930 *Nonionella turgida* (Williamson) - Cushman, p. 15, Pl. 6, figs. 1 & 4
1960 *Nonionella turgida* (Williamson) - Hofker, p. 258, Pl. F, figs. 181 & 182
1987 *Nonionella turgida* (Williamson) - Jorissen, p. 47, Pl. 4, figs. 11-13
1993 *Nonionella turgida* (Williamson) - Sgarrella & Moncharmont Zei, p. 240, Pl. 24, fig. 5
1993 *Nonionella turgida* (Williamson) - Cimerman & Langer, p. 74, Pl. 84, figs. 6-8
2003 *Nonionella turgida* (Williamson) - Murray, p. 24, fig. 9, no. 5
2005 *Nonionella turgida* (Williamson) - Rasmussen, p. 103, Pl. 16, figs. 11 & 12
2006 *Nonionella turgida* (Williamson) - Avsar et al., p. 133. Pl. 3, fig. 8
2009 *Nonionella turgida* (Williamson) - Frezza & Carboni, p. 57, Pl. 2, figs. 7 & 8

***Nonionella* sp. 1**

(Pl. 6, fig. 12)

1914 *Nonionina turgida* (Williamson) - Cushman, p. 29, Pl. 15, figs. 3 a & b
1930 *Nonionella turgida* (Williamson) - Cushman, p. 15, Pl. 6, figs. 2 & 3
1994 *Nonionella turgida* (Williamson) - Jones, p. 108, Pl. 109, fig. 17
2003 *Nonionella turgida* (Williamson) - Murray, p. 24, fig. 9, no. 4

Remarks: In our opinion, this species differs from *N. turgida* by its equilateral face view. However, specimens that look close to our specimens have been grouped to *Nonionella turgida* by Brady (see Cushman, 1930) and also by the authors listed above.

Subfamily: Astrononioninae Saidova, 1981

Genus: *Astrononion* Cushman & Edwards, 1937

***Astrononion stelligerum* (d'Orbigny)**

(Pl. 6, fig. 13)

1839 *Nonionina stelligera* d'Orbigny
1930 *Nonion stelligerum* (d'Orbigny) - Cushman, p. 7, Pl. 2, figs. 8-12; Pl. 3, figs. 1-3
1958 *Astrononion stelligerum* (d'Orbigny) - Parker, p. 258, Pl. 1, figs. 34 & 35
1988 *Astrononion stelligerum* (d'Orbigny) - Loeblich & Tappan, p. 180, Pl. 694, figs. 1 & 2; figs. 20 & 21
1990 *Astrononion stelligerum* (d'Orbigny) - Sprovieri & Hasegawa, p. 457, Pl. 3, figs. 1 & 2
1991 *Astrononion stelligerum* (d'Orbigny) - Cimerman & Langer, p. 74, Pl. 84, figs. 13-15
1993 *Astrononion stelligerum* (d'Orbigny) - Sgarrella & Moncharmont Zei, p. 238, Pl. 24, fig. 10
1994 *Astrononion stelligerum* (d'Orbigny) - Jones, p. 107, Pl. 109, figs. 3 & 4
2006 *Astrononion stelligerum* (d'Orbigny) - Avsar et al., p. 133, Pl. 3, figs. 9 & 10
2009 *Astrononion stelligerum* (d'Orbigny) - Avsar et al., p. 135, Pl. 3, fig. 9

Subfamily: Pulleniinae Schwager, 1877

Genus: *Melonis* De Montfort, 1808

***Melonis barleeanum* (Williamson)**

(Pl. 6, figs. 14 & 15)

1858 *Nonionina barleeana* Williamson
1930 *Nonion barleeanum* (Williamson) - Cushman, p. 11, Pl. 4, fig. 5
1958 *Nonion barleeanum* (Williamson) - Parker, p. 258, Pl. 1, figs. 36 & 37
1958 *Nonion barleeanum* (Williamson) - Todd, p. 190, Pl. 1, fig. 7
1979 *Melonis barleeanum* (Williamson) - Corliss, p. 10, Pl. 5, figs. 7 & 8

1987 *Nonion barleeanum* (Williamson) - Jorissen, p. 43, Pl. 4, fig. 8
1988 *Melonis barleeanum* (Williamson) - Loeblich & Tappan, p. 180, Pl. 696, figs. 5 & 6
1990 *Melonis barleeanum* (Williamson) - Sprovieri & Hasegawa, p. 457, Pl. 3, figs. 7 & 8
1993 *Melonis barleeanum* (Williamson) - Sgarrella & Moncharmont Zei, p. 242, Pl. 26, figs. 1 & 2
2003 *Melonis barleeanum* (Williamson) - Sen Gupta, p. 191, text-fig. 11.5, no. 6
2004 *Melonis barleeanum* (Williamson) - Chendes et al., p. 76, Pl. 4, fig. 1

***Melonis affinis* (Reuss)**

(Pl. 6, figs. 16 & 17)

1851 *Nonionina affinis* Reuss
1978 *Nonion affine* (Reuss) - Boltovskoy, p. 162, Pl. 5, figs. 1 & 2
1990 *Melonis affinis* (Reuss) - Sprovieri & Hasegawa, p. 457, Pl. 34, figs. 11 & 12
1994 *Melonis affinis* (Reuss) - Jones, p. 107, Pl. 109, figs. 8 & 9
2009 *Melonis pompilioides* (Fichtel & Moll) - Avsar et al., p. 135, Pl. 3, figs. 10 & 11

Genus: *Pullenia* Parker & Jones, 1862

***Pullenia quadriloba* (Reuss)**

1867 *Pullenia compressiuscula* Reuss var. *quadriloba* Reuss
1978 *Pullenia quadriloba* (Reuss) - Boltovskoy, p. 166, Pl. 6, fig. 20
1990 *Pullenia quadriloba* (Reuss) - Sprovieri & Hasegawa, p. 457, Pl. 3, figs. 19 & 20

Superfamily: Chilostomellacea Brady, 1881

Family: Alabaminidae Hofker, 1951

Genus: *Svratkina* Pokorny, 1956

***Svratkina* sp. 1**

Remarks: The test is trochospiral and biconvex. The spiral side is evolute and rather flattened. Six crescentic chambers are visible in the final whorl of the spiral side. Sutures are oblique and curved. The umbilical side is involute and convex with radial sutures. The periphery is rounded. The wall is calcareous, and coarsely perforate on the spiral side and near the periphery of the umbilical side. The aperture is an elongate, oblique opening in a slight depression, extending from near the umbilicus to the face of the last chamber.

Family: Gavelinellidae Hofker, 1956

Subfamily: Gavelinellinae Hofker, 1956

Genus: *Discanomalina* Asano, 1951

***Discanomalina semipunctata* (Bailey)**

1851 *Rotalina semipunctata* Bailey
1978 *Discanomalina semipunctata* (Bailey) - Medioli & Scott, p. 296, Pl. 1, figs. 13-16
1988 *Discanomalina semipunctata* (Bailey) - Loeblich & Tappan, p. 185, Pl. 718, figs. 1-9

Genus: *Gyroidina* d'Orbigny, 1826

***Gyroidina neosoldanii* Brotzen**

(Pl. 6, figs. 20 & 21)

1936 *Gyroidina neosoldanii* Brotzen
1993 *Gyroidina neosoldanii* Brotzen - Sgarrella & Moncharmont Zei, p. 241, Pl. 25, figs. 5 & 6

***Gyroidina umbonata* (Silvestri)**

(Pl. 6, figs. 18 & 19)

1898 *Rotalia soldanii* d'Orbigny var. *umbonata* Silvestri
1958 *Gyroidinia umbonata* (Silvestri) - Parker, p. 266, Pl. 3, figs. 19 & 20
1958 *Gyroidinia umbonata* (Silvestri) - Todd, p. 197, Pl. 1, fig. 18
1992 *Gyroidinia umbonata* (Silvestri) - Schiebel, p. 48, Pl. 4, fig. 8
1993 *Gyroidinia umbonata* (Silvestri) - Sgarrella & Moncharmont Zei, p. 241, Pl. 25, figs. 1 & 2
2005 *Gyroidinoides umbonata* (Silvestri) - Rasmussen, p. 106, Pl. 17, figs. 9-11

Family: Trichohyalidae Saidova, 1981

Genus: *Buccella* Andersen, 1952

***Buccella granulata* (Di Napoli Alliata)**

(Pl. 7, figs. 1 & 2)

1952 *Eponidus frigidus granulatus* Di Napoli Alliata
1987 *Buccella granulata* (Di Napoli Alliata) - Alberola et al., p. 308, Pl. 4, fig. 15

1987 *Buccella granulata* (Di Napoli Alliata) - Jorissen, p. 41, Pl. 3, fig. 5
1993 *Buccella granulata* (Di Napoli Alliata) - Sgarrella & Moncharmont Zei, 1993, p. 216, Pl. 16, figs. 6 & 7
1995 *Buccella granulata* (Di Napoli Alliata) - Coppa & Di Tuoro, p. 168, Pl. 2, figs. 7 & 14
2005 *Buccella granulata* (Di Napoli Alliata) - Rasmussen, p. 107, Pl. 18, figs. 1-3

Superfamily: Rotaliacea Ehrenberg, 1839

Family: Rotaliidae Ehrenberg, 1839

Subfamily: Rotaliinae Ehrenberg, 1839

Genus: *Ammonia* Bruennich, 1772

Ammonia beccarii (Linné)

(Pl. 7, figs. 5 & 6)

1767 *Nautilus beccarii* Linné
1931 *Rotalia beccarii* (Linné) - Cushman, p. 58, Pl. 12, figs. 1-7; Pl. 13, figs. 1 & 2
1960 *Streblus beccarii* (Linné) - Hofker, p. 255, Pl. E, fig. 134
2009 *Ammonia beccarii* (Linné) - Frezza & Carboni, p. 55, Pl. 1, figs. 5 & 12

Ammonia parkinsonia (d'Orbigny)

(Pl. 7, figs. 3 & 4)

1839 *Rosalina parkinsonia* d'Orbigny
1960 *Streblus parkinsonianus* (d'Orbigny) - Hofker, p. 254, Pl. E. fig. 132
1990 *Ammonia parkinsonia* (d'Orbigny) - Cimerman & Langer, p. 76, Pl. 87, figs. 7-9
1993 *Ammonia parkinsonia* (d'Orbigny) - Sgarrella & Moncharmont Zei, p. 228, Pl. 20, figs. 3 & 4
2004 *Ammonia parkinsonia* (d'Orbigny) - Chendes et al., p. 76, Pl. 4, fig. 4
2005 *Ammonia parkinsonia* (d'Orbigny) - Rasmussen, p. 107, Pl. 18, figs. 5-8
2006 *Ammonia parkinsonia* (d'Orbigny) - Avsar et al., p. 133, Pl. 3, figs. 15 & 16

Family: Elphidiidae Galloway, 1933

Subfamily: Elphidiinae Galloway, 1933

Genus: *Elphidium* De Montfort, 1808

Elphidium aculeatum (d'Orbigny)

(Pl. 7, fig. 7)

1846 *Polystomella aculeata* d'Orbigny, p. 131, Tab. 6, figs. 27 & 28
1991 *Elphidium aculeatum* (d'Orbigny) - Cimerman & Langer, p. 77, Pl. 89, figs. 1-4
1994 *Elphidium aculeatum* (d'Orbigny) - Jones, p. 109, Pl. 110, fig. 10
2005 *Elphidium aculeatum* (d'Orbigny) - Rasmussen, p. 108, Pl. 18, fig. 12

Elphidium advenum (Cushman)

(Pl. 7, fig. 8)

1922 *Polystomella advena* Cushman
1933 *Elphidium advenum* (Cushman) - Cushman, p. 50, Pl. 12, figs. 1-3
1958 *Elphidium advena* (Cushman) - Parker, p. 269, Pl. 4, figs. 3 & 4
1993 *Elphidium advenum* (Cushman) - Hottinger et al., p. 146, Pl. 207, figs. 1-7
1993 *Elphidium punctatum* (Terquem) - Sgarrella & Moncharmont Zei, p. 230, Pl. 21, figs. 3 & 4
1995 *Elphidium punctatum* (Terquem) - Coppa & Di Tuoro, p. 172, Pl. 4, fig. 11
2005 *Elphidium advenum* (Cushman) - Rasmussen, p. 108, Pl. 18, figs. 13-15

Elphidium complanatum (d'Orbigny)

(Pl. 7, figs. 9 & 10)

1839 *Polystomella complanata* d'Orbigny
1958 *Elphidium complanatum* (d'Orbigny) - Parker, p. 270, Pl. 4, fig. 5
1933 *Elphidium jenseni* (Cushman) - Cushman, p. 48, Pl. 11, figs. 6 & 7
1991 *Elphidium jenseni* (Cushman) - Cimerman & Langer, p. 78, Pl. 92, figs. 1-3
1993 *Elphidium jenseni* (Cushman) - Hottinger et al., p. 148, Pl. 211, figs. 8-14
1993 *Elphidium complanatum* (d'Orbigny) - Sgarrella & Moncharmont Zei, p. 228, Pl. 20, figs. 9 & 10
2005 *Elphidium complanatum* (d'Orbigny) - Rasmussen, p. 109, Pl. 19, fig. 2
2006 *Elphidium complanatum* (d'Orbigny) - Avsar et al., p. 134, Pl. 3, fig. 19

Elphidium complanatum var. *tyrrhenianum* Accordi

(Pl. 7, fig. 13)

1951 *Elphidium complanatum* (d'Orbigny) var. *tyrrhenianum* Accordi
2005 *Elphidium complanatum* (d'Orbigny) var. *tyrrhenianum* Accordi - Rasmussen, p. 109, Pl. 19, fig. 3

Elphidium crispum (Linné)

(Pl. 7, fig. 11 & 12)

1758 *Nautilus crispum* Linné
1846 *Polystomella crispa* Lamarck - D'Orbigny, p. 125, Tab. 6, figs. 9-14
1914 *Polystomella crispa* (Linné) - Cushman, p. 32, Pl. 18, figs. 1 a & b

1933 *Elphidium crispum* (Linné) - Cushman, p. 47, Pl. 11, fig. 4
1960 *Elphidium crispum* (Linné) - Hofker, p. 258, Pl. F, fig. 184
1987 *Elphidium crispum* (Linné) - Alberola et al., p. 322, Pl. 4, fig. 2
1987 *Elphidium crispum* forma *crispum* (Linné) - Jorissen, p. 41, Pl. 3, fig. 8
1988 *Elphidium crispum* (Linné) - Loeblich & Tappan, p. 199, Pl. 786, figs. 8 & 9; Pl. 787, figs. 1-5
1991 *Elphidium crispum* (Linné) - Cimerman & Langer, p. 77, Pl. 90, figs. 1-6
1993 *Elphidium crispum* (Linné) - Sgarrella & Moncharmont Zei, p. 228, Pl. 20, fig. 11
2005 *Elphidium crispum* (Linné) - Rasmussen, p. 109, Pl. 19, fig. 4
2006 *Elphidium crispum* (Linné) - Avsar et al., p. 134, Pl. 3, fig. 20
2009 *Elphidium crispum* (Linné) - Avsar et al., p. 135, Pl. 3, figs. 19 & 20
2009 *Elphidium crispum* (Linné) - Frezza & Carboni, p. 55, Pl. 1, fig. 16

Elphidium granosum (d'Orbigny)

(Pl. 7, fig. 14)

1826 *Nonionina granosa* d'Orbigny
1958 *Elphidium granosum* (d'Orbigny) - Parker, p. 270, Pl. 4, figs. 10 & 11
1987 *Elphidium granosum* forma *granosum* (d'Orbigny) - Jorissen, p. 39, Pl. 2, figs. 1 & 2
1993 *Elphidium granosum* (d'Orbigny) - Sgarrella & Moncharmont Zei, p. 229, Pl. 21, figs. 1 & 2
1995 *Cibroelphidium granosum* (d'Orbigny) - Coppa & Di Tuoro, p. 172, Pl. 4, fig. 2
2004 *Porosononion granosum* (d'Orbigny) - Chendes et al., p. 76, Pl. 4, fig. 7
2005 *Elphidium granosum* (d'Orbigny) - Rasmussen, p. 110, Pl. 19, fig. 8
2009 *Porosononion subgranosum* (Egger) - Avsar et al., p. 135, Pl. 3, fig. 17 & 18
2009 *Elphidium granosum* (d'Orbigny) - Frezza & Carboni, p. 57, Pl. 2, fig. 5

Elphidium incertum (Williamson)

(Pl. 7, fig. 15)

1858 *Polystomella incertum* Williamson
1930 *Elphidium incertum* (Williamson) - Cushman, p. 18, Pl. 7, figs. 4-9
1993 *Elphidium incertum* (Williamson) - Sgarrella & Moncharmont Zei, p. 229, Pl. 21, fig. 5
2005 *Elphidium excavatum* (Terquem) - Rasmussen, p. 110, Pl. 19, figs. 6 & 7

Elphidium macellum (Fichtel & Moll)

(Pl. 7, fig. 16)

1798 *Nautilus macellus* Fichtel & Moll
1914 *Elphidium macellum* (Fichtel & Moll) - Cushman, p. 33, Pl. 18, figs. 3a & b
1987 *Elphidium crispum* forma *macellum* (Fichtel & Moll) - Jorissen, p. 41, Pl. 3, figs. 9 a & b
1988 *Elphidium macellum* (Fichtel & Moll) - Loeblich & Tappan, p. 199, Pl. 789, figs. 1-5
1993 *Elphidium macellum* (Fichtel & Moll) - Sgarrella & Moncharmont Zei, p. 229, Pl. 20, fig. 12
2002 *Elphidium macellum* (Fichtel & Moll) - Kaminski, p. 179, Pl. 5, fig. 11
2004 *Elphidium macellum* (Fichtel & Moll)- Jones, p. 109, Pl. 110, figs. 8 & 11
2005 *Elphidium macellum* (Fichtel & Moll) - Rasmussen, p. 110, Pl. 19, fig. 10

Elphidium margaritaceum (Cushman)

1930 *Elphidium advenum* var. *margaritaceum* Cushman
1991 *Elphidium margaritaceum* (Cushman) - Cimerman & Langer, p. 79, Pl. 92, figs. 4-6
1993 *Elphidium pulvereum* Todd - Sgarrella & Moncharmont Zei, p. 230, Pl. 21, fig. 6
2005 *Elphidium margaritaceum* (Cushman) - Rasmussen, p. 111, Pl. 19, figs. 13 & 14

Elphidium translucens Natland

(Pl. 7, fig. 17)

1938 *Elphidium translucens* Natland
1991 *Elphidium translucens* Natland - Cimerman & Langer, p. 79, Pl. 92, figs. 7-11
2002 *Elphidium translucens* Natland - Kaminski et al., p. 176, Pl. 5, fig. 12
2009 *Elphidium translucens* Natland - Frezza & Carboni, p. 55, Pl. 1, fig. 15

Elphidium sp. 1

(pl. 7, fig. 18)

1991 *Elphidium* sp. 4 - Cimerman & Langer, p. 80, Pl. 91, figs. 5 & 6

Remarks: The test is planispiral, involute and lamellar. It is subcircular in lateral view, and broadly lenticular in profile view. The peripheral margin is acute and carinate. The at least 18 chambers in the adult coil are narrow and gradually increase when added. Sutures are arranged as rips and curved backwards. They are connected by at least 14 ponticuli (in the adult chambers) providing

slightly elongated fossettes. The wall is calcareous, finely and densely perforate.

***Parrellina verriculata* (Brady)**

(Pl. 7, figs. 19 & 20)

1881 *Polystomella verriculata* Brady
1958 *Parrellina verriculata* (Brady) - Parker, p. 271, Pl. 4, fig. 7
1993 *Parrellina verriculata* (Brady) - Sgarrella & Moncharmont Zei, p. 232, Pl. 21, fig. 7

Plate 1

1	*Reophax scorpiurus*	281x	side view
2	*Cibrostomoides subglobosum*	355x	face view
3	*Cibrostomoides jeffreysii*	635x	side view
4	*Gaudryina rudis*	506x	side view
5	*Gaudryina siciliana*	1020x	side view
6	*Gaudryina siciliana*	405x	basal view
7	*Ammoglobigerina globigeriformis*	707x	spiral view
8	*Eggerelloides scabrus*	626x	side view
9	*Bigenerina nodosaria*	242x	side view
10	*Textularia agglutinans*	266x	side view
11	*Textularia pala*	363x	side view
12	*Textularia pseudorugosa*	235x	side view
13	*Siphotextularia concava*	306x	side view
14	*Siphotextularia flintii*	509x	side view
15	*Pseudoclavulina crustata*	254x	side view
16	*Spiroplectinella sagittula* s.l.	441x	side view
17	*Spiroplectinella sagittula* s.l.	587x	side view
18	*Spirillina vivipara*	648x	side view
19	*Spirillina limbata*	383x	side view
20	*Spirillina wrightii*	411x	side view

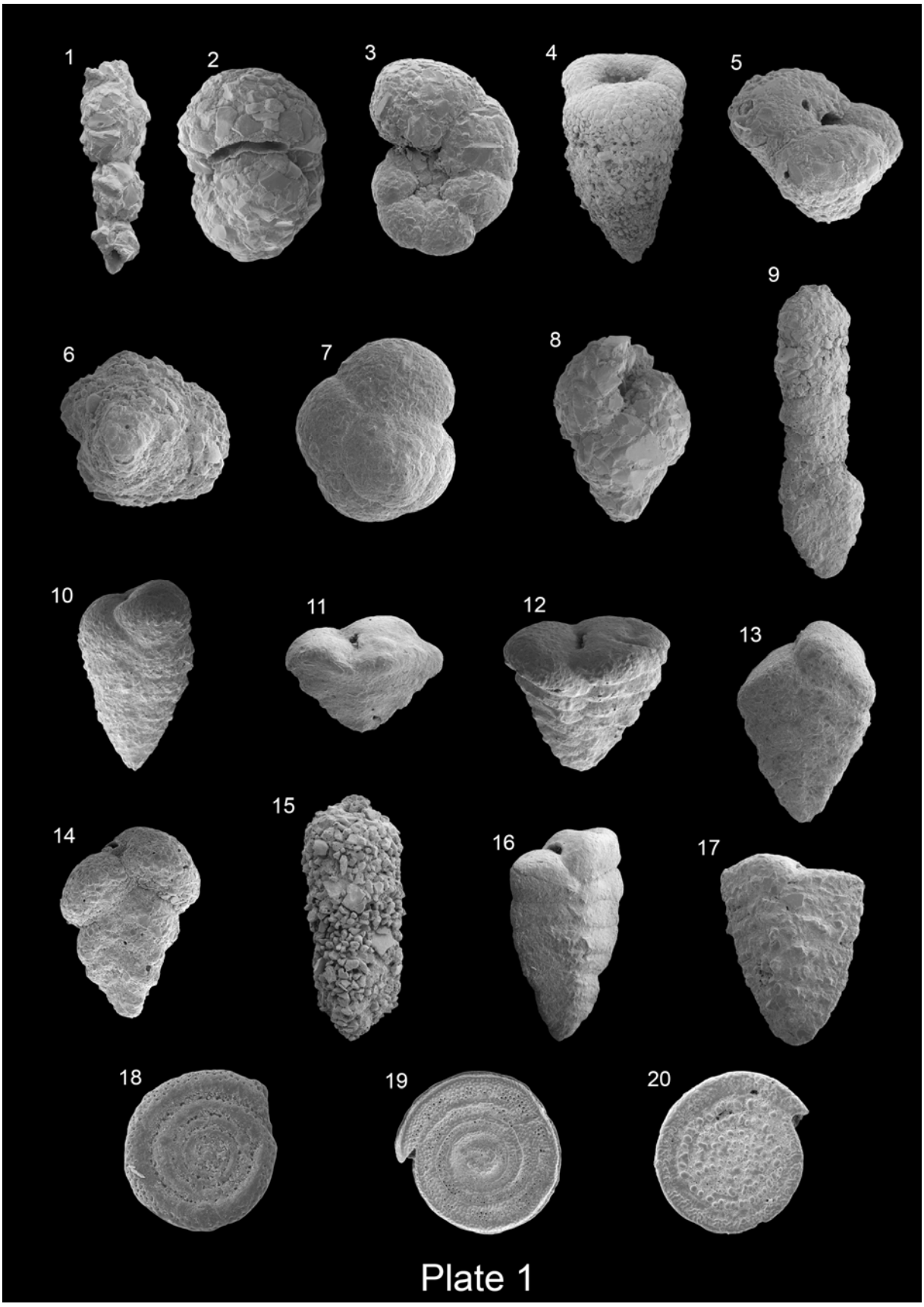
1
2
3
4
5
6
7
8
9
10
11
12
13
14
15
16
17
18
19
20
Plate 1

Plate 2

1	*Adelosina* sp. 1	293x	side view
2	*Adelosina mediterranensis*	268x	side view
3	*Spiroloculina excavata*	196x	side view
4	*Spiroloculina tenuiseptata*	391x	side view
5	*Miliolid* sp. 1	952x	side view
6	*Miliolid* sp. 2	832x	side view
7	*Siphonaperta agglutinans*	454	side view
8	*Cycloforina contorta*	861x	side view
9	*Lachlanella undulata*	861x	side view
10	*Quinqueloculina padana*	880x	side view
11	*Quinqueloculina parvula*	609x	side view
12	*Quinqueloculina seminula*	308x	side view
13	*Quinqueloculina stelligera*	717x	side view
14	*Quinqueloculina viennensis*	535x	side view
15	*Biloculinella globula*	497x	face view
16	*Miliolinella semicostata*	576x	side view
17	*Miliolinella subrotunda*	1140x	side view
18	*Miliolinella webbiana*	263x	side view
19	*Triloculina plicata*	754x	oblique face view
20	*Triloculina tricarinata*	890x	side view

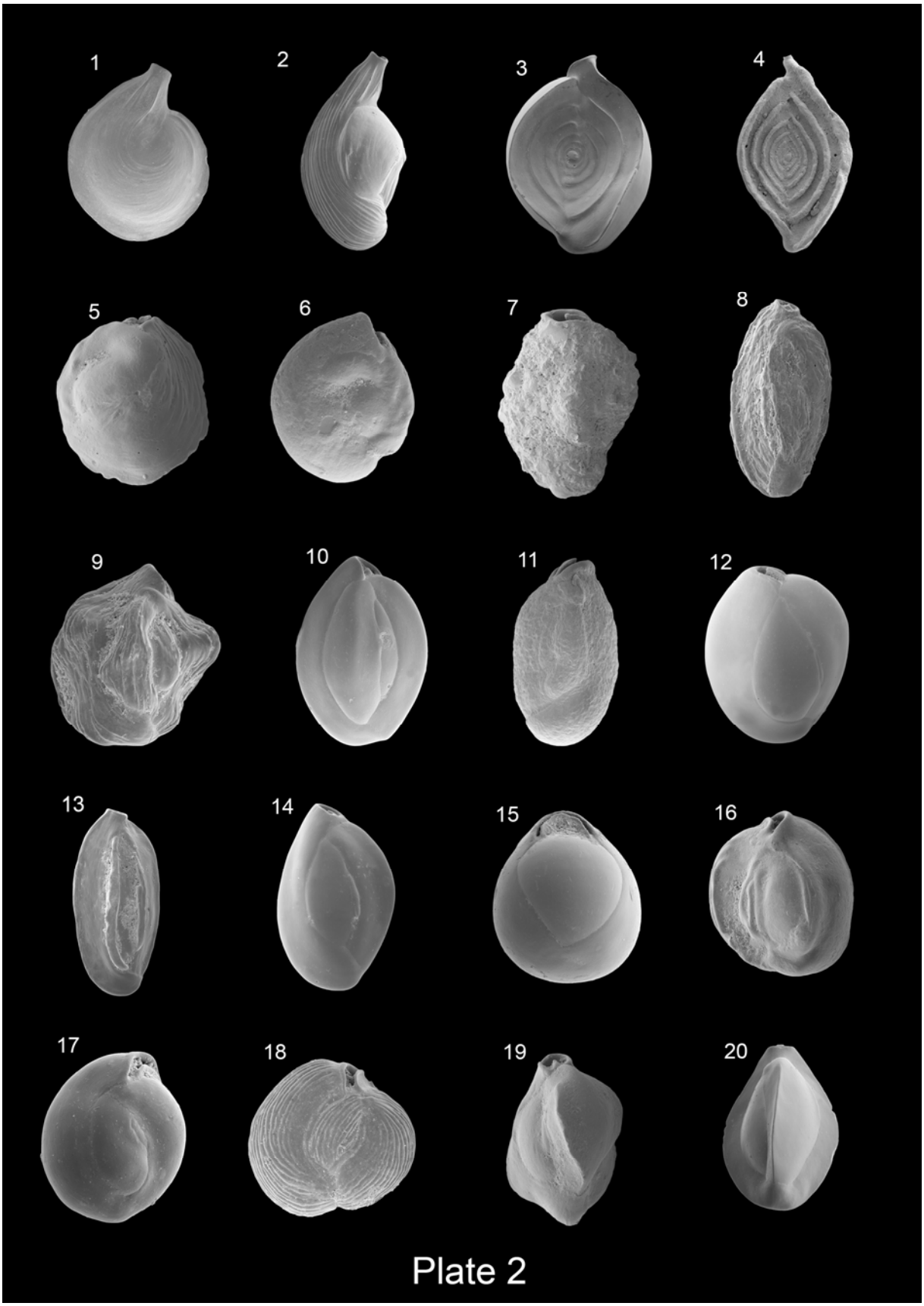
1
2
3
4
5
6
7
8
9
10
11
12
13
14
15
16
17
18
19
20
Plate 2

Plate 3

1	*Pyrgo anomala*	301x	face view
2	*Sigmoilinita costata*	460x	side view
3	*Sigmoilopsis schlumbergeri*	389x	side view
4	*Peneroplis pertusus*	388x	side view
5	*Lenticulina calcar*	438x	side view
6	*Lenticulina orbicularis*	201x	side view
7	*Amphicoryna scalaris*	375x	side view, macrospheric form
8	*Amphicoryna scalaris*	322x	side view, microspheric form
9	*Oolina hexagona*	592x	side view
10	*Bolivina pseudoplicata*	920x	side view
11	*Bolivina variablis*	549x	side view
12	*Brizalina difformis*	904	side view
13	*Brizalina striatula*	429x	side view
14	*Brizalina spathulata*	697x	side view
15	*Cassidulina crassa*	740x	side view
16	*Cassidulina laevigata* forma *carinata*	655x	side view
17	*Globocassidulina subglobosa*	1010x	oblique side view
18	*Globocassidulina oblonga*	771x	side view
19	*Rectuvigerina bononiensis*	837x	side view
20	*Rectuvigerina phlegeri*	686x	side view
21	*Bulimina aculeata*	598x	side view
22	*Bulimina elongata*	407x	side view
23	*Bulimina gibba*	509x	side view

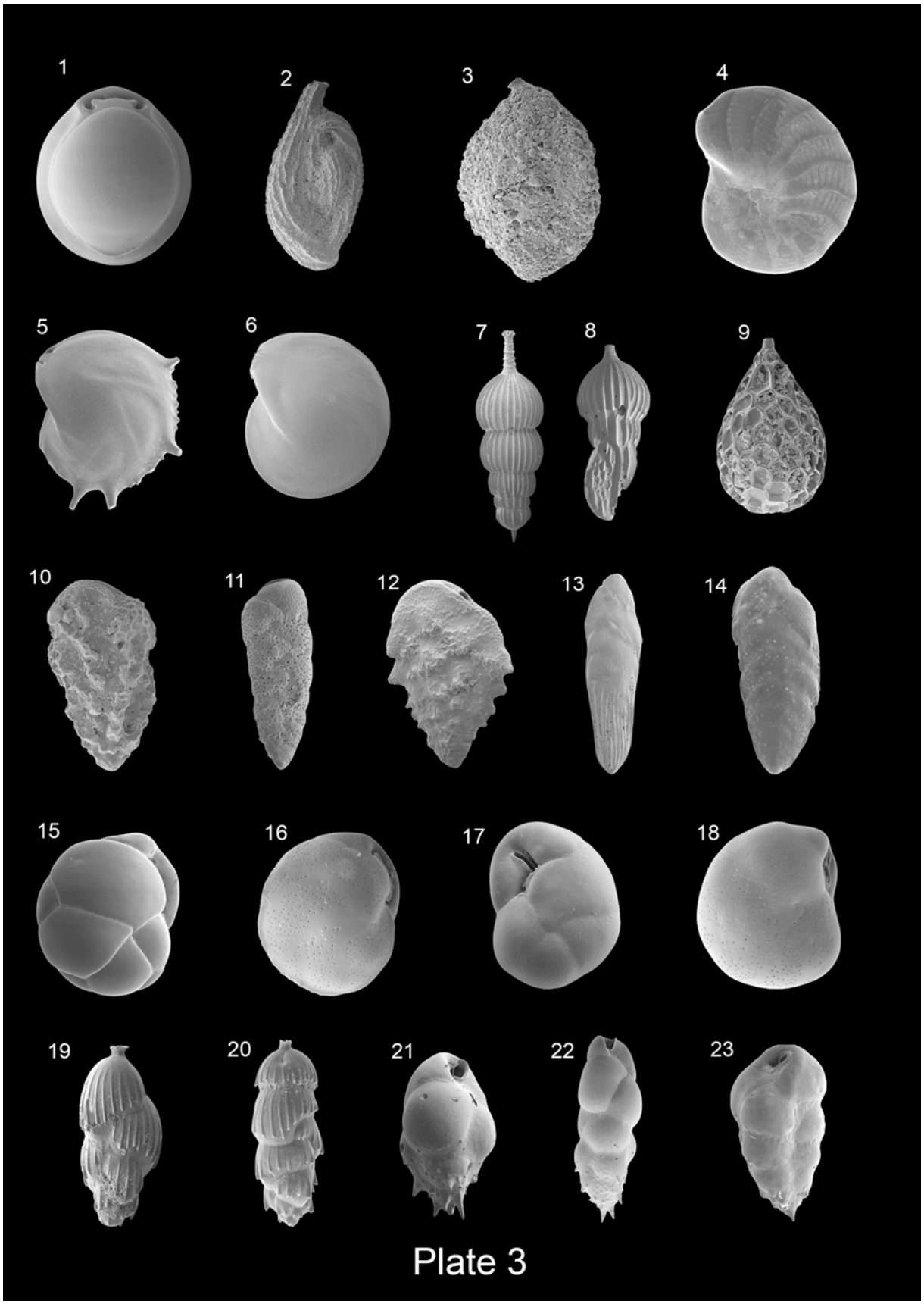
1
2
3
4
5
6
7
8
9
10
11
12
13
14
15
16
17
18
19
20
21
22
23
Plate 3

Plate 4

1	*Uvigerina peregrina*	421x	side view
2	*Angulogerina angulosa*	902x	side view
3	*Reussella spinulosa*	804x	side view
4	*Cancris auriculus*	375x	spiral side
5	*Cancris auriculus*	241x	umbilical side
6	*Valvulineria bradyana*	388x	spiral side
7	*Valvulineria bradyana*	370x	umbilical side
8	*Eponides concameratus*	188x	spiral side
9	*Eponides concameratus*	262x	umbilical side
10	*Stomatorbina concentrica*	339x	spiral side
11	*Stomatorbina concentrica*	295x	umbilical side
12	*Discorbis williamsoni*	635x	spiral side
13	*Discorbis williamsoni*	1060x	umbilical side
14	*Gavelinopsis praegeri*	785x	spiral side
15	*Gavelinopsis praegeri*	987x	umbilical side
16	*Neoconorbina terquemi*	545x	spiral side
17	*Neoconorbina terquemi*	732x	umbilical side
18	*Rosalina anomala*	243x	spiral side
19	*Rosalina anomala*	432x	umbilical side
20	*Rosalina bradyi*	782x	spiral side
21	*Rosalina bradyi*	768x	umbilical side

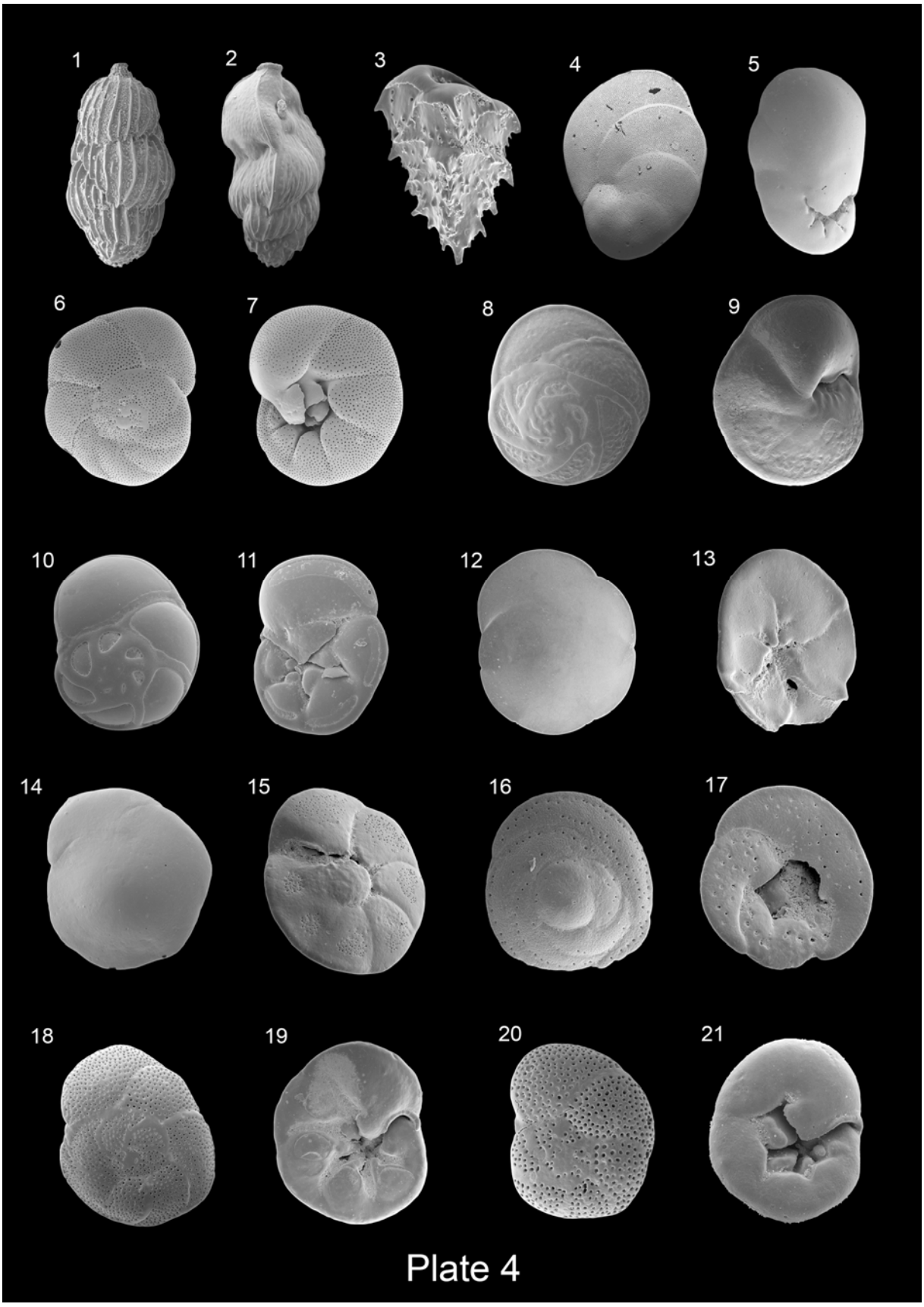
1
2
3
4
5
6
7
8
9
10
11
12
13
14
15
16
17
18
19
20
21
Plate 4

Plate 5

1	*Rosalina macropora*	609x	spiral side
2	*Rosalina macropora*	407x	umbilical side
3	*Tretomphalus concinnus*	768x	spiral side
4	*Tretomphalus* sp. 1	1090x	spiral side
5	*Conorbella pulvinata*	936x	top view
6	*Conorbella pulvinata*	931x	apertural view
7	*Glabratella hexacamerata*	907x	top view
8	*Glabratella hexacamerata*	727x	apertural view
9	*Planoglabratella opercularis*	386x	top view
10	*Planoglabratella opercularis*	473x	apertural side
11	*Discorbinella bertheloti*	603x	spiral side
12	*Discorbinella bertheloti*	500x	umbilical side
13	*Hyalinea balthica*	493x	side view
14	*Cibicides lobatulus*	244x	spiral side
15	*Cibicides lobatulus*	455x	oblique umbilical side view
16	*Cibicides pseudoungerianus*	536x	spiral side
17	*Cibicides pseudoungerianus*	409x	umbilical side
18	*Cibicides refulgens*	246x	spiral side
19	*Cibicides refulgens*	283x	side view
20	*Planorbulina mediterranensis*	580x	unattached side

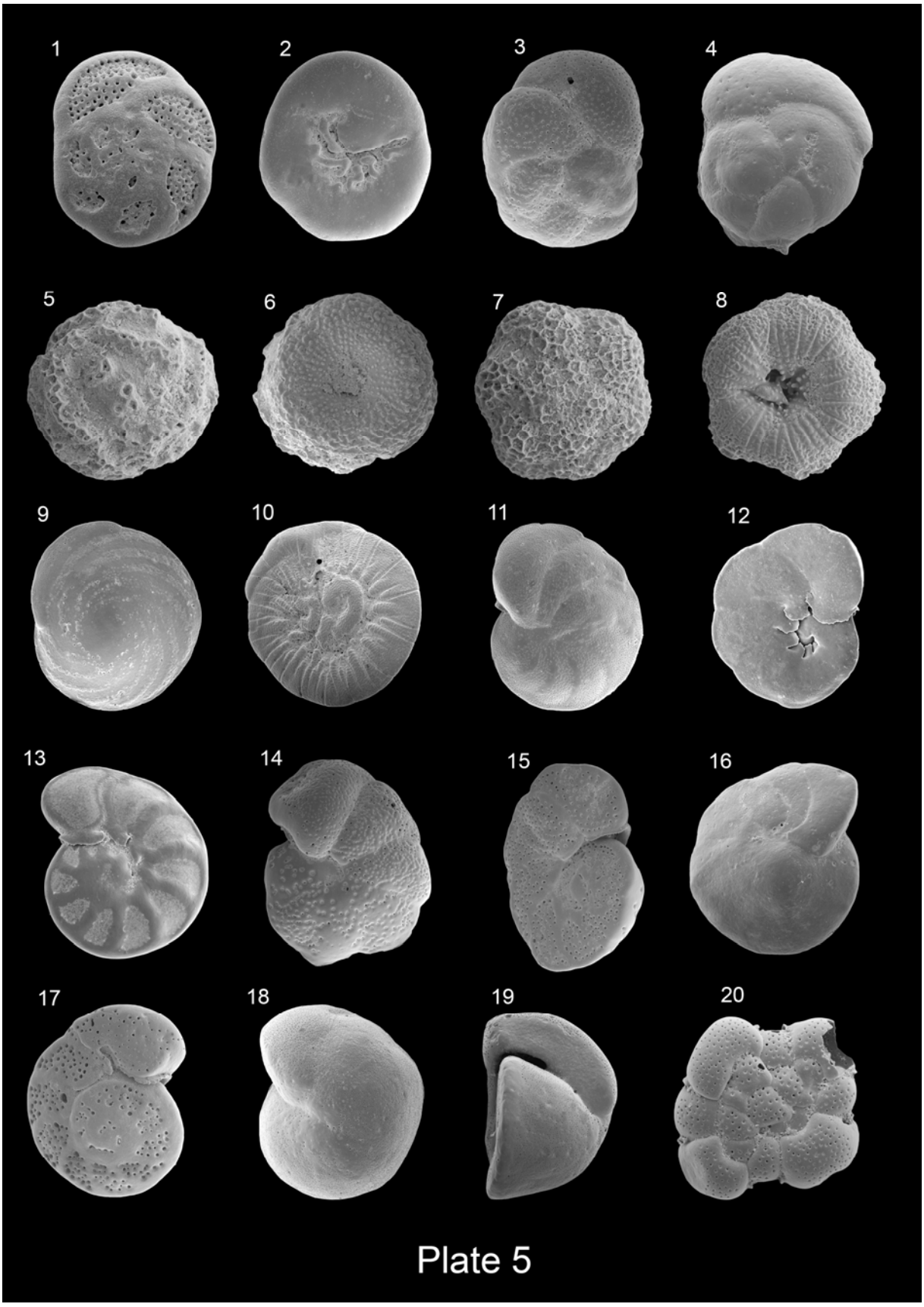
1
2
3
4
5
6
7
8
9
10
11
12
13
14
15
16
17
18
19
20
Plate 5

Plate 6

1	*Asterigerinata adriatica*	970x	spiral side
2	*Asterigerinata adriatica*	1040x	side side
3	*Asterigerinata mamilla*	868x	spiral side
4	*Asterigerinata mamilla*	1190x	side side
5	*Asterigerinata mariae*	1260x	spiral side
6	*Asterigerinata mariae*	1440x	side side
7	*Haynesina depressula*	680x	side view
8	*Haynesina* sp. 2	962x	side view
9	*Nonion fabum*	409x	side view
10	*Nonionella turgida*	852x	side view
11	*Nonionella turgida*	811	side view
12	*Nonionella* sp. 1	907x	side view
13	*Astrononion stelligerum*	372x	side view
14	*Melonis barleeanum*	538x	side view
15	*Melonis barleeanum*	597x	apertural view
16	*Melonis affinis*	446x	side view
17	*Melonis affinis*	454x	apertural view
18	*Gyroidina umbonata*	549x	spiral side
19	*Gyroidina umbonata*	776x	peripheral view
20	*Gyroidina neosoldanii*	409x	spiral side
21	*Gyroidina neosoldanii*	624x	peripheral view

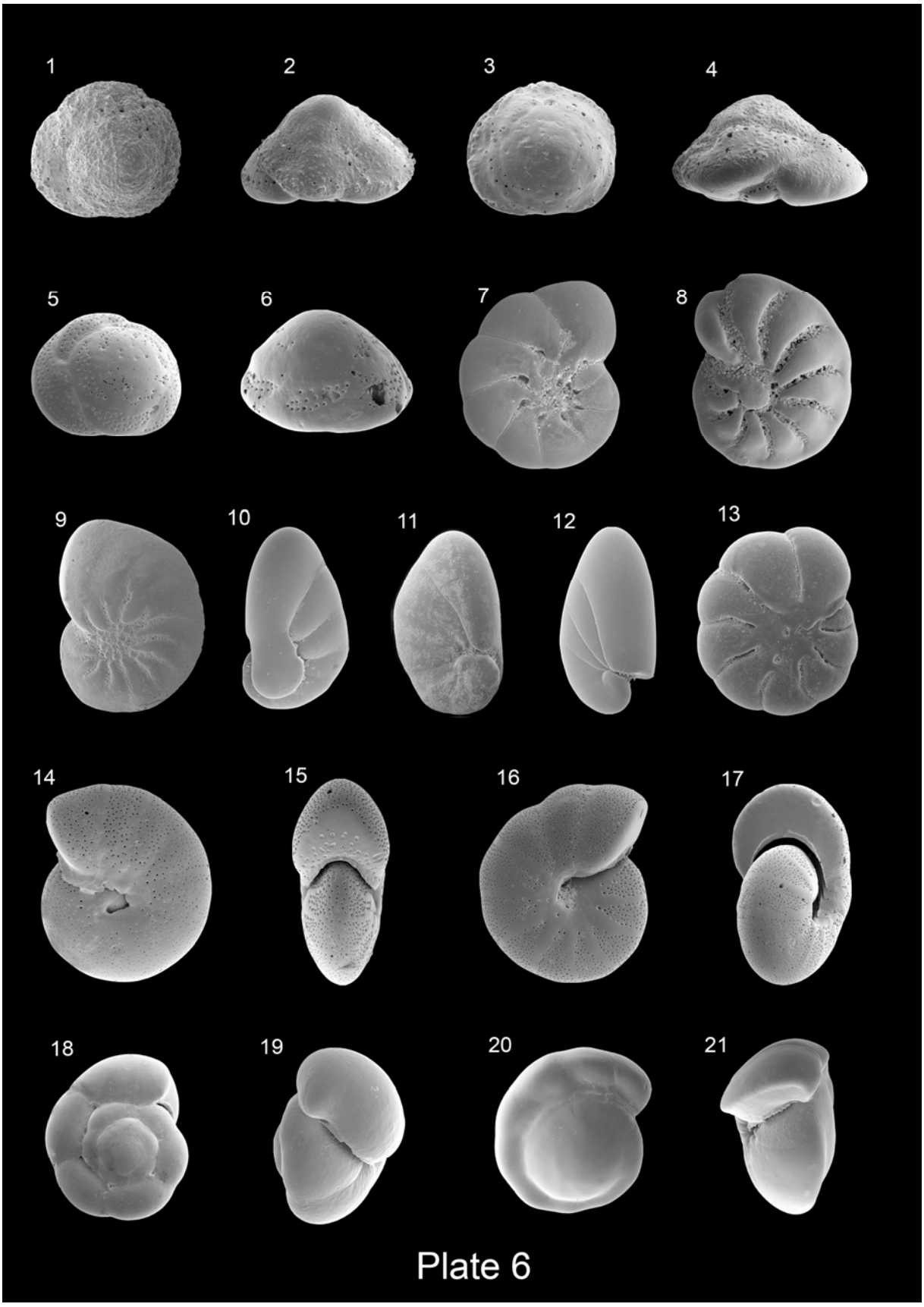
1
2
3
4
5
6
7
8
9
10
11
12
13
14
15
16
17
18
19
20
21
Plate 6

Plate 7

1	*Buccella granulata*	423x	spiral side
2	*Buccella granulata*	377x	umbilical side
3	*Ammonia parkinsonia*	703x	spiral side
4	*Ammonia parkinsonia*	591x	umbilical side
5	*Ammonia beccarii*	496x	spiral side
6	*Ammonia beccarii*	348x	umbilical side
7	*Elphidium aculeatum*	425x	side view
8	*Elphidium advenum*	301x	side view
9	*Elphidium complanatum*	295x	side view
10	*Elphidium complanatum*	310x	apertural view
11	*Elphidium crispum*	194x	side view
12	*Elphidium crispum*	242x	apertural view
13	*Elphidium complanatum* forma *tyrrhenianum*	595x	side view
14	*Elphidium granosum*	743x	side view
15	*Elphidium incertum*	1080x	side view
16	*Elphidium macellum*	418x	side view
17	*Elphidium translucens*	889x	side view
18	*Elphidium* sp. 1	266x	side view
19	*Parrellina verriculata*	613x	side view
20	*Parrellina verriculata*	613x	apertural view

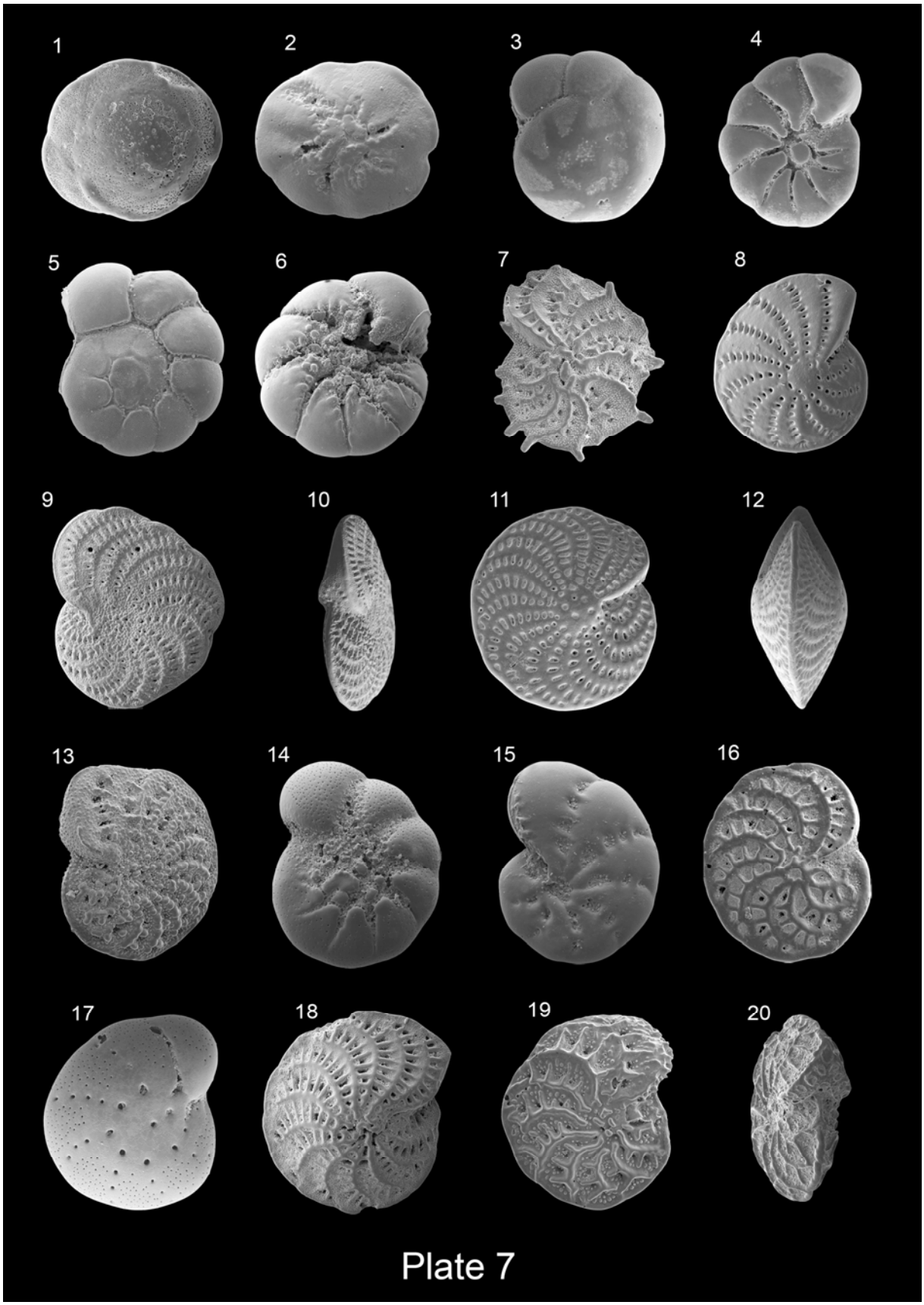
1
2
3
4
5
6
7
8
9
10
11
12
13
14
15
16
17
18
19
20
Plate 7

7 Conclusions and outlook

7.1 Conclusions

The aims of this thesis were (1) the analyses of Recent live and dead benthic shelf foraminiferal assemblages and the species-environment relationships in the western Mediterranean Sea, (2) the reconstruction of the relative sea-level development in the study areas during the latest glacial and Holocene, (3) the evaluation of climatic impacts on Mallorcan shelf ecosystems during the Holocene, and (4) a systematic description of the benthic shelf foraminifera investigated during this work.

The cool-water carbonate areas in the western Mediterranean Sea are characterized by diverse benthic foraminiferal faunas. The Recent thanatocoenoses from the shallower sites, (40 - ~80 m water depth) consist of assemblages dominated by epifaunal species such as *Asterigerinata mamilla, Neoconorbina terquemi, Rosalina macropora* and various *Cibicides* and *Elphidium* taxa. These species are permanently or temporarily attached to carbonate fragments derived from rhodoliths. A distinct faunal change between approximately 80 to 94 m water depth has been observed in all areas. On the Mallorca Shelf, the lower bathymetric limit of the shallower water assemblages coincides with the lower distribution limit of living rhodoliths, tracing the boundary of the photic zone. The assemblages from the deeper stations are characterized by higher regional contrasts, which can be related to different environmental conditions such as different substrate-type and a variable energy at the benthic boundary layer. Shallow infaunal species such as *Cassidulina laevigata* s.l. and *Bulimina elongata* occur in higher numbers in fine-grained substrates in the deeper stations on the shelf off Southwest Mallorca reflecting low energy conditions at the sea floor. These observations show that the distinct bathymetric zonation of the benthic faunas, the availability of food on the sea floor and the creation of infaunal niches are mainly controlled by the presence of different substrate-types and do not reflect regional contrasts in surface water production. In contrast, the biocoenoses in the studied areas are characterized by a low diversity and a wide range of standing stocks reflecting variable environmental conditions and a lower population dynamic in late summer 2006. In the Oran Bight, most of the biocenoses are clearly dominated by infaunal living taxa typical for areas with enhanced food fluxes such as *Cancris auriculus, Rectuvigerina* spp., bolivinids and buliminids suggesting a recent anthropogenic-induced eutrophication of the coastal region near the city of Oran. This interpretation is supported by very rare abundances of these species in middle and late Holocene assemblages analyzed in a sediment core from this region.

The shelf benthic foraminiferal assemblages from cool-water carbonate environments of the western Mediterranean Sea provide a high potential for quantitative sea-level reconstructions.

The best predictive potential is given from the Weighted Averaging-Partial Least Squares (WA-PLS) regression method resulting in an accuracy of +/- 10 m within a total sea-level rise of ~45 and ~47 m for the Alboran Platform and the shelf off Southwest Mallorca, respectively. However, transfer functions based on the Modern Analog Technique (MAT) and on Plankton/Benthos (P/B) ratios resulted in less consistent reconstructions with higher errors. The relative sea-level estimates with WA-PLS for the Alboran Platform and the Mallorca Shelf generally reflect the global and regional sea-level histories during the Holocene. Redeposition processes of foraminiferal tests can be attributed to the observed inaccuracies in the estimates in both areas. Further, the sea-level signal interferes with temporal changes in substrate on the Mallorca shelf, resulting in minor inconsistencies during the middle Holocene. In contrast, an estimated relative sea-level rise of 30 m in the Oran Bight exceeds the global sea-level rise and the rise calculated for the Alboran Platform and the Mallorca Shelf during the middle and late Holocene. While major neotectonic movements can be excluded for this region, this overestimation may be attributed to redeposition processes with enhanced relocation of benthic foraminiferal tests disturbing the sea-level signal and to a problematic age model.

Stable isotope records of planktonic and benthic foraminiferal tests provide information about the hydrological evolution and carbon cycling in marine ecosystems. Differences in the stable oxygen isotope signals of the planktonic foraminifera *Globigerina bulloides*, representing the late winter/spring situation, and *Globigerinoides ruber*, representing the late summer situation, reflect a higher seasonality on the shelf off Southwest Mallorca during the earliest Holocene and an abrupt decrease of seasonal contrasts with onset of the humid phase around 9.6 kyr. Humid conditions prevailed during the early and middle Holocene (e.g., between 9.6 and 5.5 kyr BP) and were characterized by enhanced summer rainfalls on the Mallorca Island leading to enhanced freshwater discharge and input of terrestrial disolved organic matter and nutrients to the coastal marine environments. This is documented by decreased $\delta^{18}O$ and $\delta^{13}C$ values of the planktonic foraminifer *Globigerinoides ruber* (white) in the upper surface layer, a lowering of $\delta^{13}C$ values of *Bulimina aculeata* and increased abundances of the gastropod *Turritella communis* and the infaunal benthic foraminifer *Rectuvigerina phlegeri*. This humid phase on the Mallorca Shelf was established nearly at the same time as sapropel S1 was formed in the eastern Mediterranean Sea at around 9.6 to 6.0 kyr. For the first time, the impact of this humid phase on western Mediterranean shelf ecosystems is documented.

7.2 Outlook

- The present study provides new information on shallow water benthic foraminifera from cool-water carbonate environments of the western Mediterranean Sea and their relation to different environmental settings. The more comprehensive evaluation of the distribution patterns

and ecological preferences of western Mediterranean shelf faunas would require a dense network of samples over a wide bathymteric range. For further investigations, main focus should be laid on the inclusion of further environmental parameters influencing the benthic foraminiferal assemblages such as bottom water temperatures, salinities and current velocities, organic carbon contents and other geochemical and sedimentological parameters. This would allow a more precise interpretation of species-environment relationships.

- The predictability and accuracy of the transfer functions applied for sea-level reconstruction could be improved by the creation of larger calibration data-sets, which goes hand in hand with the suggestions in the first paragraph. Furthermore, innovative methods such as Artificial Neural Networks (ANN) could be applied for relative sea-level estimates. Various potential future applications of these transfer functions are conceivable: (1) Quantification of Neogene vertical tectonic movements in coastal areas, e.g. in the eastern Mediterranean Sea, (2) Identification and provenance analysis of tsunami deposits in risk assessment studies of earthquake impacts in tectonically active areas, and (3) refining of the quantification of low-amplitude late Holocene sea-level changes on the basis of intertidal microfossil assemblages.

- The present study provides only local information on the Holocene palaeoecological and paleoceanographic development on the south-western Mallorca Shelf. Comparable geochemical and micropaleontological records should be generated for other shelf areas in the western and eastern Mediterranean Sea and compared with information from the coastal and terrestrial environments, such as pollen data from lagoonal or lacustrine environments, speleothem data etc. This would enable a more integrative and super-regional approach in the reconstruction of climate impacts on Mediterranean shelf ecosystems and the characterization of land-to-sea couplings in a marginal ocean system.

- The compilation of a comprehensive, well-illustrated and open-access benthic foraminiferal online catalogue for various applications would be very desirable. The catalogue should contain revised descriptions on the generic and species levels. This target could be realized by a close collaboration of experts for foraminiferal taxonomy.

8 References

Acosta, J., Canals, M., Carbo, A., Munoz, A., Urgeles, R., Munoz-Martin, A., Uchupi, E., 2004. Sea floor morphology and Plio-Quarternary sedimentary cover of the Mallorca Channel, Balearic Islands, western Mediterranean. Marine Geology 206, 165-179.

Alberola, C., Ferre, E.J., Usera, J., 1987. Aportacion al Conocimiento de la fauna de foraminiferos bentonicos de las Islas Columbretes: In Alonso Matilla, L.A., Carretero, J.L., Garcia-Carrascosa, A.M. (Eds.), Islas Combretes. Contribucion al estudio de su medio natural. Conselleria d'Obres Publiques, Urbanisme i Transports. Generalitat Valenciana. Valencia, 303-323.

Alberola, C., Usera, J., Garcia-Forner, A., 1991. Distribucion de las Tanatocenosis de foraminiferos arenaceos en el Puerto de Los Alfaques (Terragona). Revista Espanola de Paleontologia, Extraordinario, 77-85.

Alessio, M., Allegri, L., Antonioli, F., Belloumini, G., Improta, S., Manfra, L., Preite Martinez, M., 1994. La curva di risalita del mare Tirreno negli ultimi 43 ka ricavata da datazioni su speleotemi sommersi e dati archeoligici. Mem. Descr. Carta Geol. Ital. 52, 261-276.

Allmon, W.D., 1988. Ecology of Recent Turritelline gastropods (Prosobranchia, Turritellidae): Current knowledge and paleontological implications. PALAIOS 3, 259-284.

Allmon, W.D., 1992. Role of temperature and nutrients in extinction of turritelline gastropods: Cenozoic of the northwestern Atlantic and northeastern Pacific. Palaeogeography, Palaeoclimatology, Palaeoecology 92, 41-54

Almogi-Labin, A., Bar-Matthews, M., Shriki, D., Kolosovsky, E., Paterne, M., Schilman, B., Ayalon, A., Aizenshtat, Z., Matthews A., 2009. Climatic variability during the last 90 ka of the southern and northern Levantine Basin as evident from marine records and speleothems. Quaternary Science Reviews 28, 2882-2896.

Antoine, D., Morel A., Morel, J.-M., 1995. Algal pigment distribution and primary production in the eastern Mediterranean as derived from coastal zone color scanner observations. Journal of Geophysical Research 100(C8), 16,193-16,206.

Antonioli, F., Chemello, R., Improta, S., Riggio, S., 1999. Dendropoma lower intertidal reef formations and their palaeoclimatological significance, NW Sicily. Marine Geology 161, 155-170.

Antonioli, F., Silenzi, S., Frisia, S., 2001. Tyrrhenian Holocene palaeoclimate trends from spelean serpulids. Quarternary Science Reviews 20, 1661-1670.

Antonioli, F., Cremona, G., Immordino, F., Puglisi, C., Romagnoli, C., Silenzi, S., Valpreda, E., Verrubbi, V., 2002. New data on the Holocene sea-level rise in NW Sicily (Central Mediterranean Sea). Global and Planetary Change 34, 121-140.

Ariztegui, D., Asioli, A., Lowe, L.L., Trincardi, F., Vigliotti, L., Tamburini, F., Chondrogianni, C., Accorsi, C.A., Bandini Mazzanti, M., Mercuri, A.M., Van der Kaars, S., McKenzie, J.A., Oldfield, F., 2000. Paleoclimate and the formation of sapropel S1: inferences from Late Quarternary lacrustine and marine sequences in the central Mediterranean region. Palaeogeography, Palaeoclimatology, Palaeoecology 158, 215-240.

Arnone, R., 1994. The temporal and spatial variability of chlorophyll in the Western Mediterranean. In: La Violette P.E. (Ed.), Seasonal and Interannual Variability of the Western Mediterranean Sea. Coastal and Estuarine Studies, Vol. 46, AGU, Washington D.C., pp. 195-225.

Avsar, N., Aksu, A., Dincer, F., 2006. Benthic foraminiferal assemblage of Erdek Bay (SW Marmara Sea). Yerbilimleri 27(3), 125-141.

Avsar, N., Meric, E., Cevik, M.G., Dincer, F., 2009. Recent benthic foraminiferal assemblages on the continental shelf off the Büyük Menderes river delta (W Turkey). Yerbilimleri 30(2), 127-144.

Backhaus, K., Erichson, B., Plinke, W., Weiber, R., 2006. Multivariate Analysemethoden. Springer, Berlin, Heidelberg, New York

Bakalem, A., Ruellet, T., Dauvin, J.C., 2009. Benthic indices and ecological quality of shallow Algeria fine sand community. Ecological Indicators 9, 395-408.

Bandy, O.L., Chierici, M.A., 1966. Depth-temperature evaluation of selected California and Mediterranean bathyal foraminifera. Marine Geology 4, 259-271.

Bar-Matthews, M., Aylon, A., Kaufman, A., 2000. Timing and hydrological conditions of sapropel events in the Eastern Mediterranean, as evident from speleothemes, Soreq cave, Israel. Chemical Geology 169, 145-146.

Barale, V., Weber, B., Melin, F., Jaquet, J.M., 2005. Recurrent and anomalous algal blooms in the Mediterranean Sea as seen by seaWiFS (1998-2003), 8th Conference on Remote Sensing for Marine and Costal Environments Halifax, Nova Scotia.

Bard, E., Hamelin, B., Arnold, M., Montaggioni, L., Cabioch, G., Faure, G., Rougerie, F., 1996. Deglacial sea-level record from Tahiti corals and the timing of global meltwater discharge. Nature 382, 241-244.

Bard, E., Hamelin, B., Delanghe-Sabatier, D., 2010. Deglacial meltwater pulse 1B and Younger Dryas sea levels revisited with boreholes at Tahiti. Science 327, 1235-1237.

Barker, R.W., 1960. Taxonomic notes on the species figured by H.B. Brady in his report on the foraminifera dredged by H.M.S. Challenger during the years 1873-1876. Soc. Econ. Paleontol. Mineral. Spec. Publ. 9, 238 pp

Barmawidjaja, D.M., Jorissen, F.J., Puskaric, S., Van der Zwaan, G.J., 1992. Microhabitat selection by benthic foraminifera in the northern Adriatic Sea. Journal of Foraminiferal Research 22, 297-317.

Bartels-Jonsdottir, H.B., Knudsen, K.L., Abrantes, F., Lebreiro, S., Eriksson, J., 2006. Climate variability during the last 2000 years in the Tagus Prodelta, western Iberian Margin: Benthic foraminifera and stable isotopes. Marine Micropaleontology 59, 83-103.

Basso, D., 1997. Deep rhodolith distribution in the Pontian Islands, Italy: a model for the paleoecology of a temperate sea. Palaeogeography, Palaeoclimatology, Palaeoecology 137, 173-187.

Berne, S., Jouet, G., Bassetti, M.A., Dennielou, B., Taviani, M., 2007. Late Glacial to Preboreal sea-level rise recorded by the Rhone deltaic system (NW Mediterranean). Marine Geology 245, 65-88.

Bethoux, J.-P., 1980. Mean water fluxes across sections in the Mediterranean Sea, evaluated on the basis of water and salt budgets and of observed salinities. Oceanologica Acta 3(1), 79-88.

Betzler, C., Braga, J.C., Jaramillo-Vogel, D., Römer, M., Hübscher, C., Schmiedl, G., Lindhorst, S., in press. Late Pleistocene and Holocene cool-water carbonates in the Western Mediterranean Sea. Sedimentology.

Bijma, J., Faber Jr., W.W., Hemleben, C., 1990. Temperature and salinity limits for growths and survival of some planktonic foraminifers in laboratory cultures. J. Foraminiferal Res. 20, 95-116.

Birks, H.J.B., 1998. Numerical tools in palaeolimnology - Progress, potentialities, and problems. Journal of Paleolimnology 20, 307-332.

Birks, H.J.B., Line, J.M., Juggins, S., Stevenson, A.C., Ter Braak, C.J.F., 1990. Diatoms and pH reconstruction. Phil. Trans. R. Soc. Lond. B 327, 263-278.

Blanc, J.J., 1972. Observation sur la sédimentation bioclastique en quelques points de la marge continentale de la Méditerranée. In: Stanley D.J. (Ed.), The Mediterranean Sea. A natural sedimentation laboratory. Dowden, Hutchinson and Ross, Inc., pp. 225-240.

Boltovskoy, E., 1978. Late Cenozoic benthonic foraminifera of the Ninetyeast Ridge (Indian Ocean). Marine Geology 26, 139-175.

Boltovskoy, E., Guissani de Kahn, G., 1983. Evaluation of benthic monothalamous foraminifers as guide fossils in Cenozoic deep-sea deposits of the south Atlantic. Micropaleontology 29(3), 298-308.

Boomer, I., Horton, B.P., 2006. Holocene relative sea-level movements along the North Norfolk Coast, UK. Palaeogeography, Palaeoclimatology, Palaeoecology 230, 32-51.

Bouhadad, Y., 2001. The Murdjadjo, Western Algeria, fault-related fold: Implications for seismic hazard. Journal of Seismology 5, 541-558.

Brasseur, P., Beckers, J. M., Brankart, J. M., Schoenauen, R.,1996. Seasonal temperature and salinity fields in the Mediterranean Sea: Climatological analyses of a historical data set. Deep-Sea Research I 43(2), 159-192.

Cacho, I., Grimalt, J.O., Pelejero, C., Canals, M., Sierro, F.J., Flores, J.A., Shackleton, N.J., 1999. Dansgaard-Oeschger and Heinrich event imprints in the Alboran Sea paleotemperatures. Paleoceanography 14(6), 698-705.

Cacho, I., Grimalt, J.O., Francisco, J., Sierro, J., Shackleton, N., Canals, M., 2000. Evidence for enhanced Mediterranean thermohaline circulation during rapid climatic coolings. Earth and Planetary Science Letters 183, 417-429.

Cacho, I., Grimalt, J.O., Canals, M., Sbaffi, L., Shackleton, N.J., Schönfeld, J., Zahn, R., 2001. Variability of the western Mediterranean Sea surface temperature during the last 25,000 years and its connection with the Northern Hemisphere climatic changes. Paleoceanography 16, 40-52.

Cacho, I., Grimalt, J.O., Canals, M., 2002. Response of the Western Mediterranean Sea to rapid climatic variability during the last 50,000 years: a molecular biomarker approach. Journal of Marine Systems 33-34, 253-272.

Cantos-Figuerola, A., Parrilla, G., Werner, F.E., 1991. Modelling of the surface flow in the Alboran Sea: review of sensitivity studies of reduced gravity flows. Fisica de la Tierra 3, 307-330.

Capotondi, L., Vigliotti, L., 1999. Magnetic and microfaunal characterization of Late Quarternary sediments from the Western Mediterranean: Inferences about sapropel formation and paleoceanographic implications. In: Zahn, R. Comas, M.C., Klaus, A. (Eds.), Proceedings of the Ocean Drilling Program, Scientific Results, pp. 505-518.

Capotondi, L., Speranza Principato, M., Morigi, C., Sangiorgi, F., Maffioli, P., Giunta, S., Negri, A., Corselli, C., 2006. Foraminiferal variations and stratigraphic implications to the deposition of

sapropel S5 in the eastern Mediterranean. Palaeogeography, Palaeoclimatology, Palaeoecology 235, 48-65.

Carannante, G., Esteban, M., Milliman, J.D., Simone, L., 1988. Carbonate lithofacies as paleolatitude indicators: problems and limitations. Sedimentary Geology 60, 333-346.

Carboni, M.G., Bergamin, L., Di Bella, L., Landini, B., Manfra, L., Vesica, P., 2005. Late Quarternary paleoclimatic and paleoenvironmental changes in the Tyrrhenian Sea. Quarternary Science Reviews 24, 2069-2082.

Casford, J.S.L., Rohling, E.J., Abu-Zied, R.H., Cooke, S., Fontanier, C., Leng, M.J., Lykousis, V., 2002. Circulation changes and nutrient concentrations in the late Quarternary Aegean Sea: A nonsteady state concept for sapropel formation. Paleoceanography 17(2), 14-1 - 14-11.

Casford, J.S.L., Rohling, E.J., Abu-Zied, R.H., Fontanier, C., Jorissen, F.J., Leng, M.J., Schmiedl, G., Thomson, J., 2003. A dynamic concept for eastern Mediterranean circulation and oxygenation during sapropel formation. Palaeogeography, Palaeoclimatology, Palaeoecology 190, 103-119.

Casieri, S., Frezza, V., Mancini, S., Carboni, M.G., 2008. Epiphytic foraminifera on leaves and rhizomes of Posidonia oceanica from Ischia Island (Tyrrhenian Sea, Italy). Geophysical Research Abstracts 10, 2 p.

Caulet, J.P., 1972. Recent biogenic calcareous sedimentation on the Algerian continental shelf. In: Stanley D.J. (Ed.), The Mediterranean Sea. A natural sedimentation laboratory. Dowden, Hutchinson and Ross, Inc., pp. 261-277.

Chendes, C., Kaminiski, M.A., Filipescu, S., Aksu, A.E., Yasar, D., 2004. The response of modern benthic foraminiferal assemblages to water-mass properties along the southern shelf of Marmara Sea. Acta Palaeontologica Romaniae 4, 69-80.

Cimerman, F., Langer M.R., 1991. Mediterranean foraminifera. Slovenska Akad. Znanosti in Umetnosti. Opera. Academia Sciertiarum et Artium, Slovenca, Cl. 4, Hist. Nat. 30, Ljubljana

Cita, M. B., Zocchi, M., 1978. Distribution patterns of benthic foraminifera on the floor of the Mediterranean Sea. Oceanologica Acta 1(4), 445-462.

Comas, M.C., Zahn, R., Klaus, A., et al., 1996. Proceedings of the Ocean Drilling Program, Initial Results 161, pp. 5-18, College Station, Texas (ODP)

Comas, M.C., Platt, J.P., Soto, J.I., Watts, A.B., 1999. The origin and tectonic history of the Alboran Basin: insights from Leg 161 results. In: Zahn, R., Comas, M.C., Klaus, A. (Eds.), Proceedings of the Ocean Drilling Program, Scientific Results 161, 555-580.

Coppa, M.G., Di Tuoro, A., 1995. Preliminary data on the Holocene foraminifera of the Cilento continental shelf (Tyrrhenian Sea). Revista Espanola de Paleontologia 10(2), 161-174.

Corliss, B.H., 1979. Recent deep-sea benthonic foraminifera from the southeast Indian Ocean. Micropaleontology 25(1), 1-19.

Corliss, B.H., 1985. Microhabitats of benthic foraminifera within deep-sea sediments. Nature 314, 435-438.

Cramp, A., O'Sullivan, G., 1999. Neogene sapropels in the Mediterranean: a review. Marine Geology 153, 11-28.

Culver, S.J., Woo, H.J., Oertel, G.F., Buzas, M.A., 1996. Foraminifera of coastal depositional environments, Virginia, U.S.A., distribution and taphonomy. Palaios 11, 459-486.

Cushman, J.A., 1910. A monograph of the foraminifera of the North Pacific Ocean, Part 1: Astrorhizidae and Lituolidae. Smithonian Institution, United States National Museum, Bulletin 71, Government Print Service, Washington.

Cushman, J.A., 1911. A monograph of the foraminifera of the North Pacific Ocean, Part 2: Textularidae. Smithonian Institution, United States National Museum, Bulletin 71, Government Print Service, Washington.

Cushman, J.A., 1914. A monograph of the foraminifera on the north Pacific ocean, Part 4: Chilostomellidae, Globigerinidae, Nummulitidae. Smithonian Institution, United States National Museum, Bulletin 71, Government Print Service, Washington.

Cushman, J.A., 1915. A monograph of the foraminifera of the North Pacific Ocean, Part 5: Rotaliidae. Smithonian Institution, United States National Museum, Bulletin 71, Government Print Service, Washington.

Cushman, J.A., 1917. A monograph of the foraminifera of the North Pacific Ocean, Part 6: Miliolidae. Smithonian Institution, United States National Museum, Bulletin 71, Government Print Service, Washington.

Cushman, J.A., 1918. The foraminifera of the Atlantic Ocean, Part 1: Astrorhizidae. Smithonian Institution, United States National Museum, Bulletin 104, Government Print Service, Washington.

Cushman, J.A., 1920. The foraminifera of the Atlantic Ocean, Part 2: Lituolidae. Smithonian Institution, United States National Museum, Bulletin 104, Government Print Service, Washington.

Cushman, J.A., 1929. The foraminifera of the Atlantic Ocean, Part 6: Miliolidae, Ophthalmidiidae, Fischerinidae. Smithonian Institution, United States National Museum, Bulletin 104, Government Print Service, Washington.

Cushman, J.A., 1930. The foraminifera of the Atlantic Ocean, Part 7: Nonionidae, Camerinidae, Peneroplidae and Alveolinellidae. Smithonian Institution, United States National Museum, Bulletin 104, Government Print Service, Washington.

Cushman, J.A., 1931. The foraminifera of the Atlantic Ocean, Part 8: Rotaliidae, Amphisteginidae, Calcarinidae, Cymbalporettidae, Globorotallidae, Anomalinidae, Planorbulinidae, Pupertiidae and Homotremidae. Smithonian Institution, United States National Museum, Bulletin 104, Government Print Service, Washington.

Cushman, J.A., 1945. Foraminifera of the United States Antarctic Service Expedition 1939-1941, Proceedings of the American Philosophical Society, Reports on Scientific Results of the Antarctic Service Expedition, 1939-1941. American Philosophical Society, pp. 285-288.

DeMenocal, P., Ortiz, J., Guilderson, T., Adkins, J., Sarnthein, M., Baker, L., Yarusinsky, M., 2000. Abrupt onset and termination of the African Humid Period: rapid climate responses to gradual insolation forcing. Quarternary Science Reviews 19, 347-361.

De Rijk, S., Troelstra, S.R., Rohling, E.J., 1999. Benthic foraminiferal distribution in the Mediterranean Sea. Journal of Foraminiferal Research 29(2), 93-103.

De Rijk, S., Jorissen, F.J., Rohling, E.J., Troelstra, S.R., 2000. Organic flux control on bathymetric zonation of Mediterranean benthic foraminifera. Marine Micropaleontology 40, 151-166.

De Stigter, H.C., Jorissen, F.J., Van der Zwaan, G.J., 1998. Bathymetric distribution and microhabitat partitioning of live (Rose Bengal stained) benthic foraminifera along a shelf to bathyal transect in the southern Adriatic Sea. Journal of Foraminiferal Research 28 (1), 40-65.

Dewey, J.F., Helman, M.L., Turco, E., Hutton, D.H.W., Knott, S.D., 1989. Kinematics of the western Mediterranean. In: Coward, M.P., Dietrich, D., Park, R.G. (Eds.), Alpine Tectonics. Geological Society Special Publication, pp. 265-283.

Doglioni, C., Gueguen, E., Sabat, F., Fernandez, M., 1997. The Western Mediterranean extensional basins and the Alpine. Terra Nova 9, 109-112.

Domzig, A., Yelles, K., Le Roy, C., Deverchere, J., Bouillin, J.-P., Bracene, R., Mercier de Lepinay, B., Le Roy, P., Calais, E., Kherroubi, A., Gaullier, V., Savoye, B., Pauc, H., 2006. Searching for the Africa-Eurasia Miocene boundary offshore western Algeria (MARADJA 03 cruise). C.R. Geoscience 338, 80-91.

Dormoy, I., Peyron, O., Combooureu-Neboutb, N., Goring, S., Kotthoff, U., Magny, M., Pross, J., 2009. Terrestrial climate variablility and seasonality changes in the Mediterranean region between 15,000 and 4000 years BP deduced from marine pollen records. Clim. Past Discuss. 5, 735-770.

Drescher-Schneider, R., de Beaulieu, J.-L., Magny, M., Walter-Simonnet, A.-V., Bossuet, G., Millet, L., Brugiapaglia, E., Drescher, A., 2007. Vegetation history, climate and human impact over the last 15,000 years at Lago dell´Accesa (Tuscany, central Italy). Veget Hist Archaeobot 16, 279-299.

Duchemin, G., Fontanier, C., Jorissen, F.J., Barras, C., Griveaud, C., 2007. Living small-sized (63-150 µm) foraminifera from mid-shelf to mid-slope environments in the Bay of Biscay. Journal of Foraminiferal Research 37, 12-32.

Duijnstee, I., de Lugt, I., Vonk Noordegraaf, H., Van der Zwaan, B., 2004. Temporal variability of foraminiferal densities in the northern Adriatic Sea. Marine Micropaleontology 50, 125-148.

Emeis, K.-C., Struck, U., Schulz, H.-M., Rosenberg, R., Bernasconi, S., Erlenkeuser, H., Sakamoto, T., Martinez-Ruiz, F., 2000. Temperature and salinity variations of Mediterranean Sea surface waters over the last 16,000 years from records of planktonic stable oxygen isotopes and alkenone unsaturation ratios. Palaeogeography, Palaeoclimatology, Palaeoecology 158, 259-280.

Emeis, K.-C., Schulz, H., Struck, U., Rossignol-Strick, M., Erlenkeuser, H., Howell, M.W., Kroon, D., Mackensen, A., Ishizuka, S., Oba, T., Sakamoto, T., Koizumi I., 2003. Eastern Mediterranean surface water temperatures and $\delta^{18}O$ composition during deposition of sapropels in the late Quaternary. Paleoceanography 18, doi: 10.1029/2000PA000617.

Emiliani, C., 1971. Isotopic paleotemperatures and shell morphology of *Globigerinoides rubra* in the type section for the Pliocene-Pleistocene boundary. Micropaleontology 17, 233-238.

Fairbanks, R.G., 1989. A 17,000-year glacio-eustatic sea level record: influence of glacial melting rates on the Younger Dryas event and deep-ocean circulation. Nature 342, 637-642.

Feldman, G.C., McClain, C.R., 2006. Ocean Color Web, SeaWiFS/Chlorophyll a concentration, 07/2002-06/2006. NASA Goddard Space Flight Center, Washington, USA., http://oceancolor.gsfc.nasa.gov/

Fernandez de Puelles, M. L., Valencia, J., Vicente, L., 2004A. Zooplankton variability and climatic anomalies from 1994 to 2001 in the Balearic Sea (Western Mediterranean. Journal of Marine Science 61, 492-500.

Fernandez de Puelles, M.L., Valencia, J., Jansa, J., Morillas, A., 2004B. Hydrographical characteristics and zooplankton distribution in the Mallorca channel (Western Mediterranean): spring 2001. ICES Journal of Marine Science 61, 654-666.

Fontugne, M., Arnold, M., Labeyrie, L., Paterne, M., Calvert, S., Duplessy, J.C., 1994. Paleoenvironment, sapropel chronology, and Nile river discharge during the last 20,000 years as indicated by deep-sea sediment records in the eastern Mediterranean. Radiocarbon 34, 75-88.

Fornos, J.J., Ahr, W.M., 1997. Temperate carbonates on a modern, low-energy, isolated ramp: The Balearic Platform, Spain. Journal of Sedimentary Research 67, 364-373.

Fornos, J.J., Ahr, W.M., 2006. Present-day temperate carbonate sedimentation on the Balearic platform, western Mediterranean: compositional and textural variation along a low-energy isolated ramp. In: Pedley H.M., Carannante, G. (Eds.), Cool-water carbonates: depositional systems and palaeoenvironmental controls. London, pp. 71 - 84.

Fretter, V., Graham A., 1981. The prosobranch molluscs of Britain and Denmark, Part 6, Cerithiacea, Strombacea, Hipponicacea, Calyptraeacea, Lamellariacea, Cypracea, Naticacea, Tonnacea, Heteropoda. J. Mollus. Stud. 47, 286-293.

Frezza, V., Carboni, M.G., 2009. Distribution of recent foraminiferal assemblages near the Ombrone River mouth (Northern Tyrrhenian Sea, Italy). Revue de micropaleontologie 52, 43-66.

Frontalini, F., Coccioni, R., 2008. Benthic foraminifera for heavy metal pollution monitoring: A case study from the central Adriatic Sea coast of Italy. Estuarine, Costal and Shelf Science 76(2), 404-417.

Fujita, K., Omori, A., Yokoyama, Y., Sakai, S., Iryu, Y., 2010. Sea-level rise during Termination II inferred from large benthic foraminifers: IODP expedition 310, Tahiti sea level. Marine Geology 271, 149-155.

Garcia, E., Tintore, J., Pinot, J.M., Font, J., Manriquez, M., 1994. Surface circulation and dynamics of the Balearic Sea. In: P.E. LaViolette (Ed.), Seasonal and Interannual Variability of the Western Mediterranean Sea, Coastal and Estuarine Studies, Vol. 46. American Geophysical Union, Washington D.C., pp. 73-91.

Garthwaite, P.H., 1994. An interpretation of Partial Least Squares. Journal of the American Statistical Association 89(425), 122-127.

Gascard, J. C., Riches, C., 1985. Water masses and circulation in the Western Alboran Sea and in the Straits of Gibraltar. Progress in Oceanography 15, 157-216.

Gehrels, W.A., 2000. Using foraminiferal transfer functions to produce high-resolution sea-level records from salt-marsh deposits, Maine, USA. The Holocene 10(3), 367-376.

Giresse, P., Pauc, H., Deverchere, J., and the Maradja Shipboard Scientific Party, 2009. Sedimentary processes and origin of sediment gravity-flow deposits on the western Algerian margin during late Pleistocene and Holocene. Marine and Petroleum Geology 26, 695-710.

Goy, J. L., Zazo, C., Dabrio, C.J., 2003. A beach-ridge progradation complex reflecting periodical sea-level and climate variability during the Holocene. Geomorphology 50, 251-268.

Gueguen, E., Doglioni, C., Fernandez, M., 1998. On the post-25 Ma geodynamic evolution of the western Mediterranean. Tectonophysics 298, 259-269.

Guimerans, P. V., Currado J.L.C., 1999A. The recent uvigerinids (benthic foraminifera) in the northeastern Gulf of Cadiz. Bol.Inst.Esp.Oceanogr. 15, 191-202.

Guimerans, P.V., Currado, J.L.C., 1999B. Distribution of Planorbulinacea (benthic foraminifera) assemblages in surface sediments on the northern margin of the Gulf of Cadiz. Bol. Inst. Esp. Oceanogr. 15(1-4), 181-190.

Gündüz, M., Özsoy, E., 2005. Effects of the North Sea Caspian pattern on surface fluxes of Euro-Asian-Mediterranean Seas. Geophysical Research Letters 32, 4 pp.

Hammer, O., Harper, D.A.T., Ryan, P.D., 2001. PAST: Palaeontological statistics package for education and data analysis. Paleaeontologia Electronica 4(1), 9 pp.

Hammer, O., Harper, D.A.T., Ryan, P.D., 2008. PAST PAlaeontological STatistics, ver. 1.81., Software Documentation.

Hasegawa, S., Sprovieri, R., Poluzzi, A., 1990. Quantitative analysis of benthic foraminiferal assemblages from Plio-Pleistocene sequences in the Tyrrhenian Sea, ODP LEG 107. In: Kastens, K.A., Mascle, J. et al. (Eds.), Proceedings of the Ocean Drilling Program, Scientific Results, pp. 461-478.

Hawkes, A.D., Horton, B.P., Nelson, A.R., Hill, D.F., in press. The application of intertidal foraminifera to reconstruct coastal subsidence during the giant Cascadia earthquake of AD 1700 in Oregon, USA. Quarternary International.

Hayes, A., Rohling, E.J., De Rijk, S., Kroon, D., Zachariasse, W.J., 1999. Mediterranean planktonic foraminiferal faunas during the last glacial cycle. Marine Geology 153, 239-252.

Hayward, B. W., 2004. Foraminifera-based estimates of paleobathymetry using Modern Analoque Technique, and the subsidence history of the early Miocene Waitemata Basin. New Zealand Journal of Geology & Geophysics 47, 749-767.

Hemleben, C., Spindler, M., Anderson, O.R., 1999. Modern Planktonic Foraminifera. Springer-Verlag, New York.

Hofker, J., 1960. Foraminiferen aus dem Golf von Neapel. Paläont. Z. 34(3/4), 233-262.

Hohenegger, J., 2005. Estimation of environmental paleogradient values based on presence/absence data: a case study using benthic foraminifera for paleodepth estimation. Palaeogeography, Palaeoclimatology, Palaeoecology 217, 115-130.

Hohenegger, J., Yordanova, E., Nakano, Y., Tatzreiter, F., 1999. Habitats of larger foraminifera on the upper reef slope of Sesoko Island, Okinawa, Japan. Marine Micropaleontology 36, 109-168.

Holsten, J., Stott, L., Berelson, W., 2004. Reconstructing benthic carbon oxidation rates using $\delta^{13}C$ of benthic foraminifera, Marine Micropaleontology 53, 117-132.

Horton, B.J., Edwards R.J., 2006. Quantifying Holocene sea-level change using intertidal foraminifera: Lessons from the British Isles. Cushman Foundation for Foraminiferal Research Special Publication No. 40, 1-97.

Horton, B.J., Murray, J.W., 2006. Patterns in cumulative increase in live and dead species from foraminiferal time series of Cowpen Marsh, Tees Estuary, UK: Implications for sea-level studies. Marine Micropaleontology 58, 287-315.

Horton, B.P., Edwards, R.J., Lloyd, J.M., 1999. A foraminiferal-based transfer function: Implications for sea-level studies. Journal of Foraminiferal Research 29(2), 117-129.

Hottinger, L., Halicz, E., Reiss, Z., 1993. Recent foraminiferida from the Gulf of Aqaba, Red Sea. Slovenska Akademija Znanosti in Umetnosti, Ljubljana.

Hughen, K.A., Baillie, M.G.L., Bard, E., Bayliss, A., Beck, J.W., Bertrand, C.J.H., Blackwell, P.G., Buck, C.E., Burr, G.S., Cutler, K.B., Damon, P.E., Edwards, R.L., Fairbanks, R.G., Friedrich, M., Guilderson, T.P., Kromer, B., McCormac, F.G., Manning, S.W., Bronk Ramsey, C., Reimer, P.J., Reimer, R.W., Remmele, S., Southon, J.R., Stuiver, M., Talamo, S., Taylor, F.W., van der Plicht, J., Weyhenmeyer, C.E., 2004. Marine04 Marine radiocarbon age calibration, 26 - 0 ka BP. Radiocarbon 46, 1059-1086.

Hyams, O., Almogi-Labin, A., Benjamini, C., 2002. Larger foraminifera of the southeastern Mediterranean shallow continental shelf off Israel. Israel Journal of Earth Science 51, 169-179.

Hyams-Kaphzan, O., Almogi-Labin, A., Sivan, D., Benjamini, C., 2008. Benthic foraminifera assemblage change along the southeastern Mediterranean inner shelf due to fall-off of Nile-derived siliciclastics. N. Jb. Geol. Paläont. Abh. 248(3), 315-344.

Jimenez-Espejo, F.J., Martinez-Ruiz, F., Sakamoto, T., Iijima, K., Gallego-Torres, D., Harada, N., 2007. Paleoenvironmental changes in the western Mediterranean since the last glacial maximum: High resolution multiproxy record from the Algero-Balearic basin. Palaeogeography, Palaeoclimatology, Palaeoecology 246, 292-306.

Jimenez-Espejo, F.J., Martinez-Ruiz, F., Rogerson, M., González-Donoso, J.M., Romero, O.E., Linares, D., Sakamoto, T., Gallego-Torres, D., Rueda Ruiz, J.L., Ortega-Huertas, M., Perez Claros, J.A., 2008. Detrital input, productivity fluctuations, and water mass circulation in the westernmost Mediterranean Sea since the Last Glacial Maximum. Geochemistry, Geophysics, Geosystems 9, Q11U02, doi:10.1029/2008GC002096.

Jones, R.W., 1994. The Challenger Foraminifera, 1st Edition, Oxford University Press Inc., New York.

Jorissen, F.J., 1987. The distribution of benthic foraminifera in the Adriatic Sea. Marine Micropaleontology 12, 21-48.

Jorissen, F.J., Barmawidjaja, D.M., Puskaric, S., Van der Zwaan, G.J., 1992. Vertical distribution of benthic foraminifera in the northern Adriatic Sea: the relation with the organic flux. Marine Micropaleontology 19, 131-146.

Jorissen, F.J., de Stigter, H.C., Widmark, J.G.V., 1995. A conceptual model explaining benthic foraminiferal microhabitats. Marine Micropaleontology 26, 3-15.

Juggins, S., 2003. Software for ecological and palaeoecological data analysis and visualisation. Tutorial version 1.3, 1-24.

Kaminski, M.A., Aksu, A., Box, M., Hiscott, R.N., Filipescu, S., Al-Salameen, M., 2002. Late Glacial to Holocene benthic foraminifera in the Marmara Sea: implications for Black Sea - Mediterranean Sea connections following the last deglaciation. Marine Geology 190, 162-202.

Kayan, I., 1988. Late Holocene sea-level changes on the western Anatolian coast. Palaeogeography, Palaeoclimatology, Palaeoecology 68, 205-218.

Kotthoff, U., Pross, J., Müller, U.C., Peyron, O., Schmiedl, G., Schulz, H., Bordon A., 2008. Climate dynamics in the borderlands of the Aegean Sea during deposition of Sapropel S1 deduced from a marine pollen record. Quaternary Science Reviews 27, 832–845.

Koulouri, P., Dounas, C., Arvanitidis, C., Koutsoubas, D., Eleftheriou, A., 2006. Molluscan diversity along a Mediterranean soft bottom sublittoral ecotone. Scientia Marina 70, 573-583.

Kucera, M., Weinelt, M., Kiefer, T., Pflaumann, U., Hayes, A., Weinelt, M., Chen, M.-T., Mix, A.C., Barrows, T.T., Cortijo, E., Duprat, J., Juggins, S., Waelbroeck, C., 2005. Reconstruction of sea-surface temperatures from assemblages of planktonic foraminifera: multi-technique approach based on geographically constrained calibration data sets and its application to glacial Atlantic and Pacific Oceans. Quarternary Science Reviews 24(7-9), 951-998.

Kuhnt, T., Schmiedl, G., Ehrmann, W., Hamann, Y., Hemleben, C., 2007. Deep-sea ecosystem variability of the Aegean Sea during the past 22 kyr as revealed by benthic foraminifera. Marine Micropaleontology 64(3-4), 141-162.

Kuhnt, T., Schmiedl, G., Ehrmann, W., Hamann, Y., Andersen, N., 2008. Stable isotopic composition of Holocene benthic foraminifers from the Eastern Mediterranean Sea: past changes in productivity and deep water oxygenation. Palaeogeography, Palaeoclimatology, Palaeoecology 268, 106-115.

Kuper, R., Kröpelin S., 2006. Climate-controlled Holocene occupation in the Sahara: Motor of Africa's evolution. Science 313, 803-807.

Lambeck, K., Bard, E., 2000. Sea-level change along the French Mediterranean coast for the past 30,000 years. Earth and Planetary Science Letters 175, 203-222.

Lambeck, K., Chappell, J., 2001. Sea-level change through the last glacial cycle. Science 292, 679-686.

Lambeck, K., Antonioli, F., Purcell, A., Silenzi, S., 2004. Sea-level change along the Italian coast for the past 10,000 yr. Quarternary Science Reviews 23, 1567-1598.

Langer, M.R., Hottinger, L., 2000. Biogeography of selected "larger" foraminifera. Micropaleontology 46, 105-126.

Langer, M.R., Frick, H., Silk, M.T., 1998. Photophile and sciaphil foraminiferal assemblages from marine plant communities of Lavezzi Islands (Corsica, Mediterranean Sea). Revue Paleobiol. Geneve 17(2), 525-530.

Lee, J. J., 2006. Algal symbiosis in larger foraminifera. Symbiosis 42, 63-75.

Leiter, C., 2008. Benthos-Foraminiferen in Extremhabitaten: Auswertung von METEOR-Expeditionen vor Namibia, Ph.D. Thesis, Ludwig-Maximilians-Universität, München, 151 pp.

Leorri, E., Horton, B.P., Cearreta, A., 2008. Development of foraminifera-based transfer function in the Basque marshes, N. Spain: Implications for sea-level studies in the Bay of Biscay. Marine Geology 251, 60-74.

Leps, J., Smilauer, P., 2005. Multivariate analysis of ecological data using CANOCO. Cambridge University Press, Cambridge.

Levy, A., Mathieu, R., Poignant, A., Rosset-Moulinier, M., Ubaldo, M. de L., Ambroise, D., 1993. Recent foraminifera from the continental margin of Portugal. Micropaleontology 39, 75-87.

Leyer, I., Wesche, K., 2007. Multivariate Statistik in der Ökologie. Springer, Berlin Heidelberg.

L'Helguen, S., Le Corre, P., Madec, C., Morin, P., 2002. New and regenerated production in the Almeria-Oran front area, eastern Alboran Sea. Deep-Sea Research I 49, 83-99.

Lionello, P., Malanotte-Rizzoli, P., Boscolo, R., Luterbacher, J., 2004. The Mediterranean climate: basic issues and perspectives. In: White Paper on Mediterranean climate variability and predictability, Technical Report, 5-17

Loeblich, A.R., Tappan, H., 1988. Foraminiferal genera and their classification. Van Nostrand Reinhold Company, New York.

Luterbacher, J., Xoplaki, E., Casty, C., Wanner, H., Pauling, A., Küttel, M., Rutishauser, T., Brönnimann, S., Fischer, E., Fleitmann, D., González-Rouco, F.J., García-Herrera, R., Barriendos, M., Rodrigo, F., Gonzalez-Hidalgo, J.C., Saz, M.A., Gimeno, L., Ribera, P., Brunet, M., Paeth, H., Rimbu, N., Felis, T., Jacobeit, J., Dünkeloh, A., Zorita, E., Guiot, J., Türkes, M., Alcoforado, M.J., Trigo, R., Wheeler, D., Tett, S., Mann, M.E., Touchan, R., Shindell, D.T., Silenzi, S., Montagna, P., Camuffo, D., Mariotti, A., Nanni, T., Brunetti, M., Maugeri, M., Zerefos, C., De Zolt, S., Lionello, P., 2006. Mediterranean climate variability over the last centuries: a review. In: Lionello, P., Malanotte-Rizzoli, P., Boscolo, R. (Eds.), Mediterranean Climate variability 4. Elsevier, Amsterdam, pp. 438.

Mackensen, A., Schumacher, S., Radke, J., Schmidt, D.N., 2000. Mircrohabitat preferences and stable carbon isotopes of endobenthic foraminifera: clue to quantitative reconstruction of oceanic new production? Marine Micropaleontology 40, 233-258.

Magny, M., Miramont, C., Sivan, O., 2002. Assessment of the impact of climate and anthropogenic factors on Holocene Mediterranean vegetation in Europe on the basis of palaeohydrological records. Palaeogeography, Palaeoclimatology, Palaeoecology 186, 47-59.

Malanotte-Rizzoli, P., Hecht, A., 1988. Large-scale properties of the Eastern Mediterranean: a review. Oceanologica Acta 11(4), 323-335.

Malmgren, B.A., Haq, B.U., 1982. Assessment of quantitative techniques in paleobiogeography. Marine Micropaleontology 7, 213-230.

Malmgren, B.A., Nordlund, U., 1997. Application of artificial neural networks to paleoceanographic data. Palaeogeography, Palaeoclimatology, Palaeoecology 136, 359-373.

Martinez-Garcia, P., Soto, J.I., Comas, M., submitted. Recent structures in the Alboran Ridge and Yusuf fault-zones: interpretation from swath-bathymetry and sub-bottom profiling. Geo-Marine Letters.

Martinez-Ruiz, F., Paytan, A., Kastner, M., Gonzalez-Donoso, J.M., Linares, D., Bernasconi, S.M., Jimenez-Espejo, F.J., 2003. A comparative study of the geochemical and mineralogical characteristics of the S1 sapropel in the western and eastern Mediterranean. Palaeogeography, Palaeoclimatology, Palaeoecology 190, 23-37.

Martins, V., Dubert, J., Jouanneau, J.-M., Weber, O., Ferreira da Silva, E., Patinha, C., Alveirinho Dias, J.M., Rocha, F., 2007. A multiproxy approach of the Holocene evolution of shelf-slope circulation on the NW Iberian Continental Shelf. Marine Geology 239, 1-18.

Masque, P., Fabres, J., Canals, M., Sanchez-Cabeza, J.A., Sanchez-Vidal, A., Cacho, I., Calafat, A.M., Bruach, J.M., 2003. Accumulation rates of major constituents of hemipelagic sediments in the deep Alboran Sea: a centennial perspective of sedimentary dynamics. Marine Geology 193, 207-253.

Massuti, E., Renones, O., 2005. Demersal resource assemblages in the trawl fishing grounds off the Balearic Islands (western Mediterranean) Scientia Marina 69(1), 167-181.

McCorkle, D.C., Emerson, S.R., Quay, P.D., 1985. Stable carbon isotopes in marine porewaters. Earth and Planetary Science Letters 74, 13-26.

McCorkle, D.C., Keigwin, L.D., Corliss, B.H., Emerson, S.R., 1990. The influence of microhabitats on the carbon isotopic composition of deep-sea benthic foraminifera. Paleoceanography 5, 161-185.

Medioli, F.S., Scott, D.B., 1978. Emendation of the genus *Discanomalina* Asano and its implications on the taxonomy of some of the attached foraminiferal forms. Micropaleontology 24(3), 291-302.

Mehrnusch, M., 1993. Morhpologische und strukturelle Merkmale einiger Bolivinen (Foraminiferida). Diskussion des taxonomischen Status von *Afrobulimina, Brizalina, Bolivina* and verwandten Taxa. Paläont. Z. 67(1/2), 3-19.

Melki, T., Kallel, N., Jorissen, F.J., Guichard, F., Dennielou, B., Berne, S., Labeyrie, L., Fontugne, M., 2009. Abrupt climate change, sea surface salinity and paleoproductivity in the western Mediterranean Sea (Gulf of Lion) during the last 28 kyr. Palaeogeography, Palaeoclimatology, Palaeoecology 279, 96-113.

Mendes, I., Gonzalez, R., Dias, J.M.A., Lobo, F., Martins, V., 2004. Factors influencing Recent benthic foraminifera distribution on the Guandiana shelf (Southwestern Iberia). Marine Micropaleontology 51, 171-192.

Mercone, D., Thomson, J., Croudace, I.W., Siani, G., Paterne, M., Troelstra S., 2000. Duration of S1, the most recent sapropel in the eastern Mediterranean Sea, as indicated by accelerator mass spectrometry radiocarbon and geochemical evidence. Paleoceanography 15, 336-347.

Milker, Y., Schmiedl, G., Betzler, C., Römer, M., Jaramillo-Vogel, D., Siccha, M., 2009. Distribution of Recent benthic foraminifera in neritic carbonate environments of the Western Mediterranean Sea. Marine Micropaleontology 70, 207-225

Milker, Y., Schmiedl, G., Betzler C., submitted. Holocene sea-level change in the Western Mediterranean Sea: Quantitative reconstructions based on foraminiferal transfer functions. Quaternary Science Reviews.

Millot, C., 1999. Circulation in the Western Mediterranean Sea. Journal of Marine Systems 20, 423-442.

Millot, C., Taupier-Letage, I., 2005. Circulation in the Mediterranean Sea. In: Saliot. A. (Ed.), The Handbook of Environmental Chemistry. Springer Verlag, Heidelberg, pp. 29-66.

Millot, C., Taupier-Letage, I., Benzohra, M., 1990. The Algerian eddies. Earth-Science Reviews 27, 203-219.

Mojtahid, M., Jorissen, F., Lansard, B., Fontanier, C., Bombled, B., Rabouille, C., 2009. Spatial distribution of live benthic foraminifera in the Rhone prodelta: Faunal response to a continental-marine organic matter gradient. Marine Micropaleontology 70, 177-200.

Morhange, C., Pirazzoli, P.A., 2005. Mid-Holocene emergence of southern Tunisian coasts. Marine Geology 220, 205-213.

Morhange, C., Laborel, J., Hesnard, A., 2001. Changes of relative sea-level during the past 5000 years in the ancient harbour of Marseilles, Southern France. Palaeogeography, Palaeoclimatology, Palaeoecology 166, 319-329.

Morigi, C., Jorissen, F.J., Fraticelli, S., Horton, B.P., Principi, M., Sabbatini, A., Capotondi, L., Curzi, P.V., Negri, A., 2005. Benthic foraminiferal evidence for the formation of the Holocene mud-belt and bathymetrical evolution in the central Adriatic Sea. Marine Micropaleontology 57, 25-49.

Moutin, T., Raimbault, P., 2002. Primary production, carbon export and nutrients availability in western and eastern Mediterranean Sea in early summer 1996 (MINOS cruise). Journal of Marine Systems 33-34, 273-288.

Murgese, D.S., de Deckker, P., 2007. The Late Quarternary evolution of water masses in the eastern Indian Ocean between Australia and Indonesia, based on benthic foraminifera faunal and carbon isotopes analyses. Palaeogeography, Palaeoclimatology, Palaeoecology 247, 382-401.

Murray, J.W., 2003. An illustrated guide to the benthic foraminifera of the Hebridean shelf, west of Scotland, with notes on their mode of life. Paleaeontologia Electronica 5(1), 31 pp.

Murray, J.W., 2006. Ecology and Applications of Benthic Foraminifera. Cambridge University Press, Cambridge.

Nelson, A.R., Sawai, Y., Jennings, A.E., Bradley, L.-A., Gerson, L., Sherrod, B.L., Sabean, J., Horton, B.P., 2008. Great-earthquake paleogeodesy and tsunamies of the past 2000 years at Alsea Bay, central Oregon coast, USA. Quarternary Science Reviews 27, 747-768.

Niniyerola, M., Saez, L., Perez-Obiol, R., 2007. Relating postglacial relict plants and Holocene vegetation dynamics in the Balearic Islands trough field surveys, pollen analysis and GIS modeling. Plant Biosystems 141(3), 292-304.

Nuglisch, K., 1985. Foraminiferen - marine Mikroorganismen. A. Ziemsen Verlag, Lutherstadt Wittemberg.

Ohga, T., Kitazato, H., 1997. Seasonal changes in bathyal foraminiferal populations in response to the flux of organic matter (Sagami Bay Japan). Terra Nova 9, 33-37.

Orbigny, A. d', 1839. Foraminiferes. Voyage dans l'Amerique Meridonale 5(5), Paris and Strasbourg.

Orbigny, A. d', 1846. Foraminiferes Fossiles Du Bassin Tertiaire De Vienne (Autriche). Gide et Comp, Libraires-Editeurs, Paris.

Ortiz, J.D., Mix, A.C., Rugh, W., Watkins, J.M., Collier, R.W., 1996. Deep-dwelling planktonic foraminifera in the northeastern Pacific Ocean reveal environmental control of oxygen and carbon isotopic disequilibria. Geochimica et Cosmochimica Acta 60(22), 4509-4523.

Overpeck, J.T., Webb III. T., Prentice, I.C., 1985. Quantitative interpretation of fossil pollen spectra: Dissimilarity coefficients and the method of Modern Analogs. Quarternary Research 23, 87-108.

Panieri, G., Gamberi, F., Marani, M., Barbieri, R., 2005. Benthic foraminifera from a recent, shallow-water hydrothermal environment in the Aeolian Arc (Tyrrhenian Sea). Marine Geology 218, 207-229.

Parker, F.L., 1958. Eastern Mediterranean Foraminifera. Reports of the Swedish Deep-Sea Expedition, Sediment Cores from the Mediterranean Sea and the Red Sea 8(4), 217-285.

Pawlowski, J., Holzmann, M., Fahrni, J.F., Hallock, P., 2001. Molecular identification of algal endosymbionts in large Miliolid foraminifera: 1. Chlorophytes. Journal of Eukaryotic Microbiology 48(3), 362-367.

Pedley H.M., Carannante, G. (Eds.), 2006. Cool-Water Carbonates. Depositional Systems and Palaeoenvironmental Controls. Geological Society Special Publication, 255, London.

Peel, M.C., Finlayson, B.L., McMahon, T.A., 2007. Updated world map of the Köppen-Geiger climate classification. Hydrol. Earth Syst. Sci. 11, 1633-1644.

Pérès, J.M., Picard, J., 1964. Nouveau manuel de bionomie bentique de la Mer Mediterranée. Rec. Trav. St. Mar. Endoume 31, 1-137.

Perez-Obiol, R., 2007. Palynological evidence for climatic change along the eastern Iberian Peninsula and Balearic Islands. Contributions to Science 3(3), 415-419.

Phleger, F.B., 1965. Living benthic foraminifera from coastal marsh, southwestern Florida. Bol. Soc. Geol. Mexicana 28(1), 45-60.

Pinot, J.-M., Lopez-Jurado, J.L., Riera, M., 2002. The CANALES experiment (1996-1998). Interannual, seasonal, and mesoscale variablitiy of the circulation in the Balearic channels. Progress in Oceanography 55, 335-370.

Pirazolli, P.A., 2005. A review of possible eustatic, isostatic and tectonic contributions in eight late-Holocene relative sea-level histories from the Mediterranean area. Quarternary Science Reviews 24, 1989-2001.

Piromallo, C., Morelli, A., 2003. P wave tomography of the mantle under the Alpine-Mediterranean area. Journal of Geophysical Research 108(B2), 1-23.

Poirier, C., Sauriau, P.-G., Chaumillon, E., Allard J., 2009. Can molluscan assemblages give insights into Holocene environmental changes other than sea level rise? A case study from a macrotidal bay (Marennes-Oleron, France). Palaeogeography, Palaeoclimatology, Palaeoecology 280, 105-118.

Pomar, L., 1991. Reef geometries, erosion surfaces and high-frequency sea-level changes, upper Miocene reef complex, Mallorca, Spain. Sedimentology 38, 243-269.

Preller, R., 1986. A numerical model study of the Alboran Sea gyre. Progress in Oceanography 16, 113-146.

Pross, J., Kotthoff, U., Müller, U.C., Peyron, O., Dormoy, I., Schmiedl, G., Kalaitzidis, S., Smith, A.M., 2009. Massive perturbation in terrestrial ecosystems of the Eastern Mediterranean region associated with the 8.2 kyr B.P. climatic event. Geology 37, 887-890.

Pujol, C., Vergnaud Grazzini C., 1989. Palaeoceanography of the last deglaciation in the Alboran Sea (Western Mediterranean). Stable isotopes and planktonic foraminiferal records. Marine Micropaleontology 15, 153-179.

Pujol, A., Vergnaud-Grazzini C., 1995. Distribution patterns of live planktic foraminifera as related to regional hydrography and productive systems of the Mediterranean Sea. Marine Micropaleontology 25, 187-217.

Ramette, A., 2007. Multivariate analyses in microbial ecology. FEMS Microbiol. Ecol. 62, 142-160.

Rasmussen, T.L., 2005. Systematic paleontology and ecology of benthic foraminifera from the Plio-Pleistocene Kallithea Bay section, Rhodes, Greece. Cushman Foundation Special Publication 39, 53-157.

Rasmussen, T.L., Bäckström, D., Heinemeier, J., Klitgaard-Kristensen, D., Knutz, P.C., Kuijpers, A., Lassen, S., Thomsen, E., Troelstra, S.R., van Weering, T.C.E., 2002. The Faroer-Shetland Gateway: Late Quarternary water mass exchange between the Nordic Seas and the northeastern Atlantic. Marine Geology 188, 165-192.

Rathburn, A. E., Corliss B.H., 1994. The ecology of living (stained) deep-sea benthic foraminifera from the Sulu Sea. Paleoceanography 9, 87-150.

Reiss, Z., Halicz, E., Boaz, L., 2000. Late-Holocene foraminifera from the SE Levantine Basin. Isr. J. Earth Sci. 48, 1-27.

Reuss, A.E., 1865. Die Foraminiferen, Anthozoen und Bryozoen des deutschen Septarientons - Ein Beitrag zur Fauna der mitteloligozänen Tertiärschichten. Denkschr. Akad. Wiss. 25, 117-214.

Rixen, M., Beckers, J.-M., Levitus, S., Antonov, J., Boyer, T., Maillard, C., Fichaut, M., Balopoulos, E., Iona, S., Dooley, H., Garcia, M.-J., Manca, B., Giorgetti, A., Manzella, G., Mikhailov, N., Pinardi, N., Zavatarelli, M., and the Medar Consortium, 2005. The Western Mediterranean Deep Water: A proxy for climate change. Geophysical Research Letters 32(12), 1-9.

Robinson, A.R., Leslie, W.G., Theocharis, A., Lascaratos, A., 2001. Mediterranean Sea circulation. Encyclopedia of Ocean Science 3, 1689-1705.

Rohling, E.J., Hilgen, F.J., 1991. The eastern Mediterranean climate at times of sapropel formation: a review. Geologie en Mijnbouw 70, 253-264.

Rohling, E.J., De Rijk, S., 1999. Holocene climate optimum and Last Glacial Maximum in the Mediterranean: the marine oxygen isotope record. Marine Geology 153, 57-75.

Rohling, E.J., Cane, T.R., Cooke, S., Sprovieri, M., Bouloubassi, I., Emeis, K.-C., Schiebel, R., Kroon, D., Jorissen, F.J., Lorre, A., Kemp, A.E.S., 2002. African monsoon variability during the previous interglacial maximum. Earth and Planetary Science Letters 202, 61-75.

Rohling, E.J., Sprovieri, M., Cane, T., Casford, J.S.L., Cooke, S., Bouloubassi, I., Emeis, K.C., Schiebel, R., Rogerson, M., Hayes, A., Jorissen, F.J., Kroon, D., 2004. Reconstructing past planktic foraminiferal habitats using stable isotope data: a case history for Mediterranean sapropel S5. Marine Micropaleontology 50, 89-123.

Ros, J.D., Romero, J., Ballesteros, E., Gili, J.M., 1984. Diving in blue water. The benthos. In: Margalef R. (Ed.), Western Mediterranean, Pergamon Press, Oxford, pp. 233-295.

Rosipal, R., Krämer, N., 2006. Overview and recent advances in Partial Least Squares. Subspace, Latent Structure and Feature Selection, Lecture notes in computer science. Springer, Heidelberg-Berlin, pp. 34-51.

Rossignol-Strick, M., 1983. African monsoons, an immediate response to orbital insolation. Nature 304, 46-49.

Rossignol-Strick, M., 1995. Sea-land correlation of pollen records in the Eastern Mediterranean for the glacial-interglacial transition: biostratigraphy versus radiometric time-scale. Quarternary Science Reviews 14, 893-915.

Rossignol-Strick, M., 1999. The Holocene climate optimum and pollen records of sapropel 1 in the eastern Mediterranean, 9000-6000 BP. Quarternary Science Reviews 18, 515-530.

Rossignol-Strick, M., Nesteroff, Olive, P., Vergnaud-Grazzini, C., 1982. After the deluge: Mediterranean stagnation and sapropel formation. Nature 295, 105-110.

Romano, E., Bergamin, L., Finoia, M.G., Carboni, M.G., Ausili, A., Gabellini, M., 2008. Industrial pollution at Bagnoli (Naples, Italy): Benthic foraminifera as a tool in integrated programs of environmental characterisation. Marine Pollution Bulletin 56, 439-457.

Sabean, J.A.R., 2004. Application of foraminifera to detecting land level change associated with great earthquakes along the west coast of North America, Master Thesis, Simon Fraser University, Burnaby, British Columbia, 85 pp.

Sanz de Galdeano, C., 1990. Geologic evolution of the Betic Cordilleras in the Western Mediterranean, Miocene to the present. Tectonophysics 172, 107-119.

Saraswati, P.K., 2002. Growth and habitat of some recent miliolid foraminifera: Palaeoecological implications. Current Science 82(1), 81-84.

Saraswati, P.K., Shimoike, K., Iwao, K., Mitra, A., 2003. Distribution of larger foraminifera in the reef sediments of Akajima, Okinawa, Japan. Journal Geological Society of India 61, 16-21.

Sbaffi, L., Wezel, F.C., Kallel, N., Paterne, M., Cacho, I., Ziveri, P., Shackleton, N., 2001. Response of the pelagic environment to palaeoclimatic changes in the central Mediterranean Sea during the late Quarternary. Marine Geology 178, 39-62.

Sbaffi, L., Wezel, F.C., Curzi, G., Zoppi, U., 2004. Millenial- to centennial-scale palaeoclimatic variations during Termination I and Holocene in the central Mediterranean Sea. Global and Planetary Change 40, 201-217.

Schiebel, R., 1992. Rezente benthische Foraminiferen in Sedimenten des Schelfes und oberen Kontinentalhanges im Golf von Guinea (Westafrika). Berichte-Reports, Geol. Paläont. Inst. Universität Kiel 51, 1-126.

Schiebel, R., Waniek, J., Bork, M., Hemleben, C., 2001. Planktic foraminiferal porduction stimulated by chlorophyll redistribution and entrainment of nutrients. Deep-Sea Research I 48, 721-740.

Schilman, B., Almogi-Labin, A., Bar-Matthews, M., Labeyrie, L., Paterne, M., Luz, B., 2001. Long- and short-term carbon fluctuations in the Eastern Mediterranean during the late Holocene. Geology 29, 1099-1102.

Schönfeld, J., 2002. Recent benthic foraminiferal assemblages in deep high-energy environments from Gulf of Cadiz (Spain). Marine Micropaleontology 44, 141-162.

Schmiedl, G., Mackensen, A., Müller, P.J., 1997. Recent benthic foraminifera from the eastern South Atlantic Ocean: Dependence on food supply and water masses. Marine Micropaleontology 32, 249-287.

Schmiedl, G., de Bovée, F., Buscail, R., Charrière, B., Hemleben, C., Medernach, L., Picon, P., 2000. Trophic control of benthic foraminiferal abundance and microhabitat in the bathyal Gulf of Lions, western Mediterranean Sea. Marine Micropaleontology 40, 167-188.

Schmiedl, G., Pfeilstricker, M., Hemleben, C., Mackensen, A., 2004. Environmental and biological effects on the stable isotope composition of recent deep-sea benthic foraminifera from the western Mediterranean Sea. Marine Micropaleontology 51, 129-152.

Scott, G.A., Scourse, J.D., Austin, W.E.N., 2003. The distribution of benthic foraminifera in the Celtic Sea: the significance of seasonal stratification. Journal of Foraminiferal Research 33, 32-61.

Semeniuk, T.A., 2000. Spatial variability in epiphytic foraminifera from micro- to regional scale. Journal of Foraminiferal Research 30, 99-109.

Sen Gupta, B.K. (Ed.), 2003. Modern Foraminifera. Kluwer Academic Publishers, Dordrecht.

Sen Gupta, B.K., Machain-Castillo, M.L., 1993. Benthic foraminifera on oxygen-poor habitats. Marine Micropaleontology 20, 183-201.

Sgarrella, F., Moncharmont Zei, M., 1993. Benthic foraminifera in the Gulf of Naples (Italy): systematics and autoecology. Bollettino della Societa Paleontologica Italiana 32(2), 145-264.

Silva, K.A., Corliss, B.H., Rathburn, A.E., Thunell, R.C., 1995. Seasonality of living benthic foraminifera from the San Pedro Basin, California Borderland. Journal of Foraminiferal Research 26, 71-93.

Silva, P.G., Gonzalez Hernandez, F.M., Goy, J.L., Zazo, C., Carrasco, P., 2001. Paleo and historical seismicitiy in Mallorca (Baleares, Spain) - a preliminary approach. Acta Geologica Hispanica 36(3-4), 245-266.

Simboura, N., Zenetos, A., 2002. Benthic indicators to use in Ecological Quality classification of Mediterranean soft bottom marine ecosystems, including a new Biotic Index. Mediterranean Marine Science 3(2), 77-111.

Sivan, D., Wdowinski, S., Lambeck, K., Galili, E., Raban, A., 2001. Holocene sea-level changes along the Mediterranean coast of Israel, based on archaeological observations and numerical model. Palaeogeography, Palaeoclimatology, Palaeoecology 167, 101-117.

Spezzaferri, S., Tamburini, F., 2007. Paleodepth variations on the Eratosthenes Seamount (Eastern Mediterranean): sea-level changes or subsidence? eEarth Discussions 2, 115-132.

Sprovieri, R., Hasegawa, S., 1990. Plio-Pleistocene benthic foraminifer stratigraphic distribution in the deep-sea record of the Tyrrhenian Sea (OPD Leg 107), In: Kastens, K.A., Mascle, J. (Eds.), Proceedings of the Ocean Drilling Program, Scientific Results 107, 429-459.

Stocchi, P., Spada, G., 2007. Glacio- and hydro-isostasy in the Mediterranean Sea: Clark´s zones and role of remote ice sheets. Annals of Geophysics 50, 741-761.

Stuiver, M., Reimer, P. J., 1993. Extended ^{14}C database and revised CALIB radiocarbon calibration program. Radiocarbon 35, 215-230.

Sturrock, S., Murray, J.W., 1981. Comparison of low energy and high energy marine middle shelf foraminiferal faunas: Celtic Sea and western English Channel. In: Neale, J.W., Brasier, M.D. (Eds.), Microfossils from Recent and fossil shelf seas. Ellis Horwood, Chichester, pp. 251-260.

Taleb, Z.M., Benghali, S., Kaddour, A., Boutiba, Z., 2007. Monitoring the biological effects of pollution on the Algerian west coast using mussels Mytilus galloprovincialis. Oceanologia 49(4), 543-564.

Ter Braak, C.J.F., Juggins, S., 1993. Weighted averaging partial least squares regression (WA-PLS): an improved method for reconstructing environmental variables from species assemblages. Hydrobiologia 269/270, 485-502.

Ter Braak, C.J.F., Looman, C.W.N., 1986. Weighted averaging, logistic regression and the Gaussian response model. Vegetatio 65, 3-11.

Ter Braak, C.J.F., Smilauer, P., 2002. CANOCO Reference manual and CanoDraw for Windows User´s guide (version 4.5). Microcomputer power Ithaka, NY, USA.

Ter Braak, C.J.F., Juggins, S., Birks, H.J.B., Van der Voet, H., 1993. Weighted averaging least squares regression (WA-PLS): definition and comparison with other methods for species-environment calibration. In: Patil, G.P. Rao, C.R. (Eds.), Multivariate environmental statistics. Elsevier Science Publishers B.V. (North Holland), Amsterdam, pp. 525-560.

Thunell, R.C., 1979. Pliocene-Pleistocene paleotemperature and paleosalinity history of the Mediterranean Sea: Results from DSDP sites 125 and 132. Marine Micropalaeontology 4, 173-187.

Thunell, R., Williams, D.F., Belyea, P.R., 1984. Anoxic events in the Mediterranean Sea in relation to the evolution of late Neogene climates. Marine Geology 59, 105-134.

Tinti, S., Armigliato, A., Pagnoni, G., Zaniboni, F., 2005. Scenarios of giant tsunamis of tectonic origin in the Mediterranean. ISET Journal of Earthquake Technology 42(4), 171-188.

Tintore, J., La Violette, P.E., Blade, I., Cruzado, A., 1988. A study of an intense density from in the Eastern Alboran Sea: the Almeria-Oran Front. Journal of Physical Oceanography 18, 1384-1397.

Todd, R., 1958. Foraminifera from the Western Mediterranean deep-sea cores. Reports of the Swedish Deep-Sea Expedition, Sediment Cores from the Mediterranean Sea and the Red Sea 8(3), 167-215.

Tolderlund, D.S., Be, A.W.H., 1971. Seasonal distribution of planktonic foraminifera in the western North Atlantic, Micropaleontology 17, 297-329.

Traub, M., Fischer, H., de Reus, M., Kormann, R., Heland, J., Ziereis, H., Schlager, H., Holzinger, R., Williams, J., Warneke, C., de Gouw, J., Lelieveld, J., 2003. Chemical characteristics assigned to trajectory clusters during the MINOS campaign. Atmos. Chem. Phys. Discuss. 3, 107-134.

Van der Zwaan, G.J., Jorissen, F.J., de Stigter, H.C., 1990. The depth dependency of planktonic/benthic foraminiferal ratios: Constraints and applications. Marine Geology 95, 1-16.

Van der Zwaan, G.J., Duijnstee, I.A.P., den Dulk, M., Ernst, S.R., Jannink, N.T., Kouwenhoven, T.J., 1999. Benthic foraminifers: proxies or problems? A review of paleoecological concepts. Earth-Science Reviews 46, 213-236.

Van Hinsbergen, D.J.J., Kouwenhoven, T.J., Van der Zwaan, G.J., 2005. Paleobathymetry in the backstripping procedure: Correction for oxygenation effects on depth estimates. Palaeogeography, Palaeoclimatology, Palaeoecology 221, 245-265.

Vargas-Yanez, M., Plaza, F., Garcia-Lafuente, J., Sarhan, T., Vargas, J.M., Velez-Belchi, P., 2002. About the seasonal variability of the Alboran Sea circulation. Journal of Marine Systems 35, 229-248.

Velez-Belchi, P., Vargas-Yanez, M., Tintore, J., 2005. Observation of a western Alboran gyre migration event. Progress in Oceanography 66, 190-210.

Vergnaud Grazzini, C., Pierre, C., 1991. High fertility in the Alboran Sea since the Last Glacial Maximum. Paleoceanography 6, 519-536.

Vergnaud Grazzini, C., Pierre, C., 1992. The carbon isotope distribution in the deep $\sum CO_2$ and benthic foraminifers of the Alboran Basin, western Mediterranean: Implications for variations in primary production levels since the last deglaciation. Marine Micropaleontology 19, 147-161.

Vergnaud Grazzini, C., Ryan, W.B.F., Cita, M.B., 1977. Stable isotopic fractionation, climate change and episodic stagnation in the Eastern Mediterranean during the late Quarternary. Marine Micropaleontology 2, 353-370.

Vergnaud Grazzini, C., Devaux, M., Znaidi, J., 1986. Stable isotope "anomalies" in the Mediterranean Pleistocene records. Marine Micropaleontology 10, 35-69.

Vouvalidis, K.G., Syrides, G.E., Albanakis, K.S., 2005. Holocene morphology of the Thessaloniki Bay: impact of sea level rise. In: Fouache, E., Pavlopoulos, K. (Eds.), Sea Level Changes in Eastern Mediterranean during Holocene - Indicators and Human Impacts -. Gebrueder Bornträger, Berlin Stuttgart, pp. 147-158.

Watts, W.A., Allen, J.R.M., Huntley, B., Fritz, S.C., 1996. Vegetation history and climate if the last 15,000 years at Laghi di Monticchio, southern Italy. Quarternary Science Reviews 15, 113-132.

Weiner, S., 1975. The carbon isotopic composition of the Eastern Mediterranean planktonic foraminifera *Orbulina universa* and the phenotypes of *Globigerinoides ruber*. Palaeogeography, Palaeoclimatology, Palaeoecology 17, 149-156.

Weldeab, S., Siebel, W., Wehausen, R., Emeis, K.-C., Schmiedl, G., Hemleben, C., 2003. Late Pleistocene sedimentation in the Western Mediterranean Sea: implications for productivity changes and climatic conditions in the catchment areas. Palaeogeography, Palaeoclimatology, Palaeoecology 190, 121-137.

Werner, F.E., Vuidez, A., Tintore, J., 1993. An explanatory numerical study of the currents off the southern coast of Mallorca including the Cabrera Island complex. Journal of Marine Systems 4, 45-66.

Wilson, B., 2003. Foraminifera and paleodepths in a section of the early to middle Miocene Brasso Formation, central Trinidad. Carribean Journal of Science 39(2), 209-214.

Wisshak, M., Rueggeberg, A., 2006. Colonisation and bioerosion of experimental substrates by benthic foraminiferans from euphotic to aphotic depths (Kosterfjord, SW Sweden). Facies 52, 1-17.

Wollenburg, J., 1992. Zur Taxonomie von rezenten benthischen Foraminiferen aus dem Nansen Becken, Arktischer Ozean. Berichte zur Polarforschung 112, 137 p.

Wüst, G., 1960. Die Tiefenzirkulation des Mittelländischen Meeres. Deutsche Hydrographische Zeitschrift 13, 105-131.

Wüst, G., 1961. On the vertical circulation of the Mediterranean Sea. Journal of Geophysical Research 66(20), 3261-3271.

Yll, E.-I., Perez-Obiol, R., Pantaleon-Cano, J., Roure. J.M., 1997. Palynological evidence for climatic change and human activity during the Holocene on Minorca (Balearic Islands). Quarternary Research 48, 339-347.

Yokes, M.B., Meric, E., Avsar, N., 2007. On the presence of alien foraminifera *Amphistegina lobifera* Larsen on the coasts of the Maltese Islands. Aquatic Invasions 2(4), 439-441.

Appendix

Table A.1. Sample locations, sampling dates and water depths of the surface samples. Samples were taken with grab and box corer (BG, KG) and from core top of sediment cores drilled with vibro-corer (VC). Throughout chapter 3 and in the chapter 3 figures, sample numbers are given without the suffix for better readability.

Sample-No.	Location	Date	Latitude	Longitude	Depth [m]	Gear
326-1	Alboran Platform	16.08.2006	35°52.450´N	3°05.150´W	102	BG
327-1	Alboran Platform	16.08.2006	35°53.890´N	3°05.950´W	115	BG
328-1	Alboran Platform	16.08.2006	35°55.130´N	3°03.311´W	69	BG
329-1	Alboran Platform	16.08.2006	35°55.200´N	3°02.820´W	60	BG
330-1	Alboran Platform	16.08.2006	35°56.200´N	3°00.690´W	63	BG
331-1	Alboran Platform	16.08.2006	35°59.300´N	2°59.500´W	86	BG
332-2	Alboran Platform	16.08.2006	35°59.510´N	2°57.210´W	83	BG
333-1	Alboran Platform	16.08.2006	36°00,655´N	2°49,732´W	161	BG
334-1	Alboran Platform	16.08.2006	35°57.500´N	2°56.020´W	97	BG
335-1	Alboran Platform	16.08.2006	35°58.035´N	2°59.890´W	73	BG
336-1	Alboran Platform	16.08.2006	35°54.450´N	3°05.535´W	91	BG
341-2	Alboran Platform	17.08.2006	35°55.103´N	3°02.194´W	53	VC
342-1	Alboran Platform	17.08.2006	35°56.400´N	3°00.213´W	64	VC
343-2	Alboran Platform	17.08.2006	35°55.588´N	3°01.915´W	38	VC
351-1	Oran Bight	19.08.2006	35°48.490´N	0°34.000´W	70	BG
352-1	Oran Bight	19.08.2006	35°47.500´N	0°33.810´W	48	KG
353-1	Oran Bight	19.08.2006	35°47.230´N	0°37.650´W	73	BG
354-1	Oran Bight	19.08.2006	35°45.872´N	0°40.232´W	84	BG
355-1	Oran Bight	19.08.2006	35°50.696´N	0°35.306´W	127	BG
356-1	Oran Bight	19.08.2006	35°50.207´N	0°35.000´W	118	BG
357-1	Oran Bight	19.08.2006	35°51.204´N	0°33.092´W	100	BG
357-2	Oran Bight	19.08.2006	35°51.198´N	0°33.092´W	100	KG
358-1	Oran Bight	20.08.2006	35°50.802´N	0°32.700´W	85	BG
359-1	Oran Bight	20.08.2006	35°50.200´N	0°32.000´W	78	BG
360-1	Oran Bight	20.08.2006	35.49.890´N	0°31.600´W	83	BG
361-1	Oran Bight	20.08.2006	35°49.990´N	0°30.510´W	67	BG
362-1	Oran Bight	20.08.2006	35°50.895´N	0°29.496´W	20	KG
363-1	Oran Bight	20.08.2006	35°52.110´N	0°30.500´W	97	BG
364-1	Oran Bight	20.08.2006	35°52.900´N	0°30.800´W	121	BG
365-1	Oran Bight	20.08.2006	35°53.900´N	0°31.297´W	130	BG
373-1	Oran Bight	20.08.2006	35.49.664´N	0°34.673´W	90	BG
374-1	Oran Bight	20.08.2006	35°50.005´N	0°34.886´W	100	BG
375-1	Oran Bight	20.08.2006	35.51.105´N	0°35.526´W	115	BG
377-1	Mallorca Shelf	24.08.2006	39°18.879´N	2°47.827´E	47	BG
378-1	Mallorca Shelf	24.08.2006	39°21.192´N	2°47.810´E	40	BG
379-1	Mallorca Shelf	24.08.2006	39°19.601´N	2°46.208´E	48	BG
380-1	Mallorca Shelf	24.08.2006	39°18.098´N	2°44.702´E	56	BG
381-1	Mallorca Shelf	24.08.2006	39°17.005´N	2°43.300´E	67	BG
382-1	Mallorca Shelf	24.08.2006	39°16.101´N	2°42.196´E	74	BG
384-1	Mallorca Shelf	24.08.2006	39°18.095´N	2°49.013´E	61	BG
387-1	Mallorca Shelf	24.08.2006	39°15.503´N	2°41.498´E	80	BG
388-1	Mallorca Shelf	24.08.2006	39°15.214´N	2°41.089´E	94	BG
390-1	Mallorca Shelf	24.08.2006	39°14.830´N	2°40.532´E	116	BG
391-1	Mallorca Shelf	24.08.2006	39°13.610´N	2°39.090´E	163	BG
393-1	Mallorca Shelf	25.08.2006	39°10.601´N	2°40.398´E	235	KG
403-1	Mallorca Shelf	25.08.2006	39°14.798´N	2.45.524´E	94	BG
404-1	Mallorca Shelf	25.08.2006	39°13.970´N	2°44.496´E	105	BG

Table A.2. Summary of Principle Component Analysis (PCA) results for the Alboran Platform samples in Q-Mode. Explained variance (%) of each PC axis, and the dominant with the most important associated species and their scores are given.

Alboran Platform surface samples			
PC-axis	**Variance [%]**	**Species**	**Score**
1	56.8	***Cassidulina crassa***	3.44
		Globocassidulina subglobosa	2.96
		Gavelinopsis praegeri	1.65
		Cibicides lobatulus	1.11
2	16.8	***Asterigerinata mamilla* s.l.**	4.47
		Elphidium complanatum	1.91
		Cibicides lobatulus	1.59
3	8.4	***Elphidium complanatum***	3.28
		Cibicides refulgens	3.18
		Cibicides pseudoungerianus	1.36
4	7.7	***Cibicides pseudoungerianus***	4.71
		Cassidulina crassa	1.48
		Asterigerinata mamilla s.l.	1.26

Table A.3. Summary of Principle Component Analysis (PCA) results for the Oran Bight samples in Q-Mode. Explained variance (%) of each PC axis, and the dominant with the most important associated species and their scores are given.

Oran Bight surface samples			
PC-axis	**Variance [%]**	**Species**	**Score**
1	42.2	***Globocassidulina subglobulosa***	5.03
		Cassidulina crassa	2.03
		Spiroplectinella sagittula s.l.	1.42
		Cibicides pseudoungerianus	1.14
		Gavelinopsis praegeri	1.11
		Gaudryina siciliana	1.07
		Globocassidulina oblonga	1.03
2	15.1	***Cassidulina laevigata* s.l.**	5.59
		Globocassidulina oblonga	2.39
3	11.1	***Gaudryina rudis***	3.36
		Cibicides lobatulus	2.52
		Eponides concameratus	2.20
		Textularia pseudorugosa	2.14
		Cibicides pseudoungerianus	1.65
		Spiroplectinella sagittula s.l.	1.15
4	8.0	***Asterigerinata mamilla* s.l.**	5.26
		Rosalina macropora	1.89
		Discorbinella bertheloti	1.64
		Neoconorbina terquemi	1.13
5	5.8	***Cibicides lobatulus***	4.37
		Neoconorbina terquemi	2.31
		Cibicides pseudoungerianus	1.96
		Quinqueloculina seminula	1.90
		Elphidium crispum	1.40

Table A.4. Summary of Principle Component Analysis (PCA) results for the Mallorca Shelf samples in Q-Mode. Explained variance (%) of each PC axis, and the dominant with the most important associated species and their scores are given.

Mallorca Shelf surface samples			
PC-axis	**Variance [%]**	**Species**	**Score**
1	35.1	***Neoconorbina terquemi***	5.18
		Asterigerinata mamilla s.l.	3.71
		Cibicides lobatulus	1.45
2	25.9	***Cassidulina laevigata* s.l.**	5.72
		Bulimina elongata	2.10
		Hyalinea balthica	1.45
3	14.2	***Spiroplectinella sagittula* s.l.**	5.34
		Asterigerinata mamilla s.l.	1.66
		Cibicides lobatulus	1.54
		Globocassidulina oblonga	1.36
		Cassidulina laevigata s.l.	1.20
		Gaudryina rudis	1.13
4	7.9	***Gavelinopsis praegeri***	5.23
		Globocassidulina subglobulosa	1.91
		Cassidulina crassa	1.86
		Cibicides lobatulus	1.39
5	7.4	***Cibicides lobatulus***	4.62
		Textularia gramen	1.71
		Gaudryina rudis	1.38
		Neocornobina terquemi	1.09
		Textularia spp.	1.03
		Bigenerina nodosaria	1.02

Table A.5. Grain-size distribution of the surface samples and annual sea surface chlorophyll a, sea surface temperature and sea surface salinity data for the sample stations.

Sample-No.	Chloro-phyll a [mg/m^3]	Temp. [°C]	Sal. [psu]	>1000 µm [weight%]	500-1000 µm [weight%]	200-500 µm [weight%]	100-200 µm [weight%]	63-100 µm [weight%]	<63 µm [weight%]
326-1	0.35	20.0	36.297	25.08	22.77	42.24	7.92	0.66	1.32
327-1	0.35	20.0	36.231	31.49	22.28	26.16	12.31	2.22	5.54
328-1	0.36	19.9	36.411	55.41	17.53	16.75	7.22	1.29	1.80
329-1	0.36	19.6	36.346	47.68	21.75	25.39	4.38	0.20	0.61
330-1	0.37	20.3	36.512	28.83	21.94	29.59	12.24	1.79	5.61
331-1	0.38	20.2	36.552	29.09	20.91	30.60	14.87	1.51	3.02
332-2	0.39	20.4	36.390	37.46	22.54	17.37	6.67	2.54	13.43
333-1	0.39	20.9	36.457	50.76	31.97	14.25	0.62	0.18	2.23
334-1	0.39	20.2	36.444	34.42	25.89	32.10	5.27	0.19	2.13
335-1	0.38	20.0	36.513	40.65	22.58	20.65	11.61	2.58	1.94
336-1	0.35	20.0	36.556	58.33	12.08	14.37	9.66	2.05	3.50
341-2	0.36	20.8	36.584	44.26	14.21	15.30	9.84	4.37	12.02
342-1	0.37	20.2	36.599	48.18	20.00	22.73	4.09	0.45	4.55
343-2	0.37	20.5	36.690	29.05	30.91	30.17	3.72	0.56	5.59
351-1	0.33	24.6	36.811	12.44	22.10	35.67	17.30	2.97	9.53
352-1	0.35	24.4	36.826	x	x	x	x	x	x
353-1	0.35	24.2	36.820	59.97	19.87	10.47	1.65	0.36	7.68
354-1	0.37	24.4	36.823	32.84	27.98	26.76	4.86	1.85	5.71
355-1	0.30	22.3	36.778	16.28	13.69	36.13	13.28	4.97	15.65
356-1	0.31	24.5	36.844	16.83	14.36	21.00	18.05	8.58	21.18
357-2	0.30	23.1	36.753	31.68	27.23	19.30	5.51	2.43	13.86
357-1	0.30	23.3	36.778	31.68	27.23	19.30	5.51	2.43	13.86
358-1	0.30	24.4	36.843	42.01	27.79	20.59	3.29	0.44	5.88
359-1	0.31	24.3	36.830	30.01	36.54	22.42	3.98	0.55	6.49
360-1	0.32	24.3	36.844	17.17	22.90	24.43	10.63	4.86	20.01
361-1	0.32	24.2	36.838	3.46	1.08	51.05	35.83	0.85	7.72
362-1	x	24.2	36.862	x	x	x	x	x	x
363-1	0.29	24.2	36.820	15.52	16.60	46.55	10.19	1.92	9.23
364-1	0.29	23.6	36.789	35.74	26.13	18.07	5.73	0.93	13.40
365-1	0.29	21.7	36.695	47.29	24.68	12.66	0.99	0.63	13.74
373-1	0.31	24.2	36.809	35.27	30.10	16.70	6.82	2.59	8.52
374-1	0.31	24.5	36.824	24.77	28.03	23.82	7.96	4.50	10.92
375-1	0.30	24.4	36.813	37.59	28.39	21.56	4.03	1.51	6.92
377-1	0.19	25.4	37.377	36.48	30.90	26.47	2.90	0.74	2.50
378-1	0.21	25.8	37.376	38.62	39.83	16.58	1.53	0.41	3.03
379-1	0.19	25.6	37.328	43.71	28.42	12.13	2.60	1.76	11.37
380-1	0.18	25.6	37.367	32.80	37.67	16.95	3.77	1.99	6.82
381-1	0.18	25.7	37.317	10.78	16.07	25.05	14.27	8.67	25.17
382-1	0.17	25.7	37.281	15.90	29.32	29.84	10.23	4.43	10.29
384-1	0.19	25.8	37.359	8.57	9.11	11.09	28.76	23.44	19.03
387-1	0.17	26.0	37.273	29.10	28.91	19.38	6.12	3.22	13.26
388-1	0.17	26.3	37.273	15.55	25.77	30.66	9.95	3.82	14.25
390-1	0.17	26.1	37.301	3.92	7.46	27.47	10.53	4.97	45.65
391-1	0.16	25.6	37.297	0.38	1.89	19.90	11.84	9.57	56.42
393-1	0.16	25.3	37.290	x	x	x	x	x	x
403-1	0.17	25.8	x	0.34	0.91	6.25	16.06	16.20	60.25
404-1	0.17	25.6	x	0.33	2.49	12.47	10.17	10.47	64.07

Table A.6. Statistical results of Redundancy Analyses (RDAs) for all surface samples (excluding sample 362-1), and for all samples (excluding 362-1) with locations as binary "dummy variables", used as covariables.

RDA results							
	Axis 1	**Axis 2**	**Axis 3**	**Axis 4**	**captured variance (%)**	**F value**	**p value**
eigenvalues	0.193	0.161	0.039	0.023			
species-environment correlations	0.861	0.809	0.740	0.536			
cumulative percentage variance							
of species data	19.3	35.4	39.3	41.6			
of species-environment relation	45.5	83.6	92.7	98.0			
correlation							
temperature	-0.9345	0.2759	0.1255	0.1833	18.2	9.82	<0.0002
salinity	-0.6311	0.6160	0.2052	0.2112	14.1	7.24	<0.0002
chlorophyll a	0.6919	-0.2884	-0.6445	-0.0728	12.2	6.12	<0.0002
<63 µm	-0.5314	-0.2405	0.1171	-0.3398	6.9	3.25	<0.0034
>1000 µm	0.6838	0.2385	-0.1950	0.5994	11.0	5.42	<0.0002
water depth	-0.1846	-0.7359	0.3023	0.3155	10.1	4.92	<0.0002
RDA results with binary "dummy variables" for Oran, Alboran and Mallorca as covariables							
	Axis 1	**Axis 2**	**Axis 3**	**Axis 4**	**captured variance (%)**	**F value**	**p value**
eigenvalues	0.141	0.042	0.011	0.009			
species-environment correlations	0.778	0.619	0.595	0.553			
cumulative percentage variance							
of species data	19.0	24.7	26.2	27.4			
of species-environment relation	67.1	87.2	92.4	96.7			
correlation							
water depth	0.8071	-0.2602	0.1625	0.0757	12.9	6.25	<0.0002
salinity	-0.7063	-0.1551	-0.0939	0.0479	9.9	4.62	<0.0002
>1000 µm	-0.4778	-0.6811	0.3586	-0.3236	7.3	3.33	<0.0058
chlorophyll a	-0.5153	0.4498	0.6924	-0.0721	6.9	3.13	<0.0058
<63 µm	0.4628	0.3682	-0.4030	-0.4219	5.4	2.39	<0.0276
temperature	-0.2025	0.4289	0.2573	-0.6046	2.5	1.10	<0.3348

Table A.7. Summary of the Principle Component Analysis (PCA) results for cores 342-1, 367-1 and 401-1. The explained variance (in %) of each PC axis, the dominant and the most important associated species with their scores are given.

Core 342-1 (Alboran Platform)			
PC Axis	Variance [%]	Species	Score
1	37.8	***Asterigerinata mamilla***	5.894
		Elphidium complanatum	5.732
		Spirillina vivipara	2.389
		Brizalina difformis	1.372
2	33.7	***Cibicides lobatulus***	7.448
		Elphidium sp.1	4.296
		Elphidium complanatum forma *tyrrhenianum*	1.883
		Elphidium aculeatum	1.243
3	14.0	***Cibicides pseudoungerianus***	6.409
		Globocassidulina subglobulosa	2.724
		Cassidulina crassa	2.434
		Cibicides lobatulus	2.331
Core 367-1 (Oran Bight)			
PC Axis	Variance [%]	Species	Score
1	50.9	***Asterigerinata mamilla***	4.740
		Cibicides lobatulus	3.895
		Quinqueloculina stelligera	1.944
		Rosalina macropora	1.792
2	44.9	***Asterigerinata mamilla***	5.085
		Globocassidulina subglobulosa	2.874
		Discorbinella bertheloti	2.826
		Elphidium complanatum	2.096
Core 401-1 (Mallorca Shelf)			
PC Axis	Variance [%]	Species	Score
1	33.6	***Neoconorbina terquemi***	9.783
		Tretomphalus sp.1	2.406
2	34.1	***Tretomphalus concinnus***	7.798
		Sigmoilinita costata	2.564
		Rosalina sp.2	2.412
		Quinqueloculina stelligera	2.369
3	17.5	***Cassidulina laevigata***	9.227
		Tretomphalus sp.1	2.374
		Reussella spinulosa	1.642
		Spirillina vivipara	1.033

Table A.8. Summary of the statistical results of Weighted Averaging (WA), Partial Least Squares (PLS), WA-PLS, and Modern Analog Technique (MAT) for the Alboran Platform training data set. Shown are the root mean squared error (RMSE), the coefficient of determination (R^2), the average and maximum bias (aver. bias, max. bias), the cross validated (leave on out jack knifing) coefficient of determination (R^2_{jack}), average and maximum bias (aver. $bias_{jack}$, max. $bias_{jack}$) and the root mean squared error of prediction (RMSEP) for WA, PLS and WA-PLS, and the bootstrapped coefficient of determination (R^2_{boot}), average and maximum bias (aver. $bias_{boot}$, max. $bias_{boot}$) and the root mean squared error of prediction (RMSEP) for MAT. The selected transfer function models for core 342-1 are marked in bold.

core 342-1 (Alboran Platform)		**RMSE**	**R^2**	**Average Bias**	**Max. Bias**	**R^2_{jack}**	**Average $Bias_{jack}$**	**Max. $Bias_{jack}$**	**RMSEP**
WA	inverse	**11.116**	**0.784**	**7.93E-15**	**20.576**	**0.702**	**-0.110**	**25.468**	**13.119**
	classical	12.551	0.784	1.09E-13	14.366	0.710	-0.063	20.180	13.492
PLS	Component 1	12.233	0.739	3.97E-15	21.489	0.665	-0.430	24.964	13.876
	Component 2	**9.905**	**0.829**	**5.78E-15**	**16.682**	**0.648**	**-0.419**	**24.540**	**14.308**
	Component 3	8.056	0.887	6.28E-15	12.923	0.625	-0.361	24.868	15.008
	Component 4	6.285	0.931	1.44E-14	7.736	0.625	-0.213	25.395	15.160
	Component 5	5.013	0.956	1.32E-14	5.212	0.619	-0.502	25.579	15.398
	Component 6	4.515	0.964	1.24E-14	4.370	0.608	-0.167	24.853	15.798
WA-PLS	Component 1	11.118	0.784	0.134	20.922	0.701	0.026	25.797	13.166
	Component 2	**8.273**	**0.881**	**0.075**	**15.037**	**0.751**	**-0.057**	**23.740**	**11.959**
	Component 3	6.693	0.922	0.306	11.155	0.738	0.140	23.068	12.276
	Component 4	5.427	0.949	0.116	4.850	0.692	0.301	20.271	13.590
	Component 5	4.245	0.969	-0.006	4.120	0.660	0.463	19.786	14.509
	Component 6	3.826	0.974	-0.015	3.302	0.643	0.310	18.072	15.055
		RMSE	**R^2**	**Average Bias**	**Max. Bias**	**R^2_{boot}**	**Aver. $Bias_{boot}$**	**Max. $Bias_{boot}$**	**RMSEP**
MAT	average depth	**14.475**	**0.674**	**-4.640**	**25.083**	**0.736**	**-4.770**	**22.839**	**15.549**
	weighted average depth	14.432	0.676	-4.612	25.024	0.728	-4.959	23.160	15.864

Table A.9. Summary of the statistical results of Weighted Averaging (WA), Partial Least Squares (PLS), WA-PLS, and Modern Analog Technique (MAT) for the Oran Bight training data set. Shown are the root mean squared error (RMSE), the coefficient of determination (R^2), the average and maximum bias (aver. bias, max. bias), the cross validated (leave on out jack knifing) coefficient of determination (R^2_{jack}), average and maximum bias (aver. $bias_{jack}$, max. $bias_{jack}$) and the root mean squared error of prediction (RMSEP) for WA, PLS and WA-PLS, and the bootstrapped coefficient of determination (R^2_{boot}), average and maximum bias (aver. $bias_{boot}$, max. $bias_{boot}$) and the root mean squared error of prediction (RMSEP) for MAT. The selected transfer function models for core 367-1 are marked in bold.

core 367-1 (Oran Bight)		**RMSE**	**R^2**	**Average Bias**	**Max. Bias**	**R^2_{jack}**	**Average $Bias_{jack}$**	**Max. $Bias_{jack}$**	**RMSEP**
WA	inverse	**10.742**	**0.799**	**-2.06E-13**	**20.220**	**0.729**	**-0.228**	**24.703**	**12.511**
	classical	12.020	0.799	-2.12E-13	14.434	0.737	-0.180	19.696	12.878
PLS	Component 1	**11.324**	**0.776**	**4.96E-15**	**18.402**	**0.715**	**-0.277**	**22.202**	**12.812**
	Component 2	9.351	0.847	4.96E-15	14.055	0.718	-0.276	20.296	12.745
	Component 3	7.361	0.905	3.64E-15	9.834	0.719	-0.369	20.606	12.847
	Component 4	5.851	0.940	6.44E-15	7.370	0.739	-0.159	18.955	12.426
	Component 5	4.798	0.960	1.17E-14	7.278	0.763	-0.261	19.742	11.846
	Component 6	3.916	0.973	1.24E-14	6.407	0.774	-0.510	16.412	11.590
WA-PLS	Component 1	10.744	0.799	0.061	20.485	0.727	-0.166	24.998	12.567
	Component 2	**7.264**	**0.908**	**-0.115**	**11.020**	**0.798**	**-0.229**	**19.693**	**10.760**
	Component 3	5.644	0.944	-0.124	6.857	0.783	-0.980	17.477	11.197
	Component 4	4.275	0.968	-0.032	7.155	0.785	-0.467	14.429	11.210
	Component 5	3.788	0.975	-0.081	5.476	0.772	-0.779	14.242	11.603
	Component 6	3.338	0.981	-0.024	4.249	0.762	-0.767	15.089	11.953
		RMSE	**R^2**	**Average Bias**	**Max. Bias**	**R^2_{boot}**	**Average $Bias_{boot}$**	**Max. $Bias_{boot}$**	**RMSEP**
MAT	average depth	**14.210**	**0.697**	**-5.310**	**18.444**	**0.704**	**-4.601**	**20.247**	**16.449**
	weighted average depth	14.165	0.699	-5.294	18.328	0.688	-4.587	21.490	16.875

Table A.10. Summary of the statistical results of Weighted Averaging (WA), Partial Least Squares (PLS), WA-PLS, and Modern Analog Technique (MAT) for the Mallorca Shelf training data set. Shown are the root mean squared error (RMSE), the coefficient of determination (R^2), the average and maximum bias (aver. bias, max. bias), the cross validated (leave on out jack knifing) coefficient of determination (R^2_{jack}), average and maximum bias (aver. $bias_{jack}$, max. $bias_{jack}$) and the root mean squared error of prediction (RMSEP) for WA, PLS and WA-PLS, and the bootstrapped coefficient of determination (R^2_{boot}), average and maximum bias (aver. $bias_{boot}$, max. $bias_{boot}$) and the root mean squared error of prediction (RMSEP) for MAT. The selected transfer function models for core 401-1 are marked in bold.

core 401-1 (Mallorca Shelf)		**RMSE**	**R^2**	**Average Bias**	**Max. Bias**	**R^2_{jack}**	**Aver. $Bias_{jack}$**	**Max. $Bias_{jack}$**	**RMSEP**
WA	inverse	**11.003**	**0.789**	**6.74E-14**	**19.918**	**0.724**	**-0.257**	**24.066**	**12.633**
	classical	12.390	0.789	1.28E-13	16.150	0.731	-0.180	18.738	13.055
PLS	Component 1	11.922	0.752	6.61E-15	19.570	0.691	-0.206	23.068	13.337
	Component 2	**10.291**	**0.815**	**6.11E-15**	**17.295**	**0.718**	**-0.241**	**22.238**	**12.724**
	Component 3	7.799	0.894	6.44E-15	10.652	0.697	-0.387	19.713	13.394
	Component 4	6.280	0.931	7.44E-15	6.437	0.700	0.101	18.112	13.461
	Component 5	5.247	0.952	7.27E-15	6.332	0.695	0.148	21.120	13.728
	Component 6	3.837	0.974	8.43E-15	4.345	0.695	0.002	18.819	13.948
WA-PLS	Component 1	11.025	0.789	0.545	20.942	0.723	0.299	25.026	12.690
	Component 2	8.213	0.882	-0.188	15.895	0.803	-0.304	22.640	10.704
	Component 3	**6.110**	**0.935**	**0.064**	**9.168**	**0.830**	**-0.093**	**19.265**	**9.887**
	Component 4	4.593	0.963	0.076	3.882	0.815	0.047	16.539	10.309
	Component 5	3.799	0.975	-0.032	3.283	0.797	-0.006	15.833	10.884
	Component 6	3.208	0.982	0.092	3.464	0.780	0.082	16.952	11.405
		RMSE	**R^2**	**Average Bias**	**Max. Bias**	**R^2_{boot}**	**Average $Bias_{boot}$**	**Max. $Bias_{boot}$**	**RMSEP**
MAT	average depth	**15.660**	**0.619**	**-5.186**	**25.778**	**0.670**	**-4.952**	**24.444**	**17.104**
	weighted average depth	15.585	0.623	-5.182	25.482	0.650	-4.905	25.929	17.576

Table. A.11.: Estimated water depths (EWD) using Weighted Averaging (WA), Partial Least Square (PLS), WA-PLS, Modern Analog Technique (MAT), P/B and P/B_{mod} transfer functions for core 342-1 (Alboran Platform) versus core depth and age (C* van der Zwaan et al. (1990) transfer function).

core depth corr. [cm]	Age cal. ^{14}C years BP	EWD WA	EWD WAPLS	EWD PLS	EWD MAT	EWD P/B (transf. function A)	EWD P/B_{mod} (transf. function B)	EWD P/B_{mod} transfer funct. C*
1.0	0	76.36	73.20	63.78	70.34	71.74	76.75	229.51
5.5	89	79.08	73.47	69.79	76.45	65.33	73.06	198.22
10.5	200	76.82	72.92	76.75	78.78	61.76	72.78	195.95
15.5	555	77.54	74.29	80.44	77.07	67.35	74.06	206.45
22.5	2043	67.65	62.42	60.54	69.70	73.31	77.46	235.88
25.5	2277	70.74	71.66	71.84	70.52	75.81	77.29	234.33
30.5	2668	68.34	65.70	67.23	70.52	76.04	78.09	241.64
35.5	3058	69.54	65.43	55.81	65.36	67.78	74.33	208.61
42.5	3537	69.80	68.38	60.36	69.43	66.35	73.53	202.03
45.5	3669	63.90	60.60	56.15	60.02	63.86	72.92	197.13
50.5	3890	70.22	70.66	61.20	65.24	59.00	71.33	184.61
55.5	4111	70.49	65.79	60.02	64.21	54.44	68.33	162.48
60.5	4332	68.51	66.22	64.70	69.80	66.54	74.31	208.45
65.5	4552	73.74	69.69	71.61	72.02	55.35	68.82	166.00
70.5	4773	64.65	61.63	62.07	65.32	56.22	69.59	171.54
75.5	4994	69.06	67.37	60.88	65.74	53.60	68.23	161.79
80.5	5215	67.87	64.75	70.38	79.88	52.51	67.22	154.78
85.5	5435	59.31	52.85	57.22	54.87	50.08	66.36	148.99
90.5	5656	48.46	47.35	52.53	54.91	48.00	65.56	143.67
96.5	6230	62.78	55.07	60.24	55.30	54.12	68.22	161.72
102.5	6495	69.30	66.35	64.39	64.73	49.95	66.58	150.47
107.5	6716	62.86	55.99	63.61	58.05	57.59	71.25	183.97
111.5	6893	67.77	68.35	73.86	70.79	38.50	60.29	112.02
117.5	7157	65.42	58.12	57.12	64.36	40.10	60.20	111.55
122.5	7378	66.71	67.37	64.31	61.08	41.24	61.64	119.65
127.5	7599	56.90	45.23	48.50	57.20	47.35	65.14	141.00
132.5	7820	63.02	58.41	49.97	59.01	38.79	59.58	108.14
137.5	8041	61.67	54.96	49.74	56.81	42.92	62.05	122.04
142.5	8261	65.96	56.35	54.99	55.78	51.42	67.38	155.90
147.5	8482	65.22	60.12	53.99	55.95	51.41	66.60	150.58
152.5	8703	55.74	43.86	54.10	55.01	45.74	62.95	127.37
157.5	8924	55.78	45.57	58.16	56.07	48.82	65.17	141.18
162.5	9144	49.11	41.21	57.06	59.84	43.54	62.12	122.45
167.5	9365	48.05	36.28	57.46	54.69	47.92	64.05	134.07
172.5	9586	57.28	50.82	54.73	53.88	41.95	61.50	118.85
177.5	9723	52.78	36.09	48.27	54.61	37.84	58.80	104.01
182.5	9860	50.49	40.42	59.73	56.15	34.20	56.45	92.14
187.5	9998	49.42	38.87	61.99	59.08	32.53	56.98	94.73
196.5	10190	53.76	41.19	54.11	54.69	49.35	64.97	139.88
198.5	10245	55.61	44.46	52.98	54.95	41.48	61.08	116.46
203.5	10382	45.35	25.45	48.26	53.82	32.25	54.96	85.08
208.5	10519	41.54	29.73	63.52	54.80	34.25	56.10	90.44
213.5	10624	46.85	33.69	57.64	54.38	29.87	53.47	78.42
218.5	10716	38.35	23.69	62.13	55.15	21.92	47.28	54.42
223.5	10807	38.47	25.27	65.62	56.39	20.76	46.25	50.96

core depth corr. [cm]	Age cal. ^{14}C years BP	EWD WA	EWD WAPLS	EWD PLS	EWD MAT	EWD P/B (transf. function A)	EWD P/B_{mod} (transf. function B)	EWD P/B_{mod} transfer funct. C*
228.5	10899	44.39	35.27	69.40	63.15	18.34	44.10	44.23
233.5	10990	51.92	44.97	65.54	64.41	18.54	44.29	44.81
238.5	11082	38.70	23.99	65.33	62.35	18.03	43.80	43.35
243.5	11173	50.07	42.72	61.51	65.96	22.32	47.57	55.40
248.5	11265	41.08	36.26	71.67	62.75	17.81	43.58	42.72
253.5	11356	39.08	30.23	66.67	56.95	18.24	44.00	43.94
258.5	11448	43.12	25.12	62.63	52.29	17.45	43.21	41.64
278.5	11540	30.46	11.38	70.04	58.04	15.85	41.67	37.40
299.5	11631	35.88	17.43	66.60	55.33	16.38	42.22	38.87
319.5	11723	24.56	8.99	67.69	53.70	16.61	42.43	39.45
339.5	11814	32.83	21.79	62.49	54.88	15.89	41.71	37.51
359.5	11906	35.21	27.43	64.94	53.69	16.46	42.29	39.06
379.5	11997	41.02	28.24	75.96	76.77	15.70	41.52	37.00
399.5	12089	39.63	33.26	64.72	55.60	15.80	41.63	37.28
414.5	12180	37.78	24.59	69.66	56.96	15.92	41.75	37.61
434.5	12272	38.15	25.32	58.52	53.64	16.07	41.90	38.01
454.5	12364	37.55	21.65	59.93	56.99	15.98	41.81	37.76
469.5	12463	37.80	28.67	67.66	55.94	17.11	42.93	40.85

Table A.11 continued

Table A.12. Estimated water depths (EWD) using Weighted Averaging (WA), Partial Least Square (PLS), WA-PLS Modern Analog Technique (MAT) and P/B and P/B_{mod} transfer functions for core 367-1 (Oran Bight) versus core depth and age (C* van der Zwaan et al. (1990) transfer function).

core depth corr. [cm]	Age cal. ^{14}C years BP	EWD WA	EWD PLS	EWD WA-PLS	EWD MAT	EWD P/B (transf. function A)	EWD P/B_{mod} (transf. function B)	EWD P/B_{mod} transfer funct. C*
1.0	0	76.37	69.34	61.64	70.16	79.36	95.34	199.77
7.5	219	74.44	69.99	62.37	61.04	71.41	84.13	168.06
10.5	285	70.53	66.26	55.77	61.06	65.66	77.79	150.82
15.5	394	71.23	65.30	56.75	63.19	65.34	77.57	150.26
20.5	503	77.35	74.44	61.23	82.36	67.12	80.15	157.18
25.5	613	69.95	62.40	52.28	58.97	72.69	86.60	174.94
30.5	722	65.17	63.25	57.57	58.98	70.85	83.81	167.18
35.5	831	74.32	64.77	62.31	63.17	67.32	80.08	157.00
40.5	941	71.05	66.24	61.16	64.24	70.30	83.95	167.56
45.5	1050	75.17	68.05	61.66	60.92	76.11	91.37	188.38
50.5	1159	68.83	61.46	55.58	57.82	75.81	90.18	184.99
55.5	1269	70.43	62.18	57.89	57.79	70.53	82.62	163.91
60.5	1378	68.80	59.48	57.26	54.33	64.28	74.60	142.36
65.5	1488	71.16	62.77	59.80	62.89	68.32	81.77	161.61
70.5	1597	63.06	57.99	49.21	56.42	64.56	74.81	142.92
75.5	1706	63.70	61.37	47.84	54.45	62.63	72.61	137.13
80.5	1816	62.21	58.27	49.91	56.14	71.93	85.79	172.67
85.5	1925	71.61	61.55	57.96	61.98	70.91	85.13	170.85
90.5	2034	70.09	60.84	57.34	55.90	67.13	79.40	155.16
95.5	2144	63.19	55.65	51.36	56.74	51.41	59.06	103.11
100.5	2253	63.27	59.31	55.28	60.22	56.32	64.59	116.67
105.5	2362	68.42	59.90	53.37	56.68	54.41	61.96	110.15
110.5	2472	62.46	58.75	55.57	57.59	49.71	56.59	97.19
115.5	2581	59.35	53.79	47.60	55.54	50.60	57.20	98.64
120.5	2690	59.37	54.85	48.56	57.33	52.51	59.78	104.85
125.5	2800	62.75	56.32	49.69	56.17	52.43	60.41	106.38
130.5	2909	58.29	50.24	46.11	53.26	46.70	51.95	86.37
135.5	3018	58.98	54.95	45.39	51.71	50.89	57.10	98.40
140.5	3128	57.27	57.43	42.44	52.56	51.93	58.52	101.80
145.5	3237	50.47	47.19	34.80	51.99	46.18	50.89	83.94
150.5	3346	56.12	46.45	43.83	55.09	46.66	51.72	85.84
155.5	3456	57.29	51.49	44.02	53.27	49.25	54.74	92.84
160.5	3565	57.03	52.87	47.69	56.68	53.31	60.77	107.25
165.5	3674	57.01	51.58	42.45	54.30	47.66	52.71	88.12
170.5	3784	55.28	52.82	38.86	53.40	48.87	55.06	93.59
175.5	3893	56.93	51.91	46.76	53.37	45.46	50.47	82.99
180.5	4002	52.06	48.44	40.36	53.24	54.02	61.75	109.64
185.5	4112	59.94	54.21	46.82	55.10	49.25	55.10	93.68
190.5	4221	48.52	48.15	36.64	52.13	52.09	58.16	100.94
195.5	4330	56.57	55.00	46.03	54.99	51.78	59.25	103.57
199.5	4418	59.30	50.90	43.80	55.92	52.99	60.00	105.37

core depth corr. [cm]	Age cal. ^{14}C years BP	EWD WA	EWD PLS	EWD WA-PLS	EWD MAT	EWD P/B (transf. function A)	EWD P/B_{mod} (transf. function B)	EWD P/B_{mod} transfer funct. C*
200.5	4440	51.48	52.45	40.98	52.89	46.26	51.30	84.89
205.5	4549	51.13	48.41	42.55	51.38	51.92	57.76	99.98
210.5	4658	57.25	48.59	48.86	52.70	48.68	54.33	91.88
215.5	4768	56.93	46.31	44.99	52.85	47.17	52.71	88.11
220.5	4877	57.60	56.77	46.01	55.03	44.58	49.43	80.63
225.5	4986	54.99	52.17	44.88	53.71	52.81	59.17	103.37
230.5	5096	53.16	49.89	42.22	55.68	44.90	49.50	80.79
235.5	5205	49.32	48.94	38.14	51.82	46.86	52.26	87.07
240.5	5314	42.08	51.07	31.97	51.59	41.36	44.88	70.57
245.5	5424	47.70	51.46	41.50	54.17	40.20	43.36	67.29
250.5	5533	43.52	47.50	33.51	49.36	38.51	41.58	63.50
255.5	5642	48.26	49.92	41.33	53.26	38.97	42.20	64.81
260.5	5752	46.34	45.15	37.04	53.39	42.50	46.55	74.21
265.5	5861	45.09	54.12	29.06	51.48	38.57	41.34	62.99
270.5	5970	47.59	50.66	35.02	52.39	39.85	43.14	66.81
275.5	6080	48.26	51.03	37.32	45.34	36.62	38.96	58.04
280.5	6189	45.45	53.05	37.82	48.67	39.39	42.75	65.97

Table A.12 continued

Table A.13.: Estimated water depths (EWD) using Weighted Averaging (WA), Partial Least Square (PLS), WA-PLS Modern Analog Technique (MAT) and P/B and P/B_{mod} transfer functions for core 401-1 (Mallorca Shelf) versus core depth and age (C* van der Zwaan et al. (1990) transfer function).

core depth corr. [cm]	Age cal. ^{14}C years BP	EWD WA	EWD WAPLS	EWD PLS	EWD MAT	EWD P/B (transf. function A)	EWD P/B_{mod} (transf. function B)	EWD P/B_{mod} transfer funct. C*
0.5	0	59.05	58.47	46.36	59.34	61.05	61.54	65.39
5.5	136	62.01	64.82	55.24	61.78	65.61	68.34	71.73
10.5	272	64.78	62.23	48.65	59.33	59.24	61.29	63.11
15.5	402	65.94	67.38	60.99	60.48	65.98	65.60	66.50
20.5	532	61.82	62.38	52.28	61.23	60.17	60.56	64.44
25.5	662	63.25	60.42	51.05	61.52	60.28	60.09	65.16
30.5	792	64.00	61.36	50.73	61.31	58.10	57.72	62.53
35.5	922	67.87	62.55	61.16	60.69	68.83	67.45	72.24
40.5	1052	69.62	63.30	59.42	61.45	54.68	55.78	59.54
45.5	1182	62.60	60.80	53.52	59.15	54.76	55.53	59.86
50.5	1312	63.36	58.97	56.39	61.47	60.73	59.75	65.34
55.5	1442	65.76	62.65	58.90	61.04	55.81	61.52	60.45
60.5	1572	66.26	65.73	57.48	60.37	56.55	61.01	61.93
65.5	1703	58.51	51.53	48.94	60.95	61.13	60.97	65.28
70.5	1833	65.13	61.36	58.81	62.55	56.14	57.18	61.16
75.5	1963	62.34	56.44	61.61	66.72	57.91	58.64	63.65
80.5	2093	63.00	52.20	57.93	63.75	65.06	68.83	72.42
85.5	2223	71.36	66.44	70.15	85.41	59.05	63.50	65.30
90.5	2353	68.07	57.87	72.44	89.66	69.41	75.31	78.35
91.5	2483	70.10	68.54	61.12	66.15	64.71	64.29	71.11
96.5	2613	74.85	71.64	71.41	80.73	71.16	69.88	80.71
101.5	2743	73.63	67.41	67.70	70.11	73.86	75.65	81.67
106.5	2873	73.72	67.99	67.86	67.62	56.93	58.05	64.00
111.5	3004	80.16	70.16	71.35	85.48	73.23	73.88	83.06
116.5	3223	76.70	66.09	71.38	87.84	66.85	66.12	77.83
121.5	3443	75.11	67.66	68.37	75.46	64.61	64.57	73.38
126.5	3663	78.39	73.47	74.10	99.80	74.88	75.96	88.98
131.5	3883	70.13	63.55	67.88	77.04	58.51	61.36	67.01
136.5	4103	78.44	74.44	73.16	83.47	73.21	71.74	72.58
141.5	4323	70.77	59.05	67.54	69.74	65.79	65.89	73.40
146.5	4543	79.36	66.86	73.92	90.36	83.70	84.53	94.73
151.5	4763	79.47	68.01	73.45	91.31	84.17	79.94	94.82
156.5	5031	77.83	64.69	74.93	93.70	69.88	70.74	79.36
161.5	5300	78.56	71.15	72.89	89.01	70.72	68.25	79.94
166.5	5568	72.84	66.32	71.79	104.87	68.58	74.95	77.35
171.5	5837	66.92	52.59	60.59	62.79	65.69	66.03	70.34
176.5	6105	68.86	59.93	63.46	64.79	52.67	54.95	58.99
181.5	6374	62.80	47.71	63.02	67.14	52.89	54.10	58.28
186.5	6642	56.43	42.06	57.08	58.14	53.36	54.20	58.00
191.5	6911	68.18	60.42	60.72	61.22	58.68	60.02	63.93
196.5	7179	68.82	53.86	59.09	63.73	50.95	52.35	56.47
201.5	7447	63.33	50.89	56.14	59.62	46.49	48.37	51.21
206.5	7716	56.68	44.29	52.27	56.69	50.49	51.86	55.14
211.5	7984	51.74	40.57	51.88	52.63	47.58	49.95	51.62

core depth corr. [cm]	Age cal. ^{14}C years BP	EWD WA	EWD WAPLS	EWD PLS	EWD MAT	EWD P/B (transf. function A)	EWD P/B_{mod} (transf. function B)	EWD P/B_{mod} transfer funct. C*
216.5	8253	57.71	42.65	53.42	57.36	51.44	52.46	56.39
221.5	8521	57.26	43.89	54.30	57.52	46.51	47.91	50.62
226.5	8790	61.35	47.88	55.37	57.87	47.90	49.70	52.38
231.5	9058	54.24	43.11	51.59	56.81	46.07	47.62	50.21
236.5	9117	54.07	45.67	54.33	56.70	41.31	44.07	45.86
241.5	9177	52.66	36.31	57.88	57.89	41.75	43.24	46.30
246.5	9236	56.95	44.21	50.68	57.37	47.23	48.54	51.09
251.5	9295	47.34	38.93	55.21	55.91	46.75	48.16	50.68
256.5	9355	54.86	40.19	59.89	54.62	46.75	47.85	50.87
261.5	9414	54.23	31.00	55.93	56.72	43.16	44.35	47.42
266.5	9473	53.11	43.43	60.92	56.94	42.42	44.67	46.66
271.5	9532	56.23	34.90	54.18	56.68	38.95	40.67	42.95
276.5	9592	53.14	37.91	54.31	55.89	39.88	41.90	44.13
281.5	9651	47.94	30.86	52.61	56.33	44.31	45.40	53.66
286.5	9710	45.68	32.24	54.46	55.54	41.15	42.89	45.38
291.5	9770	41.33	24.69	48.71	52.85	41.41	42.67	45.37
296.5	9829	45.16	20.78	58.51	56.32	39.41	41.07	43.55
301.5	9888	48.16	26.81	59.38	55.96	42.62	44.11	46.59
306.5	9948	46.10	31.62	54.65	56.67	40.17	41.90	44.26
311.5	10007	43.04	19.41	54.90	51.94	41.71	42.84	45.64
316.5	10066	41.19	22.39	55.14	49.47	41.27	42.28	44.99
321.5	10125	47.92	28.61	46.03	54.86	40.13	41.89	44.33
326.5	10185	37.69	11.61	54.64	55.20	39.31	41.43	43.78
331.5	10244	42.14	18.78	48.65	53.69	44.41	45.25	47.92
336.5	10286	41.98	22.43	52.79	52.82	42.27	43.16	46.09
341.5	10329	35.24	16.12	56.19	51.52	40.51	42.71	44.34
346.5	10371	45.78	36.59	55.04	53.54	42.83	44.87	46.63
351.5	10414	38.35	12.44	53.43	54.19	40.27	45.92	44.11
356.5	10456	40.34	7.13	48.19	48.34	39.69	41.43	43.86
361.5	10498	44.86	23.66	53.96	53.33	39.79	40.98	43.84
366.5	10541	37.31	18.57	43.23	50.50	41.64	42.82	45.54
371.5	10583	45.54	25.90	43.34	53.65	40.68	42.67	44.69
376.5	10625	33.70	16.17	42.73	52.31	40.30	41.59	44.22
381.5	10668	40.08	18.71	45.52	52.99	41.47	43.37	45.49
386.5	10710	41.08	21.87	42.25	50.67	40.45	42.06	44.70
391.5	10753	39.77	19.27	41.12	53.48	38.30	39.74	42.44
396.5	10795	38.10	17.61	33.76	51.51	38.18	39.68	42.34
401.5	10837	37.84	14.19	41.78	47.75	39.53	41.36	43.65
406.5	10880	37.48	31.47	36.15	49.52	39.78	42.16	43.76
411.5	10922	40.94	19.70	50.63	52.75	37.22	38.95	41.27
416.5	10964	34.97	14.25	45.17	51.25	37.32	38.88	41.41
421.5	11007	41.15	15.26	50.38	50.32	36.78	38.64	40.95
426.5	11049	30.10	5.26	43.16	49.26	37.50	39.30	41.60
431.5	11092	35.77	30.95	42.58	48.06	40.06	42.48	43.99
436.5	11134	30.24	6.52	40.42	47.96	36.59	38.00	40.57
441.5	11176	32.80	23.27	49.08	49.90	38.65	40.44	42.63
446.5	11219	34.93	12.63	44.62	49.39	36.78	38.61	40.83
451.5	11261	37.32	16.28	49.95	49.88	36.44	38.09	40.50
456.5	11304	41.37	29.29	42.41	55.48	35.51	37.19	39.56
461.5	11346	42.76	26.48	53.44	48.19	39.82	41.07	43.80

Table A.13 continued

Table A.14. Grain-size distribution of core 401 (Mallorca Shelf) versus core depth used for Redundany Analysis (RDA). Samples were analyzed in a resolution of 20 cm.

core 401-1 depth [cm]	Fraction >1000µm (weight%)	Fraction >500 µm (weight%)	Fraction >250 µm (weight%)	Fraction >125 µm (weight%)	Fraction >63 µm (weight%)	Fraction < 63 µm (weight%)
20.5	0.59	0.59	1.19	14.20	39.05	44.38
40.5	1.40	1.87	1.40	12.15	38.32	44.86
60.5	1.14	1.14	1.52	11.41	39.55	45.25
80.5	0.95	0.94	1.27	14.87	38.92	43.04
96.5	2.41	2.00	2.00	4.82	31.72	57.03
116.5	1.55	1.55	1.93	5.02	34.36	55.59
136.5	1.68	1.68	1.68	6.15	35.75	53.07
156.5	1.48	1.48	1.77	10.91	40.41	43.95
176.5	1.69	1.69	1.69	8.08	32.32	54.54
196.5	2.43	1.35	1.62	7.82	26.95	59.83
216.5	2.19	1.36	1.36	9.86	28.50	56.72
236.5	1.46	1.48	1.71	11.95	28.53	54.87
256.5	2.03	1.62	1.62	9.50	31.31	53.93
276.5	1.08	1.34	1.88	13.68	32.17	49.85
296.5	0.82	1.64	2.20	11.50	33.15	50.68
316.5	0.62	1.72	3.09	16.50	33.01	45.05
336.5	0.62	1.53	3.36	18.65	35.78	40.06
356.5	1.43	3.44	4.87	18.06	39.25	32.95
371.5	2.93	4.74	5.48	19.70	34.31	32.85
396.5	5.51	11.97	6.14	11.01	28.16	37.21
416.5	4.16	10.94	4.53	6.41	14.72	59.25
436.5	8.30	33.16	9.76	9.03	15.37	24.38
456.5	9.60	39.90	16.41	7.32	8.33	13.38

Table A.15. Summary of the statistical results of the Redundancy Analysis (RDA) for core 401-1 (Mallorca Shelf).

Axes	**1**	**2**	**3**	**4**	**captured variance (%)**	**F-value**	**p value**
Eigenvalues	0.362	0.056	0.218	0.083			
Species-environment correlations	0.942	0.636	0.000	0.000			
Cumulative percentage variance							
of species data	36.2	41.9	63.7	72.0			
of species-environment relation	86.5	100.0	0.0	0.0			
correlations							
$ERSL_{WA\text{-}PLS}$	-0.94	-0.037	0.0000	0.0000	36.1	52.06	<0.0002
fraction <63 µm	-0.655	-0.457	0.0000	0.0000	20.5	23.66	<0.0002

Table A.16. Oxygen and carbon isotopic records in core 401-1 (Mallorca Shelf) versus calibrated radiocarbon ages and core depths.

core depth [cm]	Age cal. C^{14} years BP	$\delta^{13}C$ *G. bulloi-des*	$\delta^{13}C$ *G. ruber* (w.)	$\delta^{13}C$ *C. loba-tulus*	$\delta^{13}C$ *B. acule-ata*	$\delta^{13}C$ *R. phle-geri*	$\delta^{18}O$ *G. bulloi-des*	$\delta^{18}O$ *G. ruber* (w.)	$\delta^{18}O$ *C. loba-tulus*	$\delta^{18}O$ *B. acule-ata*	$\delta^{18}O$ *R. phle-geri*
0.5	0	-0.96	1.35	1.09	0.03		1.04	0.24	0.96	1.84	
5.5	136	-1.17	1.34	1.33	-0.07		0.94	0.20	1.10	1.82	
10.5	272	-1.12	1.43	1.26	0.40		0.93	-0.02	1.16	1.92	
15.5	402	-0.67	1.41	1.73	0.26		0.66	0.02	0.88	1.87	
20.5	532	-0.93	1.11	1.31	0.11		0.60	0.19	1.26	1.76	
25.5	662	-1.17	1.37	1.13	0.24		0.78	0.26	1.15	1.86	
30.5	792	-0.97	1.24	1.61	0.19		0.64	0.39	1.15	1.84	
35.5	922	-1.29	1.66	1.18	0.15		0.63	-0.12	1.13	1.57	
40.5	1052	-0.88	1.14	1.17	0.19		1.09	0.09	1.01	1.83	
45.5	1182	-0.81	1.22	1.31	0.19		0.87	0.36	1.12	1.76	
50.5	1312	-1.02	1.30	1.57	0.30		0.94	0.14	1.22	1.87	
55.5	1442	-0.85	1.26	1.36	0.41		0.79	0.13	1.25	1.82	
60.5	1572	-0.92	1.34	1.35			0.86	0.07	1.11		
65.5	1703	-1.07		1.06	-0.14		0.98		1.19	1.68	
70.5	1833	-1.23	1.21	1.17	0.27		1.14	0.18	1.01	1.85	
75.5	1963	-1.07	1.20	1.13	0.21		0.79	-0.12	1.22	1.90	
80.5	2093	-1.22		1.57	0.08		0.74		0.66	1.63	
85.5	2223	-1.21	1.26	1.34	-0.04		0.53	0.27	1.29	1.81	
90.5	2353	-0.71	1.42	1.63	-0.37		0.59	0.32	0.90	1.56	
91.5	2483	-0.88	1.44	1.17	-0.28		0.69	0.22	1.17	1.56	
96.5	2613	-1.18	1.26	1.18	0.14		0.95	0.20	1.15	1.96	
101.5	2743	-1.10	1.01	1.10	0.02		0.73	0.50	1.30	1.87	
106.5	2873	-0.98	1.32	1.27	-0.06		0.92	0.53	1.18	1.65	
111.5	3004		1.60	1.19	0.21			0.30	1.22	1.83	
116.5	3223	-1.25	1.38	1.39	0.02		0.75	0.30	1.28	1.75	
121.5	3443	-1.27	1.40	1.33	0.33		0.87	0.51	0.95	2.14	
126.5	3663	-1.00	1.48		-0.13		0.70	0.45		1.80	
131.5	3883	-0.69		0.46	-0.02		0.31		0.53	1.73	
136.5	4103	-1.15	1.49	1.04	-0.09		0.63	-0.12	1.12	1.94	
141.5	4323	-1.09	1.40	1.24	-0.27		0.60	0.20	1.05	1.69	
146.5	4543	-0.78	1.45	1.28	-0.27		0.41	0.25	0.98	1.65	
151.5	4763	-1.26			-0.22		0.63			1.79	
156.5	5031	-0.97	1.31		-0.16		0.65	0.15		1.73	
161.5	5300	-0.97	1.11	1.27	-0.22		0.78	0.54	1.10	1.79	
166.5	5568	-1.27	1.18	1.47	-0.20		0.57	0.27	0.98	1.79	
171.5	5837	-1.01	1.10	1.31	-0.27		0.28	0.12	0.97	1.78	
176.5	6105	-0.97	1.10	0.57	-0.40	-0.68	0.17	0.14	0.42	1.49	1.41
181.5	6374	-0.92	0.89	1.21	-0.32	-0.80	0.58	0.25	0.65	1.58	1.27
186.5	6642	-0.73	1.13	1.16	-0.55	-0.62	0.38	0.10	0.65	1.59	1.27
191.5	6911	-1.05	0.94	1.21	0.09	-0.97	0.90	0.12	0.91	1.93	1.11
196.5	7179	-0.88	1.01	1.53	-0.10	-0.68	0.81	0.36	0.78	1.75	1.09
201.5	7447	-0.86	0.59	0.99	-0.28	-1.07	0.13	-0.26	0.70	1.49	1.30
206.5	7716	-1.14	0.73	1.30	-0.43	-1.29	0.65	0.11	0.97	1.64	1.15
211.5	7984	-0.83	0.93	1.04	-0.43	-0.94	0.04	-0.40	0.63	1.50	1.18
216.5	8253	-0.80	0.80	1.28	-0.26	-1.01	0.03	-0.44	0.55	1.55	1.10
221.5	8521	-0.54	0.81		-0.71	-0.82	0.34	-0.37		1.16	1.29
226.5	8790	-0.70	0.49		-0.20	-0.93	0.35	-0.67		1.64	1.32

core depth [cm]	Age cal. C^{14} years BP	$\delta^{13}C$ *G. bulloi-des*	$\delta^{13}C$ *G. ruber* (w.)	$\delta^{13}C$ *C. loba-tulus*	$\delta^{13}C$ *B. acule-ata*	$\delta^{13}C$ *R. phle-geri*	$\delta^{18}O$ *G. bulloi-des*	$\delta^{18}O$ *G. ruber* (w.)	$\delta^{18}O$ *C. loba-tulus*	$\delta^{18}O$ *B. acule-ata*	$\delta^{18}O$ *R. phle-geri*
231.5	9058	-0.43	0.81	1.16	-0.09	-0.89	-0.11	-0.66	0.81	1.58	1.26
236.5	9117	-0.85	0.58	1.08	-0.10	-0.73	0.25	0.04	0.72	1.67	1.26
241.5	9177	-0.50	0.65	1.15	-0.14	-0.96	-0.06	-0.51	0.64	1.60	1.27
246.5	9236	-1.31	1.20	1.63	-0.43	-1.03	-0.15	-0.14	0.36	1.48	1.33
251.5	9295	-0.99	0.71	1.42	-0.41	-0.95	0.33	-0.87	0.17	1.50	1.26
256.5	9355	-0.74	0.65	1.41	-0.21	-0.90	-0.06	-0.45	0.34	1.69	1.28
261.5	9414	-0.73	0.60	1.48	0.01	-0.91	0.11	-0.47	0.34	1.59	1.12
266.5	9473	-1.30	0.74	1.31	0.07	-0.86	0.35	-0.16	0.46	1.73	1.15
271.5	9532	-0.94	0.89	1.55	-0.24	-0.63	0.39	-0.38	0.89	1.52	1.13
276.5	9592	-1.05	1.01	1.39		-0.80	0.44	-0.75	0.77		1.29
281.5	9651	-0.86	1.03	1.41	-0.16	-0.73	0.01	-0.74	1.25	1.63	1.24
286.5	9710	-1.43	1.24	1.41	-0.25	-0.77	0.37	-0.64	0.81	1.77	1.35
291.5	9770	-1.66	1.08	1.79	-0.17	-0.73	0.41	-0.82	0.72	1.55	1.12
296.5	9829	-1.15	0.70	1.83	-0.15	-0.80	0.30	-0.54	1.45	1.62	1.07
301.5	9888	-0.81	0.91	1.55	-0.21	-1.05	-0.11	-0.74	0.50	1.95	1.20
306.5	9948	-1.36	0.73	1.06	-0.28		0.68	-0.58	0.43	1.86	
311.5	10007	-1.26	0.81	1.22	-0.16		0.07	-0.74	0.64	1.78	
316.5	10066	-1.24	1.14	1.64	-0.20		0.28	-0.55	0.80	1.79	
321.5	10125	-0.87	0.79	1.44			0.44	-0.57	1.07		
326.5	10185	-1.30	1.30	1.54	-0.17		0.72	-0.38	0.91	2.15	
331.5	10244	-1.46	0.94	1.70	-0.18		0.31	-0.63	0.65	1.84	
336.5	10286	-0.98	1.23	1.27	-0.07		0.66	-0.73	1.37	2.18	
341.5	10329	-0.97	1.51	1.61	-0.25		0.32	-0.65	1.09	1.94	
346.5	10371	-0.99	1.42	1.19	-0.22		0.91	-0.45	1.34	1.82	
351.5	10414	-0.64	1.15	1.36	-0.08		0.71	-0.39	0.85	2.06	
356.5	10456	-0.71	1.31	1.41	-0.03		0.33	-0.49	1.49	2.02	
361.5	10498	-0.47	1.32	1.31	-0.06		0.12	-0.58	0.97	1.97	
366.5	10541	-0.36	1.29	1.02	-0.37		0.91	-0.54	1.06	1.91	
371.5	10583	-1.10	1.51	1.55	-0.17		0.57	-0.66	0.85	2.08	
376.5	10625	-0.25	1.48	1.68	0.07		0.25	-0.42	1.15	1.95	
381.5	10668	-0.68	1.55	1.31	-0.19		0.25	-0.54	0.82	2.01	
386.5	10710	-0.51	1.40	1.67	0.13		0.39	-0.42	1.04	2.25	
391.5	10753	-1.01	1.28	1.36	-0.21		0.36	-0.30	0.81	2.03	
396.5	10795	-0.79	1.17	1.61	-0.18		0.25	-0.32	1.00	1.82	
401.5	10837	-0.61	1.53	1.53	-0.16		0.45	-0.35	1.35	2.15	
406.5	10880	-0.57	1.23	1.52	0.16		0.65	-0.45	1.26	1.81	
411.5	10922	-0.80	1.26	1.53	-0.18		0.35	-0.44	0.97	1.94	
416.5	10964	-0.10	1.30	1.50	0.05		0.37	-0.50	1.27	2.25	
421.5	11007	-0.67	1.21	1.46			0.36	0.02	0.95		
426.5	11049	-0.62	1.10	1.25	-0.16		0.26	-0.56	0.32	2.11	
431.5	11092	-1.05	1.37	1.52	-0.23		1.11	-0.16	0.86	1.95	
436.5	11134	-1.13	1.24	1.53			0.78	0.00	0.84		
441.5	11176	-0.90	1.19	1.45	-0.41		0.96	-0.17	0.83	1.56	
446.5	11219	-0.32	1.27	1.45			0.43	-0.05	0.95		
451.5	11261	-0.73	1.26	1.46	-0.04		0.72	-0.37	0.67	2.15	
456.5	11304	-1.06	1.34	1.47	-0.24		0.36	-0.23	1.03	1.76	
461.5	11346	-0.92	1.28	1.44	-0.24		0.86	-0.20	0.96	2.08	

Table A.16 continued

The enclosure (CD-ROM) contains the following Tables:

Electronic **Table A.17**. Census counts live (Rose Bengal stained) benthic foraminifera in the surface samples from the Alboran Platform, Oran Bight, and the Mallorca Shelf with sample splits and sample volumens.

Electronic **Table A.18**. Census counts dead benthic foraminifera, sum benthic and planktonic foraminifera, sum redeposited foraminifera in the surface samples from the Alboran Platform, Oran Bight, and the Mallorca Shelf with sample splits and sample weights.

Electronic **Table A.19**. Census counts dead benthic foraminifera, sum benthic and planktonic foraminifera, sum redeposited foraminifera in sediment-core 342-1 from the Alboran Platform with sample splits and sample weights.

Electronic **Table A.20**. Census counts dead benthic foraminifera, sum benthic and planktonic foraminifera, sum redeposited foraminifera in sediment-core 367-1 from the Oran Bight with sample splits and sample weights.

Electronic **Table A.21**. Census counts dead benthic foraminifera, sum benthic and planktonic foraminifera in sediment-core 401-1 from the Mallorca Shelf with sample splits and sample weights.